PREPARATION OF NOVEL MEMBRANE DISTILLATION MEMBRANES WITH FACILE AND COST-EFFECTIVE METHODS

Miaomiao Tian

Supervisors:

Prof. Bart Van der Bruggen

Prof. Peter Van Puyvelde

Members of the Examination committee:

Prof. Dirk Vandermeulen

Prof. Rob Ameloot

Prof. Luc Pinoy

Prof. Mohamed Khayet

Dr. Kristien De Sitter

Dissertation presented in partial fulfilment of the requirements for the degree of Doctor of Engineering Science (PhD):

Chemical Engineering

March 2021

© 2021 KU Leuven, Science, Engineering & Technology

Uitgegeven in eigen beheer, Miaomiao Tian, BELGIUM

Alle rechten voorbehouden. Niets uit deze uitgave mag worden vermenigvuldigd en/of openbaar gemaakt worden door middel van druk, fotokopie, microfilm, elektronisch of op welke andere wijze ook zonder voorafgaandelijke schriftelijke toestemming van de uitgever.

All rights reserved. No part of the publication may be reproduced in any form by print, photoprint, microfilm, electronic or any other means without written permission from the publisher.

Acknowledgements

How time flies! It already comes to the end of my PhD journey. I still remember the exciting day when I arrived in Leuven, which was at the dawn of 22nd October 2016, and a beautiful city with different building styles arose. I really love the time living in Leuven. The city is old with plenty of historic buildings but also young with lots of youthful and energetic students, quiet in lots of places but also boisterous in the city center, and the people here are always nice and warmhearted. I appreciate that I can study at KU Leuven as a PhD student. During the PhD courses, I have learned different ways of thinking inspired by the teachers and classmates. While in the research time, I have learned more about my research area and improved the ability to find research topics, design experiments, analyze and prove the results. I have a lot to say about my PhD journey, and this is really a great moment to look back on my life in Leuven.

First and foremost, I want to express my greatest appreciation to my supervisor Prof. Bart Van der Bruggen for his continuous support and great encouragement. I am grateful that you gave me a chance to come here to study and to experience a different life, and I am proud to be one member of your excellent research group. I do deeply appreciate all the support from you all along my PhD process, not only the support on my research and my papers but also the support in my life when I had to stop my research to bring up a little baby. Whenever I ask you for help, you always give me the positive response. I indeed appreciate that you always stand by me and support me. When I need to go back to China with my family in the last year of my PhD, you approved this decision and encouraged me to try my best to accomplish my experiments and thesis as soon as possible, and then go back to Leuven for the defense. However, this is a special year with COVID-19 spreading, I did not finish my PhD on time because of the shut-down of the university, and it is also a pity that I did not say goodbye to you when I leave Leuven, because we thought that I could go back only after half a year. But graduation is never the end of the bond between us, and it is a new start. I will go back to visit you in the near future.

Secondly, I would like to thank my co-supervisor Prof. Peter Van Puyvelde. Thank you for opening the new world of 3D printing for me and give me the chance to explore the potential to combine this attractive technique with the membrane distillation research. You always reply to my email and give me answers very quickly, which makes me very reassured when I need your help. I'm grateful that you always support me with the printed membranes and the suggestions on my work relating to the printed membranes. 3D printing is really an interesting process, and I hope I still have the opportunity to work on it in the future.

Thirdly, I would like to express my appreciation to Prof. Yatao Zhang from Zhengzhou University, China. Thank you for giving me the support in the last year to accomplish my experiments in your group. Without your help, I cannot imagine how I can finish my PhD. As a master student in our group, I only stayed in our lab in the first year and then go to another lab for joint-supervision. But I was impressed by your kindness to us and your earnestness in research. Thank you again for giving me the opportunity to work in our lab again. I would like to appreciate Prof. Tao He from Shanghai Advanced Research Institute, China. As the leading supervisor in my master period, I was indeed impressed with your enthusiasm for research. You discuss the experiments and results with the students frequently, and you are always there to help us and give us guidance. Your attitude in research inspired me to explore further in the research area. Even during my PhD progress, you are always here to support me whenever I asked you for help. Thank you.

Fourthly, I would like to thank Prof. Dirk Vandermeulen from the Department of Electrical Engineering, KU Leuven, for being the chairman of the examination committee for my PhD defense. I would like to express my sincere appreciation to my assessors Prof. Rob Ameloot (Department of Microbial and Molecular System) and Prof. Luc Pinoy (Chemical Engineering, Ghent and Aalst Technology Campuses, KU Leuven). I also express my deep gratitude to Prof. Mohamed Khayet (University Complutense of Madrid) and Dr. Kristien De Sitter (VITO, Flemish Institute for Technological Research) for agreeing to be my examination committee members.

Thank all of you for giving me insightful and valuable comments and suggestions for my research and thesis. It is interesting to discuss my works with all of you, and the discussions inspired me to investigate more details of my research, which provided me a deeper understanding of my research area from different aspects.

Moreover, I would also express my appreciation to my colleagues who helped me a lot during my PhD. First, thanks go to Alena Vaes, Christine Wouters, Michèle Vanroelen, Herman Tollet, and Hanne Geunes. Thanks for your kind help relating to my study and my lab works in ProCESS. Then, thanks to all the colleagues in our group: Shushan Yuan, Jing Wang, Jian Li, Xin Li, Bin Liu, Ruijun Zhang, Zhijuan Zhou, Yan Zhao, Yi Li, Pengrui Jin, Junfeng Zheng, Jianxiu Wang, Xiaoyun Wu, Yaoxing Liu. Thank you for the accompany and help during the days in Leuven. It is interesting to share and discuss the research topics together, and it is also memorable we eat and travel together. I hope all of you have a nice future and realize your dreams. I also would like to thank Trang and Indah. As girls and mothers in our lab, we have special topics to talk and we have had a happy time together, and I am really happy to work with you. Wish you a happy family, a happy life, and a nice future. I would like to thank Florian Decaesstecker. When I re-started my research after my baby was sent to the daycare, you really help me a lot in exploring the experiment feasibility and MD setup construction. You are such a hardworking, earnest, and smart student, I am sure you can have a bright future. I would like to thank Dieter and Hellen. Thank you for preparing the 3D printed membranes for me, and for always answering my questions and discussions relating to the printing process. 3D printing is really an interesting area, I sincerely hope you can have great results and outputs.

Furthermore, I gratefully acknowledge China Scholarship Council (CSC) of the Ministry of Education, China, for funding me to study in KU Leuven and to give me the chance to change my views of the world and broaden my horizon.

Especially, I would like to appreciate my husband Junyong Zhu and child Yumu Zhu. Dear Junyong, thank you for all your support in both my life and my research. Without your great help and support, I cannot finish my PhD works in such a short time.

Your serious attitude toward research inspires me to do my research seriously, and the discussions about my research topic also help me a lot. I appreciate the times we spend together, the days we stay in Leuven, the days we go to travel, the days we take care of the baby together, and the days we go to the canteen together. My little baby Yumu, although you disturbed the plan I made for my PhD career, I never regret that I have such a cute baby. Every time I have problems in my research and I am upset, you can always cure me with your smiling face and your love for me. Although the days I must do experiments and take care of you are very hard, they are unforgettable and precious memories. As you grow day by day, I am more and more grateful that you can come to my family, to bring happiness to your papa and me.

Lastly, I want to thank my parents and sisters for always being with me. Thank you for all your encouragement, understanding, and support to me through all the tough times. Thank you for the endless love.

Miaomiao Tian

March 2021

Table of Content

Acknowledgements **3**

Abstract ..... **II**

Samenvatting ..... **II**

List of abbreviations and symbols ..... **II**

Chapter 1. Introduction **1**

1.1 Background 1

1.2 History of membrane distillation 4

1.3 Basic information of MD 5

1.3.1 Mechanism of membrane distillation 6

1.3.2 MD membrane characteristics 13

1.3.3 MD performance related factors 18

1.3.5 Advantages and limitations of membrane distillation 22

1.4 Fabrication of MD membranes 24

1.4.1 Membranes prepared by NIPS 27

1.4.2 Membranes prepared by electrospinning 39

1.4.3 Commercial membranes 52

1.4.4 Other methods 57

1.5 Applications of MD technology 61

1.5.1 Desalination from seawater and wastewater 61

1.5.2 Hazardous component and dye removal 62

1.5.3 Volatile and organic solvent separation and concentration 63

1.5.4 Concentration of temperature sensitive solutions 64

1.6 Objectives and outline of the thesis 64

1.7 References 67

Chapter 2 Materials and methods **83**

2.1 Preparation of PVDF coated 3D printed membranes via dip-coating 83

2.1.1 Materials and chemicals 83

2.1.2 Preparation of PVDF coated 3DP composite membranes 83

2.2 Preparation of PVDF membranes using a novel bottom-up method..... 85
2.2.1 Chemicals and materials 85
2.2.2 Membrane preparation 85
2.3 Fabrication of PVDF membranes by co-casting 87
2.3.1 Chemicals and materials 87
2.3.2 Membrane preparation 87
2.4 Characterization..... 90
2.4.1 Solution viscosity..... 90
2.4.2 Scanning electron microscope..... 90
2.4.3 Surface roughness..... 90
2.4.4 Shrinkage value 90
2.4.5 Water contact angle..... 91
2.4.6 Mean pore size..... 91
2.4.7 Porosity 92
2.4.8 Mechanical strength..... 92
2.4.9 Liquid entry pressure (LEP)..... 93
2.5 DCMD performance tests 93
Chapter 3 97
Exploring the potential usage of 3D printed membranes combined with PVDF coating in direct contact membrane distillation (DCMD) 97
3.1 Introduction..... 97
3.2 Results and discussion 100
3.2.1 Morphology and hydrophobicity of PVDF@3DP membranes 100
3.2.2 Physical properties of PVDF@3DP membranes 105
3.2.3 DCMD performance 108
3.3 Conclusions.....109
References:.....110
Chapter 4 117
One-step fabrication of isotropic poly (vinylidene fluoride) membranes for direct

contact membrane distillation (DCMD) 117
4.1 Introduction 117
4.2 Results and discussion 119
4.2.1 Membrane morphologies and hydrophobicity 119
4.2.2 Pore size, and porosity 124
4.2.3 DCMD performance 125
4.3 Conclusions 126
References: 127
Chapter 5 131
A co-casting route enables the formation of skinless, hydrophobic poly(vinylidene fluoride) membranes for DCMD 131
5.1 Introduction 131
5.2 Results and discussion 136
5.2.1 Membrane morphology 136
5.2.2 Physical properties 144
5.2.3 DCMD performance 147
5.3 Conclusions 149
References: 150
Chapter 6 155
Conclusions and outlook 155
6.1 General conclusions 155
6.2 Outlook for future work 160
Curriculum Vitae 163

Abstract

To relieve the pressure related to water scarcity in the current generation, desalination is entrusted with an important mission. Compared to the traditional desalination technologies including thermal distillation and reverse osmosis, membrane distillation (MD) has its own advantages such as mild operation conditions, a high rejection of salts, less sensitive to the feed concentration, the feasibility of low-grade heat resources, and great potential application in small scale systems. As the physical barrier to separate the hot feed solution and cool permeate side and provide the space for vapor transport while rejecting nonvolatile matters in the feed, the membrane is essential to ensure a high MD performance in terms of flux, rejection, and anti-wetting properties. Plenty of efforts have been made to fabricate MD membranes including non-solvent induced phase separation, electrospinning, combined with post modifications such as blending, coating, grafting, plasma modification, nanoimprinting. However, the complicated processing procedure and the high cost of chemicals as well as possible toxicity are major obstacles to scale up the available membranes. Therefore, exploring simple, efficient, and cost-effective membrane preparation methods is extremely important. In this thesis, three methods are discussed.

Firstly, the feasibility of using 3D printed (3DP) membranes in membrane distillation (MD) is explored for the first time in this work. Polyamide (PA) membranes were printed by a laser sintering (LS) technology, and further coated with thin poly(vinylidene fluoride) (PVDF) layers to reduce the pore size by dip-coating. The impact of PVDF concentration and immersion time on the membrane morphology, hydrophobicity, pore size, porosity, and DCMD performance were investigated. Results show that the additional PVDF layers could effectively reduce the membrane pore size from 15.9±5.3 μm to 1.0-2.5 μm. Additionally, due to the granular and rough surface of the 3DP substrates formed by the coalescence of PA powders, the hydrophobicity of the composite membranes (100°-130°) was greater than for the conventional PVDF membranes manufactured on a glass sheet or non-woven (~70°). However, considering the low porosity of the 3DP substrates (~21.7%), the PVDF coated 3DP (PVDF@3DP)

membranes are found to have relatively low porosities at a range of 45%-62%. Furthermore, the high thickness of the PA substrates of 359.6±38.9 μm lead to relatively thick composite membranes, especially for the PVDF@3DP-10 membranes of ~500 μm. Therefore, the PVDF@3DP membranes had relatively low fluxes of around 10 kg/(m^2·h) at a temperature difference of 40 °C with a feed temperature of 60 °C. The overall results indicate that the 3DP substrates significantly affect the MD performance of the composite membranes rather than the thin PVDF layer. Therefore, improving the porosity and decreasing the thickness of the printed substrates will be advantageous to prepare membranes with MD performance comparable to traditional membranes with quick fabrication and less solvent discharge.

Secondly, a facile bottom-up method using water as coagulation bath was proposed to fabricate porous PVDF membranes. By covering a piece of non-woven substrate on the nascent film on a glass plate followed by immersion into a water bath, isotropic and skinless PVDF membranes were obtained. The SEM characterization confirms the formation of a rough top surface and sponge-like granular membranes composed of spherulites. The water contact angles substantially increase from 71.7° for conventional PVDF-N membrane to ca. 144° for bottom-up membranes. The DCMD flux of the bottom-up PVDF membrane is as high as 41.4 kg/(m^2·h) with a polymer concentration of 15 wt.% when the feed and permeate temperatures were 70 °C and 20 °C, respectively.

Furthermore, porous PVDF membranes with sponge-like structure were also developed in a co-casting process. Unlike the dual-layer membranes in which dual-layers attached tightly after co-casting, the attainment of independent PVDF membranes with uniformly rough surface structures necessitates the delamination of top-layer membranes from the underlying PVDF membranes. The coverage of top-layer membranes via co-casting is expected to reduce the solvent/nonsolvent exchange rate for the underlying PVDF membranes during a phase inversion process. In this context, a polyethersulfone (PES) membrane is co-cast onto a PVDF membrane followed by phase inversion in a water bath to fabricate PVDF membranes. The spontaneous

delamination of PES from PVDF membranes occurs once the top-layer PES membrane solidifies. Due to the combined effect of the additional PES layer and the solvent retained at the PES/PVDF interface, delayed liquid-liquid (L-L) demixing of the PVDF solution take place, resulting in the formation of a porous surface with symmetric cross-section. Results show that the PVDF concentration significantly affects the membrane morphology. Increasing the PVDF content from 16 wt.% to 20 wt.% leads to a marked morphological change for membrane cross-section from cellular pores to PVDF globules, which indicates that the phase inversion mechanism varies from delayed L-L demixing to solid-liquid (S-L) demixing; this is mainly affected by the solution viscosity. Due to the roughness increment by the particulate surfaces, the hydrophobicity of PVDF-co membranes is distinctly enhanced. Furthermore, the membrane mean pore size is enlarged, and the PVDF layer thickness is reduced. Therefore, the PVDF-co membranes have much higher fluxes of 20.1-23.8 kg/(m^2·h) in comparison to the single-layer PVDF membranes of 12.5- 6.5 kg/(m^2·h) at feed and permeate temperatures of 60 °C and 20 °C, respectively, especially for PVDF-co membranes composed of PVDF particles which shows superior pore interconnectivity than the cellular pores. A long-term stability test was conducted with the PVDF-20-21 membrane for 50 h using a 3.5 wt.% NaCl solution as feed at a temperature difference of 40 °C. Fairly steady fluxes are observed over the testing course, as well as a continuous high salt rejection of above 99.9%.

Samenvatting

Om de druk door waterschaarste in de huidige generatie te verlichten, speelt ontzilting een belangrijke rol. Vergeleken met de traditionele ontziltingstechnologieën, waaronder thermische destillatie en omgekeerde osmose, heeft membraandestillatie (MD) zijn eigen voordelen, zoals milde bedrijfsomstandigheden, een hoge weerhouding van zouten, minder gevoelig voor schommelingen in de voedingsconcentratie, de mogelijkheid om laagwaardige warmtebronnen te gebruiken, en potentiële toepassing in kleinschalige systemen. Als fysieke barrière om de hete voedingsoplossing en de koele permeaatzijde te scheiden en om ruimte te bieden voor damptransport terwijl niet-vluchtige stoffen uit de voeding worden tegengehouden, is het membraan essentieel om een hoge MD-prestatie te garanderen in termen van flux, zoutverwijdering, en het vermijden van bevochtiging van het membraan. Er zijn veel methoden ontwikkeld om MD-membranen te fabriceren, waaronder fasescheiding geïnduceerd door een niet-solvent van het polymeer gebruikt als membraanmateriaal, elektrospinnen, gecombineerd met modificaties achteraf zoals mengen, coaten, enten, plasmamodificatie en nanomodificaties. De gecompliceerde verwerkingsprocedure en de hoge kosten van chemicaliën, evenals mogelijke toxiciteit, zijn echter grote obstakels om de beschikbare membranen op te schalen. Daarom is het onderzoeken naar eenvoudige, efficiënte en kosteneffectieve methoden voor het aanmaken van membranen uiterst belangrijk. In dit proefschrift worden drie methoden besproken.

Ten eerste wordt in dit werk de haalbaarheid onderzocht van het gebruik van 3D-geprinte (3DP) membranen bij membraandestillatie (MD). Polyamide (PA) membranen werden aangemaakt met een laser sintering (LS) technologie, en verder bekleed met dunne poly (vinylideenfluoride) (PVDF) lagen door onderdompeling, om de poriegrootte te verkleinen. De impact van de PVDF-concentratie en onderdompelingstijd op de membraanmorfologie, hydrofobiciteit, poriegrootte, porositeit en DCMD-prestaties werden onderzocht. De resultaten tonen aan dat de extra PVDF-lagen de poriegrootte van het membraan effectief kunnen verminderen van 15.9±5.3 μm tot 1.0-2.5 μm. Bovendien, als gevolg van het korrelige en ruwe oppervlak

van de 3DP-substraten gevormd door de coalescentie van PA-poeders, was de hydrofobiciteit van de composietmembranen (100°-130°) groter dan voor de conventionele PVDF-membranen vervaardigd op een glasplaat of niet-geweven ondergrond (~70°). Gezien de lage porositeit van de 3DP-substraten (~21.7%), blijken de PVDF @ 3DP-membranen relatief lage porositeiten te hebben, in een bereik van 45%-62%. Bovendien leidde de hoge dikte van de PA-substraten van 359.6±38.9 μm tot relatief dikke composietmembranen, vooral voor de PVDF@3DP-10-membranen van ~500 μm. Daarom hadden de PVDF@3DP-membranen relatief lage fluxen van ongeveer 10 kg/(m^2·h) bij een temperatuurverschil van 40°C. De algemene resultaten geven aan dat de 3DP-membranen de MD-prestatie van de composietmembranen aanzienlijk beïnvloeden in plaats van de dunne PVDF-laag. Daarom zal het verbeteren van de porositeit van het bedrukte membraan en het verminderen van de dikte voordelig zijn om membranen te vervaardigen met MD-prestaties die vergelijkbaar zijn met traditionele membranen met snelle fabricage en minder afvoer van solvent.

Ten tweede werd een eenvoudige *bottom-up* methode voorgesteld met water als coagulatiebad om poreuze PVDF-membranen te vervaardigen. Door met een stuk niet-geweven substraat de film te bedekken, gevolgd door onderdompeling in een waterbad, werden isotrope PVDF-membranen zonder toplaag verkregen. De SEM-karakterisering bevestigt de vorming van een ruw bovenoppervlak en sponsachtige granulaire membranen samengesteld uit sferulieten. De watercontacthoeken nemen aanzienlijk toe van 71.7° voor het PVDF-N-membraan tot ca. 144° voor *bottom-up* membranen. De DCMD-flux van het *bottom-up* PVDF-membraan is zeer hoog, 41.4 kg/(m^2h) met een polymeerconcentratie van 15 gew.%, wanneer de toevoer- en permeaattemperatuur respectievelijk 70 °C en 20 °C waren.

Verder werden ook poreuze PVDF-membranen met sponsachtige structuur ontwikkeld in een co-casting proces. In tegenstelling tot de dubbellaagse membranen, vereist het verkrijgen van onafhankelijke PVDF-membranen met uniform ruwe oppervlaktestructuren de delaminatie van de toplaag van de onderliggende PVDF-membranen. De bedekking van toplaag via co-casting zal naar verwachting de

solvent/niet-solventuitwisselingssnelheid voor de onderliggende PVDF-membranen verlagen tijdens een fase-inversieproces. In deze context wordt een polyethersulfon (PES)-membraan samen gegoten op een PVDF-membraan, gevolgd door fase-inversie in een waterbad om PVDF-membranen te fabriceren. De spontane delaminatie van PES van PVDF-membranen vindt plaats zodra het PES-membraan van de toplaag stolt. Vanwege het gecombineerde effect van de extra PES-laag en het solvent dat wordt vastgehouden op het PES/PVDF-grensvlak, vindt vertraagde vloeistof-vloeistof (L-L) ontmenging van de PVDF-oplossing plaats, wat resulteert in de vorming van een poreus oppervlak met symmetrische doorsnede. Resultaten tonen aan dat de PVDF-concentratie de membraanmorfologie significant beïnvloedt in vergelijking met de marginale invloed van de PES-concentratie. Het verhogen van het PVDF-gehalte van 16 gew.% naar 20 gew.% leidt tot een duidelijke morfologische verandering voor de membraandoorsnede van cellulaire poriën tot PVDF-bolletjes, wat aangeeft dat het fase-inversiemechanisme varieert van vertraagde LL-ontmenging tot vast-vloeistof (SL) ontmenging; dit wordt voornamelijk beïnvloed door de viscositeit van de oplossing. Vanwege de toename van de ruwheid door de deeltjesoppervlakken, wordt de hydrofobiciteit van PVDF-co-membranen duidelijk verbeterd. Bovendien wordt de gemiddelde poriegrootte van het membraan vergroot en wordt de dikte van de PVDF-laag verkleind. Daarom hebben de PVDF-co-membranen veel hogere fluxen dan de enkellaagse PVDF-membranen, vooral voor PVDF-co-membranen die zijn samengesteld uit PVDF-deeltjes die een betere poriënverbinding vertonen dan de cellulaire poriën. Een stabiliteitstest op lange termijn werd uitgevoerd met het PVDF-20-21-membraan gedurende 50 uur met een 3.5 gew.% NaCl-oplossing als voeding bij een temperatuurverschil van 40 °C. Tijdens het testtraject worden relatief constante fluxen waargenomen, evenals een continue hoge zoutverwijdering van meer dan 99.9%.

List of abbreviations and symbols

3DP	3D printed
AC	Active carbon
AFM	Atomic force microscopy
AGMD	Air gap membrane distillation
aPP	Amorphous polypropylene
APTS	3-(Aminopropyl) triethoxysilane
BNCA	Bacterial nanocellulose aerogels
CA	Contact angle
CP	Concentration polarization
CPL	ε-Caprolactam
CVD	Chemical vapor deposition
DCMD	Direct contact membrane distillation
DI	Deionized
DL	Dual-layer
DMAc	Dimethylacetamide
DMF	Dimethylformamide
DMSO	Dimethylsulfoxide
ENMs	Electrospun nanofiber membranes
ES	Electrospinning
ES^2	Electro-co-spinning/spraying
FAS	1H,1H,2H,2H-perfluorodecyltriethoxysilane
FDTS	Ferfluorodecyltrichlorosilane
FO	Forward osmosis
FPA	Fluorinated polyurethane additive
FTCS	1H,1H,2H,2H-perfluorododecyl trichlorosilane
FTES	1H,1H,2H,2H-perfluorooctyltriethoxysilane
GO	Graphene oxide
GO-NBA	N-butylamine modified graphene oxide
HF	Hollow fiber
HPI	Hydroxyl poluimide
HTAB	Hexadecyl trimethyl ammonium bromide
LEP	Liquid entry pressure
LLRW	Low-level radioactive wastewater
LMH	$L/(m^2 \cdot h)$, the flux unit
LTH	Low temperature hydrothermal
LS	Laser sintering
MCr	Membrane crystalization
MD	Membrane distillation
MED	Multiple-effect distillation
MEMD	Multi-effect MD
MF	Microfiltration

MGMD	Material-gap MD
MP	Micro-pillar
MSF	Multi-stage flash distillation
MWCNTs	Multi-walled carbon nanotubes
NCC	Nanocrystalline cellulose
NF	Nanofiltration
NIPS	Nonsolvent-induced phase separation
NMP	N-methylpyrrolidone
NPs	Nanoparticles
NTIPS	Nonsolvent thermally-induced phase separation
PA	Polyamide
PAN	Polyacrylonitrile
PBI	Polybenzimidazole
PDA	Polydopamine
PDMS	Polydimethylsiloxane
PE	Polyethylene
PEG	Polyethylene glycol
PEI	Polyetherimide
PES	Polyethersulfone
PET	Polyethylene terephthalate
PFOTS	1H, 1H, 2H, 2H-perfluorooctyltrichlorosilane
PFPE	Perfluoropolyether
POSS	Polyhedral oligomeric silsesquioxane
PP	Polypropylene
PRO	Pressure-retarded osmosis
PS	Polystyrene
PSf	Polysulfone
PTFE	Polytetrafluoroethylene
PV	Pervaporation
PVA	Polyvinyl alcohol
PVDF	Polyvinylidene fluoride
PVDF-HFP	Poly(vinylidene fluoride-co-hexafluoropropylene
PVP	Polyvinyl pyrrolidone
RO	Reverse osmosis
SA	Sliding angle
SDS	Sodium dodecyl sulfate
SEM	Scanning electron microscopy
SGMD	Sweep gas membrane distillation
SMMs	Surface modifying macromolecules
SOM	Superomniphobic
SPES	Sulfonated polyethersulfone
SSM	Stainless-steel mesh
TEOS	Tetraethyl orthosilicate
TEP	Triethyl phosphate

THF	Tetrahydrofuran
TIPS	Thermally-induced phase separation
TMSCI	Trimethylchlorosilane
TP	Temperature polarization
TPC	Temperature polarization coefficient
TR-PBOI	Thermally arranged polybenzoxazole-co-polyimide
UF	Ultrafiltration
VE-DCMD	Vacuum-enhanced DCMD
VMD	Vacuum membrane distillation
V-MEMD	Vacuum-multi-effect MD

Symbols

A	Membrane surface area in the membrane module
B	Geometric factor of a membrane pore
C_f	Electrical conductivity of the feed solution
C_p	Electrical conductivity of the permeate solution
J	MD flux in kg/(m^2·h)
K	Membrane distillation coefficient
Kn	Knudsen number
N	MD molar flux
R	Salt rejection
Δt	Time interval
T_{fb}	Bulk temperature of feed solution
T_{fm}	Membrane surface temperature at the feed side
T_{pb}	Bulk temperature of permeate solution
T_{pm}	Membrane surface temperature at the permeate side
d	Membrae pore diameter
h_m	Membrane heat transfer coefficient
h_{mg}	Heat transfer coefficient of gas
h_{ms}	Heat transfer coefficient of solid membrane matrix
m_{wet}	Mass of the wet membrane sample
$m_{wet\text{-}sub}$	Mass of the wet substrate
m_{dry}	Mass of the dry membrane sample
$m_{dry\text{-}sub}$	Mass of the dry substrate
r	Membrane pore size
r_{max}	Maximum pore size
δ	Membrane thickness
δ_{sub}	Thickness of the substrate
ε	Membrane porosity
$\varepsilon_{polymer}$	Porosity of the polymer layer
τ	Membrane tortuosity
θ	Contact angle
λ	Mean free path

γ_{SV}	Surface tension at the solid-vapor interface
γ_{SL}	Surface tension at the solid-liquid interface
γ_{LV}	Surface tension at the liquid-vapor interface
γ_{L}	Liquid surface tension
$\rho_{ethanol}$	Density of ethanol

Chapter 1. Introduction

1.1 Background

Fresh water scarcity, has been recognized as a great global risk in the current era and in the near future, as shown in Figure 1.1. As reported by "World Water Development Report 2019" of UN Water, the global water requirement is supposed to increase at 1% per year until 2050, which is mainly caused by the increasing demand in industries and cities. Paradoxically, water is also one of the most abundant resource on earth. However, 97.5% of the water resource is seawater, while only 2.5% of the total is fresh water. Furthermore, among the fresh water, most of them are glaciers, ice caps, and groundwater, and only 0.014% is easily accessible [data from *Wikipedia*]. Therefore, using saline water to produce fresh water by desalination technologies is the most technologically reliable and economically sustainable method to reduce the water scarcity stress [1-6].

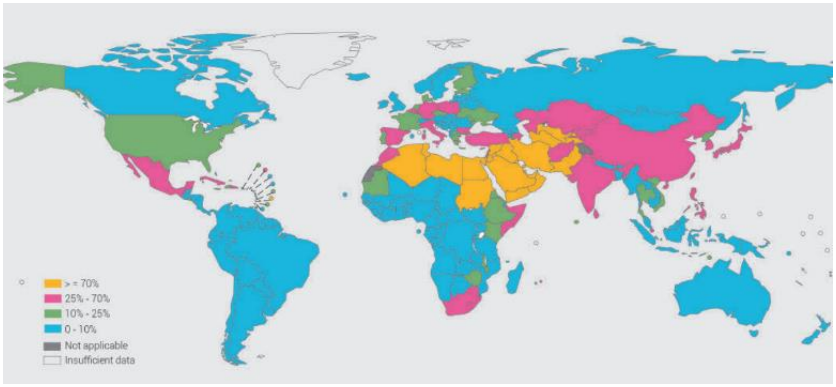


Figure 1.1 Level of water stress (*UN water*)

Desalination is a process in which freshwater is extracted from saline or contaminated streams including seawater, brackish groundwater, or wastewater. Due to the energy consumption, desalination is normally more expensive than usage of available fresh water from rivers or groundwater which are not always feasible. Approximately 1% of the world's population's daily needs for water depends on the desalinated water, which demonstrate the importance of desalination technology. The

current desalination technologies can be divided in two categories: thermal distillation technologies and membrane technologies, as depicted in Figure 1.2.

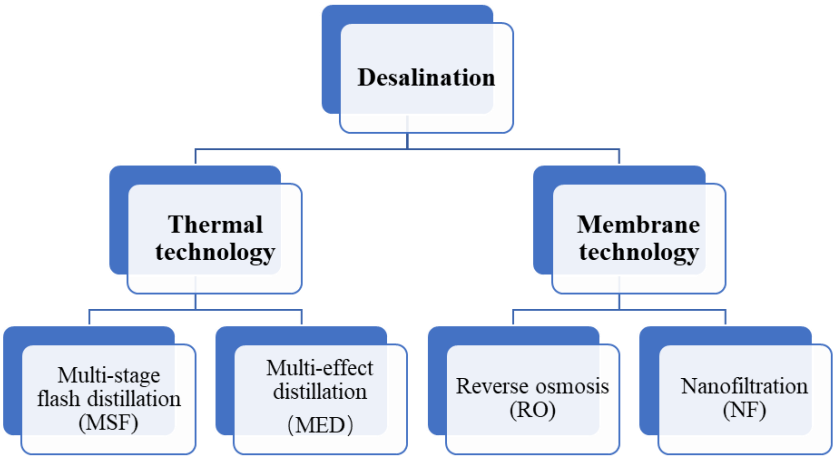


Figure 1.2 Different types of desalination technologies

The thermal technologies mainly comprise multi-stage flash distillation (MSF) and multiple-effect distillation (MED) [7, 8]. In the MSF process, a series of flash evaporation stages is employed, and water is evaporated and separated from the saline water. Each subsequent flash process utilizes the heat released from the water vapor condensation from the previous process. In the MSF process, a greater number of stages yields a better efficiency. Furthermore, as the temperature is lower than the water boiling point, steam from a heat recovery system can be used. However, the operating costs are high if waste heat is not available, and the high temperature increases the risk of corrosion and scale formation, which also increases the maintenance cost. Likewise, the MED process also consists of a series of stages. In each stage, the incoming water is sprayed onto high temperature tubes, which generate steam to heat the next batch of incoming water. The MED process has several advantages, such as a relatively low energy consumption, no pre-treatment of seawater, highly reliable and simple to operate, and low-energy heat source (hot water, waste heat from power generation, industrial processes, solar heating) can be adapted. However, heat source with a higher temperature cannot be utilized in the MED process because of the scaling issues. In addition, the MED process is difficult to scale down because of the complexity and large numbers of parts required. Among the membrane technologies, reverse osmosis (RO) is the leading desalination process, which has been commercially used since the

early 1970s, and occupies 66% of the installed desalination capacity until 2011 and nearly all the new plants [1]. In the RO process, a semipermeable membrane is utilized under high pressure to induce water permeation while rejecting salts. The energy consumption of the RO process is relatively low compared to traditional thermal technologies because there is no phase change in the process. In addition, RO can reject all dissolved minerals and micropollutants in water and it has a higher water recovery than distillation. Nonetheless, feed water pre-treatment is needed to limit fouling and scaling, and there is a salinity limit of feed solution (~80 g/L) for a RO system as the applied pressure should overcome the osmotic pressure of the feed solution. Besides, membrane cleaning and high-pressure pumps and pipes maintenance are expensive. Nanofiltration (NF) is another leading pressure-driven membrane process, mostly used in water softening due to its advantage of retaining divalent cations while passing small hydrated monovalent ions. Similar with RO, pre-treatment is needed to remove problematic particles or components that may cause membrane pore blocking and fouling of membranes. Another limitation associated with NF technology is the cost and maintenance of the membranes, which is a disadvantage of all membrane technologies. Nevertheless, due to membrane development and process combination and optimization, membrane technologies have become more efficient and affordable than the conventional treatment technologies due to advantages such as being more compact, efficient, and environmentally friendly.

In recent decades, a thermally-driven membrane technology, membrane distillation (MD), attracts more and more attention and becomes a potential promising desalination process [9-11]. MD process is a combination of a thermal process and a membrane separation process, where a porous hydrophobic membrane is utilized to isolate the hot feed solution and the cold permeate side. The primary advantage of MD is the mild operation conditions related to a relatively low feed temperature compared to distillation, and no hydraulic pressure is to be applied. Therefore, low-grade heat sources (such as solar and geothermal energy) and waste heat from industry can be integrated with MD to heat up the feed streams. Furthermore, MD has a high rejection of nonvolatile matters in the feed solution because evaporation and condensation is the

transport mechanism in the process. In addition, MD is insensitive to the feed solution salinity, which enables it to treat high salinity solutions. Moreover, the compactness and modularity of MD system because of the simplicity of the setup makes it suitable to match the dynamic demands of wastewater (the wastewater volume changes significantly over its lifetime) desalination. The details of MD process will be introduced in the following sections.

1.2 History of membrane distillation

MD started as an application in Bodell's patent [12] entitled "Silicone Rubber Vapor Diffusion in Saline water Distillation" which was proposed in 1963, and further appended in 1968 [13]. In the patent, MD was described as "… apparatus and methods for converting importable aqueous fluids to a potable water", but no information was given about the membranes being used. In 1967, the first related paper was published [14], which illustrated the basic conceptions of MD and several desirable membrane characteristics (such as hydrophobicity, membrane thickness, porosity, and material thermal conductivity). In the same year, Weyl et al. [15] applied for another patent entitled "Recovery of demineralized water from saline waters", in which MD was described as a system to "operate with a minimum external energy requirement and a minimum expenditure of capital and land for the plant". In addition, the details (*i.e.*, air-filled, porous, hydrophobic) of the membranes were given. The performance of a polytetrafluoroethylene (PTFE) membrane with a thickness of 3.175 mm, a pore size of 9 μm, and a porosity of 42% was described. The experimental flux was around 1.89 L/(m^2·h) and 3.78 L/(m^2·h) at a temperature difference of 20.5 °C and 29.8 °C, respectively. However, the interest in MD process declined sharply due to the relatively low flux compared to RO in that time.

In the early 1980s, the MD process recovered interest because of the development of new membrane fabrication technologies. By then, membranes with porosities as high as 80% and thickness as low as 50 μm were prepared, and optimization of the membrane module also decreased the concentration polarization and temperature polarization effect. Furthermore, the advantages of using low-grade energies (such as solar energy,

waste heat, geothermal energy) made MD technology more promising. Several companies made efforts to commercialize the MD process in the 1985s, such as Gore and Associates (USA) [16], Enka (Germany) [17, 18], and Swedish Nationale Development Co. (Sweden) [19]. Unfortunately, the performance and cost of MD process can hardly be compared with the developed RO process. However, because of the diversity and environmental friendliness of MD process, academic research on MD have rapidly increased. From the 1990s, MD has been further studied, including aspects such as the development of heat and mass transfer models, different configurations and membrane modules, more applications, as well as membrane preparation methods. From then on, intensive research was carried out, and a variety of applications was studied, as shown in Figure 1.3.

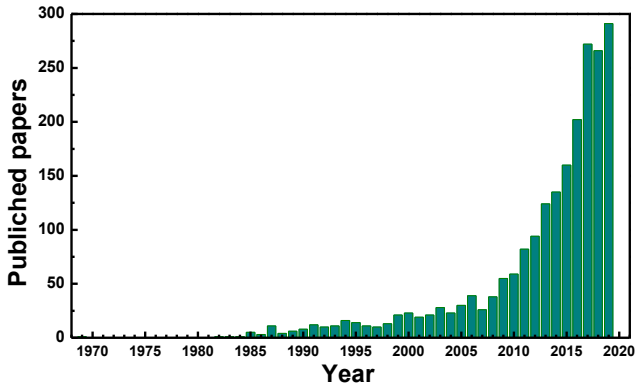


Figure 1.3 Amounts of published papers on MD development from 1963 to 2019 [Data obtained from *web of science*]

1.3 Basic information of MD

At the beginning of MD technology development, different terms were adopted to define this process, such as membrane distillation, capillary distillation, trans membrane distillation, and osmotic distillation. The standard terminology was determined by a committee "Workshop on Membrane Distillation" (Rome, 1986) and later compiled by Smolders and Franken [20]. According to the standard, "membrane distillation" should have the characteristics as following:

(1) The membrane used in MD should be *porous*.

(2) The membrane used in MD should *not be wetted* by the process liquid.

(3) The membrane should *only allow vapor* to pass through the pores.

(4) The membrane cannot change the *vapor-liquid equilibrium* of the different components in the process liquids.

(5) *No capillary condensation* occurs in the membrane pores.

(6) At least *one side* of the membrane should be in direct contact with the process liquid.

(7) For each component, the driving force of this membrane operation is a *partial pressure gradient* in the vapor phase.

1.3.1 Mechanism of membrane distillation

A schematic representation of the MD process is displayed in Figure 1.4. A hydrophobic microporous membrane is utilized as a physical barrier to insulate the high temperature feed solution and the cold permeate side. Due to the temperature difference across the membrane, a partial vapor pressure difference forms, which is the driving force for the MD process. By virtue of the membrane hydrophobicity, a vapor-liquid interface forms at each pore entrance, therefore, only vapor can pass through the pores while liquid and nonvolatile compounds will be rejected and retain in the feed solution. For desalination, only water can evaporate at the feed solution/membrane interface and pass through the membrane. When the vapor arrives the cold permeate side, it will condense to liquid as produced water.

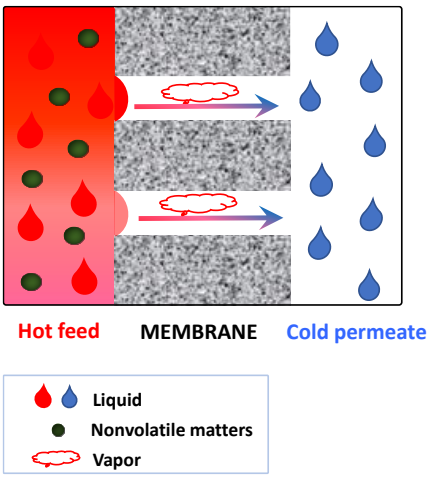


Figure 1.4 Schematic of membrane distillation process

1.3.1.1 Configurations of membrane distillation

Based on different media at the permeate side, membrane distillation has four basic configurations: (1) direct contact membrane distillation (DCMD), (2) air gap membrane distillation (AGMD), (3) vacuum membrane distillation (VMD), and (4) sweep gas membrane distillation (SGMD), as shown in Figure 1.5.

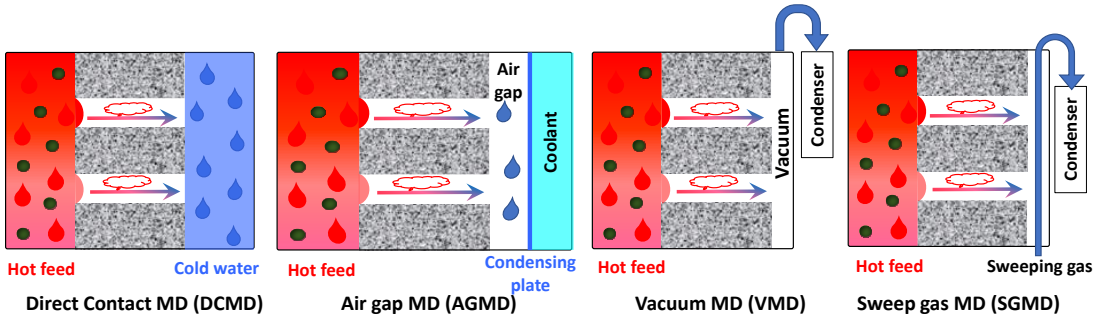


Figure 1.5 Configurations of membrane distillation

DCMD is the simplest and most studied configuration among all the MD configurations (as shown in Figure 1.6), in which a solution at a lower temperature than feed solution is directly in contact with the membrane surface to condense the vapor from the feed side. DCMD is mostly studied in desalination and for applications in the food industry. However, the major deficiency of DCMD is the conductive heat loss across the membrane, because the membrane directly contacts both the hot and cold solutions. Additionally, it is difficult to immediately detect the wetting or leakage because of the mixing of produced water with the cooling water.

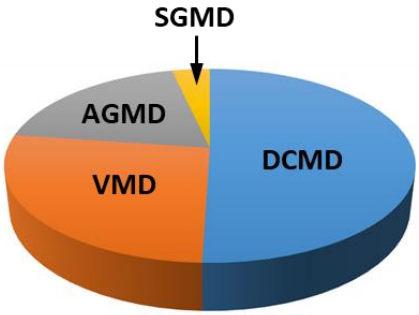


Figure 1.6 Distribution of published papers about different MD configurations

[Data obtained from *web of science*]

AGMD consists of four sections: feed solution, membrane, air gap, and cooling section. The cooling section composed of a cooling plate and coolant that flows on the opposite side of air gap. The vapor pass through the membrane and the air gap, then condense on the cooling plate which are finally drained out. As a result of the additional air gap, the mass transfer resistance is higher than in DCMD, which results in a lower flux. However, the air gap also decreases the heat conduction loss because of the low thermal conductivity of air gap, which increases the thermal efficiency of AGMD. Additionally, as the coolant does not contact with the produced water, other liquid can be used, such as cold feed solution, which can recover the latent heat in the permeate side. The applications of AGMD process are similar than for DCMD, with a particularly interest in desalination. Furthermore, AGMD can be used to remove or separate volatile chemicals (*e.g.*, alcohol) from aqueous solution [21].

In VMD, a vacuum pump is applied to generate a vacuum on the permeate side of the membrane module, and the vapors from the feed side are introduced into an external condenser for condensation. The vacuum is generally lower than the vapor pressure of the volatile matter to create the driving force. The heat conduction loss is negligible in VMD, which can be considered a main advantage. Moreover, the flux of VMD process is usually higher than in other MD configurations due to the higher partial pressure difference. However, a high pressure difference also increases the potential of liquid penetrating, which leads to membrane wetting. Moreover, the additional condenser increases the system complexity and investment. VMD is usually applied to separate volatile aqueous volatile solutions, such as binary aqueous mixtures of ethanol and ammonia removal from aqueous solution [21].

SGMD is a combination of AGMD and DCMD, in which an inert gas is used to carry the vapor from the permeate side to condense outside the module. It has a lower conductive heat loss than DCMD and a lower mass transport resistance than AGMD. However, as a large condenser is applied, the equipment cost and system complexity increases, which also results in a more difficult heat recovery. Therefore, SGMD is the least studied among the four configurations. SGMD has been utilized in desalination, separation of organic solvents from their aqueous mixtures [22], glucose concentration

[23] ammonia removal [21], and concentrate dilute glycerol wastewater [24].

In recent years, several modified MD configurations are developed to improve the energy efficiency and permeate flux, such as vacuum-enhanced DCMD (VE-DCMD) [25, 26], material-gap MD (MGMD) [27], multi-effect MD (MEMD) [28], vacuum-multi-effect MD (V-MEMD) [29, 30], multi-stage MD [31], and osmotic MD (OMD) [32, 33]. In VE-DCMD, the permeate pump is located after the membrane module, which means the permeate solution is pumped out of the module and a vacuum is generated in the permeate side. Thus, a higher flux is attained on account of the increased vapor pressure difference. MGMD refers to filling the air gap in AGMD with another material. For example, Francis et al. [27] measured the MD performance using sand, polyurethane sponge, PP mesh, and DI water in MGMD, and a flux increase of 200-800% was achieved. MEMD is introduced to represent a MD process possessing latent heat recovery. In a hollow fiber (HF)-based MEMD process [28], a low-temperature feed solution flowed through the lumen side of a non-permeable HF, which was then heated to a higher temperature by the vapor evaporated from a porous hollow fiber. After further heated by an external heater, the feed solution flowed into the counter-current porous hollow fiber AGMD module. Therefore, the latent heat of the vapor from AGMD could be recovered by heating the cold feed solution. V-MEMD associates the advantages of MED and VMD to improve the heat recovery, which is composed of a steam raiser, numerous stages, and a condenser, and each stage could reuse the heat from the precedent stage. In MSMD, several modules are placed in a particularly designed position, indicating that the vapor flows through an evaporator and enters the condenser of another module, which can decrease the energy consumption of the system. In OMD process, an osmotic agent solution is utilized at permeate side instead of water, and the generated water activity difference across the membrane induces water evaporation. Therefore, OMD has superiority in concentrating temperature-sensitive solutions, such as in food and pharmaceutic industry [34, 35].

1.3.1.2 Heat transfer in membrane distillation

Heat transfer in membrane distillation consists of four parts (as shown in

Figure 1.7) [11]: (i) heat transfer across the boundary layer from the bulk solution to the membrane surface, which is related to the feed side temperature polarization (TP) effect; (ii) heat transfer via conduction across the membrane, which is deemed as the heat loss in MD; (iii) heat for evaporation; (iv) heat transfer across the boundary layer from the permeate side membrane surface to the permeate bulk solution, which is related to the permeate side TP effect.

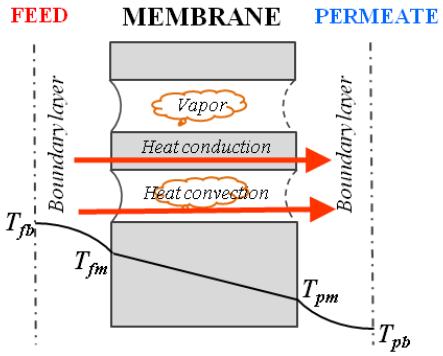


Figure 1.7 Heat transfer in MD module [*Reprinted from [9]*]

(I) Heat transfer across the feed boundary layer

The boundary layer at the membrane surface imposes the heat transfer resistance, which induces a lower temperature gradient between the liquid/membrane interfaces than the bulk solutions and reduces the driving force for mass transfer. Furthermore, the heat transfer across the boundary layer is often the rate controlling step for mass transfer in MD, since a large amount of heat should be supplied for liquid vaporization. Generally, it is agreed that the TP negatively affects the MD flux and might result in up to 80% reduction in driving force [9, 36, 37]. The TP coefficient (TPC) was defined as follows:

$$TPC = \frac{T_{fm} - T_{pm}}{T_{fb} - T_{pb}}$$

where T_{fm}, T_{pm}, T_{fb}, and T_{pb} represent the membrane surface ($_m$) temperature and bulk ($_b$) solution temperature at the feed ($_f$) and permeate ($_p$) side, respectively. As can be seen from Figure 1.7, the feed bulk temperature (T_{fb}) gradually decreases to T_{fm} across the feed boundary layer. However, it should be noted that the boundary layers are related to the fluid properties, operating conditions, and hydrodynamic conditions.

Thus, it is beneficial to operate under optimum mixing conditions to diminish the TP effects by employing high flow velocities, improved flow passage design, a better membrane arrangement, and turbulence promoters such as spacers [11]. Additionally, it was reported that the TP effect aggravates with the feed temperature increasing [36, 38-40].

(II) Heat transfer via conduction across the membrane

The heat transfer by conduction across the membrane represents a heat loss since there is no mass transfer occurs, which should be minimized to enhance the energy efficiency of the MD process. Among the four MD configurations, DCMD has the highest conduction heat loss, while VMD generally has negligible conduction heat loss due to the low vacuum pressure at the permeate side. In general, it is better to use materials with lower thermal conductivity to prepare MD membranes to decrease the conductive heat loss through the membrane matrix. Furthermore, as the thermal conductivity of air (0.022 W/(m·K)) is an order of magnitude lower than the commonly used membrane materials, it will be beneficial to fabricate membranes with a higher porosity. Additionally, thicker membranes are also recommended by most investigators to decrease the conductive heat loss.

(III) Heat transfer for evaporation

Because the MD process depends on the phase change, the quantity of heat that contributes to evaporation is regarded as the efficient heat. The energy efficiency of the MD process can be maximized if the TP effects, internal conduction heat loss, and external heat lost are reduced.

(IV) Heat transfer across the permeate boundary layer

At the permeate side, the membrane surface temperature (T_{pm}) is higher than the bulk temperature (T_{pb}) of the permeate solution due to the TP effect at the permeate side, except for the VMD configuration in which a low vacuum pressure is present at the permeate side. Similar methods with the feed side by optimizing the mixing conditions might also be applied to diminish the TP effect at the permeate side.

1.3.1.3 Mass transfer in MD

The dusty-gas model (DGM), which describes the diffusion through porous media, is generally used to describe the mass transport mechanism in a MD membrane [9, 41, 42]. The volatile components experience three steps during the MD process: (i) transport from the bulk feed solution to the feed/membrane interface; (ii) transport across the membrane pores in the gaseous phase; (iii) transport from the membrane/permeate interface to the bulk permeate phase.

(I) Mass transfer across the feed boundary layer

When the feed solution is pure water, the concentration polarization (CP) effect in the feed boundary layer can be ignored. However, it is impossible for a real MD process. If nonvolatile components exist in the feed solution, the nonvolatile component concentration becomes higher at the membrane surface than the feed bulk solution, as a separation process takes place and water evaporates. The increased solute concentration near the membrane surface not only increases the mass transfer resistance but also increases the possibility that spontaneous wetting occurs at a high or even supersaturation concentration. However, a moderate flow rate and high heat transfer coefficients could reduce the CP impact lower than the TP effect [36]. When another volatile solute is included in the feed solution, such as in the separation or removal of volatile components applications, the concentration boundary layers are made of the solvent (*i.e.*, water) instead of the volatile solute. Thus, the solute concentration decreases across the concentration boundary layer. It should be noted that in this case, the permeate usually consists of both water vapor and the volatile component transport, which alters the process separation efficiency. Therefore, selection of a proper membrane and optimization of operating conditions should be taken into consideration.

(II) Mass transfer across the membrane

There are three mechanisms of mass transport across a membrane: Knudsen-diffusion, Poiseuille-flow, Molecular-diffusion, or combinations acting as transition mechanism. Regardless of which mechanism model is included, the MD molar flux (N)

is always proportional to the vapor pressure difference (ΔP^0) across the membrane according to the following equation:

$$N = K\Delta P^0$$

where K is the membrane distillation coefficient, which is a function of the temperature, pressure, composition within the membrane, and the membrane structure. ΔP^0 is also a complex function of the temperature and compositions at the membrane surface [9]. The Knudsen number (Kn), a ratio of mean free path (λ) of the transported gas molecules through the membrane pores to the mean pore diameter (d) of the membrane, is used to determine the transport mechanism in the membrane pores. However, as the membranes always have pore size distribution instead of a uniform pore size, more than one mechanism may occur in the membrane.

1.3.2 MD membrane characteristics

As a physical barrier, a MD membrane provides a liquid/vapor interface for evaporating and condensing in the MD process, and plays an essential role in the MD process. A good MD membrane should have a low mass transfer resistance to obtain a high permeate flux, a proper liquid entry pressure to keep the membrane pores dry, a high heat transfer resistance to prevent heat loss, and good thermal stability and chemical resistance to maintain the long-term stability when dealing with various feed solutions [9, 11, 43, 44]. The relationship between the membrane characteristic parameters and the permeate flux is given as follow [9]:

$$N \propto \frac{r^a \varepsilon}{\delta_m \tau} \quad (1)$$

where r is the membrane mean pore size, a is the factor 1 or 2 for Knudsen diffusion and viscous flux, respectively, ε is the membrane porosity, δ_m is the membrane thickness, and τ is the membrane tortuosity. Apart from these membrane structure parameters, the membrane hydrophobicity, liquid entry pressure, and membrane thermal conductivity are also significant factors affecting the permeate flux. This section presents the most essential parameters for MD membranes.

1.3.2.1 Hydrophobicity

A membrane for MD should have at least one hydrophobic layer to avoid the liquid permeating in the pores. To improve the membrane anti-wetting and anti-fouling performance and the long-term stability in MD, membranes should have as high hydrophobicity as possible (such as >150° for aqueous solution), as well as high oleophobicity when treating oily feed streams.

The contact angle (CA, θ) of a droplet on a surface is used to determine whether the surface is hydrophilic ($\theta<90°$), hydrophobic ($90°<\theta<150°$), or superhydrophobic ($\theta>150°$). If the CAs of both water and oil on a surface are higher than 150°, the surface can be named as "omniphobic". The CA of a solid surface is given by Young's equation:

$$\cos\theta = \frac{\gamma_{SV}-\gamma_{SL}}{\gamma_{LV}} \quad (2)$$

where γ_{SV}, γ_{SL}, and γ_{LV} refer to the surface tensions at solid-vapor interface, sold-liquid interface, and liquid-vapor interface, respectively, as shown in Figure 1.8. Young's equation is a result of the thermodynamic equilibrium of the free energy at the flat solid-liquid-vapor interface.

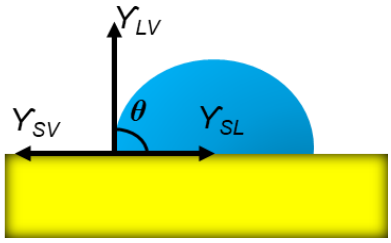


Figure 1.8 Schematic illustration of a droplet on a solid surface

However, the surfaces are not always ideally smooth, and may consist of numerous micro- and nano-scale asperities. In this condition, the CA is normally denoted as the "apparent" CA, since this value does not represent the "real" CA of the corresponding surface, as depicted in Figure 1.9. The droplet on a rough surface can either penetrate the valleys (Wenzel state) [45] or suspend above the asperities (Cassie-Baxter state) [46]. According to the Wenzel state assumption, a roughness enhancement will improve the hydrophilicity of a hydrophilic surface or hydrophobicity of a hydrophobic surface. In contrast, Cassie assumed that air is trapped in the voids, thus the water droplet

contacts not only the solid surface, but also the stranded air. As the air is totally hydrophobic (θ=*180º*), a higher CA can be achieved with less solid-liquid contact, which means a higher roughness.

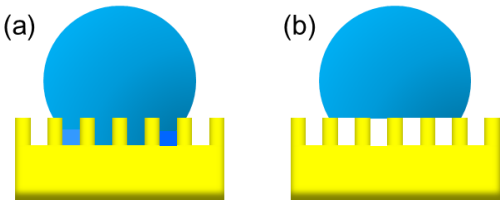


Figure 1.9 Illustration of Wenzel state (a) and Cassie-Baxter state (b)

In addition, inspired by the superhydrophobicity of lotus leaves which are composed of both a micro-/nano- hierarchical structure and a low surface energy wax coating [47-49], it is confirmed that materials with lower surface energy (such as perfluoro agents) and hierarchical roughness can be used to increase the membrane hydrophobicity. Therefore, a low surface energy and a high roughness are two crucial elements to intensify the membrane hydrophobicity.

1.3.2.2 Liquid entry pressure

During the MD process, the operating pressure difference across the membrane should be lower than the liquid entry pressure (LEP) of the membrane in case pore wetting occurs. The LEP value can be estimated by the Laplace equation [50]:

$$\text{LEP} > \Delta P_{interface} = P_{liquid} - P_{vapor} = \frac{-2B\gamma_L cos\theta}{r_{max}} \quad (3)$$

where B is a geometric factor of the membrane pore structure, γ_L is the liquid surface tension, θ is the membrane surface contact angle, and r_{max} is the maximum pore size. However, the Laplace equation should be used only as a model to interpret experimental data as B cannot be measured accurately. From the equation, it can be stated that hydrophobicity increase and maximum pore size decrease are important to improve the LEP. To avoid water penetration under produced pressure in the membrane module, a LEP higher than 2.5 bar for pure water is recommended [44].

1.3.2.3 Pore size

The pore sizes of MD membranes range from several nanometers to a few

micrometers [9, 11]. A larger pore size could lead to a higher MD flux due to the enhanced mass transport process [43]. Nevertheless, the membrane pore size should be controlled to avoid pore wetting under the MD operating conditions, which leads to a conflict with the requirement for a high flux. Therefore, an optimum pore size should be identified according to the feed solution and the operating conditions, and an ideal pore size of 0.3-0.6 μm is reported [44, 82].

1.3.2.4 Porosity

The membrane porosity (ε) is the ratio of the total void volume in a membrane to the total volume of the membrane. It is a significant parameter affecting the flux in MD. A membranes with a higher porosity can decrease the mass transfer resistance, provide more space for vapor to pass through, and exhibit a greater surface area for evaporation. Additionally, porosity is important in terms of reducing the conduction heat loss according to the heat transfer coefficient equation [9]:

$$h_m = \varepsilon h_{mg} + (1 - \varepsilon) h_{ms} \quad (4)$$

where h_m, h_{mg}, and h_{ms} represent the total membrane heat transfer coefficient, the heat transfer coefficient of the gas within the membrane pores, and the heat transfer coefficient of the solid membrane matrix, respectively. Since h_{mg} is generally an order of magnitude smaller than the h_{ms}, the value of h_m can be minimized be maximizing the membrane porosity. Thus, it is commonly understood that a membrane with a higher porosity leads to a higher permeate flux. In general, the MD membrane porosity should lie between 70-90% [11, 43].

1.3.2.5 Tortuosity

Membrane tortuosity refers to the average length of the vapor transport path compared to the membrane thickness. As a longer transport path increases the mass transport resistance, the MD flux is inversely proportional to the membrane tortuosity. Therefore, a membrane with a higher tortuosity shows a lower flux when compared to a membrane with a lower tortuosity while other structural parameters are similar. However, membrane tortuosity cannot be determined experimentally, and is generally

considered to be related to the porosity and pore interconnectivity. Various models have been built in relating the porosity with tortuosity by empirical equations, but no systematic study is performed on the effect of the pore tortuosity on the flux in MD.

1.3.2.6 Thickness

According to Eq. (1), the permeate flux is inversely proportional to the membrane thickness. To increase the MD flux, the membrane should be as thin as possible. Nevertheless, thin membranes will have more heat conduction through the membrane matrix, which leads to a higher heat loss and low thermal efficiency. Hence, there is a trade-off to find a proper thickness to achieve a high flux as well as a high energy efficiency for a MD membrane. Some researchers employed a computer simulation program to estimate the optimum membrane thickness by considering the thermal conductivity of the commercial membranes, and they found that the optimum thickness is within the range of 30-60 μm [51]. However, as the mechanical strength of thin membranes is usually insufficient to apply in the industry, most of the investigated membranes have a thickness higher than this value, or using a non-woven support. According to published results regarding membranes with different thickness but similar pore size and porosity, membranes with higher thickness have lower permeate fluxes due to increased mass transport resistance [52]. Nonetheless, in AGMD configuration, the influence of thickness is negligible, because the predominant mass transfer resistance is the stagnant air in the permeate side.

1.3.2.7 Thermal conductivity

According to the heat transfer mechanism during the MD process, the membrane thermal conductivity should be as low as possible to reduce the conductive heat lose and enhance the thermal efficiency. As most of the hydrophobic polymers have a similar thermal conductivity coefficient while air has a thermal conductivity an order of magnitude smaller than most used membrane materials, it is better to increase the membrane porosity to diminish the overall membrane thermal conductivity. Another possibility to decrease the membrane thermal conductivity is to use bi- or multi-layered

composite membranes with both hydrophobic and hydrophilic layers, as the hydrophilic layer usually possess a relatively lower thermal conductive coefficient, such as polyethersulfone (PES) of 0.13-0.18 W/(m·K), while polytetrafluoroethylene (PTFE) of 0.25-0.27 W/(m·K), polypropylene (PP) of 0.11-0.22 W/(m·K), and polyvinylidene fluoride (PVDF) of 0.17-0.25 W/(m·K). However, it should be mentioned that the hydrophilic layer should not increase the mass transfer resistance significantly.

In summary, an ideal MD membrane should have: (1) omniphobicity to treat various complicated wastewaters, (2) a LEP of pure water higher than 2.5 bar to sustain the pressure difference across the membrane, (3) a pore size of 0.3-0.6 μm to balance a fast vapor transportation and a high LEP, (4) a high porosity of 70%-90% to increase the vapor transport space for a higher flux while reducing the thermal conductivity of the membrane for less conductive heat loss, (5) a low tortuosity to decrease the vapor pass route across the membrane, (6) a polymer layer thickness of 30-60 μm with sufficient mechanical strength or 100-200 μm for composite membrane with support.

1.3.3 MD performance related factors

1.3.3.1 Operating temperature

The influence of the operating temperature on MD flux has been widely studied. The mostly used feed temperatures range from 20 ℃ to 90 ℃ (below the boiling point of the feed solution), and the permeate temperatures ranges from 5 ℃ to 30 ℃ (below the feed temperature) [53-59]. According to the obtained results, an exponential increase of MD flux with feed temperature is achieved for all the MD configurations. This can be explained that the vapor pressure increases exponentially with the feed solution temperature increase, which improves the transmembrane vapor pressure (*i.e.*, the driving force) when all the other involved MD parameters are maintained [43, 60]. In addition, it is reported that a higher feed temperature is beneficial as a higher evaporation efficiency (the ratio of efficient heat transfer to total heat transfer) could be achieved, although the TP effect increases with the feed temperature increases [38-40, 51, 61]. Furthermore, since the inlet temperature of a membrane module is generally

different from the outlet temperature in most of the MD systems, using stirred cells in the feed and permeate chambers could keep the bulk temperature homogeneous.

For the permeate side, a higher permeate temperature decreases the permeate flux, which can be ascribed to the decrease of the transmembrane vapor pressure when the feed temperature is constant. However, the effect of decreasing the permeate temperature is different for different MD configurations. In DCMD, a lower permeate temperature result in a higher flux because of the higher transmembrane vapor pressure [9, 51, 62, 63]. In contrast, the effect is negligible in AGMD, because the heat transfer coefficient in the stagnant air gap dominates the overall heat transfer coefficient, thus the permeate temperature change has little influence [64, 65]. Therefore, it is more efficient to elevate the feed solution temperature rather than to reduce the permeate temperature to obtain a higher MD permeate flux. The situation is similar in SGMD [66]. Additionally, the effect of mean temperature or the temperature difference of the feed and permeate solutions on the permeate flux is also investigated. It is found that if the mean temperature is constant, the permeate flux increases linearly with the temperature difference. In contrary, the flux increases exponentially with the mean temperature if the temperature difference is kept constant [11].

1.3.3.2 Feed concentration

The influence of feed concentration on the flux strongly depends on the separation process itself. When the feed solution only contains nonvolatile components, the most likely effect of the feed concentration increase is decreasing the permeate flux. This is due to the fact that the water partial vapor pressure goes down because of the addition of nonvolatile solutes, which consequently reduces the driving force. Additionally, the aggravated TP and CP effects also result in flux decline. On the other hand, if volatile components (such as alcohols) are included in the feed solution, the effect of an increasing feed concentration on the permeate flux is completely different. This is due to the difference in the thermodynamic properties of the volatile component and its interaction with water. In the general situation, increasing the concentration of volatile solute leads to a higher flux due to the increase of the transmembrane partial pressure.

However, possible pore wetting must be taken into consideration in this case [11, 43].

1.3.3.3 Circulation velocity

Enhancing the feed circulation velocity could increase the heat transfer at the feed side and to decrease the TP and CP effects [11]. Hence, it is better to operate with a higher circulation velocity as well as a higher mixing intensity in the feed solution to form a turbulent regime for a higher permeate flux. According to the results reported in the literature, the response of an increased circulation velocity differed from each other in different configurations and setups. In some cases, the MD flux tends to have an asymptotic value with the feed flow rate increase, while sometimes the MD flux shows a linear increase. However, the influence of the feed circulation velocity on flux in SGMD is different. When only nonvolatile components are included in the feed, the impact is negligible, which may be explained by the small effect of the feed side TP effect [62, 67, 68]. However, if volatile solutes are contained, the selectivity will be directly affected, which means that a higher feed circulation velocity results in a higher process selectivity due to better mixing and lower CP effect [69-72]. The influence of the permeate side circulation rate can only be discussed for DCMD and SGMD. If the permeate fluid is distilled water for DCMD and humid air for SGMD, the velocity affects more significantly in the latter configuration, which can be explained by the different thermal conductivities between water and air. Additionally, in SGMD, as the main TP is located on the permeate side when only nonvolatile components are present in the feed solution [37, 40, 62, 67, 68, 73], the gas flow in the permeate side can be optimized to achieve a higher flux. While if volatile matters are introduced in the feed solution, the increase of the permeate circulation velocity increases the heat transfer at the permeate side by reducing the TP and CP effect.

1.3.4.4 Membrane fouling and wetting

Flux decline in membrane distillation is caused by TP, CP, membrane wetting, and membrane fouling, especially in the long-term operation [74-77]. Membrane fouling refers to the cumulation of undesirable matters on the membrane, which is unfavorable

in the MD process due to the additional heat and mass resistance. Membrane wetting means that the pores are filled with liquid rather than gas, which leads to lower or even reverse flux and an inferior quality of produced water. It is generally assumed that the primary contributor to membrane wetting is fouling. Different membrane wetting degrees are displayed in Figure 1.10: (a) non-wetted, (b) surface-wetted, (c) partially-wetted, and (d) fully-wetted [74]. In a surface-wetted membrane, the liquid/vapor interface moves from the entrance to the inside of the membrane pores, but a gap is still maintained for vapor to pass through. In a partially-wetted membrane, some membrane pores have been filled with liquid, so that the vapor transport path is blocked. A fully-wetted membrane means the feed solution can directly flow through the wetted pores to the permeate side, which is inefficient in MD.

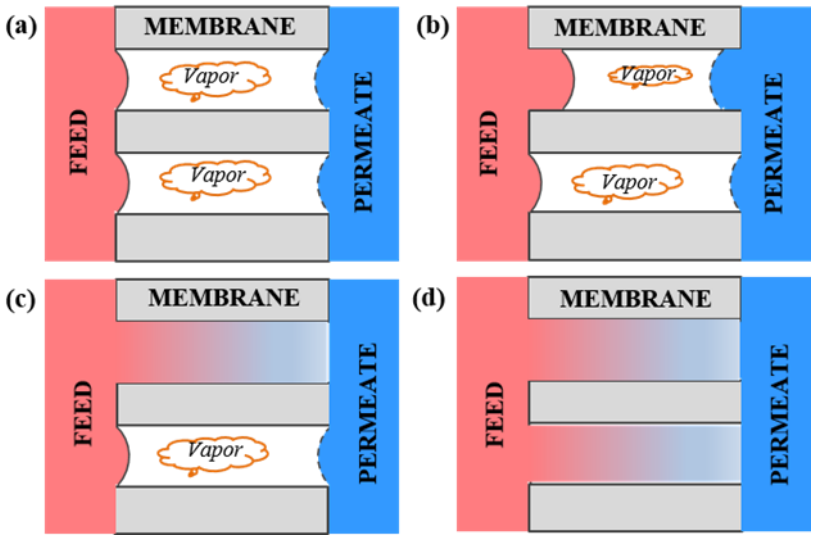


Figure 1.10 Different wetting degrees of a MD membrane: (a) non-wetted, (b) surface-wetted, (c) partially-wetted, and (d) fully-wetted [*Reprinted from [74]*]

Fouling is a complicated process, and the major factors affecting fouling formation conclude: (1) foulant characteristics, such as concentration, molecular size, solubility, diffusivity, hydrophobicity, and charge; (2) membrane surface properties, such as surface energy, roughness, charge, and functional groups; (3) operating conditions, such as temperature and flow rate; (4) feed solution characteristics, such as solution chemistry, pH, ionic strength, and the presence of organic/inorganic matter [78]. According to the different fouling sites, fouling can be categorized as external surface

fouling and pore blocking fouling [79]. The external surface fouling refers to the formation of deposits or cake layers on the feed side membrane surface, which is usually reversible by chemical cleaning. In contrast, pore blocking fouling refers to scaling and deposition inside the pores, which is irreversible in most cases. Fouling in MD can usually be classified into three categories [74]: (1) organic fouling due to the accumulation of organic matters such as humic acid and proteins; (2) inorganic fouling referring to the cumulation of inorganic colloidal particles and hard mineral salts including $CaCO_3$, $CaSO_4$, and silicate; (3) biological fouling because of the organisms such as bacteria and algae. Nonetheless, different kinds of fouling occur simultaneously in most cases, leading to a more complicated situation. Membrane fouling not only decreases the MD permeate performance, but also increases the costs including cleaning, energy depletion, setup maintenance, membrane replacement, and extra personnel costs [74, 80]. Plenty of efforts have been carried out to diminish fouling, and the frequently used techniques are novel membranes with special designs or materials, new membrane modules design, feed solution pretreatment, and membrane cleaning [43].

1.3.5 Advantages and limitations of membrane distillation

MD technology has been recognized as a promising desalination process, which can be attributed to several ***advantages*** over conventional thermal and membrane processes [7, 9, 43, 60]. Firstly, hydrophobic, microporous membranes serve as the vapor-liquid interface in MD process, while traditional distillation depends on high vapor velocities to generate an intimate vapor-liquid contact. Therefore, the MD equipment is much smaller than equipment in thermal distillation, which reduces the investment cost. Secondly, the compactness and modularity of MD desalination system resulting from the simplicity of the MD system is advantageous in small-scale and off-grid water treatment applications. In addition, MD systems are suited to match the dynamic demands of wastewater desalination (the wastewater volume changes significantly over its lifetime) because of its modularity and scalability. Thirdly, the relatively low operating temperature and small equipment surface area lead to less

thermal losses to the environment. Furthermore, when low-grade thermal energy and waste heat is available as heating source, the process investment can be reduced in an efficient way. Additionally, a lower operating temperature gives MD technology opportunities in the food industry and in the medical field. Fourthly, the operating pressure of MD process is relatively low compared to the pressure-driven membrane processes such as RO, which results in a lower equipment cost and increased process safety. Furthermore, the mechanical demands on the MD membranes are greatly reduced because there is no external pressure or a low pressure. Fifthly, the rejection of nonvolatile compounds (such as ions, macromolecules, colloids) can reach 100% as only vapor can pass through the membrane. Sixthly, the MD process is less sensitive to the feed solution salinity as it is a phase-change based process; thus, MD can treat hypersaline wastewaters compared to RO process which has a salinity limitation of ~80 g/L. MD membranes with large pores are also less prone to fouling because the process does not require hydraulic pressure. Lastly, MD shows a relatively low areal footprint and is greatly modular because of the facile, low-cost, and lightweight MD equipment.

Despite all the benefits offered by MD, it has not yet been fully industrialized due to several ***disadvantages***. Firstly, as phase change occurs during the MD separation process, the thermal efficiency is relatively low compared to the liquid phase-based membrane processes such as RO. Additionally, the heat recovery from the produced vapors is difficult than the traditional thermal processes such as MED and MSF. Therefore, the energy efficiency and heat recovery should be improved by improving the module and system design. Secondly, the relatively low flux of MD process compared to other separation techniques (such as RO) is a limitation for application. Thirdly, a specialized commercial MD membrane with high flux and stable anti-wetting performance is still on its way. The membrane preparation methods in a lab-scale are usually expensive or time-consuming, which is difficult to scale up. Fourthly, flux decline and product purity caused by membrane fouling and wetting need to be solved. Last but not the least, the gap between a lab-scale MD system to an industrial system should be investigated.

1.4 Fabrication of MD membranes

As a physical barrier to separate the hot feed solution and cold permeate side, while providing the space for vapor transport and rejecting nonvolatile matters, the membrane is essential to ensure a high MD performance in terms of flux, rejection, and anti-wetting properties.

The most investigated MD membranes can be classified into four categories [7]: hydrophobic membranes, superhydrophobic membranes, Janus membranes, and omniphobic membranes, as shown in Figure 1.11. The hydrophobic membranes are the most basic MD membranes with CA ranging from 90° to 150°, which can meet the basic demand as a MD membrane and deal with saline wastewaters with only inorganic compounds. In general, superhydrophobic membranes have a water CA higher than 150° and a sliding angle (SA) lower than 10°. These membranes usually have better anti-fouling property and stability than normal hydrophobic membranes when other parameters are similar. However, the anti-wetting performance of the superhydrophobic membranes may deteriorate if low surface tension substances exist in the feed solution. The Janus membrane refers to a composite membrane that integrates a hydrophobic layer with a hydrophilic layer. A distinct advantage of introducing a hydrophilic layer atop the hydrophobic membrane is to repel oily pollutants in the feed solution. In contrast, the Janus membranes with a hydrophobic surface and a hydrophilic matrix is advantageous to reduce the vapor transport path and increase the flux. Omniphobic membranes have CAs of the membrane surface above 150°, not only for water, but also for oily wastewater and solutions containing low surface energy components. Therefore, the preparation of omniphobic membranes is a research hotspot in the MD area because of the superior anti-wetting property, higher flux, stability, and various potential applications.

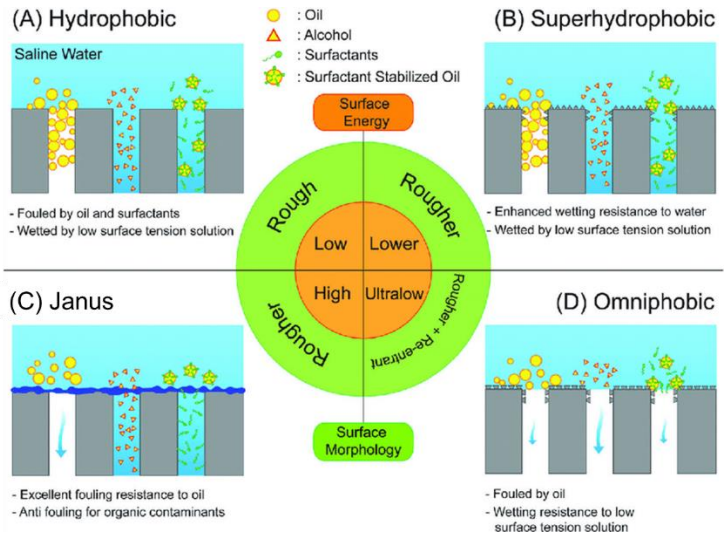


Figure 1.11 Different types of MD membrane: (A) hydrophobic, (B) superhydrophobic, (C) Janus (hydrophilic/hydrophobic), and (D) omniphobic *[7]*

The currently used commercial MD membranes are mostly microfiltration (MF) membranes which are made of polymers such as polytetrafluoroethylene (PTFE), polypropylene (PP), polyethylene (PE), or polyvinylidene fluoride (PVDF). Although these MF membranes can meet the basic need for MD membranes with a hydrophobic surface and proper pore size of 0.2-0.4 μm, there are several unsuitable properties. For instance, as the MF membranes need to withstand a relatively high pressure, the membrane thickness is usually greater than the optimal thickness of MD membranes. Additionally, although the membrane hydrophobicity is moderate which can deal with normal saline feed solutions, it is not high enough to treat complicated wastewaters in MD, especially for the oily feed solutions exhibiting low surface tensions. Moreover, a low thermal conductivity is required for MD membrane to reduce the conductive heat loss, which is not considered for the MF membranes. Therefore, special-designed MD membranes are needed to improve the MD performance.

Various efforts have been made to fabricate MD membranes by nonsolvent-induced phase separation (NIPS) [85-90], thermally-induced phase separation (TIPS) [213-216], electrospinning (ES) [91-95], and strecthing [52, 121, 122, 217, 218]. Among these technologies, NIPS and ES are most used for dedicated membranes because of its controllability and customization of the membrane structures, however,

the currently used commercial membranes are usually PTFE, PP, and PE membranes fabricated by stretching. Due to the inherent hydrophobicity of these polymers, as well as the porous structures generated during the stretching process, these commercial membranes show relatively high hydrophobicity (CA of 130°-140°), reasonable pore sizes of 0.2-0.8 μm, and high porosities of 80%-90% [217]. However, there are several limitations of this kind of membranes, such as the expensive materials, difficulty to synthesize thicker membranes, sensitive to compaction, and transformation due to the elasticity. Currently, the most investigated polymer for MD membrane in academic area is PVDF due to its several advantages over the PTFE membranes. Firstly, PVDF material is cheaper than PTFE. Secondly, PVDF can be easily dissolved in various organic solvents, thus can be prepared by different methods including NIPS, TIPS, and ES to obtain desired structures. In contrast, PTFE is hardly soluble in any solvent at room temperature [175]. In addition, due to its high melting point (327 °C) and high viscosity over its melting point [219], PTFE membrane can hardly be prepared in a melting-stretching [218]. PTFE membranes generally are fabricated through a cold stretching process including mixing with lubricant, extrusion, stretching, and sintering; thus, a high temperature is always needed in the preparation process, and the prepared membrane structure is limited. Thirdly, the structure of PVDF membranes can be tuned in a facile way by altering the dope solution composition or the preparation process (such as the coagulation bath composition and temperature in NIPS, and operating voltage, needle to support distance, chamber humidity and temperature in ES) in one step. Fourthly, it is challenging to prepare PTFE membranes with controllable thickness and pore size in the stretching process, while these parameters can be controlled easily for PVDF membranes during the NIPS and ES preparation process. However, as the hydrophobicity and pore structure of PVDF membranes prepared by single NIPS or ES technology is not optimal for MD applications in most cases, modifications are frequently employed to optimize the membrane structure, morphology, or surface chemistry. The generally used modification methods comprise blending [87, 89, 91, 93, 96-103], coating [104-110], grafting [111, 112], chemical vapor deposition (CVD) [113, 114], CF_4 plasma [53, 54, 115, 116], and nanoimprinting [117-120]. The typical

membrane fabrication methods and modification methods are summarized in this section.

1.4.1 Membranes prepared by NIPS

NIPS is one of the mostly applied approaches to fabricate polymeric membranes for separation processes. During this process, a nonsolvent of the polymer is introduced to a homogeneous polymer/solvent system to demix the solution into a polymer-rich phase and a polymer-poor phase [123]. The former phase turns into the membrane matrix and the latter phase forms the membrane pores after precipitation of the solution. There are two typical membrane structures formed by NIPS, which are sponge-like and finger-like, as shown in Figure 1.12. In general, a fast solvent/nonsolvent exchange leads to a finger-like morphology, while a slow exchange forms the sponge-like morphology. The macro-voids in the finger-like structure are considered undesirable because of the weak integrity of the membrane. However, the structure of macro-voids might be useful in right portions due to the spacious space for vapor transport. Furthermore, as the hydrophobicity of the membranes prepared by NIPS is not always high enough for MD, various modification methods have been employed to optimize the membrane morphology and hydrophobicity.

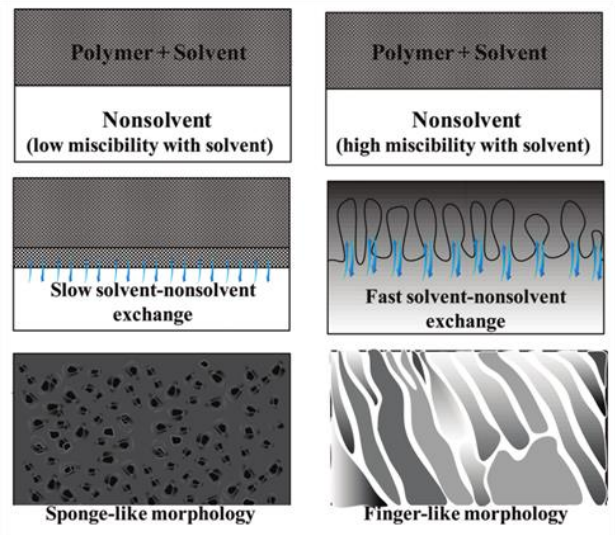


Figure 1.12 Different membrane morphologies formed by NIPS method according to different solvent/nonsolvent exchange rates *[123]*

1.4.1.1 Blending

A polymer solution usually consists of polymer and solvent, and sometimes additives. The commonly used solvents are dimethylsulfoxide (DMSO), dimethylformamide (DMF), dimethylacetamide (DMAc), N-methylpyrrolidone (NMP), while water is the commonly used nonsolvent. Early studies focus on investigating the influence of various solvent and small molecules (such as polyethylene glycol (PEG), polyvinyl pyrrolidone (PVP), acetone, LiCl, H_2O) as additives on membrane morphology and pore structures using water as coagulation bath. Khayet et al. [86] employed PEG as additive to prepare flat-sheet PVDF-co-hexafluoropropylene (PVDF-HFP) membranes, and investigated the role of the PVDF and PEG concentration, evaporation time, and coagulation bath temperature in the membrane structure and DCMD performance. The results demonstrated that the enhancement of the polymer concentration, the coagulation bath temperature and the evaporation time could result in the increased salt rejection yet declined permeate flux; however, the increase of the PEG concentration has an inverse effect: increasing the pore forming agent concentration could induce more space and increase the flux. Simone et al. [97] fabricated PVDF HF membranes assisted by the addition of hydrophilic PVP additive for VMD, and explored the role of the PVP concentration as well as the bore fluid (the coagulation reagent for the lumen side) composition in the HF structure and MD performance. The addition of small amounts of PVP induces the generation of large finger-like macro-voids, increases the membrane porosity, but reduces the strength. However, a higher PVP concentration leads to forming sponge-like structures and improves the mechanical strength, yet slightly reduces the porosity. Hou et al. [124] fabricated a series of flat-sheet PVDF membranes to investigate the effects of solvent (DMF, DMAc, DMSO, NMP), polymer concentration, additives (acetone, H_3PO_4, glycerin, LiCl, PEG400) and nonwoven fabric on the membrane physicochemical properties and DCMD performance. The results showed that DMAc was a suitable solvent adopted to attain a high permeability, and 20 wt.% PVDF was optimal to design a hydrophobic membrane. Among these additives, a mixture of 5 wt.% acetone 3 wt. %

H_3PO_4 evinced the highest permeate flux. Comparing the membranes prepared with and without nonwoven substrate, the pore size of PVDF/nonwoven composite membranes was enhanced as the nonwoven fabric can prevent membrane shrinkage.

Furthermore, blending surface modifying macromolecules (SMMs) in the polymer solution to alter the surface hydrophobicity and fabricate hydrophobic/hydrophilic composite membranes were also explored. Khayet et al. [96] incorporated fluorinated SMMs into hydrophilic base polymer polyetherimide (PEI) to prepare hydrophobic/hydrophilic membranes. During the casting and precipitation steps, the SMMs migrated to the air/polymer interface, which reduced the surface energy of the hydrophilic PEI to values close to that of PTFE. Consequently, the composite membrane containing an ultrathin hydrophobic layer atop a hydrophilic sub-layer were obtained. This type of membrane combines a low mass transport resistance due to the decline of the water vapor transport distance across hydrophobic skin layer and the decrease of heat conduction loss through the thicker hydrophilic sub-layer, which seems to be promising in MD membranes. Qtaishat et al. [58] synthesized three types of SMMs with different fluorine content, molecular weight, and glass transition temperature, and blended them with polysulfone (PSf) to prepare membranes by NIPS. It was found that the stoichiometric ratio and the SMM categories played a significant role in the membrane physicochemical properties and permeate flux. Among these three different SMMs blended membranes, the prepared membrane with SMMs possessing a higher fluorine content showed a higher MD flux but a lower LEP because of the larger pore size. The effect of solvent was also investigated using NMP and DMAc, but in contrast with the previous example, NMP was more suitable for SMMs blended PS membranes. Some of the prepared membranes even achieve better DCMD fluxes than commercial PTFE membranes, which indicates the promising application of SMMs blended membranes in DCMD.

With the development of nanomaterials in this decade, various inorganic nanoparticles (NPs), such as SiO_2, multi-walled carbon nanotubes (MWCNTs), graphene, graphene oxide (GO), are studied to improve the membrane structure or surface chemistry by adding them into the polymer solution. Hou et al. [87] introduced

hydrophobic $CaCO_3$ NPs into PVDF/DMAc/PEG/LiCl solution, and cast membranes on hydrophilic PET nonwoven substrate. The results demonstrated that the introduction of NPs increased the surface roughness, improved the pore size and porosity, and narrowed the pore size distribution. The obtained maximum flux was 49.37 kg/(m^2·h) using 35 g/L NaCl as feed solution with feed and permeate temperature at 83 °C and 20 °C, respectively. In addition, the performance stability in a 300 h test indicated the higher stability of the nano-$CaCO_3$ composite membrane compared with the virgin membrane. Efome et al. [99] investigated the influence of superhydrophobic SiO_2 NPs in PVDF membranes on the VMD performance. It was reported that the NPs enhanced the membrane performance through decreasing the thickness of sponge-like layer and enhancing the surface pore size, resulting in an elevated vapor flux. However, the sponge-like structure became dominant and the flux decreased when the SiO_2 concentration was above 7 wt.%. Graphene, an allotrope with carbon which has a high hydrophobicity, fast vapor transport, and superior thermal stability, was added in PVDF solution to fabricate membranes for AGMD to deal with real RO brine [89]. The graphene loading mass of 0.5 wt. % endowed the modified PVDF membranes with an applicable pore size (0.11 μm), suitable porosity (85%), high LEP (3.89 bar), and thus superior flux of 20.5 L/(m^2·h) (*i.e.*, LMH) at feed and coolant inlet temperature of 60 °C and 20 °C, respectively. Furthermore, GO and modified GO were used as additives as well. Lu et al. [125] prepared flat-sheet and hollow fiber PVDF membranes using n-butylamine modified GO (GO-NBA) to increase the mechanical strength and anti-wetting properties. In this work, they found that GO-NBA blended membranes showed better mechanical properties than the conventional GO blended membranes, which could be ascribed to the better compatibility, dispersity, and crystalline structure. Leaper et al. [101] functionalized GO with 3-(aminopropyl) triethoxysilane (APTS) and added the unmodified GO and GO-APTS into PVDF solutions to prepare membranes for AGMD. The permeate flux of the GO and GO-APTS modified membranes was enhanced by 52% and 86%, respectively, compared to the neat membrane. It was speculated that the improvements mainly originated from the enhanced surface porosity, enlarged pore size, and the possibly favorable water-nanofiller interactions. However,

further investigation still needs to be carried out to verify the specific interactions between water and GO embedded inside the polymer matrix.

Fluorine-containing organic polymers can also be adopted to elevate the surface hydrophobicity and optimizing the MD performance. Teoh et al. [59] incorporated PTFE particles in PVDF polymer solution to prepare single-layer and dual-layer PVDF/PTFE composite HF membranes for DCMD. The addition of PTFE particles efficiently enhanced the outer surface hydrophobicity for both kinds of HF membranes. Nevertheless, the dual-layer membranes have a higher flux than single-layer membranes, which may contribute to the reduction of the inner-layer mass transport resistance. Polydimethylsiloxane (PDMS) was also employed to modify PVDF membranes by blending instead of conventional surface coating [126]. As PVDF and PDMS can hardly dissolve in the same solvent, PVDF was dissolved in the mixed solvent of triethyl phosphate (TEP) and DMAc, while PDMS was dissolved in tetrahydrofuran (THF), followed by mixing of these two solutions. The results indicated that the finger-like structure was gradually replaced by the sponge-like structure because of the addition of PDMS. Furthermore, the membrane porosity, CA, and mean pore size increased, which led to a higher VMD flux until the PDMS: PVDF mass ratio increased to 1:5, and further increase of PDMS resulted in a reverse effect.

In general, blending is a simple method to adjust and modify membrane pore structure and characteristics. However, the homogeneous dispersion of additives (especially the NPs) in membrane matrix could not be totally controlled during the phase separation process, which might result in agglomeration and defects in the membrane structures. In addition, a large amount of the additives should be used to achieve its efficacy by locating in the overall membrane matrix, which increase the cost. Hence, plenty of other modifications methods are proposed by lots of insightful researchers to seek more possibilities to fabricate high-performance membranes for MD.

1.4.1.2 Surface modification

A high membrane surface hydrophobicity could lead to a high LEP value as well as a better anti-wetting property and a higher fouling resistance. Generally, a high

surface roughness and a low surface energy conduce to a high hydrophobicity, as mentioned in section 1.3.2.1. Therefore, diverse surface modification methods consisting of surface coating, nanoimprinting, grafting, and CF_4 plasma modification have been studied to enhance the membrane hydrophobicity.

Coating refers to the introduction of another layer on the membrane surface to increase the surface roughness, and the most used material is NPs. Zhang et al. [127] sprayed hydrophobic SiO_2 NPs on PVDF flat-sheet membranes to fabricate superhydrophobic membranes. After surface coating, the CA and LEP increased from 107° to 156° and 210 kPa to 275 kPa, respectively, while the pore size and porosity were almost unchanged. It was stated that the SiO_2 NPs mainly distributed on the top thin surface layer, resulting in a lower DCMD flux because of enhanced mass transport resistance compared to the neat PVDF membrane; but the SiO_2 modified membranes exhibited a higher rejection and a better anti-wetting performance. A similar study to modify PVDF membranes by depositing SiO_2 NPs on the surface and grafting 1H, 1H, 2H, 2H-perfluorooctyltrichlorosilane (PFOTS) was carried out by Li et al. [105]. The same observations that there is no influence on the membrane structure, a lower flux but better stability compared with virgin PVDF membrane were made. Fluorographite, a commercialized highly hydrophobic microcrystalline powder, was applied as the coating material to improve the hydrophobicity of PVDF HF membranes [128]. Unlike the previous studies, the fluorographite coating layer decreased the pore size and porosity slightly, but the flux decline is not significant. Furthermore, thus-obtained PVDF membranes displayed better anti-wetting properties during a 200 h DCMD desalination test due to the increased surface hydrophobicity.

Besides NPs, polymer particles can be used as coating materials to enhance the top surface roughness as well. Yan et al. [129] developed a modification method using etched PVDF particles in an ultrafiltration coating process. PVDF particles were etched in a mixture of DMAc and anhydrous ethanol with different volume ratio, which was followed by coating the etching suspension onto the surface of the PVDF membranes. Benefiting from the coarse surface of the etched PVDF particles (Figure 1.13), a hierarchical structure was assembled on the surface, leading to an extremely high CA

of 163.8°. Furthermore, the resulting membranes displayed a higher water flux of 29.9 kg/(m^2·h) than that of original membrane (26.0 kg/(m^2·h)) at a temperature difference of 60 °C, as well as an outstanding anti-wetting property. Additionally, Efome et al. [104] introduced thin PVDF nanofiber layers on flat-sheet PVDF membranes to enhance the hydrophobicity. The CA increased by 76% from 79° to 139°, and the LEP increased by 57% from 241 kPa to 379 kPa. In both VMD and DCMD desalination tests, the modified membranes evinced higher fluxes and a more stable rejection than the pristine membrane.

In summary, coating is an effective approach to enhance the surface hydrophobicity by improving the surface roughness, elevate the LEP value, and improve the anti-wetting and anti-fouling properties. However, as an additional layer is introduced on the surface, the coated membranes generally have a lower flux than the virgin membranes due to the increased mass transport resistance. In addition, the adhesion between the coating layer and the support membrane should be considered to maintain its stability and efficiency.

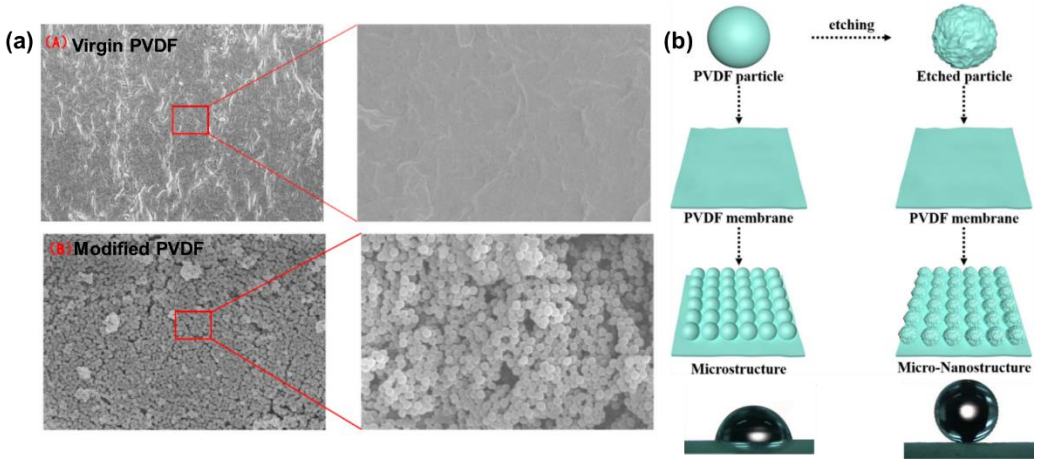


Figure 1.13 (a) SEM images of outer surfaces of the virgin and modified PVDF membranes; (b) schematic diagram of construction of micro-/nano- structure by coating etched PVDF particles on the membrane surface *[129]*

Nanoimprinting, a simple and versatile nanofabrication technique, which can manufacture structures from micro- to nano-scale on a material surface, is applied to fabricate a patterned surface morphology to increase the surface hydrophobicity by roughening the membrane surface. Zhao et al. [117] constructed hierarchical textures

on a PVDF membrane surface via nanoimprinting using a stainless-steel mesh (SSM) and its negatively PDMS template as fabrication substrates, as exhibited in Figure 1.14. The obtained PDMS-based PVDF membrane showed a plaited pattern on the membrane surface which was the same with the SSM, thus leading to a high CA of 153° yet a high SA of >90°, which can be called "petal surface". In contrast, the SSM-based PVDF membrane had a CA of 164° and a low SA of 6.8°, which can be called a "lotus leaf surface". Both the PDMS-based and SSM-based PVDF membranes had higher DCMD fluxes ascribed to the excellent hydrophobicity and enlarged pore size. However, the PDMS-based membrane showed a declined salt rejection during a long-term experiment, which might be attributed to the strong adhesion of the petal-type surface morphology.

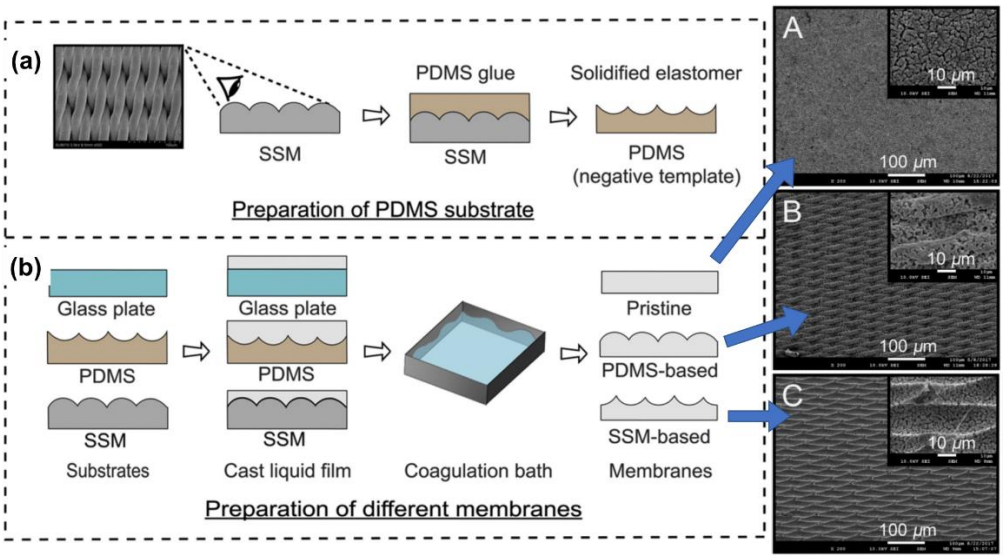


Figure 1.14 (a) Schematic protocol of preparation the PDMS substrate; (b) preparation and the SEM morphologies of the pristine, PDMS-based, and SSM-based membranes *[117]*

Similarly, Xiao et al. [118] used a lab-made silicon wafer mold with a micro-pillar (MP) array as template to prepare superhydrophobic PVDF membranes, as depicted in Figure 1.15. The obtained MP-PVDF exhibited a static CA of 166° and a SA of 15.8°. A further CF_4 plasma modification endowed the CF_4-MP-PVDF membranes with an ultrahigh CA of 175.6° and a declined SA of 3.0°. During the concentrating process of a 25 wt.% NaCl solution by DCMD, the CF_4-MP-PVDF membrane showed a superior

anti-scaling property due to the slippery surface, as shown in Figure 1.15 (d). Additionally, a superomniphobic (SOM) PVDF membrane was prepared by combination of macro-corrugation from phase separation followed by imprinting and fluorinated SiO_2 NPs coating [119]. The obtained membrane surface had remarkable anti-wetting properties repelling not only water (CA of 160.8°) but also the solutions with low surface tension (CA of 154.3°). The calculations in the study revealed that most of the water droplets were contacting with the stagnant air trapped between the neighbor SiO_2 NPs, resulting in high water repellency and self-cleaning property.

Generally, nanoimprinting can efficiently render the membrane surface macro- or nano-type surface texture to increase the membrane roughness as well as the hydrophobicity, which usually leads to a higher flux and excellent anti-wetting property. However, an initial template should be chosen carefully, and the post-modification maybe needed, which will increase the process complexity.

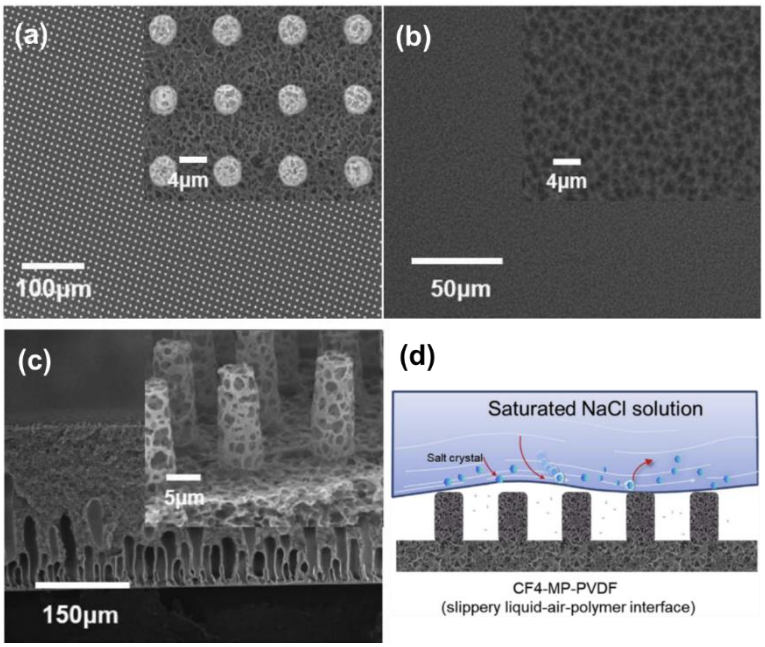


Figure 1.15 Morphologies of (a) top, (b) cross-section, (c) bottom surface of the prepared MP-PVDF membrane, and (d) schematic of the slippery interface for CF4-MP-PVDF membrane *[118]*

Grafting can be considered one of the best techniques to improve the surface hydrophobicity by reducing the surface energy. As grafting is mainly based on covalent

connection between the membrane surface and the applied chemicals, the chemical stability of the prepared membrane is superior to the membranes prepared by any physical coating process. Furthermore, grafting can be used for either hydrophilic or hydrophobic membranes. For example, a flat-sheet hydrophilic PES membrane was treated with tetraethyl orthosilicate (TEOS) and trimethylchlorosilane (TMSCI) as grafting agents to improve the membrane hydrophobicity [112]. The affecting parameters on the treatment procedure such as TMSCI to TEOS ratio, heating temperature, and heating time were explored, and the results demonstrated that all these parameters had a positive relationship with the contact angle. Moreover, the prepared membranes showed a comparable flux, stability, and rejection to a commercial PTFE membrane in the DCMD test. CF_4 plasma modification is another method to enhance the hydrophobicity without sacrificing the porosity of the membrane matrix. The created super-thin layer is achieved by monomer polymerization in a vacuum environment during the plasma polymerization procedure. Wei et al. [53] described the utilization of CF_4 plasma to transform a hydrophilic PES membrane to hydrophobic one for DCMD. The CA increased from 0° for the virgin PES membrane to 120° after the plasma modification, which can be ascribed to the fluorination via insertion and possibly deposition during the plasma process. The modified membrane exhibited a relatively high flux of 45.4 kg/(m^2·h) at a temperature difference of 40 °C using 4 wt.% NaCl as feed solution and the permeate solution conductivity continuously decreased for 54 h, indicating a successful hydrophobic modification by plasma treatment and a stable anti-wetting performance. Furthermore, CF_4 plasma modification could convert a hydrophobic PVDF membrane to a superhydrophobic membrane [116]. The DCMD flux of the superhydrophobic PVDF membrane was 30% higher than the virgin membrane due to the increase of the effective evaporation area.

The greatest advantage of grafting and CF_4 plasma modification is that the membrane structure can be maintained while decreasing the surface energy and increasing the surface hydrophobicity. Nonetheless, it is usually combined with other modifications that could roughen the surface, as both a high roughness and a low surface energy play significant roles in enhancing membrane surface hydrophobicity

and oleophobicity. However, the most used grafting agents are fluorosilanes, which are toxic and harmful to the environment, making it unpractical for a large-scale application. Meanwhile, the CF_4 plasma modification is also limited as a special equipment is required, which increases the investment. Additionally, plasma modification is system-dependent, which means that an optimal modification process should be established for each membrane with different gas, pressure, power input, and discharge time. Besides, it also faces technical challenges to scale up to a continuous process.

1.4.1.3 Tuning the precipitation process

As the solvent/nonsolvent exchange rate plays an important role in deciding the membrane morphology during the phase separation process, adjusting the solvent or nonsolvent is another efficient way to improve the membrane structure. Nejati et al. [130] employed TEP as solvent and the mixture of 2-proponal and water as nonsolvent to fabricate PVDF membranes. The obtained membrane showed an asymmetric cross-section with a relatively dense skin showing a highly fibrillated structure and an interconnected globular structure in the remainder of the membrane, as shown in Figure 1.16. It was concluded that when the propanol concentration in the coagulation bath increased, the membrane surface developed to a more open surface with reduced fiber-like structure, which is attributed to the delayed solidification of the top layer caused by the decrease of the Hansen solubility parameter of the nonsolvent-polymer system. The MD performance by using different membrane orientation demonstrated that the flux is higher when the dense surface faced the hot feed solution due to the higher vapor pressure difference and a better anti-wetting performance.

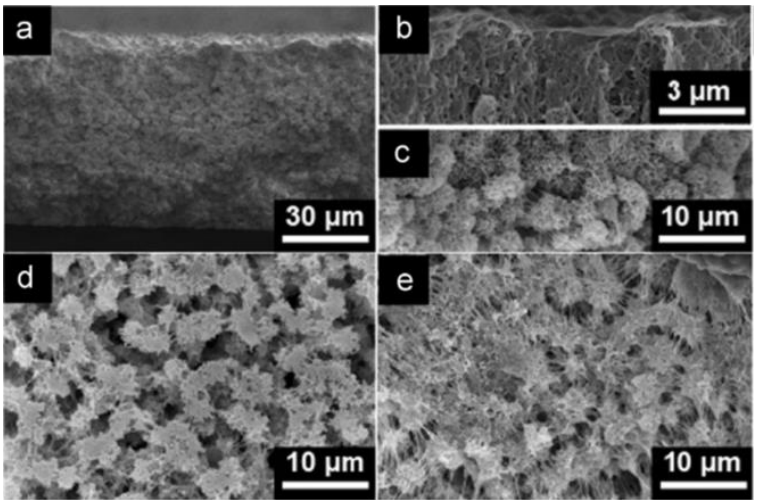


Figure 1.16 SEM images of (a)-(c) cross sections, (d) bottom surface, and (e) top surface of the prepared PVDF membrane *[130]*

Zheng et al. [131] developed PVDF-CTFE hydrophobic membranes by a two-stage phase separation process: the nascent polymer solution film was first placed in an oven for a certain time, followed by immersing into a water bath. According to the results, the exposure stage contributed to the solid-liquid demixing process because of the solvent evaporation. Therefore, a nanofibrous surface and interconnected structure was obtained, as shown in Figure 1.17, which led to a higher hydrophobicity and a better DCMD performance. Another modified dual-bath coagulation process was proposed to prepare hydrophilic skinless PSf membranes followed by CF_4 plasma modification for DCMD [54]. The nascent films were immersed into a mixture of solvent (*i.e.*, NMP) and water with different volume ratio before the water bath. The obtained results indicated that the membranes prepared using the NMP/water mixture as coagulation bath could promote the formation of an open porous surface when the NMP ratio exceeded 50%. The as-prepared membrane utilizing pure NMP as the first bath showed a high CA of 144° and a DCMD flux of 53.33 LMH using a 4 wt.% NaCl solution as feed at feed and permeate temperatures of 70.3 °C and 20 °C, respectively.

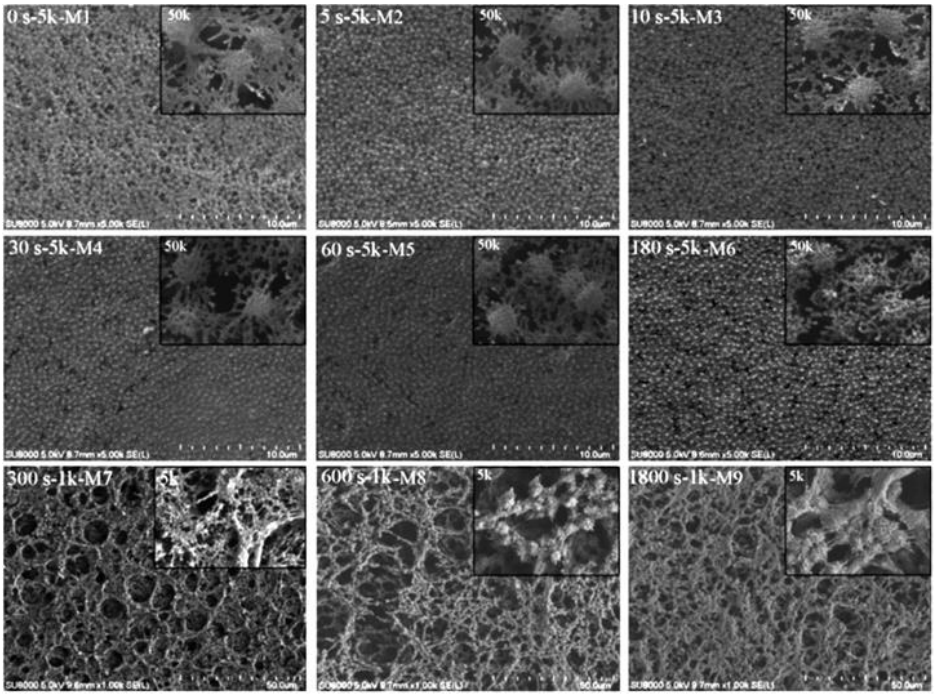


Figure 1.17 SEM images of the membrane surface with different exposure time *[131]*

Compared to the usage of nanomaterials and perfluorosilane hydrophobic agents which might threaten the produced water and environment safety, as well as the increased cost and procedure complexity, optimization of membrane structure by tuning the precipitation process is simple and efficient. However, using solvent and alcohols as coagulation bath increase the cost and wastewater discharge as well. Moreover, precise control of the preparation process is required to maintain the reproduction of the desired structures.

1.4.2 Membranes prepared by electrospinning

Electrospinning is a method of producing nanofibers, in which high electric forces are utilized to draw charged threads of polymer solution or melt up to nanofibers. Recently, electrospinning technology has been broadly investigated to fabricate MD membranes; this is because that the electrospun nanofiber membranes (ENMs) have the advantages of superior porosity, high surface area to volume ratio, and controllable pore size [132-134]. In addition, the optimization of membrane structures can be attained by tuning the polymer concentration, ambient conditions, and other electrospinning related parameters. Given the suitable surface structure and hydrophobicity of ENMs,

increasing attempts have been devoted to optimize the membrane characteristics for the enhancement of MD efficiency. ENMs can be functionalized either by incorporating functional nanofillers to the polymer solution (*i.e.*, mixing) [93, 94, 103, 135-137] to yield nanofiber membranes that contain the fillers inside, or through post-modification (such as coating, CVD, and grafting) to introduce the functional materials to the nanofiber surface [107, 108, 110, 111, 114, 115, 138, 139].

1.4.2.1 Blending

Benefitting from the nano-scale fiber size, blending NPs in the dope solution is an efficient method to impart the fiber surface protuberance and increase the roughness. Various studies show that a homogeneous NP distribution within a nanofiber is of crucial importance for the improvement of MD performance. Lilia et al. [91] constructed reinforced PVDF-HFP ENMs by incorporating nanocrystalline cellulose (NCC) for DCMD. It was reported that the introduced NCC enhanced the viscosity of spinning solution and thus resulted in larger fiber diameters. The LEP was enhanced from 19 psi to 27 psi when NCC concentration increased to 2 wt.%, and MD flux of 11.5 LMH can be obtained at a temperature difference of 22 °C (feed temperature was 60 °C) with salt rejection higher than 99.9% when treating 10 g/L NaCl solutions. Liao et al. [92] described the fabrication of PVDF ENMs containing globular silica NPs. Silica with different particle size (5-10 nm and 0.2-0.3 μm) were initially modified by perfluoropolyether before dispersed in the dope solutions. Both composite membranes were superhydrophobic (CA>150°) because of the increased roughness and lower surface energy. All the ENMs showed increased fluxes and improved product quality compared to the virgin PVDF membrane, and the membranes maintained good anti-wettability after 50 h testing. Furthermore, this group [135] investigated the fabrication of dual-layer membranes by electrospinning a superhydrophobic thin PVDF-silica layer on PVDF or polyethylene terephthalate (PET) nonwoven substrates, as depicted in Figure 1.18. The obtained PVDF composite membranes showed CA>150° to water, salty water, oil-in-water emulsion, and beverages, allowing them to be applied for diverse separation processes. In addition, the composite membranes had superior

porosities, strong mechanical properties, and remarkable wetting resistance due to the combination of the thicker 3D nanofiber with micro-/nano- structure and the underlying robust substrates. Similarly, Lee et al. [102] introduced 1H,1H,2H,2H-perfluorooctyltriethoxysilane (FTES) functionalized TiO_2 in the PVDF solution to develop PVDF-HFP ENMs for DCMD. It was found that the protruding NPs emerged visibly on the fiber surface for the modified membranes, whereas the particle aggregation occurred with the addition of 15 wt.% TiO_2 NPs. In addition to TiO_2 NPs, polymer content and solvent volatility showed a significant effect on the fiber surface structure. The incorporation of TiO_2 NPs was found to result in a decrease of pore size yet an enhancement in porosity, contact angle and LEP. The obtained membrane showed high flux of 40 LMH (feed and permeate temperatures of 60 °C and 20 °C) when treating a high concentration (7 wt.%) of NaCl solution.

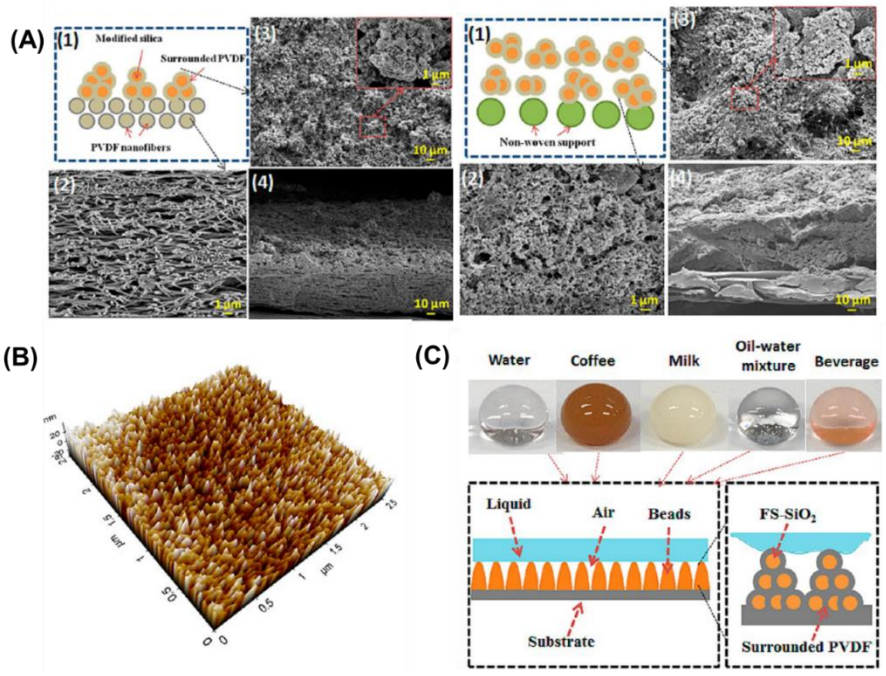


Figure 1.18 (A) Diagrams and morphologies of dual-layer membranes prepared on PVDF porous substrate (left) and PET non-woven (right): (1) schematic drawing; (2) cross-section of the middle layer; (3) surface; and (4) cross-section of the whole membrane. (B) Surface topography of the membrane prepared on PVDF nanofibrous substrate. (C) digital images of diverse liquid on the membrane surface and the liquid-membrane interface scheme on the membrane *[135]*

Carbon-based NPs, such as CNTs, GO, and active carbon (AC), are also investigated as additives. Zhao et al. [140] incorporated AC NPs into a PVDF-HFP hydrophobic active layer followed by electrospinning onto a commercial hydrophilic Nylon-6,6 substrate. Results revealed that the introduction of AC fillers increased the roughness of the fiber surface with protruding micro-wrinkles (as displayed in Figure 1.19 A) at a concentration of 1.5 wt.%. The resultant membranes showed an appropriate pore size (0.787 μm), porosity (90.5%), CA (142.7°), LEP (1.36 bar), and the highest permeate flux of 45.6 LMH compared to the virgin membrane of 36.4 LMH (feed and permeate inlet temperatures of 60 °C and 15 °C, respectively). Moreover, a possible mechanism of how AC particles influence the flux was elucidated via a proposed two-dimensional model in this work (Figure 1.19 B). In view of the inherent hydrophobicity of AC particles, the membrane hydrophobicity could be improved by both a multi-level roughness increment and a surface energy decrease. Besides, the presence of AC particles offers extra diffusion channels for rapid transport of water vapor, thereby leading to an increase of the overall vapor transport rate. Likewise, FTES modified GO sheets were introduced in the PVDF fiber via an electrospinning process to optimize the fiber characteristics for elevating the water permeability using a VMD configuration [46]. The surface hydrophobicity, LEP and water flux of the FTES-GO modified membranes experience prominent improvements compared with those of original PVDF membranes.

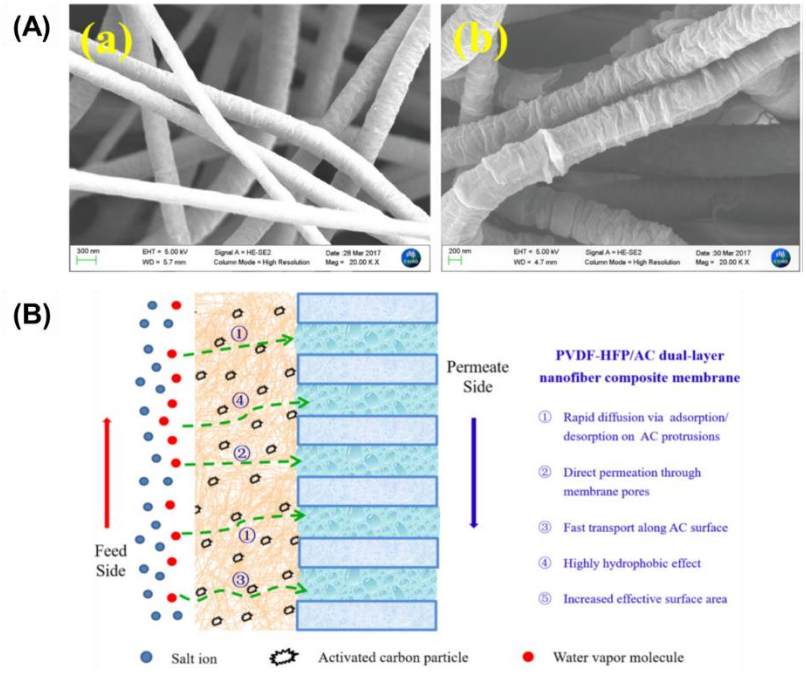


Figure 1.19 (A) Surface morphology images of (a) PVDF-HFP and (b) PVDF-HFP/AC membranes; (B) proposed schematic of AC particles effects on the membranes in DCMD *[140]*

In addition to inorganic NPs, organic NPs have been explored as well. Khayet et al. [94] attempted to fabricate self-sustained PSf-based mixed matrix ENMs using PTFE NPs. It was observed that the PTFE NPs showed a good arrangement along with the axis direction of the nanofiber at a low PTFE content. In contrast, the encapsulation of PTFE NPs by the nanofiber yields an even distribution of protruding warts on the fiber surface, which endows the modified membranes with a superhydrophobic feature and an increase of LEP. Therefore, the as-fabricated PSf/PTFE ENMs evinced a comparably high and steady MD flux with a high rejection. Their group also explored the use of fluorinated polyurethane additives (FPA) to construct PSF-based MD membranes [141]. The results displayed that the nanofibers acquired gradually more curved shapes with larger diameters and wider size distribution with the increase of the FPA content due to the significant enhancement of the dope solution viscosity. Superhydrophobic surface could be obtained for the ENMs prepared using at least 3 wt.% FPA in the PSf polymer solution. This can be explained by the assumption that FPA undergoes spontaneous surface segregation during an electrospinning process,

forming the nanofibers with an improved hydrophobic character due to the fluorine-rich surface. Moreover, for the FPA blended PSf ENMs, an enhancement of the porosity with the increase of FPA content was observed in contrast to what it was expected, which was ascribed to an enhancement of the fiber diameter and thickness of the ENMs. With an increase of the thickness, the accumulation of more electric charges within the fibers is likely to yield more obvious repulsion among the fibers, hence leading to a loosely packed fibrous web with a higher void volume fraction. The ENMs prepared with 4.5 wt.% FPA exhibited an excellent flux of 53.8 kg/(m^2·h) using 30 g/L NaCl as feed solution at feed and permeate temperatures of 80 °C and 20 °C, respectively.

Moreover, surfactants sometimes are adopted in order to decrease surface tension of the dope solution and improve the homogeneity of the electrospun nanofibers. For instance, nonionic surfactant Triton X-100 was used in polyvinyl alcohol (PVA) solution to fabricate hydrophilic electrospun nanofibers on a hydrophobic PP mat [142]. It can be observed that the quality and homogeneity of the nanofibers increased significantly due to the incorporation of Triton X-100 because of the solution conductivity and viscosity increase, as shown in Figure 1.20. During the DCMD tests, the hydrophobic PP layer faced the feed solution while the hydrophilic PVA-TX nanofiber was in contact with the permeate side. It has been well proven that dual hydrophobic/hydrophilic membranes have higher mass transport in MD due to the shortened pathway required for the vapor to transport between the two liquid/vapor interfaces. Among the prepared composite membranes, the MD flux increased with a higher Triton X-100 concentration resulting from the uniform fiber diameter and higher surface area to pore volume. In another study by Attia et al. [143], the cationic surfactant hexadecyl trimethyl ammonium bromide (HTAB) was investigated as one of the influence factors preparing PVDF ENMs for AGMD. By adding different HTAB concentrations of 0.05% and 0.5%, both membranes were bead-free. However, the nanofibers were more uniform for the membrane prepared with a lower HTAB concentration. It could be concluded that the incorporation of a surfactant is an effective method to fabricate bead-free nanofibers with uniform fiber diameter resulting from the lower surface energy.

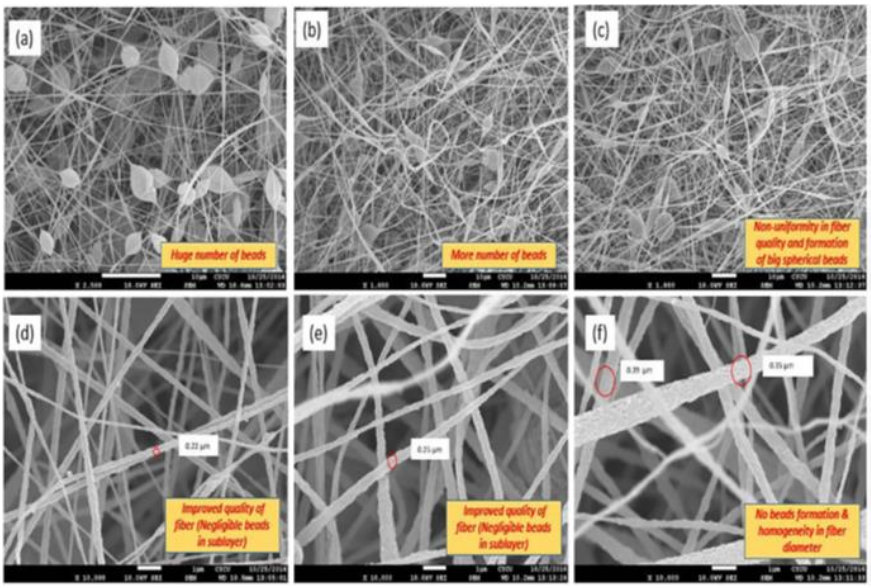


Figure 1.20 SEM micrographs analysis: before incorporation of Triton X-100 in PVA solution: (a) 4% PVA, (b) 6% PVA, and (c) 8% PVA; after incorporation of Triton X-100 in PVA solution: (d) 4% PVA-TX, (e) 6% PVA-TX, and (f) 8% PVA-TX *[142]*

Incorporation of either nanoparticles or organic particles in dope solutions for electrospinning is an efficient and facile method to increase the nanofiber roughness and leading to superhydrophobicity, which can further improve the MD performance in terms of higher fluxes and better anti-wetting properties. Generally, the dispersion uniformity of particles in ENMs is greater than in the membranes prepared in NIPS. Nonetheless, the optimization concentration of the particles should always be considered.

1.4.2.2 Surface modification

Among the established surface modification approaches, coating is the most frequently utilized method due to its simplicity and efficiency, while functional NPs are primarily implemented to construct a hierarchical structure for higher hydrophobicity and better anti-wetting properties. Liao et al. [107] fabricated superhydrophobic flat-sheet PVDF membranes by either integral or surface modification, and compared their DCMD performance with a commercial PVDF membrane. As depicted in Figure 1.21 (A), the modification procedure involved polydopamine coating, silver NPs loading, and hydrophobic modification with 1-dodecanethiol. To design the integrally

PVDF membrane (I-PVDF), the nanofiber membranes were firstly saturated with a mixture of isopropyl alcohol and water to enable the following reaction on all the fibers, whereas dry nanofiber membrane was directly implemented for surface modified membranes (S-PVDF). According to the SEM images in Figure 1.21 (B), it was obvious that silver NPs emerged on all the I-PVDF nanofiber surface, while a silver layer was produced on the top surface of the S-PVDF membrane. However, both membranes showed a high CA (>150°) and a low SA (<10°) due to the presence of a hierarchical nanostructure. The virgin PVDF membrane showed the highest flux of 35.7 LMH (feed and permeate temperatures were 333 K and 293 K, respectively) yet was the fastest one to be wetted. The S-PVDF membrane had the lowest flux since the extra silver layer posed a main hindrance for the vapor transport. In contrast, the I-PVDF membrane had a high flux of 31.6 LMH at the same operating conditions with a stable anti-wetting property.

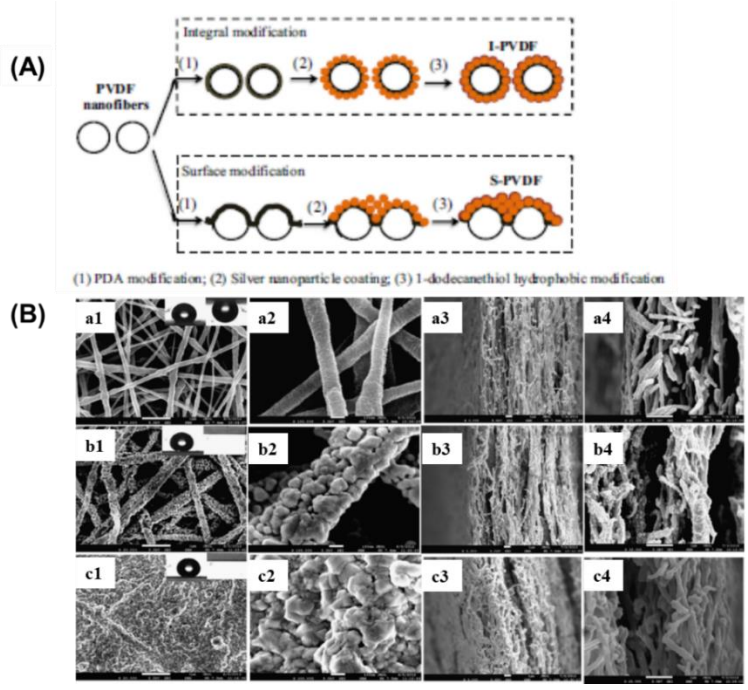


Figure 1.21 (a) Schematic diagram of preparing integrally- and surface- modified PVDF nanofiber membranes; (b) SEM images of top surface (1,2) and cross-section (3,4) for pristine PVDF (a), I-PVDF (b), and S-PVDF (c) nanofiber membranes *[107]*

A highly breathable membrane was developed via sequential electro-spraying two different solutions containing silica by integration of a superwettable selective layer

and a hydrophobic nanofiber substrate to treat with oil-in saline emulsions [144]. A PVDF-HFP/polystyrene (PS) solution with fluorosilane modified superhydrophobic silica NPs was sprayed onto the prepared PVDF nanofibers, which was followed by spraying a solution containing polyacrylonitrile (PAN) and unmodified hydrophilic silica, as illustrated in Figure 1.22. The obtained asymmetrically superwettable membrane surface was composed of micro/nanostructured nanofilaments, which showed an underwater superoleophobicity of 164° and a superhydrophobicity of 166°. When treating the oil-in-water emulsion, the superhydrophobic membrane rapidly suffered from fouling within 30 min with a distinct flux decline and permeate conductivity increase, whilst the Janus membrane showed a steady flux and superior salt rejection even after 30 h. This remarkable antifouling performance was mainly ascribed to the underwater super-oleophobic surface and the low oil adhesion force of the superhydrophilic layer. The design of constructing membranes with superwettable skins and hydrophobic support provides more possible applications in treating more complicated solutions by MD process, especially oily wastewaters.

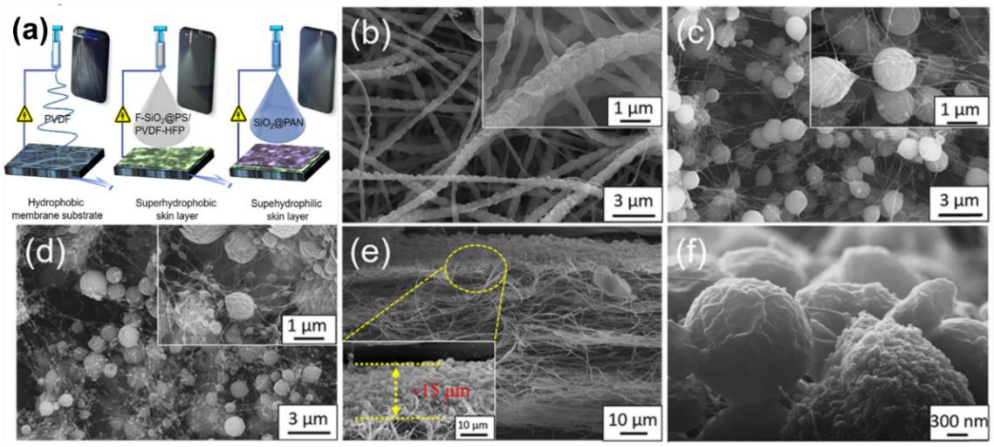


Figure 1.22 (a) Schematic illustration of the fabrication of the Janus skin layer with asymmetric superwettability on a PVDF NFM, and FE-SEM images of (b) necklace-structured PVDF NFM substrate, (c) superhyrdrophobic layer, (d) superhydrophilic layer, (e) cross-section, and (f) enlarged top layer *[144]*

Likewise, Su et al. [139] developed an approach that combined electro-co-spinning/spraying (ES^2) with DMF vapor-phase welding to fabricate superhydrophobic membranes. The electrospraying solution of silica/PVDF-HFP and the electrospinning

PVDF-HFP solution were simultaneously deposited on the PVDF-HFP support through the ES^2 technique. Afterwards, the obtained fibers were subjected to chemical phase welding to increase the mechanical properties by connecting the contact points between the fibers and the microbeads, which was followed by functionalization with 1H,1H,2H,2H-perfluorodecyltriethoxysilan (17-FAS) to enhance membrane hydrophobicity. Results showed that the membrane prepared only by electrospraying experienced contact angle decreasing and sliding angle increasing after 270 min of ultrasonication, while the hydrophobicity of ES^2 membrane remained superhydrophobic due to the composite SiO_2/PVDF-HFP microbeads which were restricted in the interconnected fibrous network reinforced by the welding process. During the MD tests for NaCl and gypsum scaling resistance, the ES^2 membrane performed better with a higher flux, a better rejection, and more stable performance than the other membranes. Apart from the electrospraying method, a low temperature hydrothermal process was utilized to coat TiO_2 NPs on the membrane surface followed by fluorosilanized with 1H,1H,2H,2H-perfluorododecyl trichlorosilane (FTCS) to fabricate superhydrophobic PVDF ENMs for DCMD [60]. The obtained membrane exhibited a superior hydrophobicity (157.1°), and an appropriate pore size (0.81 μm). Accordingly, a high flux and stable desalination performance (73.4 LMH, 99.99% rejection) using 3.5 wt.% NaCl solution as feed was achieved at feed and permeate inlet temperatures were 70 °C and 25 °C, respectively. Moreover, a high flux of 40.5 LMH with 99.98% of solute rejection in a long-term application using actual RO brine as feed solution was observed.

In addition to the NPs, PDMS (a polymeric organosilicon compound with high porosity and low surface energy) is extensively utilized to fine-tune membrane morphology and structure. For instance, An et al. [145] fabricated PVDF-HFP ENMs followed by electrospraying of hybridizing PDMS microspheres to enhance the surface hydrophobicity. Results demonstrated that monodispersed microspheres were found to emerge on the fiber surface, and wrinkling patterns appeared on the particle surface, which was possibly attributed to the interfacial behavior relative to solvent evaporation and polymer viscosity. Consequently, the PDMS microspheres distinctly enhanced the

surface hydrophobicity and roughness from 137.2° and 358 nm of PVDF-HFP ENMs to 155.4° and 1285 nm of PDMS modified membrane, respectively. The resultant membranes were tested to treat different dyeing wastewaters by DCMD, and the PDMS/PVDF-HFP membrane showed a high flux (initial flux: 33 LMH at feed and permeate temperatures of 60 °C and 20 °C, respectively) and superb anti-wetting properties. Moreover, the PDMS solution itself can be used as coating material as well instead of the formed PDMS microspheres to prepare superhydrophobic ENMs [146]. The influence of the PDMS concentration (0.5-4%) and the cold-press pressure (2-12 MPa) in the post-treatment on the membrane physicochemical characters and DCMD performance were studied. Results confirmed the formation of PDMS adhesion and/or agglomeration when the PDMS content enhanced, which imparted extra self-cleaning merit and superhydrophobicity to the modified membranes on account of the combined effect of a low surface energy of PDMS and a hierarchical roughness.

Fluorine-containing polymers are also suitable candidates as coating materials to construct a superhydrophobic surface. Amorphous PP (aPP), a byproduct of isotactic PP with low surface free energy, nontoxicity, low price, tacky property, and good solubility, was chosen to fabricate superhydrophobic membranes for DCMD by vacuum filtration onto the PVDF ENMs [147]. The coating solutions were made by the dissolution of aPP in xylene at 97 °C and then cooled down to different temperatures (90 °C, 75 °C, 60 °C, 45 °C), giving rise to gel formation due to the thermodynamic instability before filtration. When the filtration solution temperature was 90 °C and 75 °C, a large proportion of the solutions penetrated the porous substrates because the solution is transparent and homogeneous without aPP floccules. When the temperature was 60 °C, a flawless, homogenous, and porous layer comprising entangled bridges of aPP that connected the matrixes around the pores was generated on the surface (Figure 1.23). Thus, the membrane surface became superhydrophobic ascribed to rough surface and low surface free energy of aPP. Moreover, the effect of the aPP loading amount (12 g/m^2, 24 g/m^2, 48 g/m^2) was studied as well. A higher loading amount resulted in a smaller pore size, a lower porosity, a greater hydrophobicity and a higher LEP. The thin 3D network selective layer served as an extra superhydrophobic barrier

to anti-wetting purposes with a very low mass transfer resistance, and the underlying interconnected nanofibrous support was utilized to enable rapid vapor transport. The optimal aPP/PVDF-60-24 membranes showed a remarkably high flux of 135.3 $kg \cdot m^{-2}$ h^{-1} (feed and permeate temperatures are 80 °C and 20 °C, respectively) with an ultrahigh salt rejection (>99.99%), demonstrating a potential applicability for MD desalination. Additionally, Zhong et al. [110] developed a simple method to architecture a rough surface on ENM via *in situ* polymerization of aniline followed by hydrophobization. The resultant membrane with an open-cell pore structure displayed a superhydrophobic feature, a high flux of more than 28 LMH (temperature difference was 50 °C, and the permeate temperature was 15 °C), as well as superior anti-wetting properties and robust stability during a DCMD process. These studies paved a novel route in which a polymer can be used instead of inorganic NPs for the design of material surface roughness.

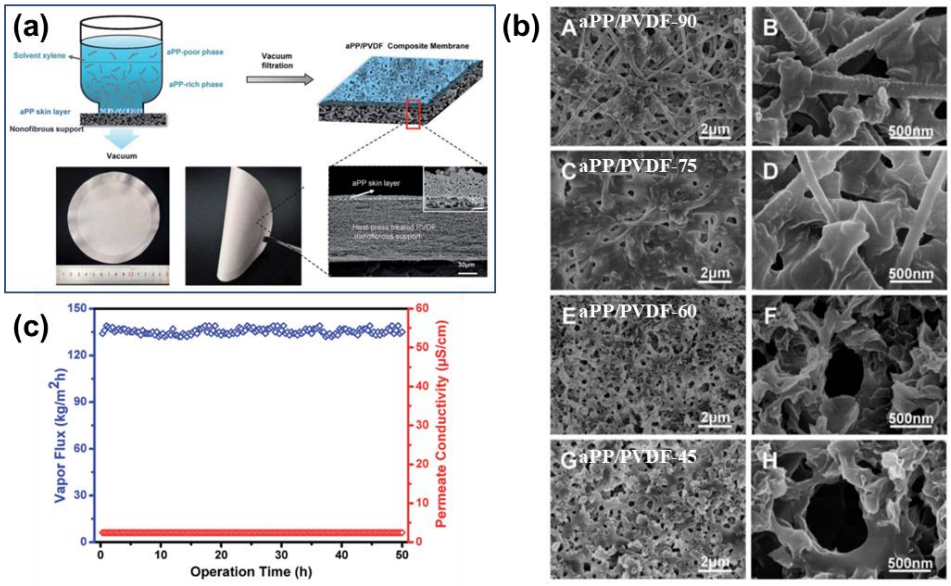


Figure 1.23 (a) Schematic of the formation process of the aPP skin layer, the digital images of a flexible aPP/PVDF composite membrane, and cross-sectional SEM images of a representative membrane; (b) SEM images of composite aPP/PVDF membranes prepared with different solution temperatures; (c) continuous DCMD test of the aPP/PVDF-60 membrane (3.5 wt.% NaCl solution, feed and permeate temperatures were 80 °C and 20 °C, respectively)) *[147]*

As mentioned before, grafting and CF_4 plasma modification can significantly reduce the surface energy by introducing more fluorine on the membrane surface without sacrificing pore size and porosity. In general, these methods are used after constructing the hierarchical structure on the surface. However, they can be used as the only modification as well. Deng et al. [111] fabricated superhydrophobic ENMs with rough fiber surfaces by directly immersing the PVDF ENM into FTCS solution without any further modification. As presented in Figure 1.24, the nanofiber surface changed substantially with different FTCS concentrations. When the FTCS concentration was low (0.5 wt.%), some teeny bumps formed on the fiber surface, and then developed into vigorous buds when the concentration was 2.0 wt.%. Finally, the flake-like structures were constructed on the fiber surfaces when the concentration enhanced to 3.5 wt.%. Due to the combination of low surface energy and hierarchical roughness, the resultant membranes were endowed with robust omniphobic feature, great mechanical strength, and excellent durability under harsh conditions. The PVDF-F-2-40 and PVDF-F-2-60 membranes showed stable permeate conductivities for over 24 h with a high permeate flux of 36.9 LMH and 25.9 LMH (feed and permeate temperatures of 60 °C and 20 °C, respectively), respectively. Likewise, CF_4 plasma modification was adopted as the only modification to prepare omniphobic PVDF ENMs for AGMD [115]. The influence of plasma treatment times on the membrane characteristics was investigated, and the results showed no significant changes of morphology and physical properties. Nonetheless, the construction of CF_3 and CF_2-CF_2 bonds on the surface lowered the surface energy, which increased the surface anti-wetting performance to various low interfacial tension liquids (such as methanol, mineral oil, and ethylene glycol). The modified membranes exhibited a stable flux of 15.3 LMH (an air gap thickness of 3 mm, feed and coolant temperatures of 60 °C and 20 °C, respectively) as well as high rejection relative to the RO brine containing 0.7 mM sodium dodecyl sulfate (SDS) surfactant, while a commercial PVDF membrane suffered wetting with merely 0.3 mM of SDS in the feed solution.

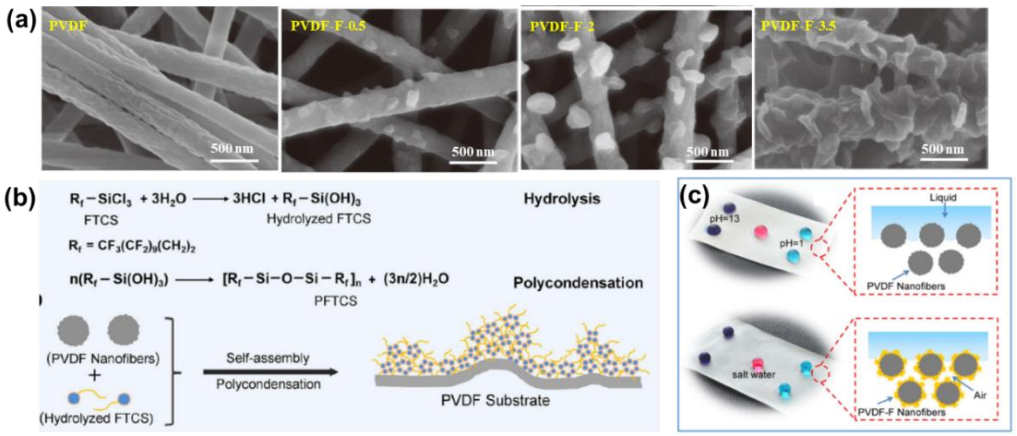


Figure 1.24 (a) SEM images PVDF ENMs modified with different FTCS concentrations; (b) schematic illustration of possible interaction among PVDF nanofibers and FTCS; (c) digital images of different droplets on the surfaces of PVDF and PVDF-F-2.0 membranes *[111]*

As mentioned before, surface modification is an effective approach to alter the membrane surface geometry or chemistry to elevate the surface coarseness or reduce the surface energy to improve the membrane hydrophobicity and oleophobicity for a better anti-wetting performance. Nonetheless, the cost of the materials and chemicals, as well as the complicated processing are big problems to be considered.

1.4.3 Commercial membranes

With the advancements of membrane-based technology, the investigation of potential commercial membranes with or without modification has been carried out to offer more possibilities for MD. Eykens et al. [213] compared the structural characteristics and the DCMD performance of 22 kinds of commercial hydrophobic membrane including PTFE, PVDF, PE, PP, and polyethersulfone (PES), which were fabricated either by stretching or phase inversion, with or without non-woven support, as well as two types of lab-made PVDF membranes prepared by ES. These membranes showed CAs ranging from 117°-149°, pore size of 0.2-3.2 μm, porosity of 66-83%, and thickness of 66-188 μm for unsupported membranes and 126-410 μm for supported membranes. By comparing the fluxes as well as the energy efficiency for seawater desalination and high-salinity water treatment, benchmarks were made where the

membrane flux and energy efficiency could exceed 75% of the obtained results, which were 20 kg/(m^2·h) and 70% for seawater while 10 kg/(m^2·h) and 57% for 23 wt.% NaCl solution at a temperature difference of 15 °C with feed temperature of 60 °C. Zuo et al. [52] explored the feasibility of commercial PE membranes in MD due to their advantages of intrinsic hydrophobicity, great chemical stability, and low heat conductivity. All the membranes were observed to have a sponge-like structure, appropriate pore size (0.06-0.2 μm), porosity (56.5%-66.1%), thickness (45-50.4 μm), and LEP (0.5-0.7 bar), which rendered the membranes proper candidates in MD desalination. The best permeation flux reached up to 123.0 LMH using 3.5 wt.% NaCl as feed solution at feed and permeate temperatures of 80 °C and 17 °C, respectively. In addition, the membrane exhibited a relatively stable MD performance with high flux and low permeate conductivity during a 100 h MD test. In another study, thin commercial PTFE flat-sheet membranes was directly used in a high-salinity concentrating DCMD process by using laminated two layers [121]. In this new strategy, the first layer act as a protecting layer to another layer. This single PTFE membrane was super-thin (11 μm) and superhydrophobicity (151.7°), and it had a proper pore size (0.248 μm), a high porosity (92.3%), a robust mechanical strength (21.1 MPa), and a great LEP (3.38 bar), which imparted the membrane a high permeate flux of 41 LMH treating 3.26 mol/L NaCl solution at feed and permeate temperatures of 60.2 °C and 20 °C, respectively. With the double-layer membrane, the flux was decreased to 32 LMH due to increased mass transport resistance, but with superior anti-fouling behavior.

Except direct usage of the commercial membranes, surface modification, especially surface coating, are employed to enhance the membrane wetting resistance to investigate the potential application in MD, especially for commercial PVDF membranes with a sponge-like structure and reasonable pore size of 0.2-0.4 μm, but a moderate hydrophobicity of 120°. Inorganic NPs (such as SiO_2, TiO_2, CNTs) are the most favorable coating materials. Razmjou et al. [56] deposited TiO_2 NPs on commercial PVDF membranes via a low temperature hydrothermal (LTH) process, which was followed by fluorosilanization using FTCS. Results showed that the CA

improved from 125° to 166° and the LEP increased from 120 kPa to 190 kPa, without compromising the pore size. Thus, the DCMD test results revealed that the anti-wetting properties of the modified membrane significantly increased although the flux was slightly lower than that of the virgin membrane due to the additional mass transport resistance on the surface. Moreover, when the feed solution contained humic acid and $CaCl_2$, the modified membrane showed a significantly higher flux recovery which indicated the enhancement of the antifouling properties. Silica NPs can be coated on the membrane surface via either chemical bonding or electrostatic adsorption, and usually combined with subsequently fluorination. Boo et al. [148] constructed an omniphobic membrane by binding negatively charged silica NPs onto the grafted positive PVDF membrane surface, which was followed by further hydrophobization with perfluorodecyltrichlorosilan (FDTS). The obtained PVDF membrane showed high liquid repellence even with low surface tension solutions, mainly owing to the stagnant air trapped between silica NPs and the low surface energy of FDTS coating layer. During the DCMD tests treating 1 mol/L NaCl solutions with different concentration of SDS and mineral oil and real shale gas produced water, the omniphobic membrane exhibited a more stable flux due to the omniphobic surface, which demonstrated its advantages in dealing with wastewaters containing various low surface tension components. Another omniphobic membrane was fabricated via spray-coating silica NPs or silica@polystyrene (PS) nano/microspheres onto a commercial PVDF membrane, followed by spraying a polymeric A 174 to immobilize the particles and further fluorination with 17-FAS [149]. The surface morphologies of virgin PVDF, silica NPs coated PVDF (NSF-PVDF), and silica@PS modified PVDF (MSF-PVDF) membranes are illustrated in Figure 1.25. It showed that the NSF-PVDF membrane possessed a silica NPs layer on the surface, while the MSF-PVDF membrane surface was bespread with uniform silica@PS spheres which was formed by electrostatic binding between silica and PS. The obtained hierarchical surface showed a great wetting resistance towards various liquids with either high or low surface tension. During the DCMD tests treating an emulsion solution, a stable flux and constant permeate conductivity was obtained for the MSF-PVDF membrane. However, for

membranes modified by coating, the coating layer as well as the possible pore block always increase the mass transport resistance, which reduces the permeate flux. Therefore, Qiu et al. [150] applied a method of dispersing graphene oxide (GO) onto the pore walls of PVDF membranes by filtering. The surface morphology of GO-PVDF membrane was not altered compared to the virgin membrane, indicating the infiltration of GO into pore channels and less blockage of pores. During the DCMD test with surfactants as foulants, the anti-fouling performance and flux of the GO-PVDF membrane were enhanced, especially when using the anionic surfactant. This approach may offer an alternative route to modify membrane pore surface properties without raising the mass transfer resistance for a better anti-wetting performance. Nonetheless, the filtered materials and the membrane pore structures should be carefully selected and considered in case blockage occurs.

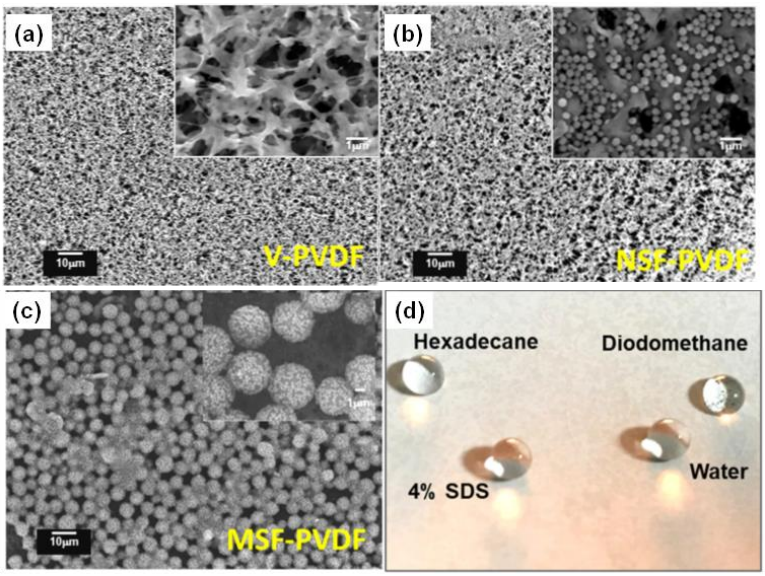


Figure 1.25 Top surface morphologies of (a) virgin PVDF membrane, (b) SiO_2 NPs coated PVDF membrane, and (c) SiO_2@PS coated PVDF membrane. (d) a photograph of various droplets on the SiO_2@PS coated PVDF membrane *[149]*

Organic polymers are studied as well to coat the membrane surface for better anti-wetting properties. For example, a hydrophobic perfluoropolyether (PFPE) compound (Fluorolink AD 1700) was coated on commercial hydrophilic polyamide (PA) membrane surfaces to enhance the membrane hydrophobicity [151]. Three PA membranes with pore sizes of 0.1 μm, 0.22 μm, and 0.45 μm were coated with different

oligomer concentrations of 5 wt.%, 10 wt.%, and 20 wt.%. The results proved that the hydrophobic coating did not change the membrane morphology, preserving the porous structure of the PA substrates. Meanwhile, the coating layer drastically increased the surface hydrophobicity leading to the production of a superhydrophobic structure composed of a thin highly hydrophobic layer (CA up to 150°) and a porous hydrophilic sub-layer (CA of about 45°) acting as a mechanical support. DCMD tests demonstrated a good stability of the coating during the experiments with both water and salty solutions. Likewise, Zhang et al. [152] coated commercial PVDF HF membranes with three hydrophobic perfluorinated copolymers, *i.e.* Hyflon AD40L, Hyflon AD40H, and Hyflon AD60. The obtained results showed that membranes modified with low viscosity coating solution leads to relatively lower porosities and smaller pore sizes, but higher contact angles, higher LEPs, higher fluxes, as well as improved mechanical strength and anti-wetting property. Additionally, Li et al. [153] fabricated a Janus membrane via layer-by layer coating of Teflon AF600 and PDA on a commercial PTFE/PP membrane. The top surface of the Janus membrane had a CA of 145.1°, while the bottom surface exhibited underwater superoleophobicity (154.2°) and in-air hydrophilicity (33.5°). Therefore, the membrane showed an enhanced wetting resistance towards various liquids comprising DI water, surfactant, alcohol, and crude oil. Another interesting work by Lee et al. [154] described a simple approach to further improve the hydrophobicity of the PDMS microspheres surface coating layer by incorporating hydrophobic silica-based aerogel particles during the electrospraying process by altering the microsphere structure because of the collisions between the aerogel particles and microspheres. When the aerogel particle concentration increased to 30%, the distortion of PDMS microspheres became distinct, such as the appearance of broken microspheres and strings, shown in Figure 1.26. Thus, this membrane showed the highest CA of 162.1° for water and 156.1° for 3.5% NaCl containing 0.1mM SDS. Moreover, the coated membrane showed a more stable flux during the DCMD test using NaCl solution containing 0.1 mM SDS as feed.

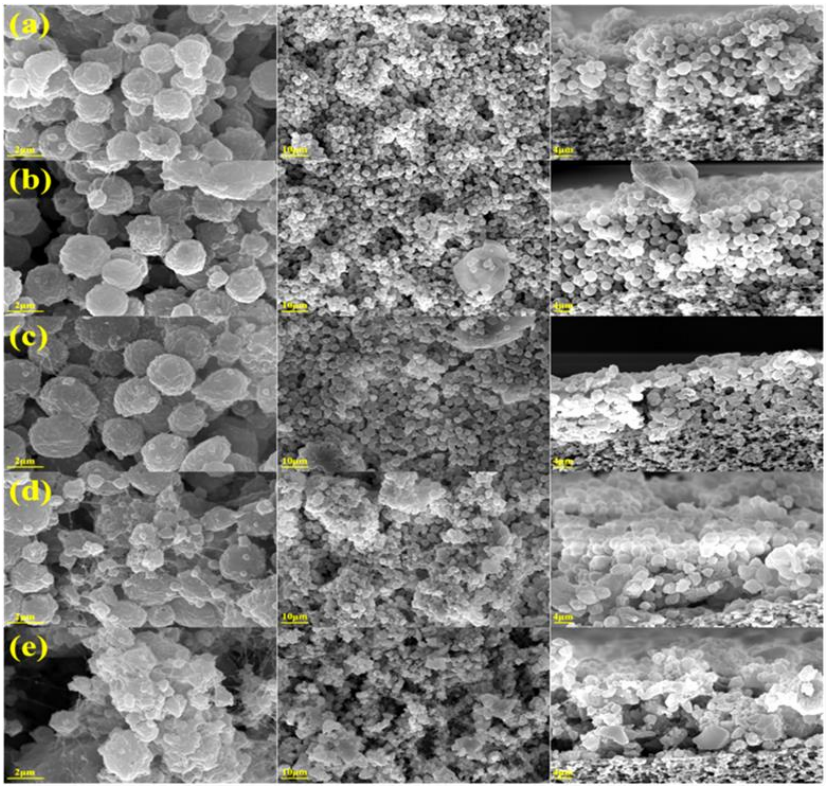


Figure 1.26 Surface and cross-sectional SEM images of the membrane coated by microspheres containing (a) 0%, (b) 5%, (c) 10%, (d) 20%, and (e) 30% of aerogel particles *[154]*

As membranes designed in lab-scale always involved complicated fabrication steps, which still need a long-time development before being manufactured in a large scale, the utilization of existing commercial membranes possessing suitable structures combined with a simple and cost-effective modification is time-saving and more promising for industrialization. However, the employment of modification which increases the process complexity and material investment may neutralize the benefits using commercial membranes, unless there are special applications that the value of the production overweighs the time and cost consumed during the preparation process.

1.4.4 Other methods

In addition to the normally used polymer membranes, other materials can be employed as membrane substrates and applied in MD with further modification as well. For instance, glass fiber membranes possessing abundant hydroxyl groups on the

surface, allows hydrophobic modification via silane grafting. A glass fiber membrane was coated with SiO_2 NPs, followed by succeeding fluorination and PVDF-HFP coating to fabricate an omniphobic membrane [155]. As shown in Figure 1.27 (A-B), the morphology showed that SiO_2 NPs coated the fiber surface, and formed agglomerates covering part of the pores. Benefitting from the hierarchical structure, the modified membrane showed a wetting resistance towards mineral oil, ethanol, and decane. During the DCMD tests treating NaCl solution containing SDS with low surface tension, the omniphobic membrane exhibited better performance with a stable flux and a high salt rejection and the hydrophobic commercial PTFE membrane, as shown in Figure 1.27 (C). When the SDS concentration increased, the rejection of the PTFE membrane reduced and the flux increased due to pore wetting which was caused by the penetrating of the feed solution through the wetted membrane pores. When the SDS concentration reached 0.3 mM, the rejection of the PTFE membrane significantly reduced to 50% while the flux increased 4 folds, while the rejection and the flux of the omniphobic membrane kept constant. The obtained results indicated the robust anti-wetting performance of the omniohobic membranes, even when treating low surface tension feed solutions.

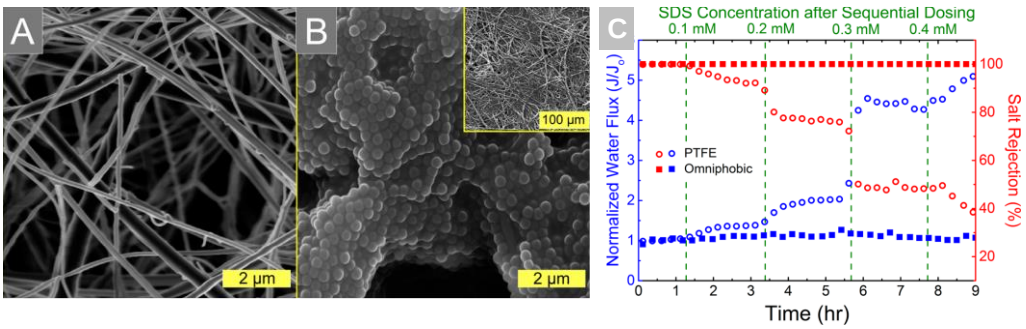


Figure 1.27 SEM images of (A) glass fiber membrane and (B) modified omniphobic membrane; (C) DCMD performance of the prepared omniphobic membrane and commercial PTFE membrane at different SDS concentrations *[155]*

A new kind of unsupported bacterial nanocellulose aerogels (BNCA) was used as membrane material and further hydrophobized via chemical vapor deposition for MD application [156]. Compared to the commercial PVDF membrane, the prepared BNCA membranes were 2.3 times thicker but showed a more open and interconnected pore

network, as well as a higher porosity (98.0% versus 62.2%) which was similar to the electrospun membranes, as showed in Figure 1.28. According to the DCMD performance, the BNCA membrane had a comparable flux with the commercial PVDF membrane, in which the advantage of the higher porosity compensated the disadvantage of the thicker structure. Additionally, the high porosity of the BNCA membrane reduced the conductive heat loss, which resulted in an increased heat efficiency compared to the PVDF membrane. Finally, they suggested that it is advantageous to decrease the density of ENMs and optimize the nanofiber diameter to improve the permeate flux, thermal efficiency, and salt rejection.

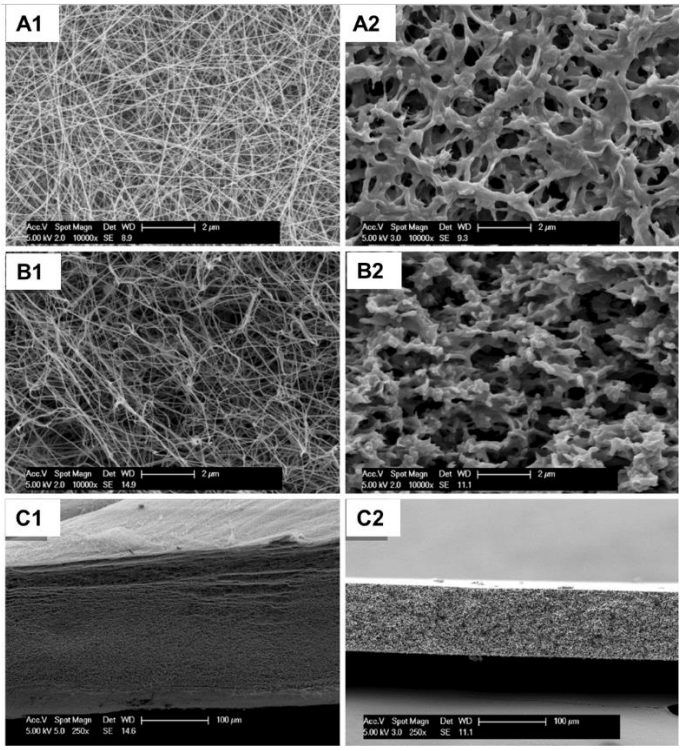


Figure 1.28 SEM images of surface (A) and cross-section (B, C) of BNCA (1) and commercial PVDF (2) membranes *[156]*

Another new type of membrane, nano-wood membrane, was developed by Ren's group from natural America basswood [157]. This membrane was prepared by clearing away lignin and semi-cellulose by means of boiling and rinsing in hot water, and subsequently immersing in boiled bleaching solution, which was followed by rinsing with cold water and freeze-drying. Finally, the hydrophilic membranes turned into hydrophobic by treating with FAS. As shown in Figure 1.29, the prepared nano-wood

membrane possessed a special structure containing xylem veins and lumens which are parallel to the surface. The obtained cellulose nanofibrils were linked with each other by intermolecular hydrogen bonds and van der Waals forces, which could reduce the heat conductivity in the transversal direction and minimize the conductive heat loss. Particularly, the eviction of lignin and semi-cellulose provided ~70% mass reduction in the wood membrane, which raised the porosity from 41% to 89% and enlarged the pore size from 0.18 μm to 0.28 μm. In the DCMD test, the nano-wood membrane showed a water flux of 20.8 LMH (feed and permeate temperatures of 60 °C and 20 °C).

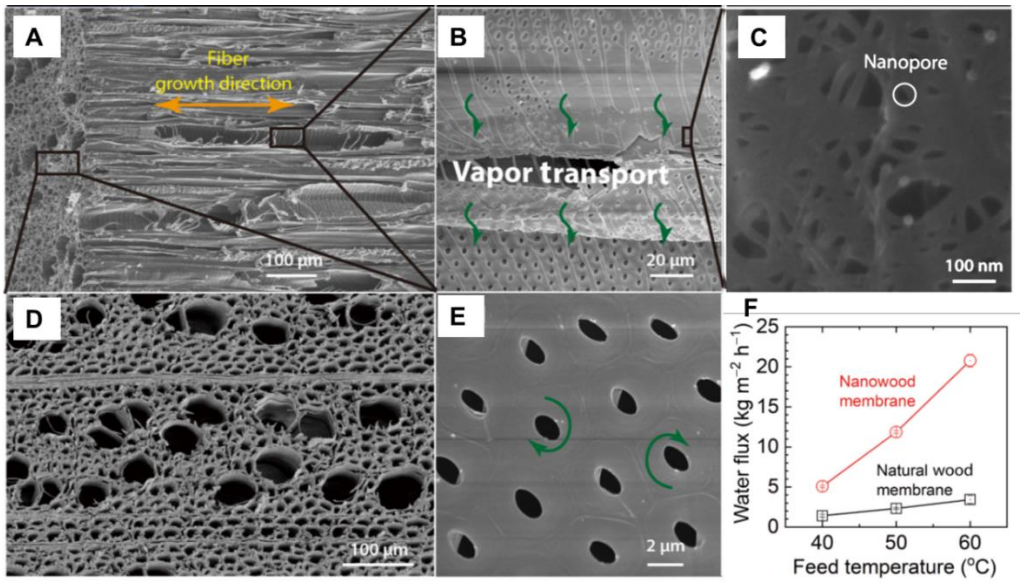


Figure 1.29 (A) SEM images of the nano-wood surface that exhibit aligned texture, xylem vessels, and lumina (channels); (B) SEM images that exhibit mesopores growing on the walls of the xylem vessels and lumina; (C) SEM images that exhibit micropores amid the cellulose fibers; Morphology of the (D) cross section and (E) pits; (F) DCMD fluxes of the nano-wood membrane at feed temperatures from 40 °C to 60 °C *[157]*

Thermally rearranged polybenzoxazole-co-polyimide (TR-PBOI) nanofiber membranes were developed for MD and membrane crystallization (MCr) for the first time by Kim et al. [158]. They utilized a TR polymer precursor, hydroxyl polyimide (HPI), to fabricate HPI nanofiber membranes (HPI-NFM-1) via electrospinning and further hot-pressing to prepare HPI-NFM-2 membranes. Furthermore, two types of HPI particles were assembled by reprecipitation using PVA and PVP as additives, which was

followed by spray coating onto HPI-NFM-2 membranes to prepare HPI-NCM-1 and HPI-NCM-2 membranes, respectively. Ultimately, the prepared membranes turned into TR-PBOI membranes after thermal rearrangement at 400 °C for 2 h. The SEM results showed that nanofibers of HPI-NFM-1 and HPI-NFM-2 membranes were merged after thermal rearrangement leading to an increase in the mechanical strengths, decrease in porosity, and increase in LEP. However, the hydrophobicity and porosity of HPI-NFM-2 were considerably lower than those of HPI-NMF, which can be ascribed to the declined surface roughness because of the hot-pressing, whereas the HPI-NCM membranes maintained their initial values due to the presence of NPs. The DCMD results demonstrated that the water fluxes increased correspondingly with the enlarged pore size, and TR-NFM-1 exhibited the highest water flux (72 LMH at 70 °C feed temperature) because of the largest pore size, while the TR-NCM membranes exhibited a lower flux than TR-NFM-1 because of the extra mass resistance resulting from the nanoparticle coating. Furthermore, the excellent chemical stability of the prepared TR-NCM-1 membrane in organic solvents, acid and base solutions was measured to check whether the TR-PBOI membrane could inherently endure harsh chemical condition.

These unconventional membranes exhibit comparable performance to polymer membranes while providing new insights into membrane preparation strategies using materials with special characteristics to diminish the drawbacks of conventional membranes such as relatively high thermal conductivity. However, complicated procedures should be utilized to make the structure or the surface chemistry of the materials more suitable for MD process, which increases the investment and process complexity.

1.5 Applications of MD technology

1.5.1 Desalination from seawater and wastewater

In traditional, MD is utilized for desalination to overcome the limitation of RO and thermal desalination techniques, due to its advantages such as the moderate operating condition, less sensitive to solution salinity, utilization of low-grade energy

resource, and system simplicity. Thus, seawater desalination is the most investigated application [8, 11, 21, 43, 60, 81, 159-167]. Besides seawater desalination, some other attracting applications have been discovered due to its lower fouling tendency and possibility to treat complicated feed solutions. For example, as its less sensitivity to solution salinity, MD can deal with highly saline wastewaters such as brine generated by RO and thermal desalination processes [168-173].

Furthermore, with the development of various technologies and industries, large amounts of wastewater are discharged every day. Therefore, treatment of different kinds of wastewater for reuse needs to be solved to release the water scarcity pressure. Among water pollutants, the most important ones are oil products, surfactants, pesticides, phenols, etc. Recently, MD has shown its potential in treating wastewaters containing oil and surfactants, especially with the development of omniphobic membranes with excellent anti-wetting performance and stability during long-term testing [155, 174-179]. For example, shale gas produced water containing a lot of salts, various hydrocarbons and chemicals, is a substantial hindrance for shale gas exploration. Nonetheless, MD has proven to be a potential candidate for treating the shale gas produced water after removing hydrocarbons by a physical process [148, 180-182].

1.5.2 Hazardous component and dye removal

In addition to produce pure water, MD can also be employed in the processes in which a high rejection of a certain component is required [62, 183-188]. Water pollution by metals is one of the most severe environmental problems, and the treatment of solutions containing heavy metals by MD has been studied. Lou et al. [188] explored the feasibility of MD combined with crystallization in dealing with concentrated heavy metal wastewater containing Zn and/or Ni to obtain pure crystals and pure water. Results showed that high concentrations of Zn and Ni did not affect the rejection, although the flux reduced due to the increased feed concentration. In addition, treatment of low-level radioactive wastewater (LLRW) by MD has also been investigated. As the LLRW from the nuclear plants should be concentrated to the largest feasible extent before the final solidification in order to minimize the costs of the final treatment and

long-term storage, MD was applied to concentrate the LLRW [186, 189, 190]. Wen et al. [186] used commercial PP membranes in DCMD to treat highly saline LLRW containing nuclides such as cobalt (Co), strontium (Sr), cesium (Cs), and a large amount of non-radioactive chemical boron (B). The results proved that DCMD is the most effective compared with other membrane technologies.

Another application of MD lies in textile industry wastewater treatment. As large amounts of freshwater are consumed in the textile industry, reuse of the textile wastewater has significant importance [191]. MD has the potential to eliminate the restrictions of pressure-driven membrane processes (*i.e.*, NF and UF) during the treatment of dye wastewater due to its low operating pressure under mild temperature [192-196]. For instance, a superhydrophobic composite PVDF hollow fiber membrane was prepared to separate dyes form water by VMD, and it showed rejections higher than 99% to Congo red and methylene blue with high flux [194].

1.5.3 Volatile and organic solvent separation and concentration

As MD is a temperature gradient based process, it provided novel opportunities to be used for concentration or separation of volatile components, such as removal of alcohol, breaking azeotropes, and concentration of acids [22, 23, 197-205, 220-223]. For instance, separation of ethanol from solutions with different concentrations in a bioreactor integrated with DCMD was examined [204]. The results demonstrated that the permeate and ethanol flux was strongly influenced by the vapor pressure, and it was also associated with the ethanol concentration in the feed. A PTFE membrane was fabricated for VMD to concentrate 2,3-butanediol from model 2,3-butanediol solutions and fermentation broths [201]. According to the results, butanediol was enriched from 40 g/L to 650 g/L in the simulated solution. When VMD was integrated with a fed-batch reactor, 2,3-butanediol could be concentrated to over 430 g/L. Separation of acids from water could be accomplished as well, such as separation of HCl from the HCl-H_2SO_4 solution [202]. It was concluded that the HCl concentration was enhanced in the permeate side with an increment in the feed solution, and the feed temperature strongly influences the HCl flux. Ammonia, which came from municipal and industrial

wastewaters, is a pollutant causing eutrophication and oxygen depletion, and MD has been investigated for ammonia removal [199, 206]. For example, a capillary PVDF membrane was studied for ammonia removal, and its performance was compared using conventional DCMD, membrane contactor, and a modified DCMD with adsorption solution containing sulfuric acid at the permeate side [206]. The results showed that the modified DCMD exhibited better ammonia removal efficiency due to the presence of sulfuric acid.

1.5.4 Concentration of temperature sensitive solutions

Furthermore, the relatively low operating temperature of MD process provides more potential applications in treating solutions containing components which are sensitive to temperatures, such as aromatic compounds, juice, dairy products, and pharmaceutical products [34, 35, 207-212]. For example, VMD was utilized to recover aroma compounds from black currant juice at low temperature of 10-45 °C, and the concentration factors increased with decreasing juice temperature [207]. Dehydration of red grape juice was also achieved by OMD using commercial PTFE membranes [34]. Moreover, the removal performance of pharmaceutical residuals from effluent was carried out using AGMD at pilot scale [212]. Almost all targeted pharmaceutical compounds were removed to a very high degree, below the method detection limit. Additionally, DCMD was applied to concentrate the wastewater from salty whey [211]. The flux decreased when trace protein presented in the feed solution, but the liquid could still be repelled. To address the advantages of MD, more potential MD applications should be discovered, and hybrid processes integrated with MD process or novel modified MD technologies can be explored.

1.6 Objectives and outline of the thesis

Various research efforts have been attempted to fabricate membranes for membrane distillation (MD), a thermally-driven membrane process which combines the advantages of high salt rejection of thermal distillation process and moderate operate condition of membrane technology together. Benefitting from several

superiorities, such as the potential usage of low-grade energy, modularity, small footprint, high rejection to non-volatile matters, MD has been envisaged as a promising desalination process. As a key part in MD, the membrane plays a significant role in rejecting unwanted matters in the feed streams and maintaining a stable flux and rejection. Therefore, many studies have been conducted to fabricate membranes possessing high flux and robust anti-fouling properties for MD. As summarized in section 1.4, the most studied membrane preparation methods are non-solvent induced phase separation (NIPS) and electrospinning (ES) combined with modification including blending, coating, and grafting, and sometimes existing commercial membranes with proper structures are studied. Although the most used commercial membranes in large-scale MD applications are PTFE, PP, and PE membranes fabricated by stretching, which show high hydrophobicity and stable chemical and thermal properties, the most investigated polymer is PVDF in the academic area, due to its lower cost, easy fabrication, proper hydrophobicity, and good thermal stability. However, modification is usually needed to improve the PVDF membrane structure or surface chemistry to enhance its anti-wetting performance and water flux, and the expensive materials and chemicals, as well as the complex fabrication procedures, make it difficult for a large-scale preparation. Therefore, it is with importance and interesting to develop facile membrane preparation methods using cost-effective polymer materials and chemicals. Although electrospinning process could produce membranes with controllable thickness and pore size, high porosities, and high hydrophobicity with proper modifications, the producing process itself limits its further industrialization, because the produce rate and the membrane area are limited. Hence, the objective of this thesis mostly lies in developing PVDF membranes using simple NIPS methods.

A benchmark is set according to the information from section 1.4.1: (1) considering a facile preparation process, the preparation process should contain less than 4 steps, such as dope solution preparation, membrane preparation, membrane solidification, and possible post-processing; (2) high temperature and high pressure should not be used in the process; (3) expensive or special materials should not be used; (4) the prepared membrane should show open and porous surface morphology; (5) the

membrane contact angle should be higher than 130°; (6) the thickness of the hydrophobic PVDF membrane should be in the range of 30-100 μm; (7) the membrane pore size should lie in 0.1-1 μm; (8) the membrane porosity should reach 70%-90%; (9) a reasonable LEP higher than 1 bar should be achieved; (10) a MD flux of 25 kg/(m^2·h) (feed and permeate temperatures of 60 °C and 20 °C, respectively) should be reached. The goal of MD flux is set according to Figure 1.30, in which one-third of the results reach or exceed this value. The values in the figure are the DCMD fluxes of the membranes prepared by NIPS (summarized in section 1.4.1) (feed and permeate temperatures of 60±5 °C and 18±5 °C, respectively).

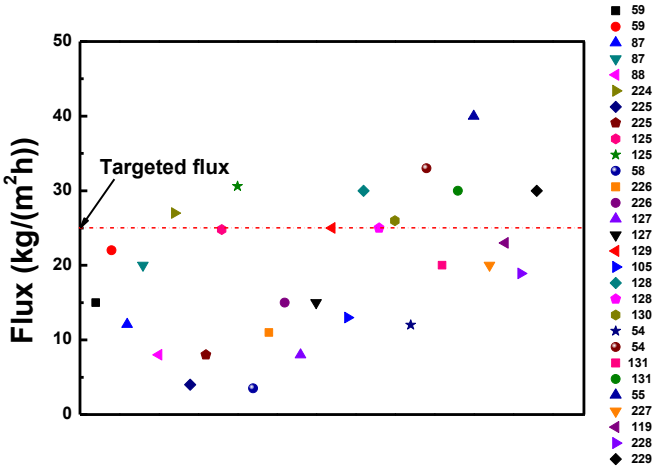


Figure 1.30 The targeted DCMD flux is set where one-third of the reported results (in section 1.4.1) reach or exceed this value. The points in the figure are the DCMD fluxes of the membranes prepared by NIPS (feed and permeate temperatures of 60±5 °C and 18±5 °C, respectively), and the numbers listed on the right hand are the reference numbers.

The chapters in this thesis are organized as follows: ***Chapter 1*** briefly discusses the desalination technologies and introduces the MD process with its mechanism and configurations. Subsequently, the MD membrane characteristics, as well as the performance-related operating parameters and their influence in MD performance are discussed. Particularly, recent advances in preparation of MD membranes are reviewed, and the applications are displayed. ***Chapter 2*** concludes the chemicals, membrane synthesis methods, and the membrane characterization for all the experiments. In

Chapter 3, the potential of using 3D printed membranes in MD application is explored. 3D printing is an attracting technology to prepare products with various shapes using a range of materials across different scales. However, using 3D printing process in membrane-related area is still in its infancy. Preparation membranes by 3D printing has several advantages of quick fabrication, less of solvent discharge, and freedom of shape design. Therefore, laser sintering (LS), a powder-based 3D printing process, is utilized to prepare rough polyamide (PA) substrates. As the pore size of printed PA membranes is too large for a MD membrane, a simple dip-coating method in PVDF solutions is utilized to decrease the pore size. The influence of PVDF solution concentration and immersion time on the membrane morphology, physical properties, and DCMD performance is discussed. In ***Chapter 4***, a novel "bottom-up" method is proposed to fabricate porous PVDF membranes by altering the sequence in traditional phase separation process, *i.e.* casting the polymer solution on a glass plate followed by covering a piece of non-woven substrate on it instead of directly casting the polymer solution on a non-woven substrate. As PVDF is a semi-crystalline polymer, the obtained membrane morphology is significantly affected by the crystallization behavior during the phase separation process. The membrane morphology, surface roughness, porosity and pore size of the normal casting and bottom-up membranes are investigated, as well as the MD performance at different feed solution temperatures. ***Chapter 5*** introduces another porous PVDF membrane preparation method named "co-casting". After the PVDF solution is cast on the nonwoven substrates, a PES solution layer is cast onto the PVDF layer immediately before immersing into a water bath for phase separation. Due to the shrinkage rate difference between PES and PVDF membranes, delamination between the two layers occurs, and the underlying PVDF membranes are reserved for MD measurements. The influence of the PES and PVDF concentration on PVDF morphology and MD performance are studied. Finally, the conclusions and future perspectives are presented in ***Chapter 6***.

1.7 References

[1] M. Elimelech, William A. Phillip, The Future of Seawater Desalination: Energy,

Technology, and the Environment, Science, 333 (2011) 712-717.
[2] R.F. Service, Desalination Freshens Up, Science, 313 (2006) 1088-1090.
[3] A. Mark, Science and Technology for water purification in the coming decades, Nature, 452 (2008) 20.
[4] J.R. Werber, C.O. Osuji, M. Elimelech, Materials for next-generation desalination and water purification membranes, Nat. Mater., 1 (2016) 1-16.
[5] M.A. Abdelkareem, M. El Haj Assad, E.T. Sayed, B. Soudan, Recent progress in the use of renewable energy sources to power water desalination plants, Desalination, 435 (2018) 97-113.
[6] E. Jones, M. Qadir, M.T.H. van Vliet, V. Smakhtin, S.M. Kang, The state of desalination and brine production: A global outlook, Sci. Total Environ., 657 (2019) 1343-1356.
[7] A. Deshmukh, C. Boo, V. Karanikola, S. Lin, A.P. Straub, T. Tong, D.M. Warsinger, M. Elimelech, Membrane distillation at the water-energy nexus: limits, opportunities, and challenges, Energy Environ. Sci., 11 (2018) 1177-1196.
[8] B. Van der Bruggen, Carlo Vandecasteele, Distillation vs. membrane filtration: overview of process evolutions in seawater desalination, Desalination, 143 (2002) 207-218.
[9] K.W. Lawson, D.R. Lloyd, Membrane distillation, J. Membr. Sci., 124 (1997) 1-25.
[10] E. Curcio, E. Drioli, Membrane distillation and related operations - A review, Sep. Purif. Rev., 34 (2005) 35-86.
[11] M.S. El-Bourawi, Z. Ding, R. Ma, M. Khayet, A framework for better understanding membrane distillation separation process, J. Membr. Sci., 285 (2006) 4-29.
[12] B.R. Bodell, Silicone rubber vapor diffusion in saline water distillation, in, U.S., 1963.
[13] B.R. Bodell, Distillation of saline water using silicone rubber membrane, in, U.S., 1968.
[14] M.E. Findley, Vaporization through porous membranes, Ind. Eng. Chem. Process Des. Dev., 6 (1967) 226-230.
[15] P.K. Weyl, Recovery of demineralized water from saline waters, in, U.S., 1967.
[16] D.W. Gore, Gore-Tex membrane distillation, Proc. 10th Ann. Con. Water, (1982) 25-29.
[17] L. Carlsson, The new generation in sea water desalination SU membrane distillation system, Desalination, 45 (1983) 221-222.
[18] S. I. Andersson, N. Kjellander, B. Rodesjo, Design and field tests of a new membrane distillation desalination process, Desalination, 56 (1985) 345-354.
[19] K. Schneider, W. Holz, R. Wollbeck, S. Ripperger, Membranes and modules for transmembrane distillation, J. Membr. Sci., 39 (1988) 25-42.
[20] K. Smolders, A. Franken, Terminology for membrane distillation, Desalination, 72 (1989) 249-262.
[21] D. González, J. Amigo, F. Suárez, Membrane distillation: Perspectives for sustainable and improved desalination, Renew. Sust. Energ. Rev., 80 (2017) 238-259.
[22] O. Gupta, S. Roy, S. Mitra, Enhanced membrane distillation of organic solvents

from their aqueous mixtures using a carbon nanotube immobilized membrane, J. Membr. Sci., 568 (2018) 134-140.
[23] M.M.A. Shirazi, A. Kargari, Concentrating of Sugar Syrup in Bioethanol Production Using Sweeping Gas Membrane Distillation, Membranes, 9 (2019) 14.
[24] S. Kalla, S. Upadhyaya, K. Singh, Principles and advancements of air gap membrane distillation, Rev. Chem. Eng., 35 (2019) 817-859.
[25] T.Y. Cath, V.D. Adams, A.E. Childress, Experimental study of desalination using direct contact membrane distillation: a new approach to flux enhancement, J. Membr. Sci., 228 (2004) 5-16.
[26] G. Naidu, S. Jeong, S. Vigneswaran, E.K. Jang, Y.J. Choi, T.M. Hwang, Fouling study on vacuum-enhanced direct contact membrane distillation for seawater desalination, Desalin. Water Treat., 57 (2016) 10042-10051.
[27] L. Francis, N. Ghaffour, A.A. Alsaadi, G.L. Amy, Material gap membrane distillation: A new design for water vapor flux enhancement, J. Membr. Sci., 448 (2013) 240-247.
[28] X.J. Li, Y.J. Qin, R.L. Liu, Y.P. Zhang, K. Yao, Study on concentration of aqueous sulfuric acid solution by multiple-effect membrane distillation, Desalination, 307 (2012) 34-41.
[29] K. Zhao, W. Heinzl, M. Wenzel, S. Buttner, F. Bollen, G. Lange, S. Heinzl, N. Sarda, Experimental study of the memsys vacuum-multi-effect-membrane-distillation (V-MEMD) module, Desalination, 323 (2013) 150-160.
[30] G. Braun, C. Kleffner, Industrial water desalination by vacuum multi-effect membrane distillation, Chemie Ingenieur Technik, 91 (2019) 1400-1408.
[31] J.C. Vega-Beltran, L. Garcia-Rodriguez, I. Martin-Mateos, J. Blanco-Galvez, Solar membrane distillation: theoretical assessment of multi-stage concept, Desalin. Water Treat., 18 (2010) 133-138.
[32] B.R. Babu, N.K. Rastogi, K. Raghavarao, Mass transfer in osmotic membrane distillation of phycocyanin colorant and sweet-lime juice, J. Membr. Sci., 272 (2006) 58-69.
[33] B. Ravindra Babu, N.K. Rastogi, K.S.M.S. Raghavarao, Concentration and temperature polarization effects during osmotic membrane distillation, J. Membr. Sci., 322 (2008) 146-153.
[34] W. Kujawski, A. Sobolewska, K. Jarzynka, C. Güell, M. Ferrando, J. Warczok, Application of osmotic membrane distillation process in red grape juice concentration, J. Food Eng., 116 (2013) 801-808.
[35] J. Kujawa, E. Guillen-Burrieza, H.A. Arafat, M. Kurzawa, A. Wolan, W. Kujawski, Raw Juice Concentration by Osmotic Membrane Distillation Process with Hydrophobic Polymeric Membranes, Food Bioproc. Tech., 8 (2015) 2146-2158.
[36] L. Martinez-Diez, M.I. Vazquez-Gonzalez, Temperature and concentration polarization in membrane distillation of aqueous salt solutions, J. Membr. Sci., 156 (1999) 265-273.
[37] M. Khayet, M.P. Godino, J.I. Mengual, Study of asymmetric polarization in direct contact membrane distillation, Sep. Sci. Technol., 39 (2004) 125-147.
[38] J. Phattaranawik, R. Jiraratananon, A.G. Fane, Heat transport and membrane

distillation coefficients in direct contact membrane distillation, J. Membr. Sci., 212 (2003) 177-193.
[39] L. Martinez-Diez, M.I. Vazquez-Gonzalez, A method to evaluate coefficients affecting flux in membrane distillation, J. Membr. Sci., 173 (2000) 225-234.
[40] M. Khayet, M.P. Godino, J.I. Mengual, Thermal boundary layers in sweeping gas membrane distillation processes, AICHE J., 48 (2002) 1488-1497.
[41] R.W. Schofield, A.G. Fane, C.J.D. Fell, Heat and mass transfer in membrane distillation, J. Membr. Sci., 33 (1987) 299-313.
[42] J. Phattaranawik, R. Jiraratananon, A.G. Fane, Effect of pore size distribution and air flux on mass transport in direct contact membrane distillation, J. Membr. Sci., 215 (2003) 75-85.
[43] A. Alkhudhiri, N. Darwish, N. Hilal, Membrane distillation: A comprehensive review, Desalination, 287 (2012) 2-18.
[44] L. Eykens, K. De Sitter, C. Dotremont, L. Pinoy, B. Van der Bruggen, How To Optimize the Membrane Properties for Membrane Distillation: A Review, Ind. Eng. Chem. Res., 55 (2016) 9333-9343.
[45] R.N. Wenzel, Surface roughness and contact angle, J. Phys. Chem., 53 (1949) 1466-1467.
[46] A. Cassie, Contact angles, Discuss. Faraday Soc., 3 (1948) 11-16.
[47] W. Barthlott, C. Neinhuis, Purity of the sacred lotus, or escape from contamination in biological surfaces, Planta, 202 (1997) 1-8.
[48] L. Feng, S.H. Li, Y.S. Li, H.J. Li, L.J. Zhang, J. Zhai, Y.L. Song, B.Q. Liu, L. Jiang, D.B. Zhu, Super-hydrophobic surface: From Natural to Artificial, Adv. Mater., 14 (2002) 1857-1860.
[49] H.J. Ensikat, P. Ditsche-Kuru, C. Neinhuis, W. Barthlott, Superhydrophobicity in perfection: the outstanding properties of the lotus leaf, Beilstein J. Nanotech., 2 (2011) 152-161.
[50] A.C.M. Franken, J.A.M. Nolten, M.H.V. Mulder, D. Bargeman, C.A. Smolders, Wetting criteria for the applicability of membrane distillation, J. Membr. Sci., 33 (1987) 315-328.
[51] F. Lagana, G. Barbieri, E. Drioli, Direct contact membrane distillation: modelling and concentration experiments, J. Membr. Sci., 166 (2000) 1-11.
[52] J. Zuo, S. Bonyadi, T.S. Chung, Exploring the potential of commercial polyethylene membranes for desalination by membrane distillation, J. Membr. Sci.,497 (2016) 239-247.
[53] X. Wei, B. Zhao, X.-M. Li, Z. Wang, B.-Q. He, T. He, B. Jiang, CF4 plasma surface modification of asymmetric hydrophilic polyethersulfone membranes for direct contact membrane distillation, J. Membr. Sci., 407-408 (2012) 164-175.
[54] M. Tian, Y. Yin, C. Yang, B. Zhao, J. Song, J. Liu, X.-M. Li, T. He, CF4 plasma modified highly interconnective porous polysulfone membranes for direct contact membrane distillation (DCMD), Desalination, 369 (2015) 105-114.
[55] S. Munirasu, F. Banat, A.A. Durrani, M.A. Haija, Intrinsically superhydrophobic PVDF membrane by phase inversion for membrane distillation, Desalination, 417 (2017) 77-86.

[56] A. Razmjou, E. Arifin, G.X. Dong, J. Mansouri, V. Chen, Superhydrophobic modification of TiO_2 nanocomposite PVDF membranes for applications in membrane distillation, J. Membr. Sci., 415-416 (2012) 850-863.
[57] D. Hou, J. Wang, D. Qu, Z. Luan, X. Ren, Fabrication and characterization of hydrophobic PVDF hollow fiber membranes for desalination through direct contact membrane distillation, Sep. Purif. Technol., 69 (2009) 78-86.
[58] M. Qtaishat, M. Khayet, T. Matsuura, Novel porous composite hydrophobic/hydrophilic polysulfone membranes for desalination by direct contact membrane distillation, J. Membr. Sci., 341 (2009) 139-148.
[59] M.M. Teoh, T.-S. Chung, Y.S. Yeo, Dual-layer PVDF/PTFE composite hollow fibers with a thin macrovoid-free selective layer for water production via membrane distillation, Chem. Eng. J., 171 (2011) 684-691.
[60] A.M. Alklaibi, N. Lior, Membrane-distillation desalination: Status and potential, Desalination, 171 (2005) 111-131.
[61] K.W. Lawson, D.R. Lloyd, Membrane distillation .1. Module design and performance evaluation using vacuum membrane distillation, J. Membr. Sci., 120 (1996) 111-121.
[62] M. Khayet, M.P. Godino, J.I. Mengual, Possibility of nuclear desalination through various membrane distillation configurations: a comparative study, International Journal of Nuclear Desalination, 1 (2003) 30-46.
[63] L. Martinez, F.J. Florido-Diaz, A. Hernandez, P. Pradanos, Estimation of vapor transfer coefficient of hydrophobic porous membranes for applications in membrane distillation, Sep. Purif. Technol., 33 (2003) 45-55.
[64] F.A. Banat, J. Simandl, Theoretical and experimental study in membrane distillation, Desalination, 95 (1994) 39-52.
[65] F.A. Banat, J. Simandl, Desalination by membrane distillation: A parametric study, Sep. Sci. Technol., 33 (1998) 201-226.
[66] C.A. Rivier, M.C. Garcia-Payo, I.W. Marison, U. von Stockar, Separation of binary mixtures by thermostatic sweeping gas membrane distillation I. Theory and simulations, J. Membr. Sci., 201 (2002) 1-16.
[67] M. Khayet, P. Godino, J.I. Mengual, Theory and experiments on sweeping gas membrane distillation, J. Membr. Sci., 165 (2000) 261-272.
[68] M. Khayet, P. Godino, J.I. Mengual, Nature of flow on sweeping gas membrane distillation, J. Membr. Sci., 170 (2000) 243-255.
[69] S. Bandini, C. Gostoli, G.C. Sarti, Separation efficiency in vacuum membrane distillation, J. Membr. Sci., 73 (1992) 217-229.
[70] M.C. Garcia-Payo, M.A. Izquierdo-Gil, C. Fernandez-Pineda, Air gap membrane distillation of aqueous alcohol solutions, J. Membr. Sci., 169 (2000) 61-80.
[71] S. Bandini, G.C. Sarti, Heat and mass transport resistances in vacuum membrane distillation per drop, AICHE J., 45 (1999) 1422-1433.
[72] C.H. Lee, W.H. Hong, Effect of operating variables on the flux and selectivity in sweep gas membrane distillation for dilute aqueous isopropanol, J. Membr. Sci., 188 (2001) 79-86.
[73] M. Khayet, M.P. Godino, J.I. Mengual, Theoretical and experimental studies on

desalination using the sweeping gas membrane distillation method, Desalination, 157 (2003) 297-305.
[74] L.D. Tijing, Y.C. Woo, J.-S. Choi, S. Lee, S.-H. Kim, H.K. Shon, Fouling and its control in membrane distillation—A review, J. Membr. Sci., 475 (2015) 215-244.
[75] D.M. Warsinger, J. Swaminathan, E. Guillen-Burrieza, H.A. Arafat, J.H. Lienhard V, Scaling and fouling in membrane distillation for desalination applications: A review, Desalination, 356 (2015) 294-313.
[76] M. Rezaei, D.M. Warsinger, J.H. Lienhard V, M.C. Duke, T. Matsuura, W.M. Samhaber, Wetting phenomena in membrane distillation: Mechanisms, reversal, and prevention, Water Res., 139 (2018) 329-352.
[77] M. Rahman Choudhury, Nawrin Anwar, David Jassby, M.S. Rahaman, Fouling and wetting in themembrane distillation driven wastewater reclamation process - A review, Adv. Colloid Interface Sci., 269 (2019) 370-399.
[78] C.Y. Tang, T.H. Chong, A.G. Fane, Colloidal interactions and fouling of NF and RO membranes: A review, Adv. Colloid Interface Sci., 164 (2011) 126-143.
[79] T.V. Knyazkova, A.A. Maynarovich, Recognition of membrane fouling: testing of theoretical approaches with data on NF of salt solutions containing a low molecular weight surfactant as a foulant, Desalination, 126 (1999) 163-169.
[80] M. Gryta, Fouling in direct contact membrane distillation process, J. Membr. Sci., 325 (2008) 383-394.
[81] P. Wang, T.-S. Chung, Recent advances in membrane distillation processes: Membrane development, configuration design and application exploring, J. Membr. Sci., 474 (2015) 39-56.
[82] L. Eykens, K. De Sitter, C. Dotremont, L. Pinoy, B. Van der Bruggen, Membrane synthesis for membrane distillation: A review, Sep. Purif. Technol., (2017) 36-51.
[83] N.G.P. Chew, S. Zhao, R. Wang, Recent advances in membrane development for treating surfactant- and oil-containing feed streams via membrane distillation, Adv. Colloid Interface Sci., (2019) 102022.
[84] M.K. Alsebaeai, A.L. Ahmad, Membrane distillation: Progress in the improvement of dedicated membranes for enhanced hydrophobicity and desalination performance, J. Ind. Eng. Chem., 86 (2020) 13-34.
[85] M. Khayet, T. Matsuura, J. Mengual, Porous hydrophobic/hydrophilic composite membranes: Estimation of the hydrophobic-layer thickness, J. Membr. Sci., 266 (2005) 68-79.
[86] M. Khayet, C. Cojocaru, M.C. García-Payo, Experimental design and optimization of asymmetric flat-sheet membranes prepared for direct contact membrane distillation, J. Membr. Sci., 315 (2010) 234-245.
[87] D. Hou, G. Dai, H. Fan, J. Wang, C. Zhao, H. Huang, Effects of calcium carbonate nano-particles on the properties of PVDF/nonwoven fabric flat-sheet composite membranes for direct contact membrane distillation, Desalination, 347 (2014) 25-33.
[88] J. Zhu, L. Jiang, T. Matsuura, New insights into fabrication of hydrophobic/hydrophilic composite hollow fibers for direct contact membrane distillation, Chem. Eng. Sci., 137 (2015) 79-90.
[89] Y.C. Woo, Y. Kim, W.-G. Shim, L.D. Tijing, M. Yao, L.D. Nghiem, J.-S. Choi, S.-

H. Kim, H.K. Shon, Graphene/PVDF flat-sheet membrane for the treatment of RO brine from coal seam gas produced water by air gap membrane distillation, J. Membr. Sci., 513 (2016) 74-84.
[90] R. Zhou, D. Rana, T. Matsuura, C.Q. Lan, Effects of multi-walled carbon nanotubes (MWCNTs) and integrated MWCNTs/SiO2 nano-additives on PVDF polymeric membranes for vacuum membrane distillation, Sep. Purif. Technol., 217 (2019) 154-163.
[91] B.S. Lalia, E. Guillen, H.A. Arafat, R. Hashaikeh, Nanocrystalline cellulose reinforced PVDF-HFP membranes for membrane distillation application, Desalination, 332 (2014) 134-141.
[92] Y. Liao, R. Wang, A.G. Fane, Fabrication of bioinspired composite nanofiber membranes with robust superhydrophobicity for direct contact membrane distillation, Environ. Sci. Technol., 48 (2014) 6335-6341.
[93] A. Kyoungjin An, E.J. Lee, J. Guo, S. Jeong, J.G. Lee, N. Ghaffour, Enhanced vapor transport in membrane distillation via functionalized carbon nanotubes anchored into electrospun nanofibres, Sci. Rep., 7 (2017) 41562.
[94] M. Khayet, R. Wang, Mixed Matrix Polytetrafluoroethylene/Polysulfone Electrospun Nanofibrous Membranes for Water Desalination by Membrane Distillation, ACS Appl. Mater. Interfaces, 10 (2018) 24275-24287.
[95] H. Li, W. Shi, X. Zeng, S. Huang, H. Zhang, X. Qin, Improved desalination properties of hydrophobic GO-incorporated PVDF electrospun nanofibrous composites for vacuum membrane distillation, Sep. Purifi. Technol., 230 (2020) 115889.
[96] M. Khayet, J.I. Mengual, T. Matsuura, Porous hydrophobic/hydrophilic composite membranes, J. Membr. Sci., 252 (2005) 101-113.
[97] S. Simone, A. Figoli, A. Criscuoli, M.C. Carnevale, A. Rosselli, E. Drioli, Preparation of hollow fibre membranes from PVDF/PVP blends and their application in VMD, J. Membr. Sci., 364 (2010) 219-232.
[98] M. Baghbanzadeh, D. Rana, T. Matsuura, C.Q. Lan, Effects of hydrophilic CuO nanoparticles on properties and performance of PVDF VMD membranes, Desalination, 369 (2015) 75-84.
[99] J.E. Efome, M. Baghbanzadeh, D. Rana, T. Matsuura, C.Q. Lan, Effects of superhydrophobic SiO2 nanoparticles on the performance of PVDF flat sheet membranes for vacuum membrane distillation, Desalination, 373 (2015) 47-57.
[100] T.L.S. Silva, S. Morales-Torres, J.L. Figueiredo, A.M.T. Silva, Multi-walled carbon nanotube/PVDF blended membranes with sponge- and finger-like pores for direct contact membrane distillation, Desalination, 357 (2015) 233-245.
[101] S. Leaper, A. Abdel-Karim, B. Faki, J.M. Luque-Alled, M. Alberto, A. Vijayaraghavan, S.M. Holmes, G. Szekely, M.I. Badawy, N. Shokri, P. Gorgojo, Flux-enhanced PVDF mixed matrix membranes incorporating APTS-functionalized graphene oxide for membrane distillation, J. Membr. Sci., 554 (2018) 309-323.
[102] E.-J. Lee, A.K. An, T. He, Y.C. Woo, H.K. Shon, Electrospun nanofiber membranes incorporating fluorosilane-coated TiO2 nanocomposite for direct contact membrane distillation, J. Membr. Sci., 520 (2016) 145-154.
[103] Q. Huang, S. Gao, Y. Huang, M. Zhang, C. Xiao, Study on photothermal

PVDF/ATO nanofiber membrane and its membrane distillation performance, J. Membr. Sci., 582 (2019) 203-210.
[104] J.E. Efome, D. Rana, T. Matsuura, C.Q. Lan, Enhanced performance of PVDF nanocomposite membrane by nanofiber coating: A membrane for sustainable desalination through MD, Water Res., 89 (2016) 39-49.
[105] W. Zhang, Y. Li, J. Liu, B. Li, S. Wang, Fabrication of hierarchical poly (vinylidene fluoride) micro/nano-composite membrane with anti-fouling property for membrane distillation, J. Membr. Sci., 535 (2017) 258-267.
[106] Y.C. Woo, Y. Kim, M. Yao, L.D. Tijing, J.-S. Choi, S. Lee, S.-H. Kim, H.K. Shon, Hierarchical Composite Membranes with Robust Omniphobic Surface Using Layer-By-Layer Assembly Technique, Environ. Sci. Technol., 52 (2018) 2186-2196.
[107] Y. Liao, R. Wang, A.G. Fane, Engineering superhydrophobic surface on poly(vinylidene fluoride) nanofiber membranes for direct contact membrane distillation, J. Membr. Sci., 440 (2013) 77-87.
[108] L.-F. Ren, F. Xia, V. Chen, J. Shao, R. Chen, Y. He, TiO2 -FTCS modified superhydrophobic PVDF electrospun nanofibrous membrane for desalination by direct contact membrane distillation, Desalination, 423 (2017) 1-11.
[109] E. Shaulsky, S. Nejati, C. Boo, F. Perreault, C.O. Osuji, M. Elimelech, Post-fabrication modification of electrospun nanofiber mats with polymer coating for membrane distillation applications, J. Membr. Sci., 530 (2017) 158-165.
[110] L. Zhong, Z. Zhu, Y. Han, Q. Wang, D. Liu, F. Cui, B. Li, W. Wang, One-step nanotopography construction by polyaniline polymerization for a superhydrophobic nanofibrous membrane towards direct contact membrane distillation, Environ. Sci. Nano, (2019).
[111] L. Deng, H. Ye, X. Li, P. Li, J. Zhang, X. Wang, M. Zhu, B.S. Hsiao, Self-roughened omniphobic coatings on nanofibrous membrane for membrane distillation, Sep. Purif. Technol., 206 (2018) 14-25.
[112] A. Rastegarpanah, H.R. Mortaheb, Surface treatment of polyethersulfone membranes for applying in desalination by direct contact membrane distillation, Desalination, 377 (2016) 99-107.
[113] S. Cong, F. Guo, Janus Nanofibrous Membranes for Desalination by Air Gap Membrane Distillation, ACS Appl. Polym. Mater., (2019).
[114] X.-Q. Wu, X. Wu, T.-Y. Wang, L. Zhao, Y.B. Truong, D. Ng, Y.-M. Zheng, Z. Xie, Omniphobic surface modification of electrospun nanofiber membrane via vapor deposition for enhanced anti-wetting property in membrane distillation, J. Membr. Sci., 606 (2020) 118075.
[115] Y. Chul Woo, Y. Chen, L.D. Tijing, S. Phuntsho, T. He, J.-S. Choi, S.-H. Kim, H. Kyong Shon, CF4 plasma-modified omniphobic electrospun nanofiber membrane for produced water brine treatment by membrane distillation, J. Membr. Sci., 529 (2017) 234-242.
[116] C. Yang, X.-M. Li, J. Gilron, D.-f. Kong, Y. Yin, Y. Oren, C. Linder, T. He, CF_4 plasma-modified superhydrophobic PVDF membranes for direct contact membrane distillation, J. Membr. Sci., 456 (2014) 155-161.
[117] F. Zhao, Z. Ma, K. Xiao, C. Xiang, H. Wang, X. Huang, S. Liang, Hierarchically

textured superhydrophobic polyvinylidene fluoride membrane fabricated via nanocasting for enhanced membrane distillation performance, Desalination, 443 (2018) 228-236.
[118] Z. Xiao, R. Zheng, Y. Liu, H. He, X. Yuan, Y. Ji, D. Li, H. Yin, Y. Zhang, X.M. Li, T. He, Slippery for scaling resistance in membrane distillation: A novel porous micropillared superhydrophobic surface, Water Res., 155 (2019) 152-161.
[119] J.A. Kharraz, M.U. Farid, N.K. Khanzada, B.J. Deka, H.A. Arafat, A.K. An, Macro-corrugated and nano-patterned hierarchically structured superomniphobic membrane for treatment of low surface tension oily wastewater by membrane distillation, Water Res., 174 (2020) 115600.
[120] Y. Liu, J. Wang, Z. Xiao, L. Liu, D. Li, X. Li, H. Yin, T. He, Anisotropic performance of a superhydrophobic polyvinyl difluoride membrane with corrugated pattern in direct contact membrane distillation, Desalination, 481 (2020) 114363.
[121] Y. Chen, R. Zheng, J. Wang, Y. Liu, Y. Wang, X.-M. Li, T. He, Laminated PTFE membranes to enhance the performance in direct contact membrane distillation for high salinity solution, Desalination, 424 (2017) 140-148.
[122] A.L. McGaughey, P. Karandikar, M. Gupta, A.E. Childress, Hydrophobicity versus Pore Size: Polymer Coatings to Improve Membrane Wetting Resistance for Membrane Distillation, ACS Appl. Polym. Mater., 2 (2020) 1256-1267.
[123] G.R. Guillen, Y. Pan, M. Li, E.M.V. Hoek, Preparation and Characterization of Membranes Formed by Nonsolvent Induced Phase Separation: A Review, Ind. Eng. Chem. Res., 50 (2011) 3798-3817.
[124] D. Hou, H. Fan, Q. Jiang, J. Wang, X. Zhang, Preparation and characterization of PVDF flat-sheet membranes for direct contact membrane distillation, Sep. Purif. Technol., 135 (2014) 211-222.
[125] K.-J. Lu, J. Zuo, T.-S. Chung, Novel PVDF membranes comprising n-butylamine functionalized graphene oxide for direct contact membrane distillation, J. Membr. Sci., 539 (2017) 34-42.
[126] D. Sun, M.-Q. Liu, J.-H. Guo, J.-Y. Zhang, B.-B. Li, D.-Y. Li, Preparation and characterization of PDMS-PVDF hydrophobic microporous membrane for membrane distillation, Desalination, 370 (2015) 63-71.
[127] J. Zhang, Z. Song, B. Li, Q. Wang, S. Wang, Fabrication and characterization of superhydrophobic poly (vinylidene fluoride) membrane for direct contact membrane distillation, Desalination, 324 (2013) 1-9.
[128] D. Zhao, J. Zuo, K.-J. Lu, T.-S. Chung, Fluorographite modified PVDF membranes for seawater desalination via direct contact membrane distillation, Desalination, 413 (2017) 119-126.
[129] H. Yan, X. Lu, C. Wu, X. Sun, W. Tang, Fabrication of a super-hydrophobic polyvinylidene fluoride hollow fiber membrane using a particle coating process, J. Membr. Sci., 533 (2017) 130-140.
[130] S. Nejati, C. Boo, C.O. Osuji, M. Elimelech, Engineering flat sheet microporous PVDF films for membrane distillation, J. Membr. Sci., 492 (2015) 355-363.
[131] L. Zheng, J. Wang, Z. Wu, J. Li, Y. Zhang, M. Yang, Y. Wei, Preparation of Interconnected Biomimetic Poly(vinylidene fluoride-co-chlorotrifluoroethylene)

Hydrophobic Membrane by Tuning the Two-Stage Phase Inversion Process, ACS Appl. Mater. Interfaces, 8 (2016) 32604-32615.
[132] F.E. Ahmed, B.S. Lalia, R. Hashaikeh, A review on electrospinning for membrane fabrication: Challenges and applications, Desalination, 356 (2015) 15-30.
[133] C.-Y. Pan, G.-R. Xu, K. Xu, H.-L. Zhao, Y.-Q. Wu, H.-C. Su, J.-M. Xu, R. Das, Electrospun nanofibrous membranes in membrane distillation: Recent developments and future perspectives, Sep. Purif. Technol., 221 (2019) 44-63.
[134] F. Yalcinkaya, A review on advanced nanofiber technology for membrane distillation, J. Eng. Fibers Fabr., 14 (2019) 1-12.
[135] Y. Liao, C.H. Loh, R. Wang, A.G. Fane, Electrospun superhydrophobic membranes with unique structures for membrane distillation, ACS Appl. Mater. interfaces, 6 (2014) 16035-16048.
[136] E.-J. Lee, A.K. An, P. Hadi, S. Lee, Y.C. Woo, H.K. Shon, Advanced multi-nozzle electrospun functionalized titanium dioxide/polyvinylidene fluoride-co-hexafluoropropylene (TiO 2 /PVDF-HFP) composite membranes for direct contact membrane distillation, J. Membr. Sci., 524 (2017) 712-720.
[137] M. Reza Shirzad Kebria, Ahmad Rahimpour, Saeed Khoshhal Salestan, S. Fatemeh Seyedpour, Arman Jafari, Fatemeh Banisheykholeslami, Naser Tavajohi Hassan Kiadeh, Hyper-branched dendritic structure modified PVDF electrospun membranes for air gap membrane distillation, Desalination, 479 (2020) 114307.
[138] E.J. Lee, B.J. Deka, J. Guo, Y.C. Woo, H.K. Shon, A.K. An, Engineering the Re-Entrant Hierarchy and Surface Energy of PDMS-PVDF Membrane for Membrane Distillation Using a Facile and Benign Microsphere Coating, Environ. Sci. Technol. 51 (2017) 10117-10126.
[139] C. Su, T. Horseman, H. Cao, K.S.S. Christie, Y. Li, S. Lin, Robust Superhydrophobic Membrane for Membrane Distillation with Excellent Scaling Resistance, Environ. Sci. Technol., 53 (2019) 11801-11809.
[140] L. Zhao, C. Wu, X. Lu, D. Ng, Y.B. Truong, Z. Xie, Activated carbon enhanced hydrophobic/hydrophilic dual-layer nanofiber composite membranes for high-performance direct contact membrane distillation, Desalination, 446 (2018) 59-69.
[141] M. Khayet, C. García-Payo, T. Matsuura, Superhydrophobic nanofibers electrospun by surface segregating fluorinated amphiphilic additive for membrane distillation, J. Membr. Sci., 588 (2019) 117215.
[142] S.S. Ray, S.-S. Chen, N.C. Nguyen, H.-T. Hsu, H.T. Nguyen, C.-T. Chang, Poly(vinyl alcohol) incorporated with surfactant based electrospun nanofibrous layer onto polypropylene mat for improved desalination by using membrane distillation, Desalination, 414 (2017) 18-27.
[143] H. Attia, S. Alexander, C.J. Wright, N. Hilal, Superhydrophobic electrospun membrane for heavy metals removal by air gap membrane distillation (AGMD), Desalination, 420 (2017) 318-329.
[144] Z. Zhu, Z. Liu, L. Zhong, C. Song, W. Shi, F. Cui, W. Wang, Breathable and asymmetrically superwettable Janus membrane with robust oil-fouling resistance for durable membrane distillation, J. Membr. Sci., 563 (2018) 602-609.
[145] A.K. An, J. Guo, E.-J. Lee, S. Jeong, Y. Zhao, Z. Wang, T. Leiknes, PDMS/PVDF

hybrid electrospun membrane with superhydrophobic property and drop impact dynamics for dyeing wastewater treatment using membrane distillation, J. Membr. Sci., 525 (2017) 57-67.
[146] X. Li, M.C. Garcia-Payo, M. Khayet, M. Wang, X. Wang, Superhydrophobic polysulfone/polydimethylsiloxane electrospun nanofibrous membranes for water desalination by direct contact membrane distillation, J. Membr. Sci., 542 (2017) 308-319.
[147] L. Deng, P. Li, K. Liu, X. Wang, B.S. Hsiao, Robust superhydrophobic dual layer nanofibrous composite membranes with a hierarchically structured amorphous polypropylene skin for membrane distillation, J. Mater. Chem. A, 7 (2019) 11282-11297.
[148] C. Boo, J. Lee, M. Elimelech, Omniphobic Polyvinylidene Fluoride (PVDF) Membrane for Desalination of Shale Gas Produced Water by Membrane Distillation, Environ. Sci. Technol., 50 (2016) 12275-12282.
[149] R. Zheng, Y. Chen, J. Wang, J. Song, X.-M. Li, T. He, Preparation of omniphobic PVDF membrane with hierarchical structure for treating saline oily wastewater using direct contact membrane distillation, J. Membr. Sci., 555 (2018) 197-205.
[150] H. Qiu, Y. Peng, L. Ge, B. Villacorta Hernandez, Z. Zhu, Pore channel surface modification for enhancing anti-fouling membrane distillation, Appl. Surf. Sci., 443 (2018) 217-226.
[151] A. Figoli, C. Ursino, F. Galiano, E. Di Nicolò, P. Campanelli, M.C. Carnevale, A. Criscuoli, Innovative hydrophobic coating of perfluoropolyether (PFPE) on commercial hydrophilic membranes for DCMD application, J. Membr. Sci., 522 (2017) 192-201.
[152] Y. Zhang, X. Wang, Z. Cui, E. Drioli, Z. Wang, S. Zhao, Enhancing wetting resistance of poly(vinylidene fluoride) membranes for vacuum membrane distillation, Desalination, 415 (2017) 58-66.
[153] M. Li, K.J. Lu, L. Wang, X. Zhang, T.-S. Chung, Janus membranes with asymmetric wettability via a layer-by-layer coating strategy for robust membrane distillation, J. Membr. Sci., 603 (2020) 118031.
[154] E.-J. Lee, B.J. Deka, A.K. An, Reinforced superhydrophobic membrane coated with aerogel-assisted polymeric microspheres for membrane distillation, J. Membr. Sci., 573 (2019) 570-578.
[155] S. Lin, S. Nejati, C. Boo, Y. Hu, C.O. Osuji, M. Elimelech, Omniphobic Membrane for Robust Membrane Distillation, Environ. Sci. Technol. Lett., 1 (2014) 443-447.
[156] M.E. Leitch, C. Li, O. Ikkala, M.S. Mauter, G.V. Lowry, Bacterial Nanocellulose Aerogel Membranes: Novel High-Porosity Materials for Membrane Distillation, Environ. Sci. Technol. Lett., 3 (2016) 85-91.
[157] D. Hou, T. Li, X. Chen, S. He, J. Dai, S.A. Mofid, D. Hou, A. Iddya, D. Jassby, R. Yang, Hydrophobic nanostructured wood membrane for thermally efficient distillation, Sci. Adv., 5 (2019) 3203.
[158] J.H. Kim, S.H. Park, M.J. Lee, S.M. Lee, W.H. Lee, K.H. Lee, N.R. Kang, H.J. Jo, J.F. Kim, E. Drioli, Y.M. Lee, Thermally rearranged polymer membranes for

desalination, Energy Environ. Sci., 9 (2016) 878-884.
[159] B.L. Pangarkar, S.K. Deshmukh, V.S. Sapkal, R.S. Sapkal, Review of membrane distillation process for water purification, Desalin. Water Treat., 57 (2014) 2959-2981.
[160] E. Drioli, A. Ali, F. Macedonio, Membrane distillation: Recent developments and perspectives, Desalination, 356 (2015) 56-84.
[161] N. Ghaffour, S. Soukane, J.G. Lee, Y. Kim, A. Alpatova, Membrane distillation hybrids for water production and energy efficiency enhancement: A critical review, Appl. Energ., 254 (2019) 113698.
[162] M.R. Qtaishat, F. Banat, Desalination by solar powered membrane distillation systems, Desalination, 308 (2013) 186-197.
[163] R.B. Saffarini, E.K. Summers, H.A. Arafat, J.H. Lienhard V, Technical evaluation of stand-alone solar powered membrane distillation systems, Desalination, 286 (2012) 332-341.
[164] N. Dow, S. Gray, J.-d. Li, J. Zhang, E. Ostarcevic, A. Liubinas, P. Atherton, G. Roeszler, A. Gibbs, M. Duke, Pilot trial of membrane distillation driven by low grade waste heat: Membrane fouling and energy assessment, Desalination, 391 (2016) 30-42.
[165] R.G. Raluy, R. Schwantes, V.J. Subiela, B. Peñate, G. Melián, J.R. Betancort, Operational experience of a solar membrane distillation demonstration plant in Pozo Izquierdo-Gran Canaria Island (Spain), Desalination, 290 (2012) 1-13.
[166] E. Guillén-Burrieza, G. Zaragoza, S. Miralles-Cuevas, J. Blanco, Experimental evaluation of two pilot-scale membrane distillation modules used for solar desalination, J. Membr. Sci., 409-410 (2012) 264-275.
[167] G. Zaragoza, A. Ruiz-Aguirre, E. Guillén-Burrieza, Efficiency in the use of solar thermal energy of small membrane desalination systems for decentralized water production, Appl. Energ., 130 (2014) 491-499.
[168] X. Ji, E. Curcio, S. Al Obaidani, G. Di Profio, E. Fontananova, E. Drioli, Membrane distillation-crystallization of seawater reverse osmosis brines, Sep. Purif. Technol., 71 (2010) 76-82.
[169] S. Adham, A. Hussain, J.M. Matar, R. Dores, A. Janson, Application of Membrane Distillation for desalting brines from thermal desalination plants, Desalination, 314 (2013) 101-108.
[170] H.C. Duong, A.R. Chivas, B. Nelemans, M. Duke, S. Gray, T.Y. Cath, L.D. Nghiem, Treatment of RO brine from CSG produced water by spiral-wound air gap membrane distillation — A pilot study, Desalination, 366 (2015) 121-129.
[171] J.A. Bush, J. Vanneste, T.Y. Cath, Membrane distillation for concentration of hypersaline brines from the Great Salt Lake: Effects of scaling and fouling on performance, efficiency, and salt rejection, Sep. Purif. Technol., 170 (2016) 78-91.
[172] J.A. Sanmartino, M. Khayet, M.C. García-Payo, H. El-Bakouri, A. Riaza, Treatment of reverse osmosis brine by direct contact membrane distillation: Chemical pretreatment approach, Desalination, 420 (2017) 79-90.
[173] A. Kullab, A. Martin, Membrane distillation and applications for water purification in thermal cogeneration plants, Sep. Purif. Technol., 76 (2011) 231-237.
[174] S. Jamaly, A. Giwa, S.W. Hasan, Recent improvements in oily wastewater treatment: Progress, challenges, and future opportunities, J. Environ. Sci., 37 (2015)

15-30.
[175] B.B. Ashoor, S. Mansour, A. Giwa, V. Dufour, S.W. Hasan, Principles and applications of direct contact membrane distillation (DCMD): A comprehensive review, Desalination, 398 (2016) 222-246.
[176] C. Boo, J. Lee, M. Elimelech, Engineering Surface Energy and Nanostructure of Microporous Films for Expanded Membrane Distillation Applications, Environ. Sci. Technol., 50 (2016) 8112-8119.
[177] M. Yao, L.D. Tijing, G. Naidu, S.-H. Kim, H. Matsuyama, A.G. Fane, H.K. Shon, A review of membrane wettability for the treatment of saline water deploying membrane distillation, Desalination, 479 (2020) 114312.
[178] M.I. Siyal, C.K. Lee, C. Park, A.A. Khan, J.O. Kim, A review of membrane development in membrane distillation for emulsified industrial or shale gas wastewater treatments with feed containing hybrid impurities, J. Environ. Manage., 243 (2019) 45-66.
[179] F. Ricceri, M. Giagnorio, G. Farinelli, G. Blandini, M. Minella, D. Vione, A. Tiraferri, Desalination of Produced Water by Membrane Distillation: Effect of the Feed Components and of a Pre-treatment by Fenton Oxidation, Sci. Rep., 9 (2019) 12.
[180] Q.Y. Li, B.Y. Lian, W.W. Zhong, A. Omar, A. Razmjou, P. Dai, J. Guan, G. Leslie, R.A. Taylor, Improving the performance of vacuum membrane distillation using a 3D-printed helical baffle and a superhydrophobic nanocomposite membrane, Sep. Purif. Technol., 248 (2020) 11.
[181] S. Tavakkoli, O. Lokare, R. Vidic, V. Khanna, Shale gas produced water management using membrane distillation: An optimization-based approach, Resour. Conserv. Recycl., 158 (2020) 13.
[182] Y.X. Du, D. Wang, W. Wang, J.J. Fu, X.M. Chen, L.J. Wang, W. Yang, X. Zhang, Electrospun Nanofibrous Polyphenylene Oxide Membranes for High-Salinity Water Desalination by Direct Contact Membrane Distillation, ACS Sustain. Chem. Eng., 7 (2019) 20060-20069.
[183] P.P. Zolotarev, V.V. Ugrozov, I.B. Volkina, V.N. Nikulin, Treatment of wastewater for removing heavy metals by membrane distillation, J. Hazard. Mater., 37 (1994) 77-82.
[184] A. Criscuoli, E. Rossi, F. Cofone, E. Drioli, Boron removal by membrane contactors: the water that purifies water, Clean Technol. Envir., 12 (2009) 53-61.
[185] C. Teng-Chien, H. Gaw-Hao, C. Chuh-Shun, H. Yao-Hui, Reducing industrial wastewater and recovery of gold by direct contact membrane distillation with electrolytic system, Sustain. Environ. Res., 23 (2013) 209-214.
[186] X. Wen, F. Li, X. Zhao, Removal of nuclides and boron from highly saline radioactive wastewater by direct contact membrane distillation, Desalination, 394 (2016) 101-107.
[187] I.V. Korolkov, A.B. Yeszhanov, M.V. Zdorovets, Y.G. Gorin, O. Güven, S.S. Dosmagambetova, N.A. Khlebnikov, K.V. Serkov, M.V. Krasnopyorova, O.S. Milts, D.A. Zheltov, Modification of PET ion track membranes for membrane distillation of low-level liquid radioactive wastes and salt solutions, Sep. Purif. Technol., 227 (2019) 115694.

[188] X.Y. Lou, Z. Xu, A.P. Bai, M. Resina-Gallego, Z.G. Ji, Separation and Recycling of Concentrated Heavy Metal Wastewater by Tube Membrane Distillation Integrated with Crystallization, Membranes, 10 (2020).
[189] M. Khayet, Treatment of radioactive wastewater solutions by direct contact membrane distillation using surface modified membranes, Desalination, 321 (2013) 60-66.
[190] H. Liu, J. Wang, Treatment of radioactive wastewater using direct contact membrane distillation, J. Hazard. Mater., 261 (2013) 307-315.
[191] H. Ramlow, R.A.F. Machado, C. Marangoni, Direct contact membrane distillation for textile wastewater treatment: a state-of-the-art review, Water Sci. Technol., 76 (2017) 2565-2579.
[192] F. Banat, S. Al-Asheh, M. Qtaishat, Treatment of waters colored with methylene blue dye by vacuum membrane distillation, Desalination, 174 (2005) 87-96.
[193] A. Criscuoli, J. Zhong, A. Figoli, M.C. Carnevale, R. Huang, E. Drioli, Treatment of dye solutions by vacuum membrane distillation, Water Res., 42 (2008) 5031-5037.
[194] H. Li, X. Feng, W. Shi, H. Zhang, Q. Du, L. Qin, X. Qin, Dye removal using hydrophobic polyvinylidene fluoride hollow fibre composite membrane by vacuum membrane distillation, Color. Technol., 135 (2019) 451-466.
[195] S. Parakala, S. Moulik, S. Sridhar, Effective separation of methylene blue dye from aqueous solutions by integration of micellar enhanced ultrafiltration with vacuum membrane distillation, Chem. Eng. J., 375 (2019) 122015.
[196] N.P. Khumalo, L.N. Nthunya, E. De Canck, S. Derese, A.R. Verliefde, A.T. Kuvarega, B.B. Mamba, S.D. Mhlanga, D.S. Dlamini, Congo red dye removal by direct membrane distillation using PVDF/PTFE membrane, Sep. Purif. Technol., 211 (2019) 578-586.
[197] M.C. Garcıa-Payo, M.A. Izquierdo-Gil, C. Fernández-Pineda, Air gap membrane distillation of aqueous alcohol solutions, J. Membr. Sci., 169 (2000) 61-80.
[198] A. Kujawska, J.K. Kujawski, M. Bryjak, M. Cichosz, W. Kujawski, Removal of volatile organic compounds from aqueous solutions applying thermally driven membrane processes. 2. Air gap membrane distillation, J. Membr. Sci., 499 (2016) 245-256.
[199] W. Intrchom, S. Roy, S. Mitra, Functionalized carbon nanotube immobilized membrane for low temperature ammonia removal via membrane distillation, Sep. Purif. Technol., 235 (2020) 116188.
[200] R. Thiruvenkatachari, M. Manickam, T.O. Kwon, I.S. Moon, J.W. Kim, Separation of water and nitric acid with porous hydrophobic membrane by air gap membrane distillation (AGMD), Sep. Sci. Technol., 41 (2006) 3187-3199.
[201] N. Qureshi, M.M. Meagher, R.W. Hutkins, Recovery of 2,3-butanediol by vacuum membrane distillation, Sep. Sci. Technol., 29 (1994) 1733-1748.
[202] M. Tomaszewska, A. Mientka, Separation of HCl from HCl–H2SO4 solutions by membrane distillation, Desalination, 240 (2009) 244-250.
[203] G. Lewandowicz, W. Białas, B. Marczewski, D. Szymanowska, Application of membrane distillation for ethanol recovery during fuel ethanol production, J. Membr. Sci., 375 (2011) 212-219.

[204] M. Tomaszewska, L. Bialoñczyk, The investigation of ethanol separation by the membrane distillation process, Pol. J. Chem. Technol., 13 (2011) 66-69.
[205] P.M. Duyen, P. Jacob, R. Rattanaoudom, C. Visvanathan, Feasibility of sweeping gas membrane distillation on concentrating triethylene glycol from waste streams, Chem. Eng. Process, 110 (2016) 225-234.
[206] D. Qu, D. Sun, H. Wang, Y. Yun, Experimental study of ammonia removal from water by modified direct contact membrane distillation, Desalination, 326 (2013) 135-140.
[207] R. Bagger-Jørgensen, A.S. Meyer, C. Varming, G. Jonsson, Recovery of volatile aroma compounds from black currant juice by vacuum membrane distillation, J. Food Eng., 64 (2004) 23-31.
[208] S. Al-Asheh, F. Banat, M. Qtaishat, M. Al-Khateeb, Concentration of sucrose solutions via vacuum membrane distillation, Desalination, 195 (2006) 60-68.
[209] A. Hausmann, P. Sanciolo, T. Vasiljevic, M. Weeks, K. Schroën, S. Gray, M. Duke, Fouling of dairy components on hydrophobic polytetrafluoroethylene (PTFE) membranes for membrane distillation, J. Membr. Sci., 442 (2013) 149-159.
[210] P. Onsekizoglu, Production of high quality clarified pomegranate juice concentrate by membrane processes, J. Membr. Sci., 442 (2013) 264-271.
[211] K. Kezia, J. Lee, M. Weeks, S. Kentish, Direct contact membrane distillation for the concentration of saline dairy effluent, Water Res., 81 (2015) 167-177.
[212] D. Woldemariam, A. Kullab, U. Fortkamp, J. Magner, H. Royen, A. Martin, Membrane distillation pilot plant trials with pharmaceutical residues and energy demand analysis, Chem. Eng. J., 306 (2016) 471-483.
[213] N. Tang, Q. Jia, H. Zhang, J. Li, S. Cao, Preparation and morphological characterization of narrow pore size distributed polypropylene hydrophobic membranes for vacuum membrane distillation via thermally induced phase separation, Desalination, 256 (2010) 27-36.
[214] C. Fang, W. Liu, P. Zhang, S. Rajabzadeh, N. Kato, Y. Sasaki, H.K. Shon, H. Matsuyama, Hollow fiber membranes with hierarchical spherulite surface structure developed by thermally induced phase separation using triple-orifice spinneret for membrane distillation, J. Membr. Sci., 618 (2020) 118586.
[215] N. Tang, C. Feng, H. Han, X. Hua, L. Zhang, J. Xiang, P. Cheng, W. Du, X. Wang, High permeation flux polypropylene/ethylene vinyl acetate co-blending membranes via thermally induced phase separation for vacuum membrane distillation desalination, Desalination, 394 (2016) 44-55.
[216] J. Zhao, L. Shi, C.H. Loh, R. Wang, Preparation of PVDF/PTFE hollow fiber membranes for direct contact membrane distillation via thermally induced phase separation method, Desalination, 430 (2018) 86-97.
[217] L. Eykens, K. De Sitter, C. Dotremont, L. Pinoy, B. Van der Bruggen, Characterization and performance evaluation of commercially available hydrophobic membranes for direct contact membrane distillation, Desalination, 392 (2016) 63-73.
[218] K. Li, Y. Zhang, L. Xu, F. Zeng, D. Hou, J. Wang, Optimizing stretching conditions in fabrication of PTFE hollow fiber membrane for performance improvement in membrane distillation, J. Membr. Sci., 550 (2018) 126-135.

[219] I. Ochoa, S.G. Hatzikiriakos, Paste extrusion of polytetrafluoroethylene (PTFE): Surface tension and viscosity effects, Powder Technol., 153 (2005) 108-118.
[220] S. Kalla, S. Upadhyaya, K. Singh, R. Baghel, Experimental and mathematical study of air gap membrane distillation for aqueous HCl azeotropic separation, J. Chem. Technol. Biotechnol., 94 (2019) 63-78.
[221] F.A. Banat, F.A. Al-Rub, R. Jumah, M. Shannag, On the effect of inert gases in breaking the formic acid–water azeotrope by gas-gap membrane distillation, Chem. Eng. J., 73 (1999) 37-42.
[222] F.A. Banat, F.A. Al-Rub, R. Jumah, M. Shannag, Theoretical investigation of membrane distillation role in breaking the formic acid-water azeotropic point: comparison between Fickian and Stefan-Maxwell-based models, Int. Commun. Heat. Mass, 26 (1999) 879-888.
[223] H. Udriot, A. Araque, U. Von Stockar, Azeotropic mixtures may be broken by membrane distillation, Chem. Eng. J. Biochem. Eng. J., 54 (1994) 87-93.
[224] L. Zheng, Z. Wu, Y. Wei, Y. Zhang, Y. Yuan, J. Wang, Preparation of PVDF-CTFE hydrophobic membranes for MD application: Effect of LiCl-based mixed additives, J. Membr. Sci., 506 (2016) 71-85.
[225] X. Feng, L.Y. Jiang, T. Matsuura, P. Wu, Fabrication of hydrophobic/hydrophilic composite hollow fibers for DCMD: Influence of dope formulation and external coagulant, Desalination, 401 (2017) 53-63.
[226] T.A. Agbaje, S. Al-Gharabli, M.O. Mavukkandy, J. Kujawa, H.A. Arafat, PVDF/magnetite blend membranes for enhanced flux and salt rejection in membrane distillation, Desalination, 436 (2018) 69-80.
[227] L. Zheng, J. Wang, J. Li, Y. Zhang, K. Li, Y. Wei, Preparation, evaluation and modification of PVDF-CTFE hydrophobic membrane for MD desalination application, Desalination, 402 (2017) 162-172.
[228] Minwei Yao, Jiawei Ren, Nawshad Akther, Yun Chul Woo, Leonard D. Tijing, Seung-Hyun Kim, H.K. Shon, Improving membrane distillation performance: morphology optimization of hollow fiber membranes with selected non-solvent in dope solution, Chemosphere, (2019).
[229] H. Fan, A. Gao, G. Zhang, S. Zhao, J. Cui, Y. Yan, A facile strategy towards developing amphiphobic polysulfone membrane with double Re-entrant structure for membrane distillation, J. Membr. Sci., 602 (2020) 117933.

Chapter 2 Materials and methods

2.1 Preparation of PVDF coated 3D printed membranes via dip-coating

2.1.1 Materials and chemicals

Polyamide-12 powder (PA2200) with an average diameter of 59 μm was supplied by EOS GmbH (Germany). For the 3D printed (3DP) membrane preparation, 30% recycled powders from previous printing process mixed with new powders were used. Polyvinylidene fluoride (PVDF, Solef® 1015/1001, Mw: 570,000-600,000 Da) was purchased from Solvay. The organic solvent n-methyl-2-pyrrolidone (NMP, ≥99%) was obtained from Honeywell. Tap water was used as the coagulation bath during the NIPS process. Deionized (DI) water was used to rinse and store the prepared membranes.

2.1.2 Preparation of PVDF coated 3DP composite membranes

2.1.2.1 Synthesis of 3DP membranes by laser sintering

Laser sintering (LS) of PA powders was carried out on a DTM Sinterstation 2000, and the printing process was conducted in nitrogen atmosphere. Before the printing process, the powder bed was preheated to 173 °C. When the pre-set temperature was reached, the laser scanned the powder bed according to the designed CAD model. After the printing process finished, the build platform temperature decreased slowly to room temperature to avoid shrinkage and distortion of the printed products. In this work, the operation parameters were fixed at a laser power of 15 W, hatch space of 0.15 mm, scanning count of 1, and a scanning speed of 1000 mm/s. Seven circular membranes with a diameter of 8 cm were printed in one batch, as depicted in Figure 2.1. The printed membranes were rinsed in deionized (DI) water to clear away residual powder on the surface. Finally, the 3DP membranes were dried at room temperature for further modification.



Figure 2.1 A photo of the 3D printed PA membranes in the laser sintering (LS) printer. The diameter of the circular membranes is 8 cm.

2.1.2.2 Fabrication of PVDF@3DP composite membranes

Before the dip-coating experiments, PVDF solutions with concentrations of 3 wt.%, 5 wt.%, 7 wt.%, 10 wt.%, 12 wt.%, and 15 wt.% were prepared, and a small piece of 3DP membrane was immersed into these solutions for 1 min to check the operational feasibility. Results showed that the 3 wt.% solution was difficult to retained on the sample surface due to its low viscosity, while the 12 wt.% and 15 wt.% solutions were too viscous and it took a long time for the entire membrane to be coated. Additionally, the sample pieces coated by these two high viscous solutions were too thick, which was not desired in MD as a thick membrane usually leads to a low flux. Thus, the concentrations of 5 wt.%, 7 wt.%, and 10 wt.% were chosen for the subsequent experiments. To determine the immersion times, a piece of 3DP membrane (the circle membrane with a diameter of 8 cm) was immersed into the 10 wt.% solution (the highest viscosity among these three solutions) to check the time needed for the entire membrane to be totally immersed into the solution, and the result was 12 s. Therefore, the shortest immersion time of 15 s was chosen by extending a short period for solution penetration. Then, the immersion time was doubled (30 s, 60 s, and 120 s) to investigate the influence of the immersion time.

The 3DP membranes were modified with PVDF dope solutions via dip-coating followed by NIPS, as illustrated in Figure 2.2. Firstly, PVDF/NMP dope solutions with

different PVDF concentrations (5 wt.%, 7 wt.%, 10 wt.%) were prepared by magnetic agitation at room temperature, then the solutions were left for 4 h for degassing. During the dip-coating process, the 3DP membranes were immersed in the PVDF solutions for a given time (15 s, 30 s, 60 s, and 120 s). Subsequently, the membranes were pulled out from the polymer solution and hung up for 1.5 min, followed by rotating the membranes upside-down for another 1.5 min for redundant PVDF solution on the surface to drip off. Ultimately, the prepared membranes were soaked in water for PVDF layers solidification. The composite membranes were labeled as PVDF@3DP-x-y, in which the x and y refers to the PVDF concentration and immersion time, respectively.

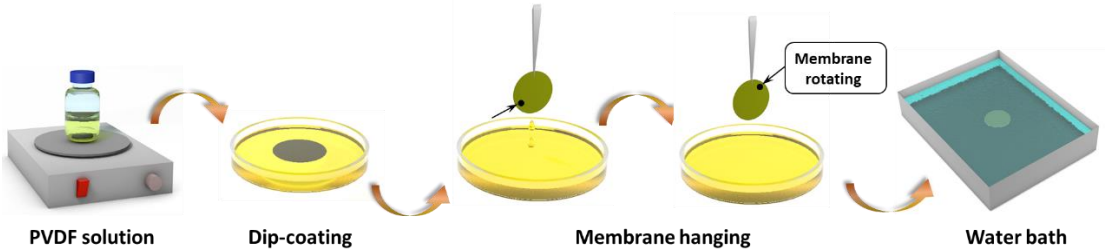


Figure 2.2 Schematic illustration of preparing PVDF@3DP composite membranes

2.2 Preparation of PVDF membranes using a novel bottom-up method

2.2.1 Chemicals and materials

Polyvinylidene fluoride (PVDF, Solef® 1015/1001, Mw: 570,000-600,000 Da) was purchased from Solvay. NMP (AR, ≥99%) was obtained from Honeywell. Novatexx 2471 non-woven support was provided by Freudenberg Performance Materials. Tap water was used as the coagulation bath during the NIPS process. DI water was used to rinse and store the prepared membranes.

2.2.2 Membrane preparation

The membranes were constructed through a “bottom-up” method, as shown in Figure 2.3. Firstly, a certain amount of PVDF was dissolved in NMP under mechanical stirring for 24 h to achieve a uniform solution. Secondly, the solution was allowed to

stand for 4 h for degasification. Thirdly, the polymer solution was cast onto a clean glass plate by a casting knife with 330 μm thickness. Afterward, a piece of non-woven was carefully placed on the nascent film, which was then soaked in the water bath. Due to the viscosity of the polymer solution, the PVDF membrane and the non-woven substrate attached together, and the surface delaminated from the glass plate turned to be the top surface of the prepared membrane. The resultant membranes were left in water for at least 12 h for complete release of solvent. As a contrast, the normal casting membrane, labeled as PVDF-N, was prepared via directly casting on the non-woven substrate with 15 wt.% PVDF solution using the same casting knife gap.

The most used PVDF concentrations for membrane preparation by NIPS process in the literature range from 12 wt.% to 20 wt.% (references in chapter 1 [55, 57, 59, 87, 90, 97-101, 105]). For the bottom-up method, a piece of non-woven covered the nascent polymer solution layer; thus, a dilute polymer solution could not maintain the homogeneous layer (the non-woven was not covered by the polymer solution in some positions) after non-woven coverage (such as 12-14 wt.%). Therefore, a 15 wt.% concentration was chosen as the lowest concentration. Moreover, an 18 wt.% solution with a higher viscosity was chosen to investigate the influence of solution viscosity on the membrane morphology. During the membrane preparation process with the 18 wt.% solution, it took more than ten minutes before the membrane separated from the glass plate; thus, this concentration was used as the highest concentration due to the purpose of developing a facile and time-saving method. In addition, a 16.5 wt.% solution was chosen as a medial concentration. The prepared bottom-up membranes with different PVDF concentrations (15 wt.%, 16.5 wt.%, and 18 wt.%) were labeled as PVDF-15, PVDF-16.5, and PVDF-18, respectively.

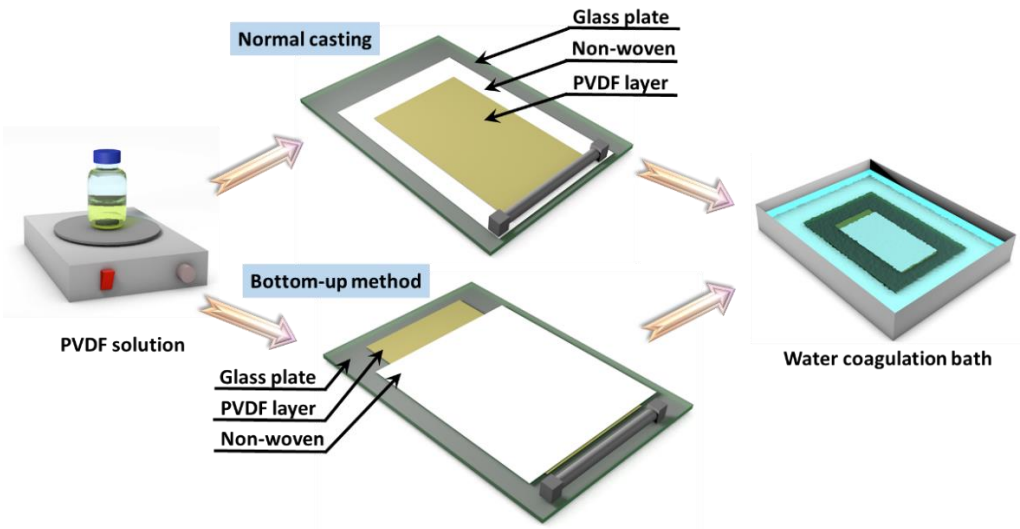


Figure 2.3 Schematic of the normal casting and bottom-up casting procedures

2.3 Fabrication of PVDF membranes by co-casting

2.3.1 Chemicals and materials

Polyvinylidene fluoride (PVDF, Solef® 1015/1001) and polyethersulfone (PES, Veradel® 3000P) were supplied by Solvay. NMP (AR, ≥99%) and dimethyl sulfoxide (DMSO, AR, ≥99%) were purchased from Sinopharm. Novatexx 2471 non-woven support was provided by Freudenberg Performance Materials. Tap water was used as the coagulation bath during the phase separation process. DI water was used to rinse and store the prepared membranes.

2.3.2 Membrane preparation

Similar to the membrane preparation in the bottom-up method, a PES layer was co-cast to cover the underlying PVDF solution layer; thus, a dilute PVDF solution (such as 12 wt.%) is not suitable in the co-casting method. During the early-stage exploration to investigate whether delamination between PES and PVDF membranes could occur, a most used 15 wt.% PES solution and a 16 wt.% PVDF solution for membrane preparation were used. Results showed that delamination occurred as expected, thus different PES and PVDF concentrations were considered to investigate the influence on the membrane morphology and performance. As the PES membrane prepared with

a higher concentration could form a thicker layer which might further reduce the water diffusion rate into the underlying PVDF layer, higher PES concentrations (*e.g.*, 18 wt.% and 21 wt.%) were investigated. Moreover, by preparing membranes with different PVDF concentrations, it was found that if the viscosity of PVDF solution was lower than that of PES solution, a homogeneous polymer layer was difficult to be formed, and the two layers could hardly be separated, as shown in Figure 2.4, in which the membrane was prepared with 14 wt.% PVDF solution (viscosity of 2722 mPa·s at 25 °C) and 21 wt.% PES solution (viscosity of 4540 mPa·s at 25 °C). Therefore, 16 wt.% was chosen as the lowest PVDF concentration, and higher PVDF concentrations of 18 wt.% and 20 wt.% were used to investigate the impact of the PVDF concentration.

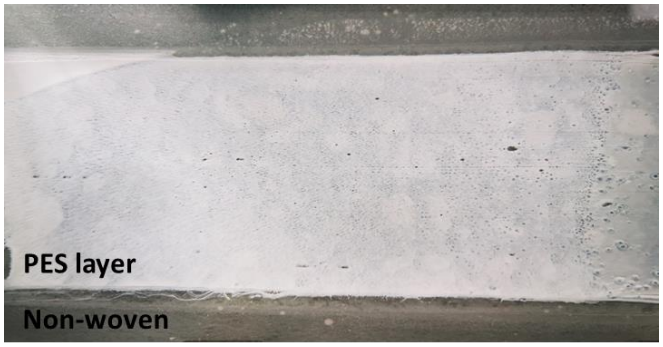


Figure 2.4 A digital image of the inhomogeneous co-cast membrane with 14 wt.% PVDF solution and 21 wt.% PES solution. The PVDF layer was totally covered by PES layer, which cannot be seen from this picture.

The membrane preparation in a co-casting process is depicted in Figure 2.5. First, PES solutions with different concentrations (15 wt.%, 18 wt.%, 21 wt.%) were prepared in different solvents (*e.g.*, NMP and DMSO) via magnetic stir at room temperature, while PVDF was solved in NMP under mechanical agitation at 60 °C to prepare solutions with different concentrations (16 wt.%, 18 wt.%, 20 wt.%). After homogeneous solutions were obtained, degasification was conducted by placing the solutions at room temperature overnight. In the co-casting process, a PVDF solution was spread on the non-woven by a casting knife with a thickness of 300 μm. Subsequently, the PES layer was immediately cast on the PVDF nascent solution film with a thickness of 500 μm, thus a 200 μm PES solution layer was created. Finally, the

obtained dual-layer films with non-woven were dipped into water for phase separation. After the PES and PVDF layers both precipitated, the two layers separated spontaneously, as shown in Figure 2.6, and the PES layer could be removed easily. The PVDF membranes on the non-woven substrates were stored in fresh DI water for one day. Afterwards, the membranes were dried at ambient environment for further characterization. The prepared membranes were labelled as PVDF-x-y, where x and y were the concentration of PVDF and PES solutions, respectively. The control single-layer PVDF membranes were prepared by directly casting the PVDF solutions (16 wt.%, 18 wt.%, 20 wt.%) with a thickness of 300 μm on nonwoven and subsequently soaked in water bath for phase separation.

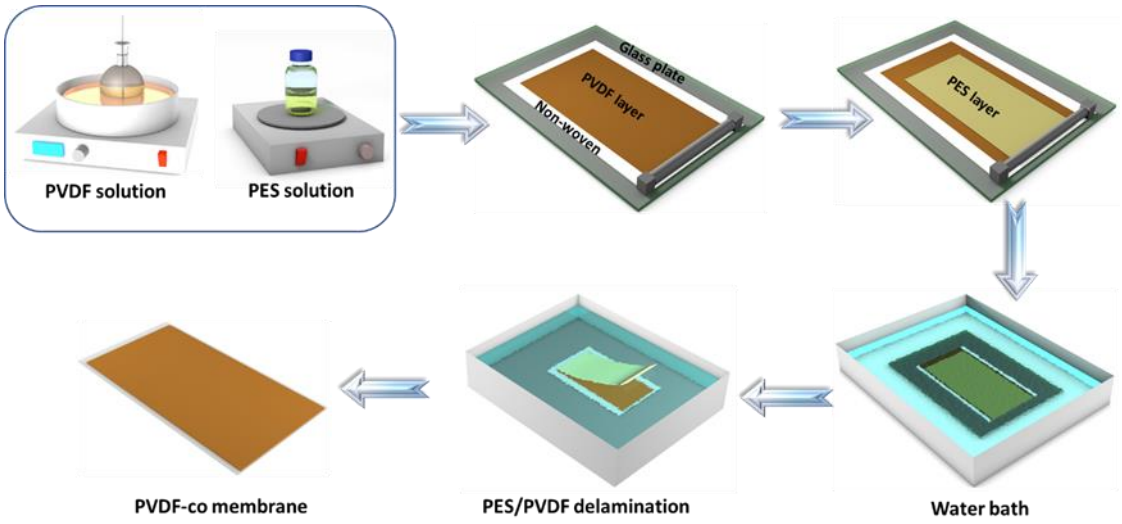


Figure 2.5 Schematic diagram of preparing PVDF membranes by co-casting

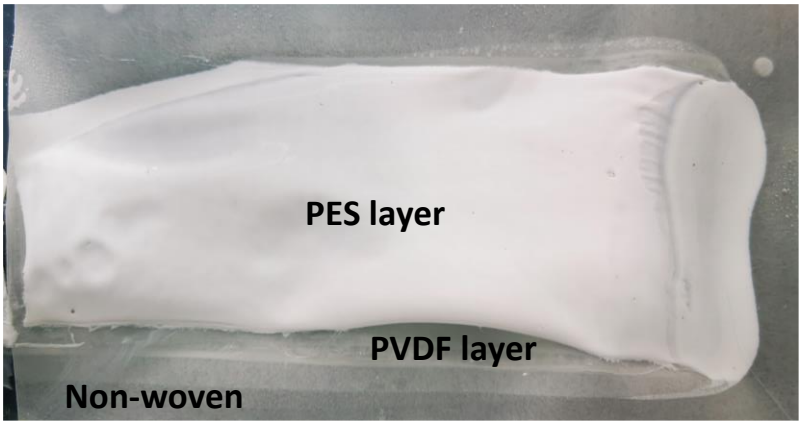


Figure 2.6 A digital image of the delaminated PES/PVDF membrane

2.4 Characterization

2.4.1 Solution viscosity

The polymer solution viscosities were analyzed by an NDJ-8S viscosimeter (Shanghai Yueping Equipment Co., Ltd., China) at room temperature. A suitable rotor and rotational speed were selected for each sample. Each solution was tested at least three times, and the average values were recorded.

2.4.2 Scanning electron microscope

The surface morphologies and cross-section structures of the prepared membranes were characterized by scanning electron microscopy (SEM, Philips XL30 FEG, Netherlands). The cross-section samples were prepared by cryogenic breaking in liquid nitrogen. The membrane samples were totally dried under vacuum and then sputter coated with gold, followed by imaging at 10 kV.

2.4.3 Surface roughness

Atomic force microscopy (AFM, Dimension 3100 AFM device, Bruker) was utilized to measure the membrane surface roughness. The images were performed using SSS-NCHR probes (NanoAndMore GmbH, Germany). The roughness parameters, Ra (average roughness), Rrms (root mean square roughness), and Rmax (maximum vertical difference between the highest peaks and the lowest valleys) were calculated using the ISO 25178-2 standard.

2.4.4 Shrinkage value

The membrane shrinkage values were evaluated in width, length, and thickness directions. After co-cast PVDF and PES solutions on the non-woven substrate, a piece of the nascent film on the substrate with a certain area at 5 cm*5cm was cut and immersed into a water bath. The shrinkage value at different temperatures (1.1 °C, 22 °C, 70 °C, and 92 °C) were measured for membranes cast with 16 wt.% PVDF solution and 15 wt.% PES solution. The width, length, and thickness of the obtained

membranes were measured after these membranes were dried in the oven at 30 °C. In addition, co-casting of PVDF and PES on the glass plate was conducted.

2.4.5 Water contact angle

The membrane hydrophobicity was determined by measuring the water contact angles using a sessile drop method by applying the contact angle goniometer (OCA20, Dataphysics Instruments, Germany). A water droplet of 3 μL was used for each measurement at 10 random locations on 3 independent membrane pieces. The average values were reported.

2.4.6 Mean pore size

Mean pore size of the prepared membranes was determined with Capillary Flow Porometry (Porolux 1000), as shown in Figure 2.7 (A). The membrane samples were prepared in a tablet press machine with a module diameter of 10.2 mm. The samples were placed into the test cell and wetted by a commercial low surface tension liquid Porefil (perfluoroether, surface tension of 16 mN/m) before measuring. The measurement was managed with a program consisting of a wet-run and a dry-run, as shown in Figure 2.7 (B). The nitrogen flows through the wetted samples during a stepwise increase of the applied pressure, and the flow could be detected at a certain pressure which can be called the bubble point, where the corresponding pore size is the maximum pore size of the sample. With the further increase of the pressure, the membrane can be totally dried out, and the generated curve is called the wet-curve. Then the nitrogen flow rate of this dry sample was tested in an increased pressure process, which formed the linear dry-curve. At a certain pressure, the nitrogen flow rate of the dry-curve and the wet-curve are the same, which means that at this point, the wetted membrane sample is totally dried out during the wet-curve measurement, and the corresponding pore size at this pressure is the smallest pore size. The half-dry curve is calculated by dividing the flow rate values of the dry-curve by 2. The mean pore size is the pore size at which 50% of the gas flow can be reached, which is determined by fitting the wet curve and the half-dry curve.

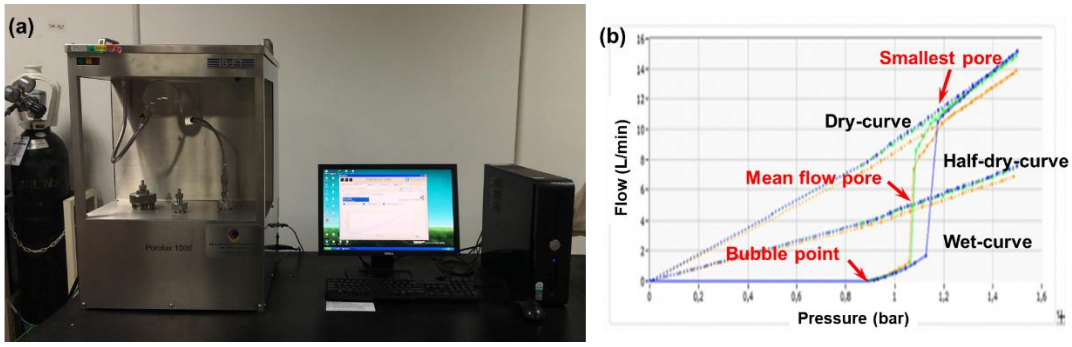


Figure 2.7 A picture of the pore size measurement instrument (a) and a result sheet from Porolux 1000 (b)

2.4.7 Porosity

The porosity represents the ratio of the pore volume to the apparent membrane volume of a certain piece of membrane sample. It was determined using gravimetrical method by comparing the wet weight (m_{wet}) and the dry weight (m_{dry}) of the membrane. As the prepared membranes are hydrophobic, ethanol was used to wet the membrane samples. The increased weight of the wet sample compared to the dry sample is the amount of ethanol retained in the pores, thus the porosity can be calculated as follows

$$\varepsilon = \frac{m_{wet} - m_{dry}}{\rho_{Ethanol} \cdot A \cdot \delta} \times 100\%$$

in which $\rho_{Ethanol}$ is the density of ethanol (789 kg/m^3), A is the area of the membrane sample (m^2), and δ is the membrane thickness (m). For each membrane, at least four pieces were taken and the average value was registered.

To estimate the porosity of the polymer layer ($\varepsilon_{polymer}$) rather than the whole membrane with the non-woven substrate, a similar calculation was utilized as follows:

$$\varepsilon_{polymer} = \frac{(m_{wet} - m_{wet-sub}) - (m_{dry} - m_{dry-sub})}{\rho_{Ethanol} \cdot A \cdot (\delta - \delta_{sub})}$$

where $m_{wet\text{-}sub}$ and $m_{dry\text{-}sub}$ are the wet and dry weight of the substrate (*i.e.*, 3D printed membrane and non-woven support), and δ_{sub} is the substrate thickness.

2.4.8 Mechanical strength

The mechanical strength of the 3DP membrane and PVDF@3DP composite

membranes were measured by a tensile testing machine (UTM T150, USA). A membrane sample with a width of 5 mm was prepared and fixed by two holding grips. The samples were slowly pulled lengthwise with a rate of 5 mm/min until it broke. At least three samples were measured.

2.4.9 Liquid entry pressure (LEP)

The LEP values of the prepared membranes were tested in a dead-end module and a picture of the setup is shown in Figure 2.8. The membrane samples were fixed into the sample testing module between two silicon pads, and the top surface of the membrane faced the water reservoir side. The pressure was introduced from a nitrogen cylinder step by step with a 0.05 bar increment. The water from the water tank was pushed into the testing module and imposed pressure on the membrane samples. At each step, the pressure was maintained for 15 s. The testing process terminated until the first water droplet was observed from the open-side of the testing module. Three membrane pieces were measured for each membrane.

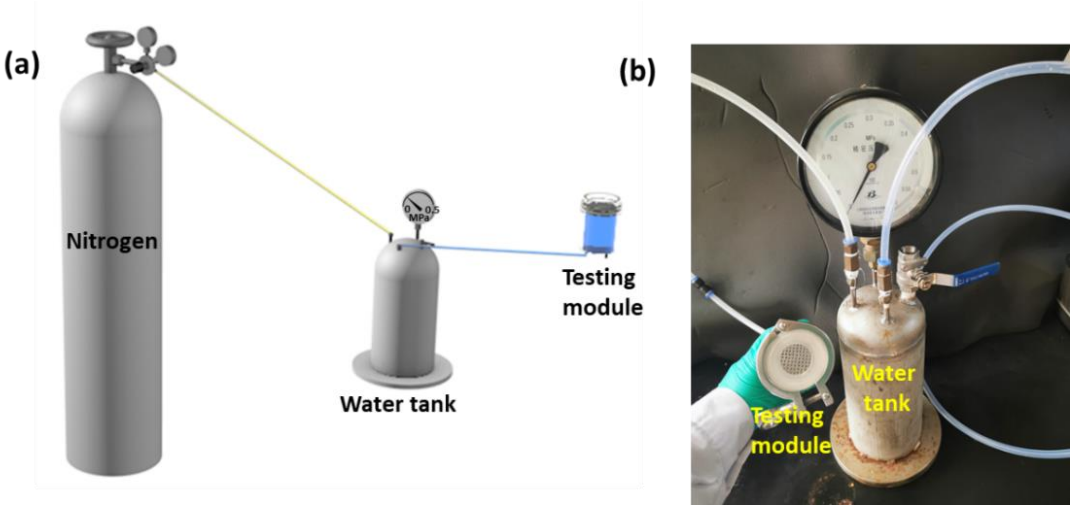


Figure 2.8 The schematic (a) and a digital picture (b) of the LEP test system

2.5 DCMD performance tests

A schematic illustration of the DCMD setup is presented in Figure 2.9. As the experiments were conducted in different laboratories, there are two DCMD setups, as shown in Figure 2.10. The setup in Figure 2.10 (a) was used to measure the DCMD

performance of the PVDF membranes prepared by bottom-up method, and the performance of PVDF coated 3D printed membranes and PVDF-co membranes was evaluated by the setup in Figure 2.10 (b). The membrane modules in these two setups are totally the same, with an effective membrane area of 50*20 mm. Peristaltic pumps were used in both setups, and Watson-Marlow Sci-Q 300 pumps were used in Figure 2.10 (a) while Longer BT300-2J pumps were used in Figure 2.10 (b). External heating bath and cooling bath were used to maintain the desired feed and permeate solution temperatures. The tubes were covered with insulation materials to reduce the heat loss during circulation.

The MD performance of the prepared membranes was usually measured for two hours using 35 g/L NaCl as feed solution and deionized (DI) water as permeate solution, respectively. For the PVDF membranes prepared by bottom-up methods, the feed solution temperatures during the MD tests ranged from 40 °C to 70 °C, while the permeate temperature was fixed at 20.0±0.5 °C, and the measurements continued for two hours at each temperature. For the PVDF coated 3D printed membranes (PVDF@3DP) and PVDF-co membranes, the MD performance were tested at feed and permeate solution temperatures of 60.2±0.5 °C and 19.8±0.5 °C, respectively. As the MD flux always increases with a higher feed temperature, the influence of feed temperature was not carried out for these two types of membranes. During the two-hour MD tests, the feed solution volume only decreased slightly compared to the initial volume (2 L) according to the corresponding flux, thus the solution concentration only changed marginally.

A long-term stability test of a PVDF-co membrane was conducted for 48 h intermittently. After a 12 h-test for each day, the pumps, the heating bath, and the cooling bath were turned off during the night while the other sections were kept the same. During the long-term test, the feed concentration was kept constant by a big external DI water reservoir as shown in Figure 2.11. A soft tube filled with DI water is used to connect the external water reservoir and feed tank. The initial water level of the feed tank and reservoir was at the same height. Thus, if the water level in the feed tank

decreases due to the flux through the membrane, the water reservoir could replenish the feed tank to keep the water level the same due to the siphon phenomenon and keep the solution concentration constant.

The produced water in the permeate side was collected as an overflow from the permeate vessel to a beaker, and the weight and conductivity of the permeate were measured in a certain time interval. The permeate flux J (kg/(m^2·h)) was calculated according to

$$J = \frac{\Delta m}{A \cdot \Delta t}$$

where Δm (kg) represents the mass of water transported from feed to permeate in the certain time interval (Δt, h), and A (m^2) is the available membrane area (0.001 m^2 in this experiment). The salt rejection (R) was defined as follow:

$$R = \left(1 - \frac{V_p \cdot C_p}{J \cdot A \cdot \Delta t \cdot C_f}\right) \times 100\%$$

where C_f and C_p represent the NaCl concentration in the feed and permeate solution, respectively. V_p is the volume of the increased permeate solution.

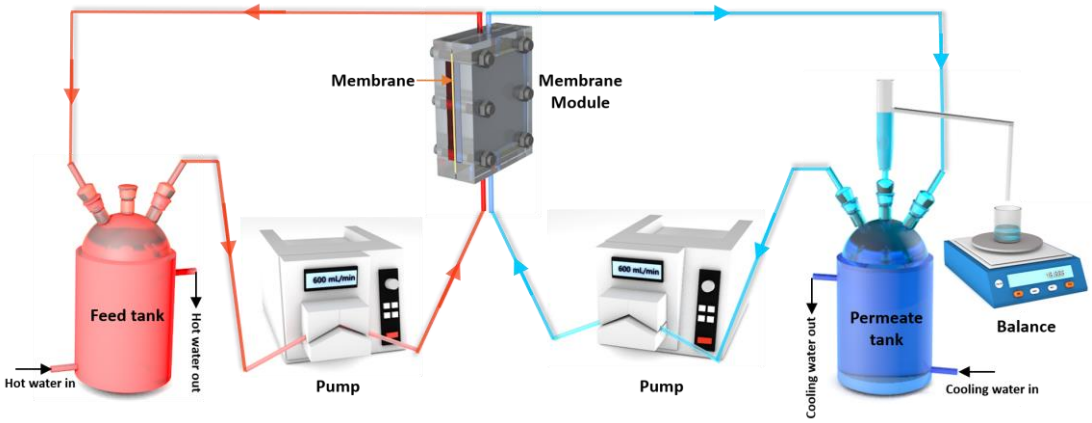


Figure 2.9 Schematic illustration of the DCMD setup

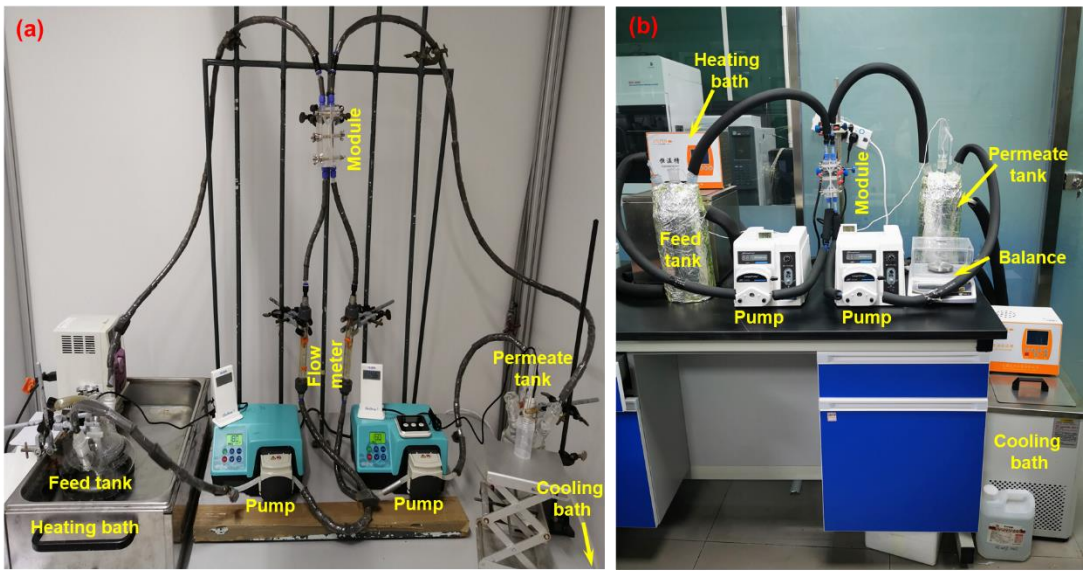


Figure 2.10 Digital photos of the lab-scale DCMD setups. (a) this setup was used to measure the MD performance of the PVDF membranes prepared by bottom-up method, and (b) this setup was used to measure the membrane performance of PVDF coated 3D printed membranes and PVDF membranes fabricated in co-casting process.

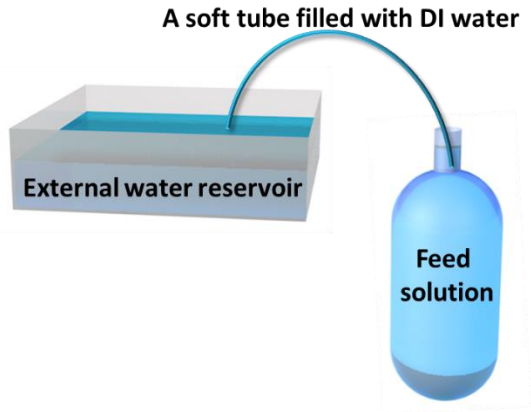


Figure 2.11 A schematic illustration of the external water reservoir to keep the feed concentration constant during the long-term test

Chapter 3

Exploring the potential usage of 3D printed membranes combined with PVDF coating in direct contact membrane distillation (DCMD)

Adapted from: Miaomiao Tian, Hellen De Coninck, Junyong Zhu, Yatao Zhang, Shushan Yuan, Brecht Van Hooreweder, Peter Van Puyvelde, Bart Van der Bruggen, Exploring the potential usage of 3D printed membranes combined with PVDF coating in direct contact membrane distillation (DCMD) (in preparation for submission)

3.1 Introduction

As reviewed in Chapter 1, a proper membrane has primary importance to attain a good performance with regard to flux and permeate quality, as well as a higher energy efficiency [1-4]. The currently investigated membranes can be divided into three categories: (i) sponge-like or macro-voids membranes prepared by nonsolvent induced phase separation (NIPS) [5-15], (ii) nanofibrous membranes prepared by electrospinning (ES) [16-29], and (iii) existing commercial membranes [30-37]. As a traditional membrane fabrication method with super simplicity, NIPS is most studied in both laboratories and industries [38, 39]. In recent years, electrospinning stands out in preparing MD membranes by virtue of its several advantages of the superior pore interconnectivity, a high porosity, a controllable thickness, and a high surface area to volume ratio [40-42]. However, the scale up of the electrospun membranes is still challenging due to its low production rate. Furthermore, modifications and post-treatments are required to enhance the membrane hydrophobicity and integrity, which expands the process complexity and cost. Several novel and biological materials were also examined about their capability in MD, such as an unsupported nanofibrous membrane made by bacterial nanocellulose aerogels [43], and a nanowood membrane prepared by removing the lignin and semi-cellulose from natural wood [44].

Nonetheless, these new methods need further improvement and investigation to confirm the feasibility in large-scale membrane preparation.

Over the last decades, 3D printing technology has been studied intensively because of its promising characteristics such as freedom of design, less waste formation, and automation [45, 46]. This evolution provides great opportunities to develop products with complicated features using a range of materials in various shapes with great precision. In the last five years, 3D printing technology has gained special attention and has been explored in membrane fabrication for wastewater treatment applications [47, 48]. The first printed membrane emerged in 2015 [49]. Femmer et al. fabricated polydimethylsiloxane (PDMS) membranes for gas-liquid-contacting with various 3D geometries using 3D printed (3DP) templates as sacrificial models. It was reported that precise fabrication can be achieved, and the designed geometries greatly enhanced the mass transport of carbon dioxide due to the improved flow characteristics. Unlike the indirect usage of the 3D printing technique, Mattia's group developed composite membranes composed of a thick 3DP wavy support followed by attaching a thin polyethersulfone (PES) selective layer under vacuum filtration for ultrafiltration (UF) [50, 51]. The results showed that the wavy support membranes led to a higher pure water flux, a better recovery ratio, and superior anti-fouling properties compared to the flat support membranes due to the localized turbulence resulting from the curved structure. Apart from the use of 3DP membrane supports, direct usage of the printed membranes was also carried out. Yuan et al. [52] prepared polyamide (PA) membranes by laser sintering (LS), a powder-based 3D printing process, and investigated the influence of printing parameters on the membrane structures. The results indicated that a higher laser energy led to a better coalescence of PA particles, and hence to a denser membrane with a lower porosity and water flux. Furthermore, Yuan constructed superhydrophobic membranes by adding a ZIF-L layer on the 3DP PA substrates and subsequently a polydimethylsiloxane (PDMS) coating, and the obtained membranes showed an excellent oil-water separation performance [53]. Yang et al. [54] printed membranes with eggbeater heads by an immersed surface accumulation process with a

hydrophilic material. The designed structure imparted the membrane superhydrophobicity with good water adhesion, which can be called the “petal effect”. By printing different structures with this advanced technique, it was concluded that the adhesive behavior of the membrane surface could be adjusted by varying the number of eggbeater arms, which was helpful to further understand the relationship between the surface structure and the adhesive force. Chowdhury et al. [55] utilized an additive method to prepare polyamide membranes with controllable thickness and roughness by electrospraying the monomers directly onto a substrate. This precisely controlled process could reach a 4 nm increment in layer thickness. 3DP ceramic membranes were also prepared and investigated by Hwa et al. [56]. Porous and strong membranes with a book-like structure were obtained. The water filtration performance was measured, and it was found to be related to the particle size, in which the flux decreased with increasing particle diameter. However, due to the relatively low resolution of various 3D printing technologies (usually a few tens of micrometers or even hundreds of micrometers, except two-photon polymerization which could reach 100 nm [45]) and available material limitation, direct usage of the 3D printed membranes is still challenging. However, it is promising in the membrane-related area because of the quick fabrication, less solvent discharge, feasibility of the complex design, and precise control for each layer compared to the traditional membrane preparation methods.

LS, which can build designed parts by sintering particles layer-by-layer, is promising to prepare membranes with a rough surface and inherent porosity (10-30%, [52]) due to particles coalescence [47, 52, 64-66]. Therefore, the potential usage of LS membranes in membrane distillation (MD) was explored in this work for the first time. Among the polymers used in LS process, polyamide (PA) is favored due to the advantages of its powder form which could reduce the additional costs for cryo-milling, as well as the suitable particles size for the printing process. Additionally, PA is also a general polymer material for membrane fabrication; thus, PA is chosen as the printing material in this work. However, since the pore size of the LS printed membrane is decided by the particle size which is usually tens of micrometers, while the optimal pore size for

MD membrane locates in 0.1-1 μm, thin poly (vinylidene fluoride) (PVDF) layers were introduced on the 3DP membranes by dip-coating to reduce the overall membrane pore size while not to add significant mass transfer resistance was proposed. The membrane morphology, hydrophobicity, pore size, porosity were measured, and the DCMD performance was tested in a lab-scale setup.

3.2 Results and discussion

3.2.1 Morphology and hydrophobicity of PVDF@3DP membranes

The morphologies of the top surface, cross section, and bottom surface, as well as the water contact angles on each surface of the 3DP PA membrane are shown in Figure 3.1. As presented in the images, the membrane exhibits a relatively dense and flat top layer obtained by melting and coalescence of PA powders, which has a contact angle of 94.6°. While the bottom surface is particulate, porous, and rough due to the adhesion of the less coalesced PA particles owing to the reduced energy [52], which shows a higher contact angle (*i.e.*, 124.3°) than the top surface owing to a higher roughness.

Although a well-ordered pore structure (such as circular pores distribute uniformly, or straight pores across the two membrane surfaces) was expected for the printed membranes, membranes composed of particles and random pores was printed due to the limitation of the printing resolution (80-150 μm, [45]), the powder size, and the printing principle of sintering. Nonetheless, since the 3DP membrane is formed by particle coalescence, the gaps between the particles are the only route for vapor transport, which is similar with the PVDF membranes with a structure composed of PVDF crystals as shown in Figure 1.16, further characterizations were carried out to explore the potential of the 3DP membranes. Firstly, the printed membrane was directly tested in DCMD and the membrane was immediately wetted, which could be ascribed to the large pore size. Subsequently, the CF_4 plasma modification was conducted on the printed membrane to increase the hydrophobicity as well as liquid entry pressure; however, the membrane was wetted immediately again. Then, a PVDF layer coating was conducted on the 3DP membranes, and the properties as well as the DCMD

performance of the composite membrane was studied. As the particulate and more hydrophobic bottom surface of the printed membrane was adopted as the surface in contact with the feed solution during the DCMD measurement in the initial exploration (the printed membrane was directly used in DCMD), this side was utilized as the top surface of the composite membranes after PVDF coating as well.

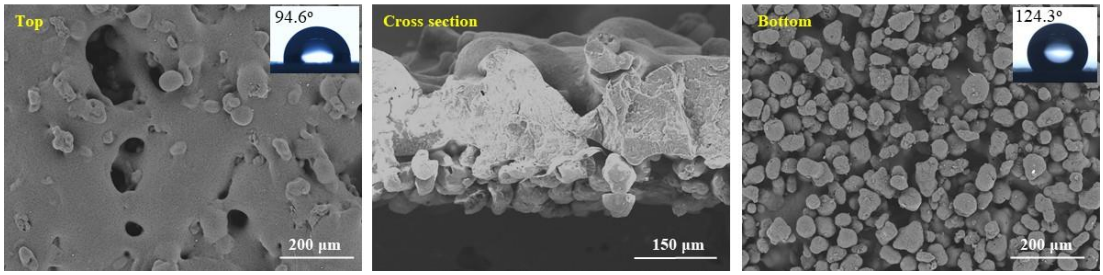


Figure 3.1 SEM images of the polyamide (PA) membrane printed by laser sintering (LS). The insert images are the contact angles on the membrane surfaces.

The morphologies of composite PVDF@3DP membranes prepared using PVDF solutions with different concentrations are shown in Figure 3.2. It can be observed that the PVDF layers become denser and thicker with a higher PVDF concentration. In addition, as the thickness of the PVDF layer is greater than the size protrudent particles, the surface of the coated membranes became flat, and no distinct roughness could be maintained. Furthermore, there is no significant disparity between the top and bottom surfaces for each concentration. When the PVDF concentration is 5 wt.%, the PA particles can be easily detected on the surface, which could be ascribed to the non-continuous PVDF layer formed by the low polymer concentration. With the concentration increased to 7 wt.%, a flat and uniform polymer layer is built on both sides. When the polymer concentration is further increased to 10 wt.%, a relatively dense and smooth surface is generated. As shown in the cross-section images, the PVDF layers are composed of flat skin layers and various macro-voids, which is a typical structure of PVDF membranes prepared in a water bath [57, 58]. Additionally, the PVDF layer thickness increases from 48.6 µm to 94.6 µm when the PVDF concentration increased from 5 wt.% to 10 wt.%. The membrane morphologies demonstrate that the coated PVDF layers could efficiently decrease the pore size of 3DP

substrates, yet neutralized the roughness of the substrates.

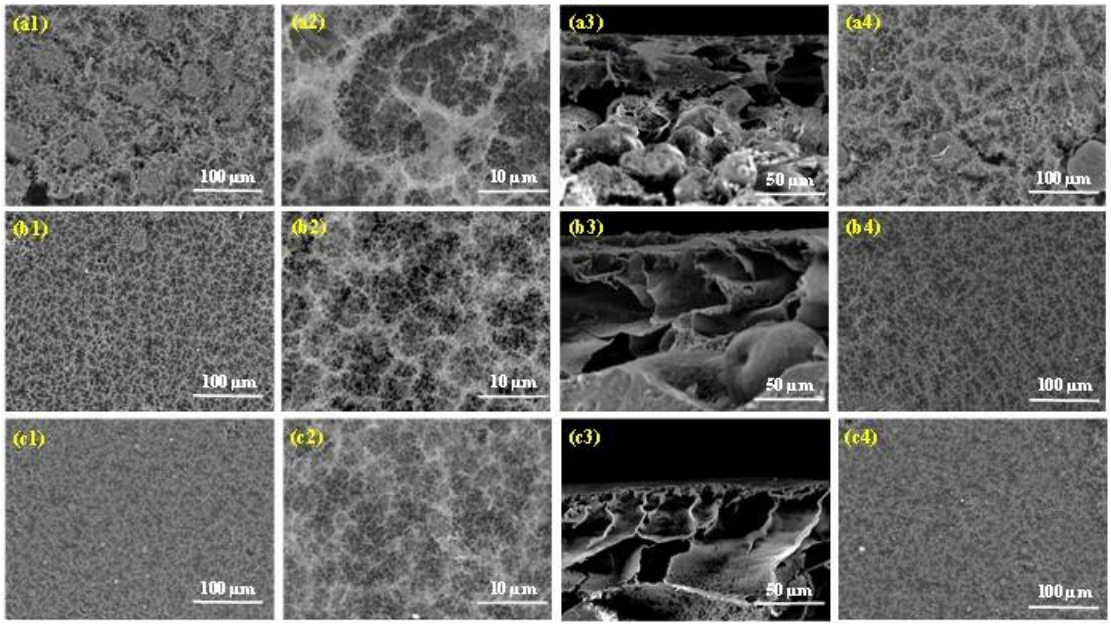


Figure 3.2 The morphologies of top (1-2), cross-section (3), and bottom (4) surfaces of PVDF@3DP membranes with different PVDF concentrations: (a) 5 wt.%, (b) 7 wt.%, and (c) 10 wt.%. The immersion time during the dip-coating procedure is 15 s.

The structures of PVDF@3DP membranes with different immersion times are depicted in Figure 3.3, Figure 3.4, and Figure 3.5. As shown in Figure 3.3, steady PVDF layers could be formed on the substrates when the immersion time exceeded 30 s, and the PA particles could not be recognized. In addition, the PVDF layer become more compact with a longer immersion time due to the presence of more residual polymer solution on the substrates. In contrast, no major difference in the surface morphology could be found for the membranes experiencing an immersion time less than 60 s with 7 wt.% PVDF solution, as displayed in Figure 3.4. Nonetheless, when the immersion time is doubled to 120 s, the PVDF layer becomes denser. Moreover, the morphology distinction is negligible between different immersion times for the PVDF@3DP-10 membranes, as shown in Figure 3.5. The disparity in the surface morphology tendency among these composite membranes may result from the viscosity difference, as listed in Table 3.1. Considering the lowest viscosity of the 5 wt.% solution, the amount of the retaining solution varies greatly according to the immersion time, thus the PVDF layer

morphology changes significantly with immersion time. Nevertheless, the 10 wt.% solution shows the highest viscosity, and it exhibits the slowest spreading and penetration rate on the PA membranes, which leads to little variation in morphology with different immersion times.

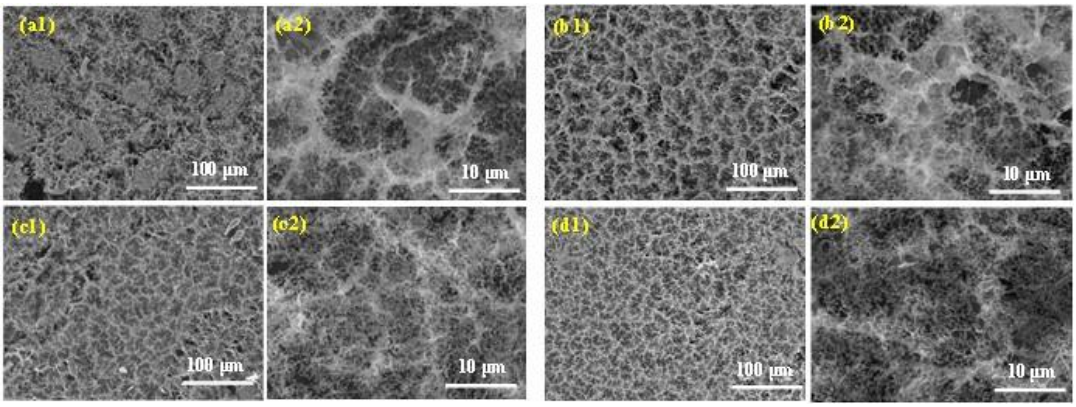


Figure 3.3 The morphologies of top surface and enlarged images of PVDF@3DP-5 membranes with different immersion times: (a) 15 s, (b) 30 s, (c) 60 s, and (d) 120 s

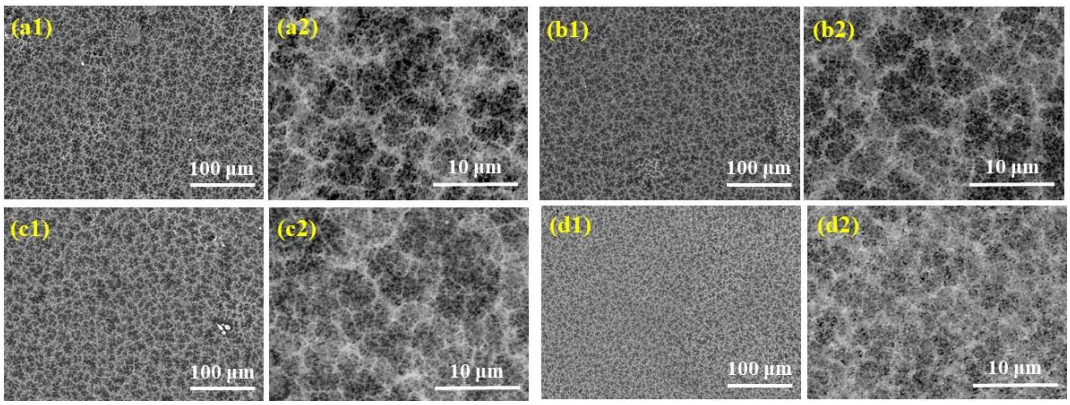


Figure 3.4 The morphologies of top surface and enlarged images of PVDF@3DP-7 membranes with different immersion times: (a) 15 s, (b) 30 s, (c) 60 s, and (d) 120 s

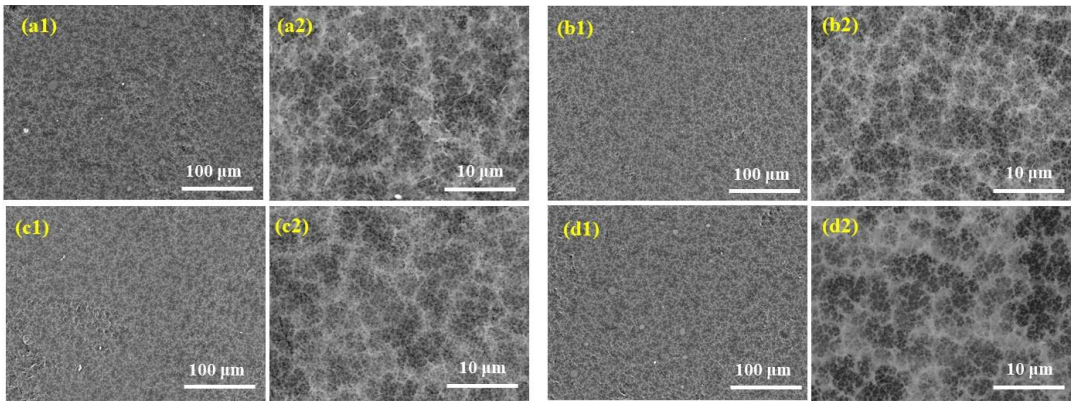


Figure 3.5 The morphologies of top surface and enlarged images of PVDF@3DP-10 membranes with different immersion times: (a) 15 s, (b) 30 s, (c) 60 s, and (d) 120 s

Table 3.1 Viscosities of PVDF solutions at 25 °C

PVDF concentration	Viscosity (mPa·s)
5 wt.%	164±8
7 wt.%	275±16
10 wt.%	814±22

The contact angles on both sides of the PVDF@3DP membranes are shown in Figure 3.6. For both sides, the surface hydrophobicity follows a sequence of PVDF@3DP-5> PVDF@3DP-7>PVDF@3DP-10. As the surface roughness plays an important role in deciding the membrane hydrophobicity when the surface energy is similar, the highest contact angles of PVDF@3DP-5 membranes can be attributed to the maintained particulate structure and high roughness due to the thinnest PVDF layer, although the particulate surface is inconspicuous. Oppositely, the relatively low contact angles of PVDF@3DP-10 membranes could result from the most flat and dense surfaces. In addition, although the roughness between the two sides of the 3DP membrane shows great difference, the surface morphologies shift similar after PVDF coating. Thus, all the top surfaces of the composite PVDF@3DP membranes only show

marginally higher contact angles than the bottom surfaces. Nonetheless, the hydrophobicity of the PVDF@3DP membranes is higher than the conventional PVDF membranes cast on a glass plate or nonwoven of ~70°, which manifests the advantage of the rougher surface than the smooth substrates.

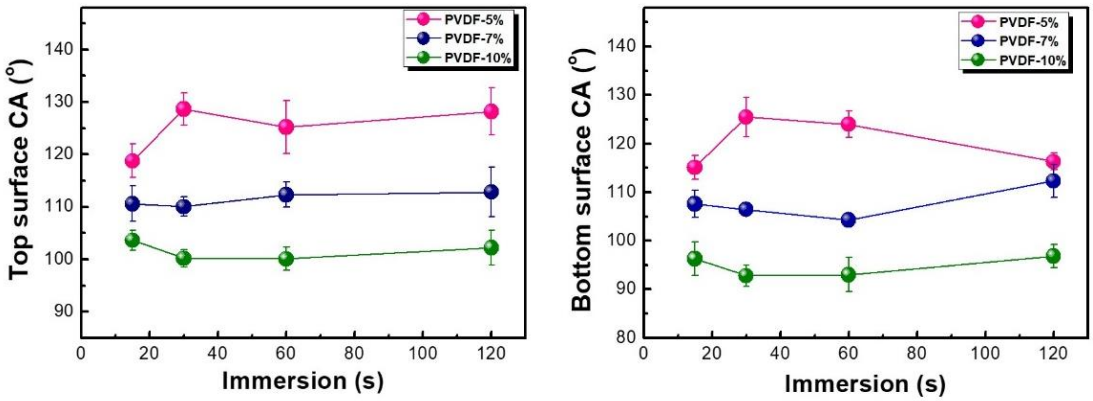


Figure 3.6 The contact angles on the top (left) and bottom (right) surfaces of the prepared PVDF@3DP membranes.

3.2.2 Physical properties of PVDF@3DP membranes

The physical properties including membrane thickness, mean pore size, porosity, and mechanical strength of the 3DP PA membranes and PVDF@3DP composite membranes are shown in Table 3.2 and Figure 3.7, respectively. However, as the diameter of the PA powders is significantly greater than the PVDF crystals, the printed PA membrane show a relatively low porosity of 21.7% compared to the PVDF membranes with similar structures as the PA powders occupy a lot of space in a same area. It should be mentioned that the large deviation in thickness and pore size results from the manufacturing process. In the sintering process, the PA powders were fused together by laser scanning in only one cycle. Thus, the distribution of the powders and the powder quality (new powder or recycled powder) may affect the physical properties of the printed membranes in different piece.

Table 3.2 Physical properties of 3DP PA membranes

Property	PA membrane
Thickness (μm)	359.6±38.9
Mean pore size (μm)	15.9±5.3
Porosity (%)	21.7±4.4
Mechanical strength (MPa)	10.7±1.8

Figure 3.7 (a) indicates the membranes thickness variation tendency of the PVDF@3DP composite membranes, which shows a greater membrane thickness with a higher PVDF concentration. On the one hand, a higher polymer concentration contains more polymer chains which leads to a thicker layer. On the other hand, more polymer solution was retained on the substrate surface during the dip-coating procedure due to a higher viscosity of solutions with a higher concentration. The mean pore sizes of the PVDF@3DP membranes are shown in Figure 3.7 (b). The pore size reduces from 15.9±5.3 μm to 1.0-2.5 μm ascribed to the coated PVDF layers, which confirms the effectiveness of the dip-coating process. Besides, the PVDF@3DP-10 membranes possess the lowest pore size while PVDF@3DP-5 membranes show the largest pore size, which is consistent with the tendency in morphology. The membranes porosities are shown in Figure 3.7 (c), and they fall into a range of 46%-62%. The relatively low porosity is limited by the low porosity of the 3DP substrates. As the reported porosity is an average of the porosity of both PVDF layer and the 3DP substrate, a higher porosity of the polymer layer could lead to a high porosity of the composite membrane than the virgin substrate. The mechanical properties were tested for PVDF@3DP-x -15 and PVDF@3DP-x-120 membranes, as shown in Figure 3.7 (d). The results show that all the samples display a tensile strength higher than 10 MPa; thus, they are stronger than most conventional polymer membranes [59-63]. However, it should be noted that the mechanical strength of the composite membranes mostly depended on the thickness of the virgin 3DP substrate rather than the entire composite membranes, which can be

concluded from the testing process; thus, the tendency of the mechanical strength is random as the substrate thickness is different from each other. Therefore, although the PVDF@3DP-10-15 membrane had a higher thickness than the PVDF@3DP-7 membranes, it was found to have a lower tensile strength due to the relatively thinner 3DP membrane. In addition, although with strong mechanical strength, some tiny cracks occurred on the membrane surface under 0.1 bar during the LEP tests, as depicted in Figure 3.8. As the 3DP membranes were formed by coalescence and adhesion of PA particles, voids may generate between the incompletely melted particles leading to insufficient adhesion.

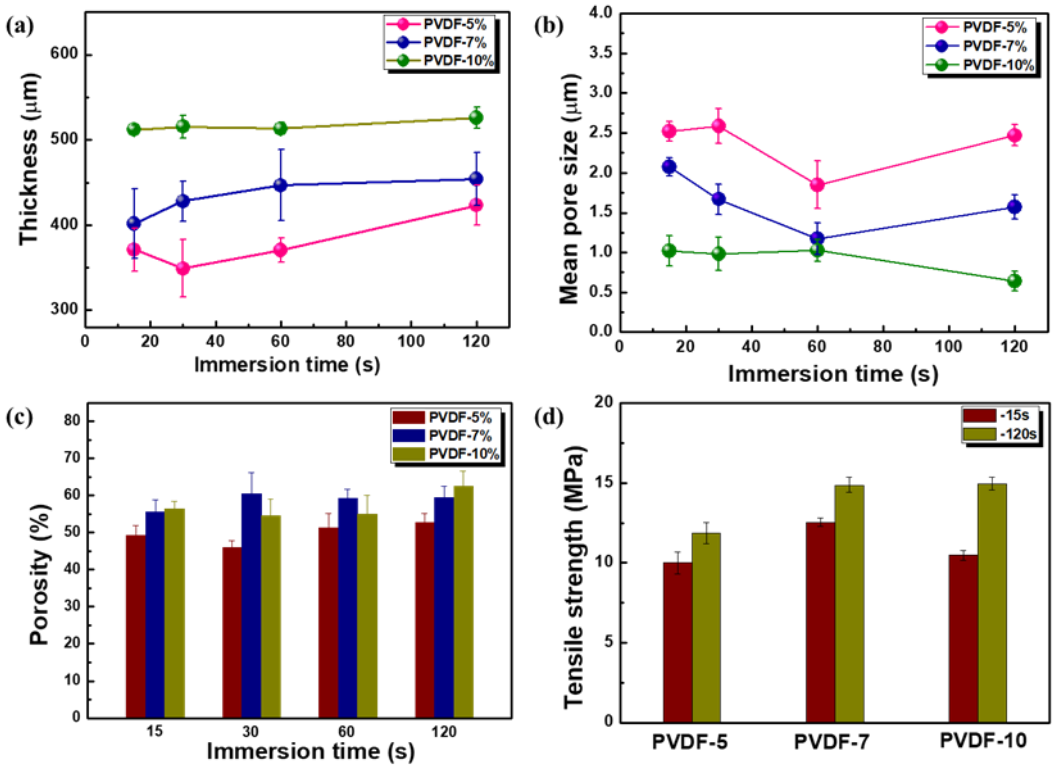


Figure 3.7 Physical properties of PVDF@3DP membranes: (a) thickness, (b) pore size, (c) porosity, and (d) mechanical strength

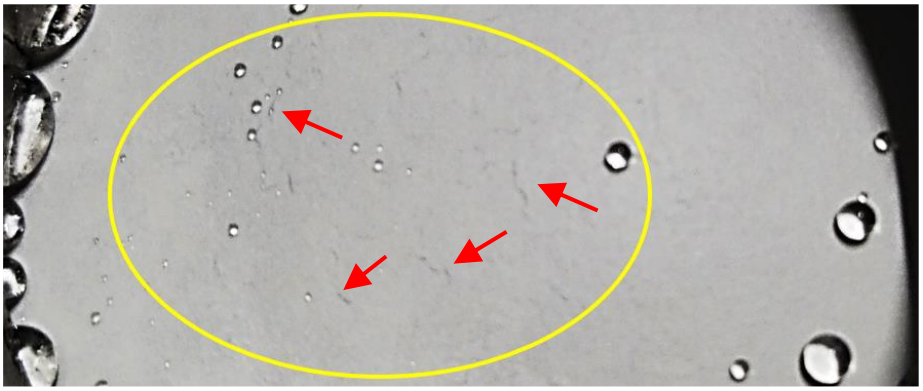


Figure 3.8 The defects formed during the LEP tests

3.2.3 DCMD performance

The DCMD fluxes of the PVDF@3DP membranes are presented in Figure 3.9. Because the PVDF@3DP-5-15 and PVDF@3DP-5-30 membranes consisted of non-continuous thin PVDF layers, these two membranes were immediately wetted at the beginning of the DCMD tests` due to the large pores. All the other tested membranes had NaCl rejections above 99.9%, but with slightly permeate solution conductivity increase. It can be obtained from the results that all the PVDF@3DP membranes show relatively low fluxes of 5-10 kg/(m^2·h) at feed and permeate temperatures of 60 °C and 20 °C, respectively, which can be ascribed to the low porosity and great thickness, as well as some closed pores formed by fully-sintered particles. Among the membranes prepared with different PVDF concentrations, PVDF@3DP-10 have the lowest fluxes because they have the lowest hydrophobicity, the highest thickness, and the narrowest pore size. In addition, although the PVDF@3DP-5-y membranes have thinner PVDF layer thickness and higher contact angles, they had lower fluxes than for the PVDF@3DP-7-15 membrane due to the thicker 3DP substrates and the comparable pore size. From all the obtained results, it can be concluded that the 3DP PA substrates significantly affect the MD performance of the PVDF@3DP composite membranes. Therefore, it is beneficial and essential to improve the structure of the 3DP PA membranes, such as decreasing the thickness while increasing the porosity by printing with the powders with a small diameter. In addition, if the powder size is sufficient low, a further modification might not be needed, thus the flux could also be improved.

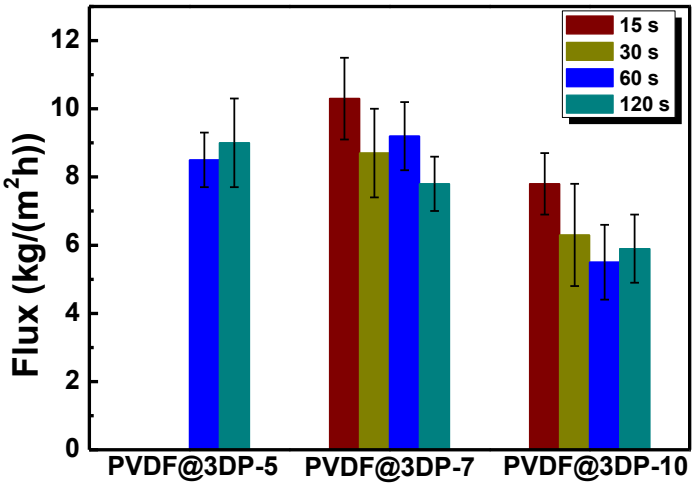


Figure 3.9 The DCMD fluxes of the PVDF@3DP membranes. The feed solution is 35 g/L NaCl. The feed and permeate temperatures are 60.2±0.5 °C and 19.8 ±0.5 °C, respectively. The flow rate is 36 L/h on both sides.

3.3 Conclusions

The potential of using 3D printed (3DP) membranes in membrane distillation is firstly explored in this work. Polyamide (PA) membranes with particulate and porous surface were printed in a laser sintering (LS) process. Thin PVDF layers were coated on the PA membranes utilizing different PVDF concentrations (5 wt.%, 7 wt.%, and 10 wt.%) by dip-coating with different immersion time (15 s, 30 s, 60 s, and 120 s) to reduce the oversized pores. The obtained composite membranes were labeled as PVDF@3DP-x-y, where x and y represent the PVDF concentration and immersion time, respectively. The membrane morphology and pore size results demonstrate the effectiveness of the dip-coating procedure. A continuous and uniform PVDF layer can be constructed with 5 wt.% PVDF solution with immersion intervals above 30 s or a higher concentration. Results showed that the hydrophobicity, thickness, and pore size of the composite membranes are significantly influenced by the PVDF concentration. A lower concentration induces a thinner PVDF layer and the granular morphology of PA membranes could be retained to some degree, which leads to a higher contact angle of 130°; while a higher PVDF concentration generates a thicker and denser flat layer with a relative lower contact angle of 100°. Additionally, PVDF@3DP-10 membranes

show the highest thickness of 512-526 μm and pore size of 0.64-1.02 μm, while the PVDF@3DP-5 membranes have the lowest thickness of 350-420 μm and pore size of 1.85-2.58 μm. However, the membrane porosity does not display a substantial difference due to the limitation of the low porosity of the 3DP PA membranes. Moreover, although the composite membranes show a mechanical strength of over 10 MPa, cracks emerged under 0.1 bar during the LEP tests, which may result from the relatively weak adhesion between the not-fully melted PA particles. In the DCMD tests, the composite membranes show relatively low fluxes, below 10 kg/(m^2·h) (feed and permeate temperatures of 60 °C and 20 °C, respectively), due to the rather low porosity and great thickness, as well as some closed pores formed by powder coalescence. This work explored the potential application of 3D printing membranes in MD, and demonstrated the significant role of the membrane substrates in the MD performance. However, comparing to the benchmarks in section 1.6, 3DP membrane is far from what is needed for MD membranes. On the one hand, a high temperature, a special laser beam, the printing instrument, and high-cost printing materials are needed. On the other hand, the dip-coating procedure using PVDF solutions diminish the advantages of no solvent and wastewater discharge, as well as quick fabrication for 3D printing process. Moreover, the great thicknesses (350-520 μm), low porosities (45%-60%), and relatively weak coalescence between powder particles under pressure, lead to a low MD flux and LEP compared to the desired properties. According to the results, further improving the structure of the printed membranes is essential. For example, since the LS technology is a powder-based process, the structural parameters could be optimized by applying PA particles with a smaller size, which could lead to a thinner thickness and a higher porosity. Moreover, incorporation of small water-soluble materials with PA particles during the printing process followed by washing away after membrane printing may be helpful in enhancing the membrane porosity.

References:

[1] K. W. Lawson, D.R. Lloyd, Membrane distillation, J. Membr. Sci., 124 (1997) 1-25.
[2] P. Wang, T.-S. Chung, Recent advances in membrane distillation processes:

Membrane development, configuration design and application exploring, J. Membr. Sci., 474 (2015) 39-56.
[3] L. Eykens, K. De Sitter, C. Dotremont, L. Pinoy, B. Van der Bruggen, How To Optimize the Membrane Properties for Membrane Distillation: A Review, Ind. Eng. Chem. Res., 55 (2016) 9333-9343.
[4] L. Eykens, K. De Sitter, C. Dotremont, L. Pinoy, B. Van der Bruggen, Membrane synthesis for membrane distillation: A review, Sep. Purif. Technol., (2017).
[5] M. Qtaishat, M. Khayet, T. Matsuura, Novel porous composite hydrophobic/hydrophilic polysulfone membranes for desalination by direct contact membrane distillation, J. Membr. Sci., 341 (2009) 139-148.
[6] D. Hou, G. Dai, H. Fan, J. Wang, C. Zhao, H. Huang, Effects of calcium carbonate nano-particles on the properties of PVDF/nonwoven fabric flat-sheet composite membranes for direct contact membrane distillation, Desalination, 347 (2014) 25-33.
[7] Y.C. Woo, Y. Kim, W.-G. Shim, L.D. Tijing, M. Yao, L.D. Nghiem, J.-S. Choi, S.-H. Kim, H.K. Shon, Graphene/PVDF flat-sheet membrane for the treatment of RO brine from coal seam gas produced water by air gap membrane distillation, J. Membr. Sci., 513 (2016) 74-84.
[8] K.-J. Lu, J. Zuo, T.-S. Chung, Novel PVDF membranes comprising n-butylamine functionalized graphene oxide for direct contact membrane distillation, J. Membr. Sci., 539 (2017) 34-42.
[9] S. Leaper, A. Abdel-Karim, B. Faki, J.M. Luque-Alled, M. Alberto, A. Vijayaraghavan, S.M. Holmes, G. Szekely, M.I. Badawy, N. Shokri, P. Gorgojo, Flux-enhanced PVDF mixed matrix membranes incorporating APTS-functionalized graphene oxide for membrane distillation, J. Membr. Sci., 554 (2018) 309-323.
[10] L. Deng, P. Li, K. Liu, X. Wang, B.S. Hsiao, Robust superhydrophobic dual layer nanofibrous composite membranes with a hierarchically structured amorphous polypropylene skin for membrane distillation, J. Mater. Chem. A, 7 (2019) 11282-11297.
[11] J. Zhang, Z. Song, B. Li, Q. Wang, S. Wang, Fabrication and characterization of superhydrophobic poly (vinylidene fluoride) membrane for direct contact membrane distillation, Desalination, 324 (2013) 1-9.
[12] W. Zhang, Y. Li, J. Liu, B. Li, S. Wang, Fabrication of hierarchical poly (vinylidene fluoride) micro/nano-composite membrane with anti-fouling property for membrane distillation, J. Membr. Sci., 535 (2017) 258-267.
[13] Y.C. Woo, Y. Kim, M. Yao, L.D. Tijing, J.-S. Choi, S. Lee, S.-H. Kim, H.K. Shon, Hierarchical Composite Membranes with Robust Omniphobic Surface Using Layer-By-Layer Assembly Technique, Environ. Sci. Technol., 52 (2018) 2186-2196.
[14] S. Nejati, C. Boo, C.O. Osuji, M. Elimelech, Engineering flat sheet microporous PVDF films for membrane distillation, J. Membr. Sci., 492 (2015) 355-363.
[15] H. Fan, A. Gao, G. Zhang, S. Zhao, J. Cui, Y. Yan, A facile strategy towards developing amphiphobic polysulfone membrane with double Re-entrant structure for membrane distillation, J. Membr. Sci., 602 (2020) 117933.
[16] B.S. Lalia, E. Guillen, H.A. Arafat, R. Hashaikeh, Nanocrystalline cellulose reinforced PVDF-HFP membranes for membrane distillation application, Desalination,

332 (2014) 134-141.
[17] E.-J. Lee, A.K. An, T. He, Y.C. Woo, H.K. Shon, Electrospun nanofiber membranes incorporating fluorosilane-coated TiO2 nanocomposite for direct contact membrane distillation, J. Membr. Sci., 520 (2016) 145-154.
[18] C. Su, J. Chang, K. Tang, F. Gao, Y. Li, H. Cao, Novel three-dimensional superhydrophobic and strength-enhanced electrospun membranes for long-term membrane distillation, Sep. Purif. Technol., 178 (2017) 279-287.
[19] L. Zhao, C. Wu, X. Lu, D. Ng, Y.B. Truong, Z. Xie, Activated carbon enhanced hydrophobic/hydrophilic dual-layer nanofiber composite membranes for high-performance direct contact membrane distillation, Desalination, 446 (2018) 59-69.
[20] M. Khayet, C. García-Payo, T. Matsuura, Superhydrophobic nanofibers electrospun by surface segregating fluorinated amphiphilic additive for membrane distillation, J. Membr. Sci., 588 (2019) 117215.
[21] M. Reza Shirzad Kebria, A. Rahimpour, S. Khoshhal Salestan, S. Fatemeh Seyedpour, A. Jafari, F. Banisheykholeslami, Naser Tavajohi Hassan Kiadeh, Hyper-branched dendritic structure modified PVDF electrospun membranes for air gap membrane distillation, Desalination, 479 (2020) 114307.
[22] E.J. Lee, B.J. Deka, J. Guo, Y.C. Woo, H.K. Shon, A.K. An, Engineering the Re-Entrant Hierarchy and Surface Energy of PDMS-PVDF Membrane for Membrane Distillation Using a Facile and Benign Microsphere Coating, Environ. Sci. Technol., 51 (2017) 10117-10126.
[23] E. Shaulsky, S. Nejati, C. Boo, F. Perreault, C.O. Osuji, M. Elimelech, Post-fabrication modification of electrospun nanofiber mats with polymer coating for membrane distillation applications, J. Membr. Sci., 530 (2017) 158-165.
[24] Z. Zhu, Z. Liu, L. Zhong, C. Song, W. Shi, F. Cui, W. Wang, Breathable and asymmetrically superwettable Janus membrane with robust oil-fouling resistance for durable membrane distillation, J. Membr. Sci., 563 (2018) 602-609.
[25] C. Su, T. Horseman, H. Cao, K.S.S. Christie, Y. Li, S. Lin, Robust Superhydrophobic Membrane for Membrane Distillation with Excellent Scaling Resistance, Environ. Sci. Technol., 53 (2019) 11801-11809.
[26] Y. Liao, G. Zheng, J.J. Huang, M. Tian, R. Wang, Development of robust and superhydrophobic membranes to mitigate membrane scaling and fouling in membrane distillation, J. Membr. Sci., 601 (2020) 117962.
[27] Y. Fan, S. Chen, H. Zhao, Y. Liu, Distillation membrane constructed by TiO2 nanofiber followed by fluorination for excellent water desalination performance, Desalination, 405 (2017) 51-58.
[28] H. Qiu, Y. Peng, L. Ge, B. Villacorta Hernandez, Z. Zhu, Pore channel surface modification for enhancing anti-fouling membrane distillation, Appl. Surf. Sci., 443 (2018) 217-226.
[29] A. Razmjou, E. Arifin, G.X. Dong, J. Mansouri, V. Chen, Superhydrophobic modification of TiO_2 nanocomposite PVDF membranes for applications in membrane distillation, J. Membr. Sci., 415-416 (2012) 850-863.
[30] C. Boo, J. Lee, M. Elimelech, Omniphobic Polyvinylidene Fluoride (PVDF) Membrane for Desalination of Shale Gas Produced Water by Membrane Distillation,

Environ. Sci. Technol., 50 (2016) 12275-12282.
[31] X. Zhang, L. Shen, W.-Z. Lang, Y. Wang, Improved performance of thin-film composite membrane with PVDF/PFSA substrate for forward osmosis process, J. Membr. Sci., 535 (2017) 188-199.
[32] H. Shan, J. Liu, X. Li, Y. Li, F.H. Tezel, B. Li, S. Wang, Nanocoated amphiphobic membrane for flux enhancement and comprehensive anti-fouling performance in direct contact membrane distillation, J. Membr. Sci., 567 (2018) 166-180.
[33] J. Li, S. Guo, Z. Xu, J. Li, Z. Pan, Z. Du, F. Cheng, Preparation of omniphobic PVDF membranes with silica nanoparticles for treating coking wastewater using direct contact membrane distillation: Electrostatic adsorption vs. chemical bonding, J. Membr. Sci., 574 (2019) 349-357.
[34] M. Han, T. Dong, D. Hou, J. Yao, L. Han, Carbon nanotube based Janus composite membrane of oil fouling resistance for direct contact membrane distillation, J. Membr. Sci., 607 (2020) 118078.
[35] J. Zuo, S. Bonyadi, T.-S. Chung, Exploring the potential of commercial polyethylene membranes for desalination by membrane distillation, J. Membr. Sci., 497 (2016) 239-247.
[36] Y. Chen, R. Zheng, J. Wang, Y. Liu, Y. Wang, X.-M. Li, T. He, Laminated PTFE membranes to enhance the performance in direct contact membrane distillation for high salinity solution, Desalination, 424 (2017) 140-148.
[37] A.L. McGaughey, P. Karandikar, M. Gupta, A.E. Childress, Hydrophobicity versus Pore Size: Polymer Coatings to Improve Membrane Wetting Resistance for Membrane Distillation, ACS Appl. Polym. Mater., 2 (2020) 1256-1267.
[38] G.R. Guillen, Y. Pan, M. Li, E.M.V. Hoek, Preparation and Characterization of Membranes Formed by Nonsolvent Induced Phase Separation: A Review, Ind. Eng. Chem. Res., 50 (2011) 3798-3817.
[39] D.-M. Wang, J.-Y. Lai, Recent advances in preparation and morphology control of polymeric membranes formed by nonsolvent induced phase separation, Curr. Opin. Chem. Eng., 2 (2013) 229-237.
[40] F.E. Ahmed, B.S. Lalia, R. Hashaikeh, A review on electrospinning for membrane fabrication: Challenges and applications, Desalination, 356 (2015) 15-30.
[41] C.-Y. Pan, G.-R. Xu, K. Xu, H.-L. Zhao, Y.-Q. Wu, H.-C. Su, J.-M. Xu, R. Das, Electrospun nanofibrous membranes in membrane distillation: Recent developments and future perspectives, Sep. Purif. Technol., 221 (2019) 44-63.
[42] F. Yalcinkaya, A review on advanced nanofiber technology for membrane distillation, J. Eng. Fibers Fabr., 14 (2019) 1-12.
[43] M.E. Leitch, C. Li, O. Ikkala, M.S. Mauter, G.V. Lowry, Bacterial Nanocellulose Aerogel Membranes: Novel High-Porosity Materials for Membrane Distillation, Environ. Sci. Technol. Lett., 3 (2016) 85-91.
[44] D. Hou, T. Li, X. Chen, S. He, J. Dai, S.A. Mofid, D. Hou, A. Iddya, D. Jassby, R. Yang, Hydrophobic nanostructured wood membrane for thermally efficient distillation, Sci. Adv., 5 (2019) 3203.
[45] Z.-X. Low, Y.T. Chua, B.M. Ray, D. Mattia, I.S. Metcalfe, D.A. Patterson, Perspective on 3D printing of separation membranes and comparison to related

unconventional fabrication techniques, J. Membr. Sci., 523 (2017) 596-613.
[46] C. Parra-Cabrera, C. Achille, S. Kuhn, R. Ameloot, 3D printing in chemical engineering and catalytic technology: structured catalysts, mixers and reactors, Chem. Soc. Rev., 47 (2018) 209-230.
[47] L.D. Tijing, J.R.C. Dizon, I. Ibrahim, A.R.N. Nisay, H.K. Shon, R.C. Advincula, 3D printing for membrane separation, desalination and water treatment, Appl. Mater. Today, (2019) 100486.
[48] N. Yanar, P. Kallem, M. Son, H. Park, S. Kang, H. Choi, A New Era of Water Treatment Technologies: 3D Printing for Membranes, J. Ind. Eng. Chem., (2020).
[49] T. Femmer, A.J.C. Kuehne, J. Torres-Rendon, A. Walther, M. Wessling, Print your membrane: Rapid prototyping of complex 3D-PDMS membranes via a sacrificial resist, J. Membr. Sci., 478 (2015) 12-18.
[50] A. Al-Shimmery, S. Mazinani, J. Ji, Y.M.J. Chew, D. Mattia, 3D printed composite membranes with enhanced anti-fouling behaviour, J. Membr. Sci., 574 (2019) 76-85.
[51] S. Mazinani, A. Al-Shimmery, Y.M.J. Chew, D. Mattia, 3D Printed Fouling-Resistant Composite Membranes, ACS Appl. Mater. Interfaces, 11 (2019) 26373-26383.
[52] S. Yuan, D. Strobbe, J.-P. Kruth, P. Van Puyvelde, B. Van der Bruggen, Production of polyamide-12 membranes for microfiltration through selective laser sintering, J. Membr. Sci., 525 (2017) 157-162.
[53] S. Yuan, J. Zhu, Y. Li, Y. Zhao, J. Li, P. Van Puyvelde, B. Van der Bruggen, Structure architecture of micro/nanoscale ZIF-L on a 3D printed membrane for a superhydrophobic and underwater superoleophobic surface, J. Materi. Chem. A, 7 (2019) 2723-2729.
[54] X.L. Yang Yang, Xuan Zheng, Zeyu Chen, Qifa Zhou, Yong Chen, 3D-Printed Biomimetic Super-Hydrophobic Structure for Microdroplet Manipulation and Oil/Water Separation, Adv. Mater., 30 (2018) 1704912.
[55] M. R. Chowdhury, J. Steffes, B. D. Huey, J. R. McCutcheon, 3D printed polyamide membranes for desalination, Science, 361 (2018) 682-686.
[56] L.C. Hwa, M.B. Uday, N. Ahmad, A.M. Noor, S. Rajoo, K.B. Zakaria, Integration and fabrication of the cheap ceramic membrane through 3D printing technology, Mater. Today Commun., 15 (2018) 134-142.
[57] A. Bottino, G. Camera-Roda, G. Capannelli, S. Munari, The formation of polyvinylidene difluoride microporous membranes by phase separation, J. Membr. Sci., 57 (1991) 1-20.
[58] M.-m. Tao, F. Liu, B.-r. Ma, L.-x. Xue, Effect of solvent power on PVDF membrane polymorphism during phase inversion, Desalination, 316 (2013) 137-145.
[59] X. Zhang, L. Shen, W.-Z. Lang, Y. Wang, Improved performance of thin-film composite membrane with PVDF/PFSA substrate for forward osmosis process, J. Membr. Sci., 535 (2017) 188-199.
[60] K.-J. Lu, J. Zuo, T.-S. Chung, Novel PVDF membranes comprising n-butylamine functionalized graphene oxide for direct contact membrane distillation, J. Membr. Sci., 539 (2017) 34-42.
[61] E.C. Mapunda, B.B. Mamba, T.A.M. Msagati, Carbon nanotube embedded PVDF membranes: Effect of solvent composition on the structural morphology for membrane

distillation, Phys. Chem. Earth, 100 (2017) 135-142.
[62] T.A. Agbaje, S. Al-Gharabli, M.O. Mavukkandy, J. Kujawa, H.A. Arafat, PVDF/magnetite blend membranes for enhanced flux and salt rejection in membrane distillation, Desalination, 436 (2018) 69-80.
[63] H. Zhang, B. Li, D. Sun, X. Miao, Y. Gu, SiO2-PDMS-PVDF hollow fiber membrane with high flux for vacuum membrane distillation, Desalination, 429 (2018) 33-43.
[64] S. Dupin, O. Lame, C. Barrès, J.-Y. Charmeau, Microstructural origin of physical and mechanical properties of polyamide 12 processed by laser sintering, Eur. Polym. J., 48 (2012) 1611-1621.
[65] G. Wang, P. Wang, Z. Zhen, W. Zhang, J. Ji, Preparation of PA12 microspheres with tunable morphology and size for use in SLS processing, Mater. Design, 87 (2015) 656-662.
[66] L. Verbelen, S. Dadbakhsh, M. Van den Eynde, J.-P. Kruth, B. Goderis, P. Van Puyvelde, Characterization of polyamide powders for determination of laser sintering processability, Eur. Polym. J., 75 (2016) 163-174.

Chapter 4

One-step fabrication of isotropic poly (vinylidene fluoride) membranes for direct contact membrane distillation (DCMD)

Adapted from: Miaomiao Tian, Shushan Yuan, Florian Decaesstecker, Junyong Zhu, Alexander Volodine, Bart Van der Bruggen. One-step fabrication of isotropic poly (vinylidene fluoride) membranes for direct contact membrane distillation (DCMD). Desalination, 477(2020), 114265

4.1 Introduction

As mentioned in Chapter 1, developing MD membranes generally involves nonsolvent induced phase separation (NIPS) [1-4], electrospinning [5-11], and/or modification [12-20]. Electrospun membranes have received growing attention in recent years due to the high porosity, good interconnectivity, and high surface area. However, thermally or chemically post-treatment is normally required to optimize the membrane structure and physicochemical properties, such as pore size, hydrophobicity, and/or mechanical integrity [21]. Surface modification, such as coating [12,16], chemical vapor deposition [22], and CF_4 plasma 13,23], is another efficacious means to fabricate high-performance MD membranes [24]. In general, nanoparticles are mostly utilized in the surface modification process to form a micro-/nano- hierarchical structure, notably elevating the surface roughness and improving the MD performance. Nevertheless, the instability, the possibility of particle aggregation, and the high cost of the nanoparticles significantly hinder the industrialization of such membranes. In addition, NIPS is the commonly used method for MD membrane fabrication with desired pore structure and hydrophobicity by incorporating various additives, such as small nonsolvent molecules, inorganic materials, macromolecules, as well as their combinations [4, 25-29]. Furthermore, the control of the phase inversion process by

altering the composition of the coagulation bath is also adopted to optimize the membrane structure, such as the well-known dual coagulation bath [30]. Nonetheless, the major issues of preparing MD membranes via NIPS are the non-uniformity of the membrane structure, the defects caused by aggregation of the additives, as well as the use of environmentally unfriendly solvents.

Using water as coagulation bath, asymmetric PVDF membranes with dense top surface and macro-voids were generally obtained due to the fast solvent/nonsolvent exchange during phase separation [31, 32], which will severely reduce the membrane performance in MD process: it increases the mass transfer resistance, or decreases the liquid entry pressure (LEP). Thus, it is beneficial to prepare membranes with a symmetric, sponge-like, and macro-voids free structure to improve the membrane performance by decreasing the precipitation rate. Several studies were performed to use a soft nonsolvent (such as methanol, ethanol, propanol, octanol) as coagulation bath instead of water, which could change the membrane formation mechanism and thus generate membranes with skinless top surface and symmetrical structure without macro-voids [33-37]. For instance, Lin et al. [33] fabricated porous PVDF membranes using 1-octanol as coagulation bath, and the fabricated membranes exhibited a uniform cross-section composed of interlocked crystal elements coexisting with the network of continuous pores. Similarly, Nejati et al. [34] reported the construction of PVDF membranes using 2-propanol/water mixture as the coagulation bath. It was found that increasing the concentration of propanol could substantially enhance the membrane surface porosity and roughness, thus obviously heightening the water flux. In another report, Munirasu et al. [35] fabricated PVDF membranes using methanol as nonsolvent. The resultant membranes had intrinsically superhydrophobic characteristics due to the formation of a sponge-like interconnected fibrous microstructure. The MD flux of the superhydrophobic PVDF membranes was more than twice the flux of conventional water induced membranes. However, the use of alcohols as nonsolvent inevitably increases the preparation cost, prolongs the preparation processes, and is environmentally unfriendly. Therefore, it is envisaged that it will be more cost-effective

to decrease the solvent/nonsolvent exchange rate while using water as coagulation bath.

To address the above-mentioned issues, the use of water as coagulation bath to prepare isotropic and porous PVDF membranes in one step is reported in this paper. Briefly, the PVDF/NMP casting solution was cast on the glass plate, followed by simply covering a piece of non-woven substrate on the nascent film. The following wet phase inversion process was performed by soaking them into the water coagulation bath. In this regard, the solvent/nonsolvent exchange rate could be considerably reduced due to the barrier effect of the non-woven support, thus largely changing the membrane morphology and structure. Such one-step, bottom-up strategy facilitates the formation of the skinless, isotropic, highly hydrophobic, and porous membranes. The effect of different polymer concentration on the surface structure and separation performance of the obtained PVDF membranes was studied in detail. In addition, the synthesized membranes were characterized using SEM, AFM, contact angle, pore size, porosity, and direct contact membrane distillation (DCMD) performance.

4.2 Results and discussion

4.2.1 Membrane morphologies and hydrophobicity

The membrane morphologies (surface and cross-section) characterized by SEM images are separately illustrated in Figure 4.1 and Figure 4.2, respectively. It can be found that the membrane surface morphology and overall structure change drastically by using the bottom-up method compared to the traditional phase inversion. A dense top surface with macro-voids structure is observed for the PVDF-N membrane, while skinless, isotropic, and spherulites composed membranes are obtained assisted by the bottom-up strategies.

As a semi-crystalline polymer, two kinds of membrane formation mechanisms will occur for the PVDF dope solution in the NIPS process: solid-liquid demixing (crystallization) and liquid-liquid demixing [33,39]. Generally, the liquid–liquid demixing engenders membranes with dense top layer, macro-voids, and cellular pores due to the rapid solvent/nonsolvent exchange, as shown in Figure 4.1 and Figure 4.2

(PVDF-N). In contrast, the crystallization process typically results in the formation of granular membranes with bi-continuous structure composed of globules joined together [33, 36, 39], as depicted in Figure 4.1 and Figure 4.2 (PVDF-15). Occasionally, crystallization may take place simultaneously with liquid–liquid demixing to form membranes having the features of crystallization (*i.e.*, crystalline particles) and liquid–liquid demixing (*i.e.*, macro-voids). In general, the phase separation mechanism can be properly tailored by changing the polymer dope solution to metastable dopes, which is on the edge of precipitation. Therefore, a skinless membrane could be obtained by immersing into a soft nonsolvent bath [37, 39].

In this work, the strong nonsolvent (i.e., water) instead of soft nonsolvent is firstly utilized as the coagulation bath to prepare isotropic membranes. Different from the traditional phase inversion process, a piece of non-woven substrate is used to cover the nascent dope solution film, aiming to prevent the solvent/nonsolvent from exchanging immediately upon contacting with water. The non-woven is hydrophobic (the contact angle is ~130°), thus can slow down the penetration of water into the dope solution film. Therefore, the solvent/nonsolvent exchange rate is largely reduced through physical barrier effect in the early stage, which results in the crystallization process. Furthermore, the surface morphologies of the bottom-up membranes comprise the flattened structure (*i.e.*, truncated globules), which is because the growth is largely limited by the substrate, as shown in Figure 4.1 [36]. Besides, by elevating the polymer concentration, it can be found that the size of the globules increases significantly, and the interglobular connections change dramatically, especially for PVDF-18 membrane. In view of PVDF-15 and PVDF-16.5 membranes, the particles are found to be evenly distributed throughout the whole membranes with a typical diameter of about 0.9 μm and 1.2 μm, respectively. The presence of these globules is probably because of radially growth of individual PVDF nuclei in the meantime until it reaches the point of mutual restriction. The globular-globular connections are in the form of a group of sheets or in the form of a set of fibrils; it can be assumed that these features are most probably one or a few folded lamellae thick [33]. However, the globules of PVDF-18 membrane are further

perfected and larger than PVDF-15 and PVDF-16.5, but not uniform in diameter (*i.e.*, 1.8-3.7 μm). Furthermore, a large quantity of sheaf-like textures can be observed among the globules except the sheets and fibrils. The polymer solution viscosity is thought to affect the crystallization process, where the increased viscosity could result in an impediment of nonsolvent diffusion into polymer solution layer during the precipitation process [31, 33], as shown in Table 4.1. In addition, the rate of formation of nuclei is reduced, which gives the spherulites more time to grow.

Table 4.1 Viscosities of PVDF solutions at 25 °C

PVDF concentration	Viscosity (mPa·s)
15 wt.%	3956±87
16.5 wt.%	6160±107
18 wt.%	8666±143

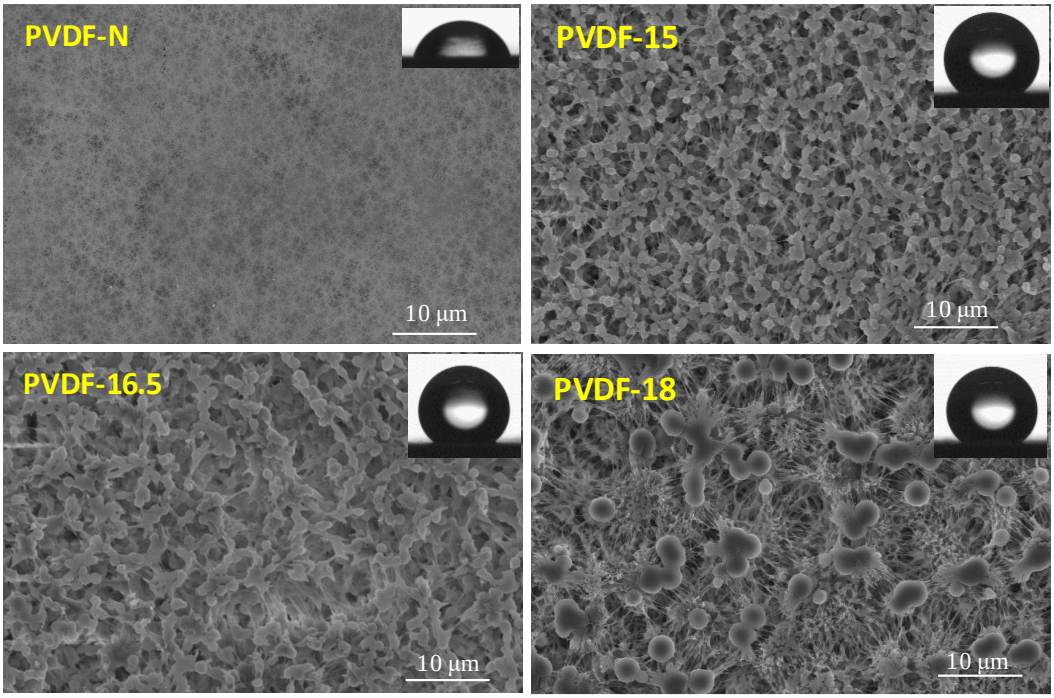


Figure 4.1 SEM images of the top surface of the normal casting and bottom-up membranes. The insert photos are 3 μL water droplets on the top surface.

The images of water droplets (3 μL) on the membrane surfaces and the contact angles are shown in Figure 4.1 and Table 4.3, respectively. The contact angles dramatically increase from 71.7° for PVDF-N membrane to ~144° for bottom-up membranes, which can be attributed to the particulate rough surface of the bottom-up membranes compared to the smooth surface of PVDF-N membrane. However, the contact angles are similar for the bottom-up membranes fabricated by different polymer concentration, which might be ascribed to the same surface energy and similar magnitude roughness.

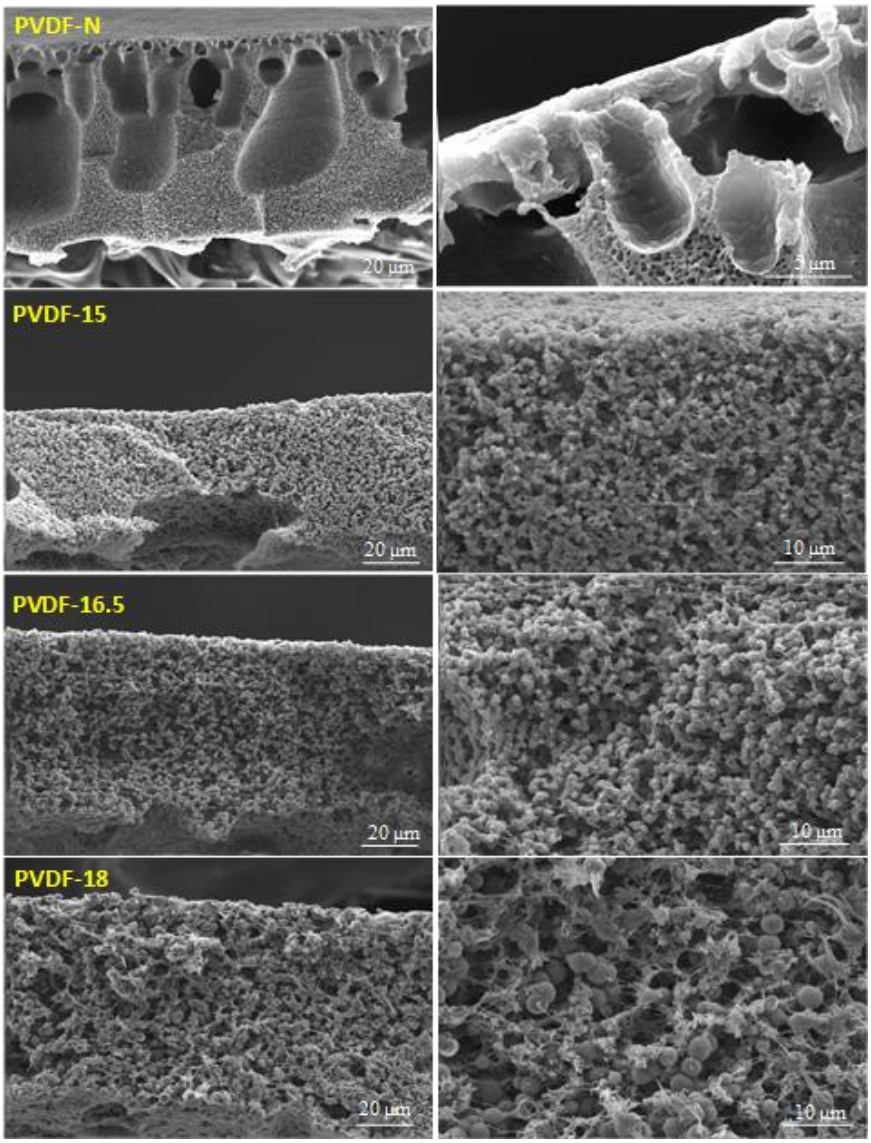


Figure 4.2 SEM images of the cross-section of the PVDF membranes prepared by normal casting and bottom-up methods

Figure 4.3 depicts the AFM images, and Table 4.2 summarizes the surface roughness parameters. The surface roughness increases from 0.0255 µm for the PVDF-N membrane to 0.179 µm for the bottom-up membrane using the same concentration of the PVDF dope solution. Such high increment can be explained by the formed particulate surface, which is in accordance with the SEM images. The roughness decreases slightly with the polymer concentration increase, which is probably resulting from the larger globules size but less globule quantity in the same area.

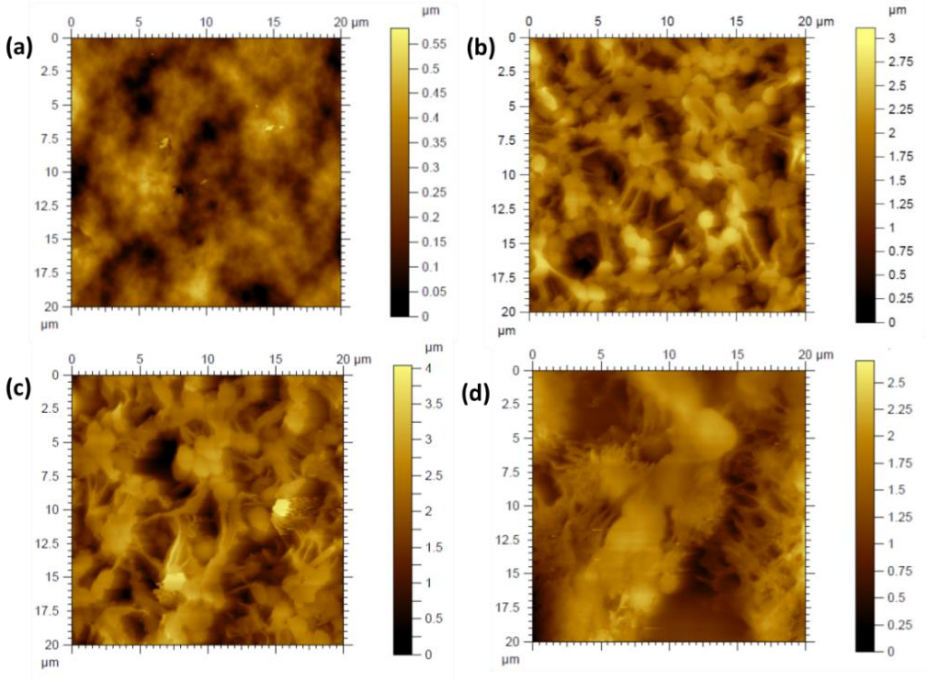


Figure 4.3 AFM images of the normal casting and bottom-up membranes. (a) PVDF-N, (b) PVDF-15, (c) PVDF-16.5, and (d) PVDF-18

Table 4.2 AFM results for the prepared membranes

Membrane Label	R_a (µm)	R_{rms} (µm)	R_{max} (µm)
PVDF-N	0.0255	0.0336	0.268
PVDF-15	0.179	0.218	1.68
PVDF-16.5	0.165	0.215	1.50
PVDF-18	0.110	0.148	1.61

R_a: average roughness

R_{rms}: root mean square roughness

R_{max}: maximum vertical difference between the highest peaks and the lowest valleys

4.2.2 Pore size, and porosity

Table 4.3 lists the contact angle, thickness, porosity, pore size, and LEP of the fabricated membranes. Apparently, the enhancement of the polymer concentration leads to an enhanced membrane thickness. Additionally, the thickness of PVDF-15 is lower than PVDF-N using the same dope solution. This is mainly attributed to the fact that the process of covering the non-woven leads to the thinner nascent film than normal casting. The overall porosity is lower than the assumed results from the SEM images, as the calculated results for the PVDF layer is 90%-92%. It may be postulated that the low porosity of the non-woven substrate dominates the overall porosity. Although the porosity of the PVDF layer is relatively high, the thickness of the polymer layer is only a small portion of the entire thickness, leading to a low porosity compared to the pure PVDF layer. The porosities of the bottom-up membranes are lower than those of PVDF-N membranes, which might be due to the absence of macro-voids. Furthermore, the porosity elevates when the polymer concentration increases, which can be explained by the larger globule sizes and interglobular voids, as well as a greater thickness. The mean pore sizes of the bottom-up membranes greatly enlarge compared to the PVDF-N membrane of 0.17 μm, which is accordance with the SEM images. The PVDF-18 membrane has the highest pore size due to the largest globule size and internal voids. According to section 1.3.2.3, an optimum pore size for MD membrane is 0.3-0.6 μm; thus, PVDF-16.5 membrane showed the closest value of 0.74 μm to the optimal pore size. In addition, a larger pore size leads to a low LEP, which increases the tendency of feed solution leakage at a high pressure difference across the membrane. Therefore, the LEP results of the bottom-up membranes are relatively low due to the large pores. For the PVDF-N membrane, the LEP could be obtained as the non-woven substrate has a high contact angle of 130° although the PVDF layer is not hydrophobic. PVDF-18 membrane shows the lowest LEP values is predictable as it exhibits the largest pore size while similar hydrophobicity among these three membranes.

Table 4.3 Comparison of contact angle, thickness, porosity, and mean pore size of the prepared membranes

Membrane label	PVDF-N	PVDF-15	PVDF-16.5	PVDF-18
Contact angle (°)	71.7±1.7	144.0±2.2	144.5±1.5	144.4±0.7
Thickness, δ (μm)	254±2	227±3	248±2	257±3
Porosity, ε (%)	44.4±2.6	35.1±1.2	37.9±2.8	41.7±1.2
Mean pore size, d (μm)	0.17±0.01	0.99±0.04	0.74±0.09	1.81±0.27
LEP, (bar)	0.63±0.05	0.72±0.05	0.7±0.08	0.52±0.1

* The thickness of the non-woven substrate is 180 μm.

4.2.3 DCMD performance

The DCMD fluxes of the prepared membranes at different feed solution temperatures are displayed in Figure 4.4. The fluxes typically boost with the increase of temperature, which is related to the increment in the vapor pressure difference, *i.e.* the driving force [10, 40]. The rejection is 99.97% in all cases. In addition, the fluxes of the PVDF-15 membrane are almost a factor two higher than the PVDF-N membrane, which is primarily due to the combination of a skinless surface, a larger pore size, a lower thickness, and the well interconnected pore structure generated by the particles. Although the difference among these membranes is not significant, the PVDF-15 membrane shows the highest flux while the PVDF-18 membrane has the lowest flux. It can be suggested that PVDF-15 has the thinnest polymer layer, which generates the lowest mass transfer resistance. Meanwhile, the lowest flux of the PVDF-18 membrane may be caused by the large amount of the inter-globule connections and the thickest polymer layer. Compared to the benchmark in chapter 1, the PVDF-15 and PVDF-16.5 membranes reach the targeted MD flux at feed and permeate temperatures of 60 °C and 20 °C, while the PVDF-18 membrane has a slightly lower flux of 24.2 kg/(m^2·h).

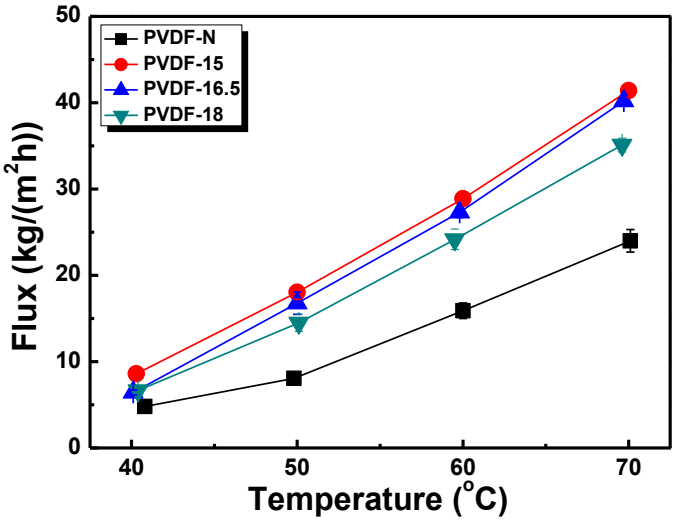


Figure 4.4 DCMD fluxes at different feed temperatures of the prepared PVDF membranes. The permeate temperature is 20.0±0.5 °C. The feed solution is 35 g/L NaCl solution. The flow rate of feed and permeate solution is 40 L/h.

4.3 Conclusions

This work proposed a cost-effective bottom-up method for the preparation of symmetric PVDF membranes using water as coagulation bath, which might be a feasible approach of manufacturing MD membranes with desirable separation performance. As confirmed from the SEM images, the obtained membranes composed of interlinked globules are isotropic and porous. A sharp increase of water contact angles from normal casting membranes (71.7°) to the bottom-up membrane (144°) confirms the successful preparation of highly hydrophobic PVDF membranes using water bath for phase inversion. This ingenious design could effectively delay the solvent/non-solvent exchange rate via the physical barrier effect. Meanwhile, the surface roughness significantly augments from 0.0255 μm of the normal casting membrane to 0.179 μm of the bottom-up membrane using the same dope solution composition. The DCMD fluxes of bottom-up membranes at different feed solution temperatures are almost twice as the normal casting membrane. Comparing to the benchmark described in section 1.6, a simple preparation process and cost-effective materials are used at ambient temperature and pressure, the surface hydrophobicity is satisfied with contact angles higher than 130°, the pore sizes of PVDF-15 and

PVDF-16.5 membranes locate in the range of 0.1-1 μm, the PVDF layer thicknesses are 47-77 μm, and the MD fluxes of PVDF-15 and PVDF-16.5 membranes reach 28.9 kg/(m^2·h) and 27.3 kg/(m^2·h) at feed and permeate temperatures of 60 °C and 20 °C, respectively. However, the LEP values of the prepared membrane are relatively lower due to the large pores, especially for PVDF-18 membrane. Additionally, the membrane porosities are too low than the desired values. Although the PVDF polymer layer has a high porosity of 90%-92%, the less-porous non-woven substrate reduces the overall porosity. Therefore, a more porous substrate with less thickness should be chosen to further improve the MD performance.

References:

[1] S. Leaper, A. Abdel-Karim, B. Faki, J.M. Luque-Alled, M. Alberto, A. Vijayaraghavan, S.M. Holmes, G. Szekely, M.I. Badawy, N. Shokri, P. Gorgojo, Flux-enhanced PVDF mixed matrix membranes incorporating APTS-functionalized graphene oxide for membrane distillation, J. Membr. Sci., 554 (2018) 309-323.
[2] K.-J. Lu, J. Zuo, T.-S. Chung, Novel PVDF membranes comprising n-butylamine functionalized graphene oxide for direct contact membrane distillation, J. Membr. Sci., 539 (2017) 34-42.
[3] H. Zhang, B. Li, D. Sun, X. Miao, Y. Gu, SiO2-PDMS-PVDF hollow fiber membrane with high flux for vacuum membrane distillation, Desalination, 429 (2018) 33-43.
[4] M. Khayet, C. Cojocaru, M.C. García-Payo, Experimental design and optimization of asymmetric flat-sheet membranes prepared for direct contact membrane distillation, J. Membr. Sci., 351 (2010) 234-245.
[5] H. Maab, L. Francis, A. Al-saadi, C. Aubry, N. Ghaffour, G. Amy, S.P. Nunes, Synthesis and fabrication of nanostructured hydrophobic polyazole membranes for low-energy water recovery, J. Membr. Sci., 423-424 (2012) 11-19.
[6] Y. Liao, R. Wang, M. Tian, C. Qiu, A.G. Fane, Fabrication of polyvinylidene fluoride (PVDF) nanofiber membranes by electro-spinning for direct contact membrane distillation, J. Membr. Sci., 425-426 (2013) 30-39.
[7] Y. Chul Woo, Y. Chen, L.D. Tijing, S. Phuntsho, T. He, J.-S. Choi, S.-H. Kim, H. Kyong Shon, CF4 plasma-modified omniphobic electrospun nanofiber membrane for produced water brine treatment by membrane distillation, J. Membr. Sci., 529 (2017) 234-242.
[8] Y. Zhang, B. Yang, K. Li, D. Hou, C. Zhao, J. Wang, Electrospun porous poly(tetrafluoroethylene-co-hexafluoropropylene-co-vinylidene fluoride) membranes for membrane distillation, RSC Adv., 7 (2017) 56183-56193.
[9] Z. Zhu, Z. Liu, L. Zhong, C. Song, W. Shi, F. Cui, W. Wang, Breathable and asymmetrically superwettable Janus membrane with robust oil-fouling resistance for

durable membrane distillation, J. Membr. Sci., 563 (2018) 602-609.
[10] L. Deng, P. Li, K. Liu, X. Wang, B.S. Hsiao, Robust superhydrophobic dual layer nanofibrous composite membranes with a hierarchically structured amorphous polypropylene skin for membrane distillation, J. Mater. Chem. A, 7 (2019) 11282-11297.
[11] B.S. Lalia, E. Guillen-Burrieza, H.A. Arafat, R. Hashaikeh, Fabrication and characterization of polyvinylidenefluoride-co-hexafluoropropylene (PVDF-HFP) electrospun membranes for direct contact membrane distillation, J. Membr. Sci., 428 (2013) 104-115.
[12] A. Razmjou, E. Arifin, G.X. Dong, J. Mansouri, V. Chen, Superhydrophobic modification of TiO2 nanocomposite PVDF membranes for applications in membrane distillation, J. Membr. Sci., 415-416 (2012) 850-863.
[13] X. Wei, B.L. Zhao, X.M. Li, Z.W. Wang, B.Q. He, T. He, B. Jiang, CF4 plasma surface modification of asymmetric hydrophilic polyethersulfone membranes for direct contact membrane distillation, J Membr Sci, 407-408 (2012) 164-175.
[14] N.G.P. Chew, S. Zhao, C. Malde, R. Wang, Polyvinylidene fluoride membrane modification via oxidant-induced dopamine polymerization for sustainable direct-contact membrane distillation, J. Membr. Sci., 563 (2018) 31-42.
[15] H. Shan, J. Liu, X. Li, Y. Li, F.H. Tezel, B. Li, S. Wang, Nanocoated amphiphobic membrane for flux enhancement and comprehensive anti-fouling performance in direct contact membrane distillation, J. Membr. Sci., 567 (2018) 166-180.
[16] J. Li, S. Guo, Z. Xu, J. Li, Z. Pan, Z. Du, F. Cheng, Preparation of omniphobic PVDF membranes with silica nanoparticles for treating coking wastewater using direct contact membrane distillation: Electrostatic adsorption vs. chemical bonding, J. Membr. Sci., 574 (2019) 349-357.
[17] Z. Xiao, R. Zheng, Y. Liu, H. He, X. Yuan, Y. Ji, D. Li, H. Yin, Y. Zhang, X.M. Li, T. He, Slippery for scaling resistance in membrane distillation: A novel porous micropillared superhydrophobic surface, Water Res., 155 (2019) 152-161.
[18] C. Boo, J. Lee, M. Elimelech, Engineering Surface Energy and Nanostructure of Microporous Films for Expanded Membrane Distillation Applications, Environ. Sci. Technol., 50 (2016) 8112-8119.
[19] M. Xie, W. Luo, S.R. Gray, Surface pattern by nanoimprint for membrane fouling mitigation: Design, performance and mechanisms, Water Res., 124 (2017) 238-243.
[20] T. Horseman, C. Su, K.S.S. Christie, S. Lin, Highly Effective Scaling Mitigation in Membrane Distillation Using a Superhydrophobic Membrane with Gas Purging, Environ. Sci. Tech. Let., 6 (2019) 423-429.
[21] F.E. Ahmed, B.S. Lalia, R. Hashaikeh, A review on electrospinning for membrane fabrication: Challenges and applications, Desalination, 356 (2015) 15-30.
[22] M.M. Aljumaily, M.A. Alsaadi, N.A. Hashim, Q.F. Alsalhy, R. Das, F.S. Mjalli, Embedded high-hydrophobic CNMs prepared by CVD technique with PVDF-co-HFP membrane for application in water desalination by DCMD, Desalination Water Treat., 142 (2019) 37-48.
[23] C. Yang, X.M. Li, J. Gilron, D.f. Kong, Y. Yin, Y. Oren, C. Linder, T. He, CF4 plasma-modified superhydrophobic PVDF membranes for direct contact membrane

distillation, J. Membr. Sci., 456 (2014) 155-161.
[24] P. Wang, T.-S. Chung, Recent advances in membrane distillation processes: Membrane development, configuration design and application exploring, J. Membr. Sci., 474 (2015) 39-56.
[25] M. Yeow, Y. Liu, K. Li, Preparation of porous PVDF hollow fibre membrane via a phase inversion method using lithium perchlorate (LiClO) as an additive, J. Membr. Sci., 258 (2005) 16-22.
[26] S. Simone, A. Figoli, A. Criscuoli, M.C. Carnevale, A. Rosselli, E. Drioli, Preparation of hollow fibre membranes from PVDF/PVP blends and their application in VMD, J. Membr. Sci., 364 (2010) 219-232.
[27] K. Gethard, O. Sae-Khow, S. Mitra, Water desalination using carbon-nanotube-enhanced membrane distillation, ACS Appl. Mater. Interfaces, 3 (2011) 110-114.
[28] T.A. Agbaje, S. Al-Gharabli, M.O. Mavukkandy, J. Kujawa, H.A. Arafat, PVDF/magnetite blend membranes for enhanced flux and salt rejection in membrane distillation, Desalination, 436 (2018) 69-80.
[29] A. Politano, P. Argurio, G. Di Profio, V. Sanna, A. Cupolillo, S. Chakraborty, H.A. Arafat, E. Curcio, Photothermal Membrane Distillation for Seawater Desalination, Adv. Mater., 29 (2017).
[30] M. Tian, Y. Yin, C. Yang, B. Zhao, J. Song, J. Liu, X.-M. Li, T. He, CF4 plasma modified highly interconnective porous polysulfone membranes for direct contact membrane distillation (DCMD), Desalination, 369 (2015) 105-114.
[31] C. Alexowsky, M. Bojarska, M. Ulbricht, Porous poly(vinylidene fluoride) membranes with tailored properties by fast and scalable non-solvent vapor induced phase separation, J. Membr. Sci., 577 (2019) 69-78.
[32] F. Abdulla AlMarzooqi, M. Roil Bilad, H. Ali Arafat, Improving Liquid Entry Pressure of Polyvinylidene Fluoride (PVDF) Membranes by Exploiting the Role of Fabrication Parameters in Vapor-Induced Phase Separation VIPS and Non-Solvent-Induced Phase Separation (NIPS) Processes, Appl. Sci., 7 (2017) 181.
[33] D.-J. Lin, K. Beltsios, C.-L. Chang, L.-P. Cheng, Fine Structure and Formation Mechanism of Particulate Phase-Inversion Poly(vinylidene fluoride) Membranes, J. Polym. Sci. B, 41 (2003) 1578-1588.
[34] S. Nejati, C. Boo, C.O. Osuji, M. Elimelech, Engineering flat sheet microporous PVDF films for membrane distillation, J. Membr. Sci., 492 (2015) 355-363.
[35] S. Munirasu, F. Banat, A.A. Durrani, M.A. Haija, Intrinsically superhydrophobic PVDF membrane by phase inversion for membrane distillation, Desalination, 417 (2017) 77-86.
[36] D.-J. Lin, H.-H. Chang, T.-C. Chen, Y.-C. Lee, L.-P. Cheng, Formation of porous poly(vinylidene fluoride) membranes with symmetric or asymmetric morphology by immersion precipitation in the water/TEP/PVDF system, Eur. Polym. J., 42 (2006) 1581-1594.
[37] X. Li, Y. Wang, X. Lu, C. Xiao, Morphology changes of polyvinylidene fluoride membrane under different phase separation mechanisms, J. Membr. Sci., 320 (2008) 477-482.
[38] Y. Chen, M. Tian, X. Li, Y. Wang, A.K. An, J. Fang, T. He, Anti-wetting behavior

of negatively charged superhydrophobic PVDF membranes in direct contact membrane distillation of emulsified wastewaters, J. Membr. Sci., 535 (2017) 230-238.
[39] D.-J. Lin, K. Beltsios, T.-H. Young, Y.-S. Jeng, L.-P. Cheng, Strong effect of precursor preparation on the morphology of semicrystalline phase inversion poly(vinylidene fluoride) membranes, J. Membr. Sci., 274 (2006) 64-72.
[40] C. Su, Y. Li, H. Cao, C. Lu, Y. Li, J. Chang, F. Duan, Novel PTFE hollow fiber membrane fabricated by emulsion electrospinning and sintering for membrane distillation, J. Membr. Sci., 583 (2019) 200-208.

Chapter 5

A co-casting route enables the formation of skinless, hydrophobic poly(vinylidene fluoride) membranes for DCMD

Adapted from: Miaomiao Tian, Junyong Zhu, Shushan Yuan, Yatao Zhang, Bart Van der Bruggen, A co-casting route enables the formation of skinless, hydrophobic poly(vinylidene fluoride) membranes for DCMD, (Journal of Membrane Science, major revision)

5.1 Introduction

Polyvinylidene fluoride (PVDF) is the mostly investigated polymer for MD membranes considering its inherent hydrophobicity and solubility in diverse organic solvents [1]. Various methods have been explored to fabricate skinless and porous PVDF membranes with highly hydrophobicity, such as adding solvent or soft nonsolvent (*i.e.*, alcohols) to the coagulation bath, elevating the coagulation bath temperature, and exposing the nascent film to a humid environment [2-8]. However, addition of a solvent or an alcohol as nonsolvent is environmentally unfriendly and costly. Raising the bath temperature needs an accurate control during the preparation process to maintain the same membrane morphology, meanwhile, it is also energy-intensive. Accordingly, it is of great significance from both scientific and practical perspectives to utilize a simple and cost-effective polymer system with only a water bath at room temperature to fabricate porous and symmetric membranes for MD.

Co-casting and co-extrusion, referring to prepare membranes by simultaneously casting or extruding two different polymer solutions, has been extensively studied to prepare dual-layer (DL) membranes for various applications including gas separation [9-11], pervaporation (PV) [12], ultrafiltration (UF) [13], nanofiltration (NF) [14, 15], forward osmosis (FO), pressure retarded osmosis (PRO) [16], and MD [17-20]. The

main advantages of this technology are the convenience and simplicity to prepare composite membranes by merging the prominent performance of each layer in one step which is time-saving, as well as the low cost by adopting a more economical polymer as the support layer material [21, 22]. He et al. [14] developed DL hollow fiber (HF) membranes with a thin ion exchange layer (hydrophilic sulfonated polyethersulfone (SPES)) and a polysulfone (PSf) support by co-extruding. The mechanical stability and the adhesion of the coating layer on the supporting layer were investigated, and it was found that the SPES concentration played a significant role. With SPES concentration increased from 20 wt.% to 30 wt.%, the SPES layer transformed from a brittle film to a more flexible one, which had enough mechanical strength to avoid broken after drying. Moreover, with a high concentration, delamination of the two layers could be avoided, and it can be ascribed to the high solution viscosity which led to slow water in-diffusion and longer time for polymer chains interdiffusion. In addition, the as-fabricated membranes exhibited a good nanofiltration performance with high rejection of large charged molecules and easy penetration of inorganic salts. Liu et al. [12] spun composite membranes containing an expensive P84 (co-polyimide) layer onto a low-cost PES support layer for isopropanol dehydration in the PV process. To avoid the interfacial layer delamination, three factors were considered: (1) material compatibility (PES was chosen as PES showed good interactions with most polyimides), (2) a proper polymer concentration with a high viscosity, and (3) a suitable ration of the outer-layer to inner-layer dope solution flow rate during the spinning process. Two kinds of DL HF membranes were prepared through wet-spun (the spinneret is submerged in the coagulation bath) and dry-jet wet-spun (the spinneret is located above the coagulation bath) processes, and the influence of spinning conditions (air gap, outer solution flow rate, and inner solution flow rate) were studied. Results showed that a higher air gap resulted in a poor pervaporation performance, a higher outer-layer flow rate improved the selectivity while reduced the flux for wet-spun membranes (no improvement for dry-jet wet-spun membranes), and a higher inner flow rate led to a decrease in both flux and selectivity, as well as defects in the outer-layer (no influence on the performance of

dry-jet wet-spun membranes). Moreover, post modifications were utilized to improve the poor selectivity of the as-spun membranes, and two kinds of post-modifications (*i.e.*, heat treatment and chemical cross-linking with *p*-xylenediamine) were compared. Results demonstrated that the selectivity enhancement by heat treatment was limited due to the closure of the pores in the substrate in high temperatures, and the flux was sharply decreased. For the chemical modification, *p*-xylenediamine was chosen due to its effect in densifying the skin layer while not affect the PES layer. With an optimal immersion time in *p*-xylenediamine solution, a better performance improvement (separation factor increased 15 times while flux decreased 43%) was obtained than heat treatment (separation factor increased 1.8 times while flux decreased 60%). Moreover, the overall material cost was saved by using a cheaper PES support layer. Matrimid, a commercial material with superior O_2/N_2 permeation properties, was co-extruded as an outer layer with PSf as an inner layer to prepare dual-layer membranes [9]. The influence of solution composition and the spinning conditions on the membrane separation performance was evaluated. In the outer layer dope solution, a mixed solvent of NMP and THF with different ratio was used, and it was found that a higher THF concentration led to a higher selectivity but lower permeance. This can be explained by the high volatility of THF, where a high THF concentration resulted in a higher polymer concentration after evaporation through the air gap, which led to a thicker and denser membrane. Additionally, the critical air gap distance and spinning temperature were determined at 3 cm and 45 °C, respectively. Especially, after a 3 wt.% silicon coating was conducted on the as-spun membrane, a higher O_2/N_2 selectivity than the intrinsic value of Matrimid could be reached after heat-treatment. In addition, dual-layer HF membranes comprising a dense polybenzimidazole/ polyhedral oligomeric silsesquioxane (PBI/POSS) selective outer layer and a cheaper polyacrylonitrile/polyvinylpyrrolidone (PAN/PVP) inner layer was co-extruded for PRO process [23]. Results showed that the addition of PVP could effectively reduce the finger-like structures in the support layer and avoid delamination due to the increased solution viscosity. Additionally, the incorporation of POSS into the PBI layer reduced

the dense layer thickness, thus enhanced both the water and salt permeability across the membrane. Composite HF membranes with a hydrophobic PVDF outer layer and a hydrophilic PVDF/ polyacrylonitrile (PAN) inner layer were fabricated by co-extrusion for DCMD for the first time by Bonyadi and co-workers [17]. Clay particles were added in both dope solutions to enhance the mechanical strength, and the PVDF in the inner layer solution was used to avoid delamination. The effect of the coagulation reagent on the membrane morphology was studied by increasing the methanol content in a water bath. The PVDF surface transformed from dense and smooth in a pure water bath to porous and fiber-like morphology in an 80 wt.% methanol bath due to the delayed demixing during the phase separation process. In the DCMD test using a 3.5 wt.% NaCl as feed solution, a high flux of 55 kg/(m^2·h) based on the outer diameter can be achieved at feed and permeate inlet temperatures of 90.3 °C and 16.5 °C, respectively. Likewise, a flat-sheet Janus membrane with a thin hydrophobic PVDF layer and a hydrophilic PVDF-polyvinyl alcohol (PVA) layer were prepared by co-casting combined with a nonsolvent TIPS (NTIPS) for MD [20]. In this work, a special solvent, ε-Caprolactam (CPL), was used to prepare the dope solutions. The membrane preparation process consisted of co-casting dope solutions of PVDF/CPL and PVDF/PVA/CPL (the ratio of PVDF to PVA was 8:2) at 150 °C, followed by immersing the nascent film into a cold coagulation bath (5-50 °C). After the obtained membranes were soaked in DI water for 24 h to complete the solvent exchange, the membranes were frozen in a refrigerator for 12 h followed by drying in a freeze drier. The composite membrane showed a dense skin with finger-like macro-voids beneath the skin for the hydrophobic layer and a highly porous cellular pore structure for the support layer. It was reported that no delamination occurred between these two layers due to the use of the same solvent and bulk polymer in both layers. By varying the PVDF concentration in the top layer, it was found that the finger-like structures became shorter with a higher concentration due to the reduced CPL/water exchange rate resulting from the higher viscosity. Additionally, due to the very thin PVDF layer, the MD flux of the DL membranes marginally changed with different PVDF concentration when the membrane thickness was kept constant.

Nonetheless, if the thickness of the PVDF layer was constant while increasing the support layer thickness, the flux reduced significantly due to the increased temperature polarization effect across the thicker hydrophilic layer. Moreover, when the water bath temperature increased from 5 to 50 °C, the skin layer became rougher while the finger-like pores grow longer, which mainly ascribed to the weakened TIPS mechanism resulting from the decreased temperature difference between the nascent polymer film and the water bath. The MD flux increased slightly when the bath temperature increased to 40 °C, then sharply decreased when the bath temperature increased to 50 °C due to the denser structure caused by the increased NIPS phenomenon. Finally, an optimal Janus membrane was decided using 15 wt.% PVDF solution as the top layer in 20 °C water bath with a total membrane thickness of 120 μm, and it showed a high porosity of 85%, a contact angle of 74 °, a high LEP of 3.6 bar, and a high flux of 85.1 kg/(m^2·h) using 3.5 wt.% NaCl solution at feed and permeate temperatures of 60 °C and 17.5 °C, respectively.

However, delamination, which can be considered a failure in DL membranes, occurs in some cases [10, 19, 21, 24-26]. The adhesion/delamination mechanism has been widely investigated, and the factors affecting this phenomenon are summarized into two categories: (i) thermodynamics and kinetics of polymers and (ii) mechanical properties of each layer [27]. The thermodynamic and kinetic factors comprise the interpenetration time between two polymer solutions before solidification, the relative energy difference, the difference in diffusion rate of nonsolvent into polymer solutions, and the hydrophilicity gradient of two layers [10, 21, 22]. The mechanical properties mainly refer to the discrepancy of the shrinkage value of the two polymer layers [25, 28]. Nevertheless, delamination is beneficial in some cases. He's group [24, 29] prepared microfiltration (MF) membranes by co-casting polyetherimide (PEI)/PSf solutions. Due to the separation of the two layers after phase separation induced by the shrinkage value difference in thickness, porous PSf membranes with concave surface were obtained. Furthermore, membranes were prepared by changing the sequence of the two layers (PSf as the top layer and the PEI as the sub-layer), and PSf membranes

with highly-open bottom surfaces were obtained [30, 31]. Using this membrane as the substrate with further interfacial polymerization in FO, it was demonstrated that a remarkably lower structure parameter, significantly reduced internal concentration polarization, and a great higher flux was achieved than with the single layer PSf membrane.

During the phase separation process of a PVDF polymer solution, the obtained PVDF membrane morphology is significantly affected by the solvent/nonsolvent exchange rate. A barrier between the PVDF solution and nonsolvent could reduce the exchange rate, which will be advantageous to prepare a skinless and porous PVDF membrane. Hence, a co-casting method is employed in this work to take advantage of the delamination, in which the PVDF was cast as the sub- layer while PES was used as the top layer to reduce the solvent/water exchange rate during the precipitation of PVDF layer. The effect of PES and PVDF concentration on the membrane morphology and permeate performance were measured in view of membrane morphology, hydrophobicity, pore size, porosity, as well as the DCMD behavior. In addition, the influence of the solvent in the top layer solution on the PVDF morphology was investigated as well.

5.2 Results and discussion

5.2.1 Membrane morphology

5.2.1.1 Delamination mechanism

Due to the obvious hydrophobicity difference of PES and PVDF membrane, the hydrophilicity gradient was first considered to induce the delamination. According to this theory, no delamination should occur if the sub-layer is more hydrophilic than the top layer as a more hydrophilic sub-layer could absorb more water from the top layer and show better infiltration [27]. Therefore, a membrane using PVDF as top-layer and PES as sub-layer was co-cast, but delamination still occurred. Subsequently, the shrinkage value was used to explain the delamination due to the huge shrinkage value

difference between the two layers, as shown in Figure 5.1. By varying the coagulation bath temperature from 1 °C to 92 °C, different shrinkage values were obtained, but delamination always occurred. As the PVDF membrane was cast on the non-woven substrate, its shrinkage in the width and length directions was limited, while the values of the PES membrane decreased from 14% to 6%. Nonetheless, in the thickness direction, the shrinkage values slightly increased from 77.9% to 90.3% of PVDF membranes and from 13.8% to 36.4% of PES membranes. Although the shrinkage in width and length was diminished by means of a high temperature water bath, the shrinkage value difference in thickness was only slightly affected (declined from 64.1% to 48.6%). According to [25], the membranes with a shrinkage value difference from 40% to 20% showed delamination, while a difference of 8% could form a well-adhesion DL membrane. Therefore, it is possible to state that the delamination between PVDF and PES membranes resulted from the shrinkage value difference in thickness.

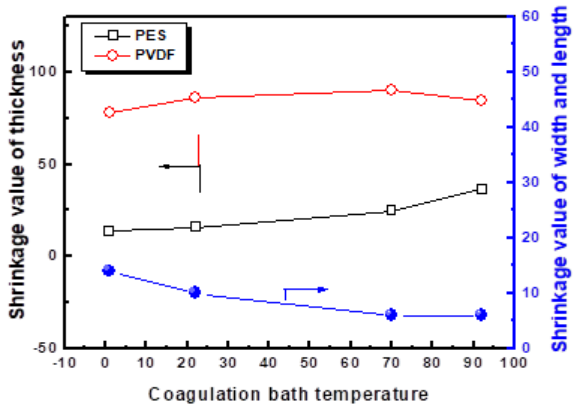


Figure 5.1 The shrinkage values in thickness direction of PES and PVDF membranes prepared in a water bath at different temperatures, and the shrinkage values in width and length directions of the PES membrane. The membranes were prepared with a 15 wt.% PES solution and a 16 wt.% PVDF solution.

5.2.1.2 Membrane morphologies using PES/NMP solution as top layer

The morphology of the sacrificial PES layer is depicted in Figure 5.2. A typical structure of a dense surface and finger-like structure was obtained. However, the large circular pores formed on the bottom surface differs from the traditional PES membranes

cast on a glass plate [32-34], which may be caused by the inter-penetration of the NMP between the PES layer and the PVDF layer during the phase separation process.

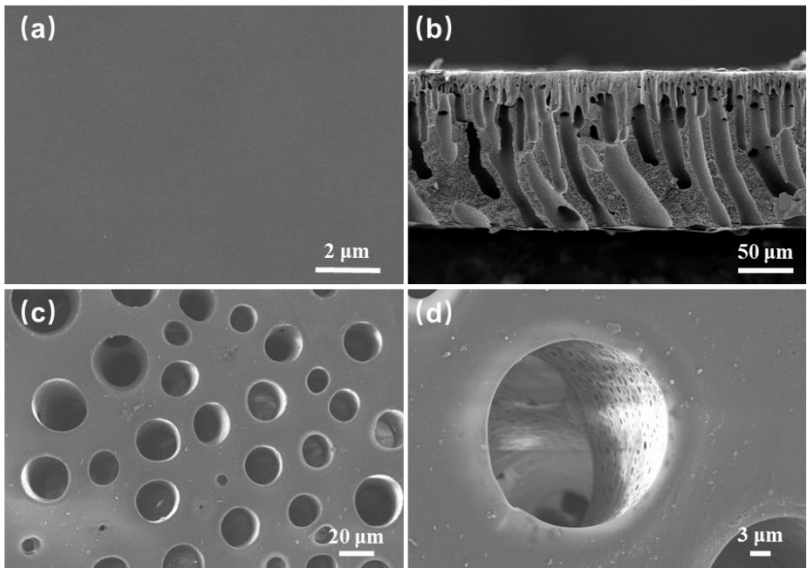


Figure 5.2 Morphologies of the top surface (a), cross-section (b), and bottom surface (c, d) of the PES membrane

As shown in Figure 5.3, compared to the relatively dense surface and macro-voids of the single-layer PVDF-16 membrane, the PVDF-co membranes exhibit porous surface and a sponge-like structure. Because PVDF is a semi-crystalline polymer, three possible mechanisms may occur during a phase separation procedure, which are liquid-liquid (L-L) demixing, solid-liquid demixing (crystallization), and their combination [3, 35, 36]. It is generally understood that a fast solvent/nonsolvent exchange rate leads to a membrane with macro-voids and cellular pores beneath a dense surface, as shown in Figure 5.3 (a). When a slow solvent/nonsolvent exchange starts, S-L demixing may occur first, which induces the crystallization and forms a membrane with cross-linked PVDF spherulites. In contrast, if a combination mechanism occurs, a symmetric membrane with cellular pores is created, as exhibited in Figure 5.3 (b-d). During the co-casting process, the coagulation reagent (*i.e.*, water) should first penetrate the PES membrane before contacting with the PVDF solution, which slows down the water diffusion rate into PVDF solution. In addition, the solvent for the PES solution (*i.e.*, NMP) diffuses inward the PVDF layer or is retained at the PES/PVDF interface; thus,

the coagulation bath for PVDF solution was NMP/water mixture instead of pure water. Therefore, delayed L-L demixing and S-L demixing occurred under the combined effect of these two factors, resulting in skinless and sponge-like structures. However, there are disparities among the PVDF-co-16 membranes prepared with different PES concentration. On the PVDF-16-15 and PVDF-16-18 membrane surfaces, polygonal plates are formed, which can be ascribed to the two-dimensional growth of the nuclei formed just beneath the top surface. Furthermore, the bumps in the center of each plate may result from the rejection of impurities during the crystallization process [37]. In comparison, a net-like surface composed by fibrils is generated on the PVDF-16-21 membrane surface. The difference in the surface morphology may arise from the solution composition and viscosity, as summarized in Table 5.1. When the PES concentration was low, a higher NMP content may be generated at the PES/PVDF interface, thus crystallization tends to occur from the surface. However, as the separation of PES and PVDF layer occurs faster at a low PES concentration, water diffusion started quickly and L-L demixing took place. When the PES concentration increased to 21 wt.%, the viscosity significantly increased compared to 18 wt.%, and a thicker PES layer was formed which further limits the intrusion of water to the PVDF layer. Therefore, the PVDF crystallization occurs more uniformly, and the initial thread-like crystalline and nodules are generated.

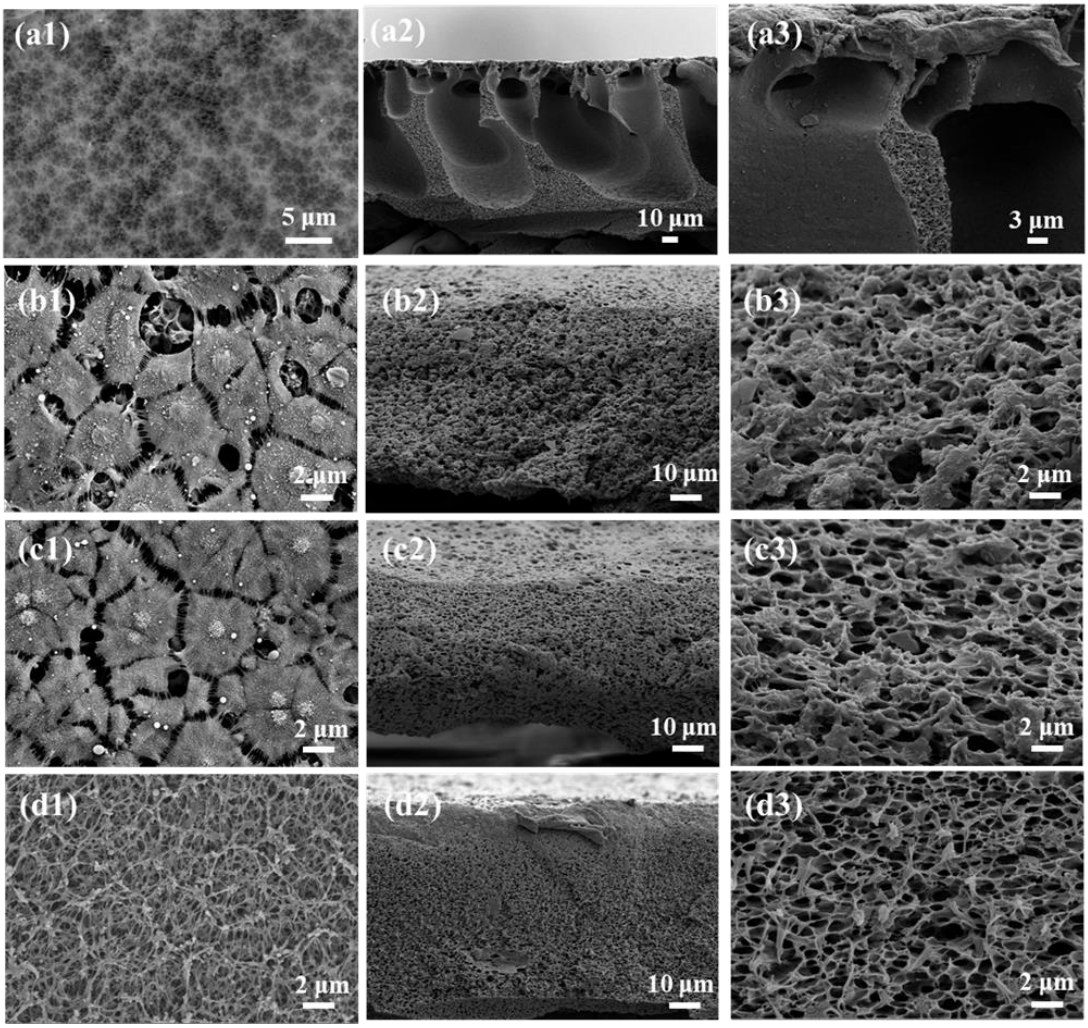


Figure 5.3 SEM images of the (1) top surface and (2, 3) cross-sections of the (a) single layer PVDF-16 membrane and (b-d) PVDF-co-16 membranes using different PES concentrations (b: 15 wt.%, c: 18 wt.%, d: 21 wt.%)

Table 5.1 Viscosity of the PVDF and PES solutions at 25 °C

PVDF/NMP	Viscosity (mPa·s)	PES/NMP	Viscosity (mPa·s)
16 wt.%	5288±156	15 wt.%	408±16
18 wt.%	8666±183	18 wt.%	945±35
20 wt.%	14879±259	21 wt.%	2496±78

The morphologies of PVDF-co membranes with 18 wt.% and 20 wt.% PVDF solutions are exhibited in Figure 5.4 and Figure 5.5. Unlike the polygonal plates and

cellular pores in PVDF-co-16 membranes, completely open surfaces composed of small spherulites and fibrils are formed in PVDF-co-18 membranes (as shown in Figure 5.4). As the 18 wt.% PVDF solution has a higher viscosity than the 16 wt.% solution, the nonsolvent diffusion rate into PVDF solution is slower, and the S-L demixing dominates the phase separation process [37, 38]. Thus, small particles are detected from the cross-section images, which confirms the PVDF crystallization behavior during phase separation. Additionally, a rather looser layer can be observed in the upper part from the cross-section images of the PVDF-18-15 and PVDF-18-18 membranes. This may be ascribed to the lower concentration of PES solutions which contain more solvent. The solvent dilutes the top layer of the PVDF solution before the PVDF precipitation, which results in a lower PVDF concentration on the top layer and accordingly a loose structure on the upper part. For the PVDF-20-y membranes, larger PVDF particles than for the PVDF-18-y membranes are observed from the membrane cross-section images, as presented in Figure 5.5 (a3-c3). This can be ascribed to the higher viscosity of 20 wt.% solution (see Table 5.1), which further impedes the water penetration into the polymer solution and reduces the formation rate of PVDF nuclei, leading to a longer growth time for the globules. Furthermore, the PVDF-co-18 and PVDF-co-20 membranes composed of particulates show better pore interconnectivity compared to the PVDF-co-16 membranes consisted of cellular pores, because no closed pores are formed.

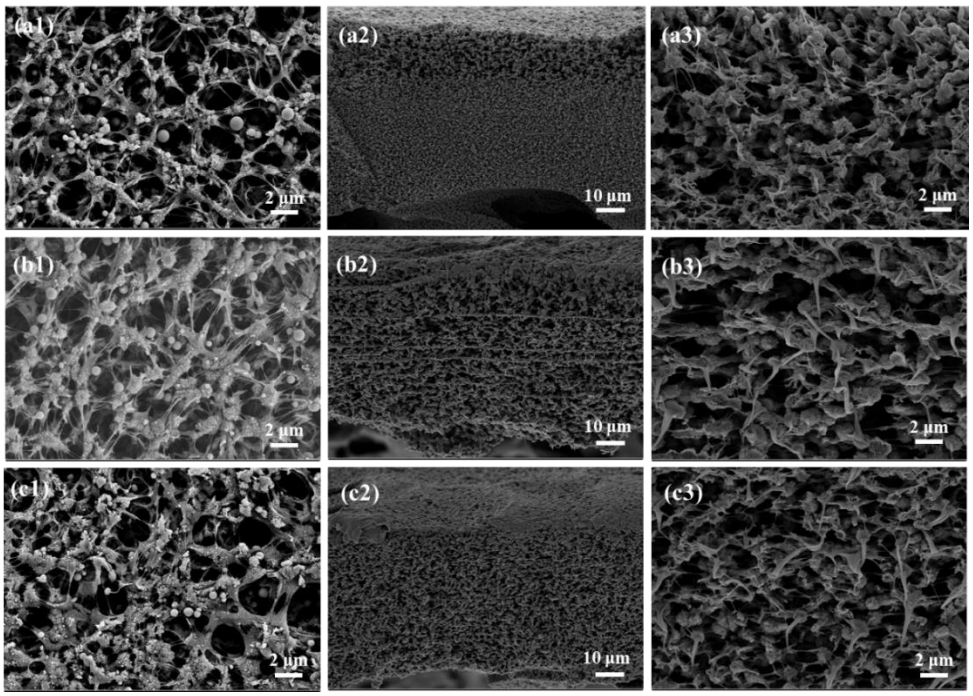


Figure 5.4 SEM images of the (1) top surface and (2, 3) cross-section of the PVDF-co-18 membranes with different PES concentrations (a: 15 wt.%, b: 18 wt.%, c: 21 wt.%)

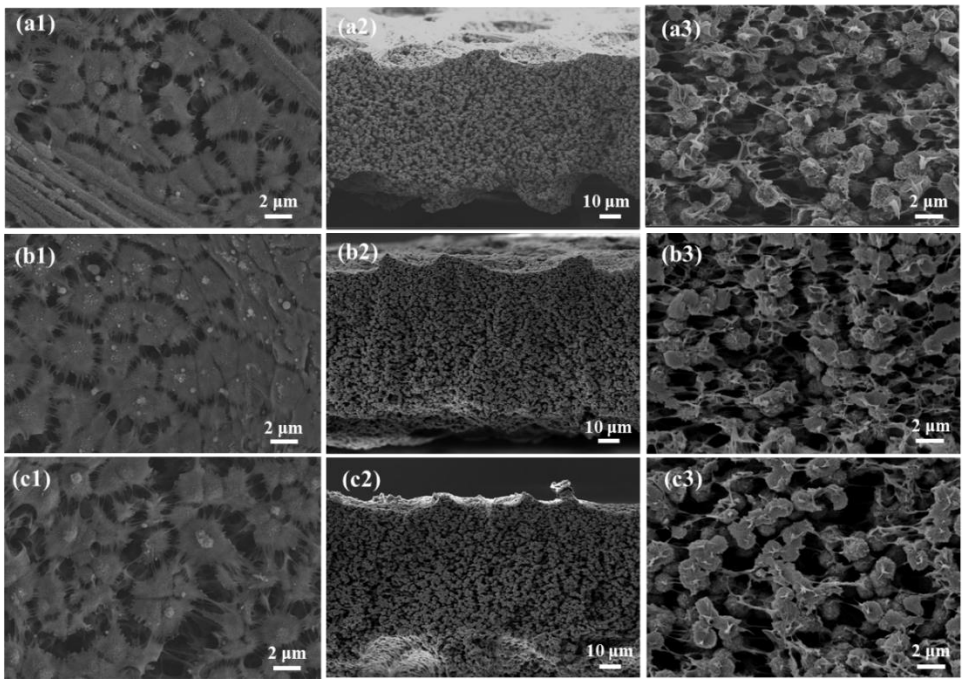


Figure 5.5 SEM images of the (1) top surface and (2, 3) cross-section of the PVDF-co-20 membranes with different PES concentrations (a: 15 wt.%, b: 18 wt.%, c: 21 wt.%)

5.2.1.3 Membrane morphologies using PES/DMSO solution as top layer

The influence of a different solvent for the PES solution on the membrane morphology is represented in Figure 5.6 and Figure 5.7. DMSO was chosen because it can dissolve both PES and PVDF, and more importantly, it has a lower toxicity than other normally used solvents. As shown in Figure 5.6, a significant difference occurs in the bottom surface of the PES membrane and the top surface of PVDF membranes. In the phase separation process, nonsolvent in-diffusion and solvent out-diffusion occurs simultaneously in the polymer solution layer [40], as shown in Figure 1.12. Each solvent has its own diffusivity in different medium, and the solvent-nonsolvent mutual diffusion plays an important role in determining the membrane structures. To compare the PVDF-co membranes prepared with different PES solutions, the solvent for PES is the only variate. Thus, it can be concluded that the morphology difference between Figure 5.2 and Figure 5.6 results from the different solvents of the two layers. Considering the disparity in diffusivity between DMSO and NMP, the mutual diffusion between NMP/NMP and DMSO/NMP is different. For the PES/NMP+PVDF/NMP system, NMP can penetrate freely in these two layers and at the interface, while for the PES/DMSO+PVDF/NMP system, the mutual diffusion will be affected, and the penetration of DMSO to the PVDF/NMP solution layer may be not perpendicular to the PVDF layer. When the bottom surface morphologies of the two different PES membranes are compared, it seems to be that there is slippage at the PES/PVDF interface, which can be verified by the irregular circles of PES/DMSO membrane and the extremely circular pores of PES/NMP membrane. Moreover, since DMSO is a relatively weaker solvent than NMP for PVDF [2, 39], the influence of DMSO on the PVDF top surface is less than NMP. Thus, globular structures are not evident although porous surfaces are generated. In addition, the effect of the PES and PVDF concentrations on the PVDF surface morphology is marginal, and all the membrane surfaces show a similar morphology with open but flat pores, as shown in Figure 5.7. This morphology difference between PVDF-co membranes using PES/DMSO and PVDF/NMP solutions demonstrate the significant impact of the coagulation bath

composition on the membrane morphology during a phase separation process. As these membranes do not show comparable structures (open and rough surface) to the membranes prepared with PES/NMP+PVDF/NMP system, which may lead to relatively lower hydrophobicity and lower fluxes, further characterization was not conducted for these membranes.

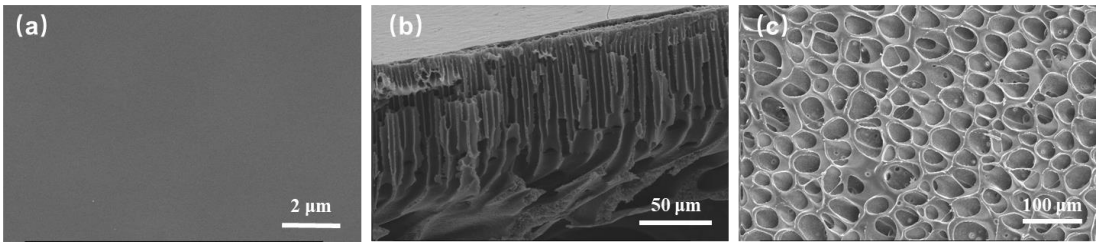


Figure 5.6 Morphologies of the (a) top surface, (b) cross-section, and (c)bottom surface of the PES membrane prepared with PES/DMSO+PVDF/NMP system

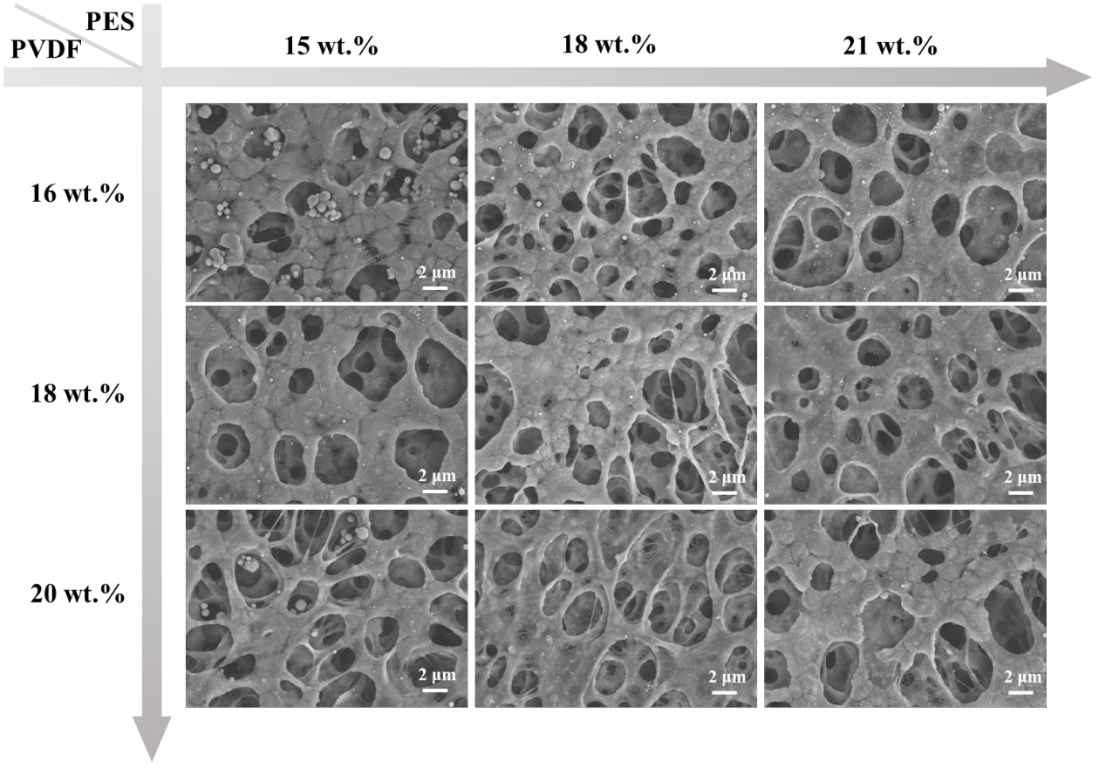


Figure 5.7 SEM images of PVDF-co membranes prepared using PES/DMSO solution as the top layer

5.2.2 Physical properties

The hydrophobicity and other characters of the single layer PVDF membranes and

PVDF-co membranes are shown in Table 5.2 and Figure 5.8, respectively. Higher contact angles ranging from 125° to 133° are achieved due to the rougher surface with particulate structures of PVDF-co membranes compared to the single layer PVDF membranes, as displayed in Figure 5.8 (a). Moreover, due to the small spherulites and nodule-like structures on the PVDF-18 membrane surface which may lead to a higher roughness than the surface composed of larger particles, PVDF-18 membranes show slightly higher contact angles. As shown in Figure 5.8 (b), the thicknesses of the PVDF-co membranes are significantly less than the single-layer PVDF membranes, which can be ascribed to the compression of the PES solution layer and the partial dissolution by the solvent for PES solution at the PES/PVDF interlayer. Among the PVDF-co membranes, the membrane thickness increases with a higher PVDF concentration. This can be explained by the higher polymer content, as well as less PVDF dissolution due to the higher solution viscosity. The membrane porosities are presented in Figure 5.8 (c). Due to the limitation of the nonwoven substrate showing a low porosity of 17%, the PVDF-co membranes show relatively low porosities in the range of 37.4%-49.6%. Nonetheless, if the porosities of the PVDF layer are calculated, they could reach 80-90%. However, as the composite membranes composed of PVDF layer and nonwoven substrate were tested in MD, the overall porosities should be reported. As the reported porosity is the average of the PVDF layer and the non-woven support, a thicker polymer layer with a high porosity could result in a higher overall porosity, such as the PVDF-20-y membranes. During the membrane fabrication of PVDF membranes in NIPS, non-woven substrate is essential to limit the membrane shrinkage and provide sufficient mechanical strength, but more porous substrate should be considered in the future work. The membrane mean pore sizes are given in Figure 5.8 (d), and a significant increment can be obtained compared to the single layer PVDF membranes. The PVDF-20-y membranes show the highest pore size because the membrane structure is formed by only large particulates, thus the voids between the particles are larger than PVDF-18 membranes with smaller particles. For the PVDF-16-y membranes, the relatively large pore size may result from the low PVDF

concentration. Moreover, the LEP values are shown in Figure 5.8 (e), ranging from 0.75-1.0 bar. Since the hydrophobicity of the PVDF-co membranes are similar, the highest LEP of PVDF-18-15 membrane may result from the smallest pore size. In summary, the prepared PVDF-co membranes show a higher hydrophobicity, a thinner thickness, a larger pore size, a comparable porosity to the single-layer PVDF membrane, and a medium LEP, which may be a better candidate than the normal casting membranes for MD.

Table 5.2 The characteristics of single layer PVDF membranes

Properties	PVDF-16	PVDF-18	PVDF-20
Contact angle (°)	75.6±0.9	73.9±4.4	76.8±1.5
Thickness (μm)	262.2±4.5	273.9±1.9	285.3±3.9
Porosity (%)	45.7±1.6	51.2±2.9	53.1±2.4
Pore size (μm)	0.142±0.055	0.125±0.014	0.106±0.016
LEP (bar)	0.73±0.12	0.81±0.07	0.91±0.08

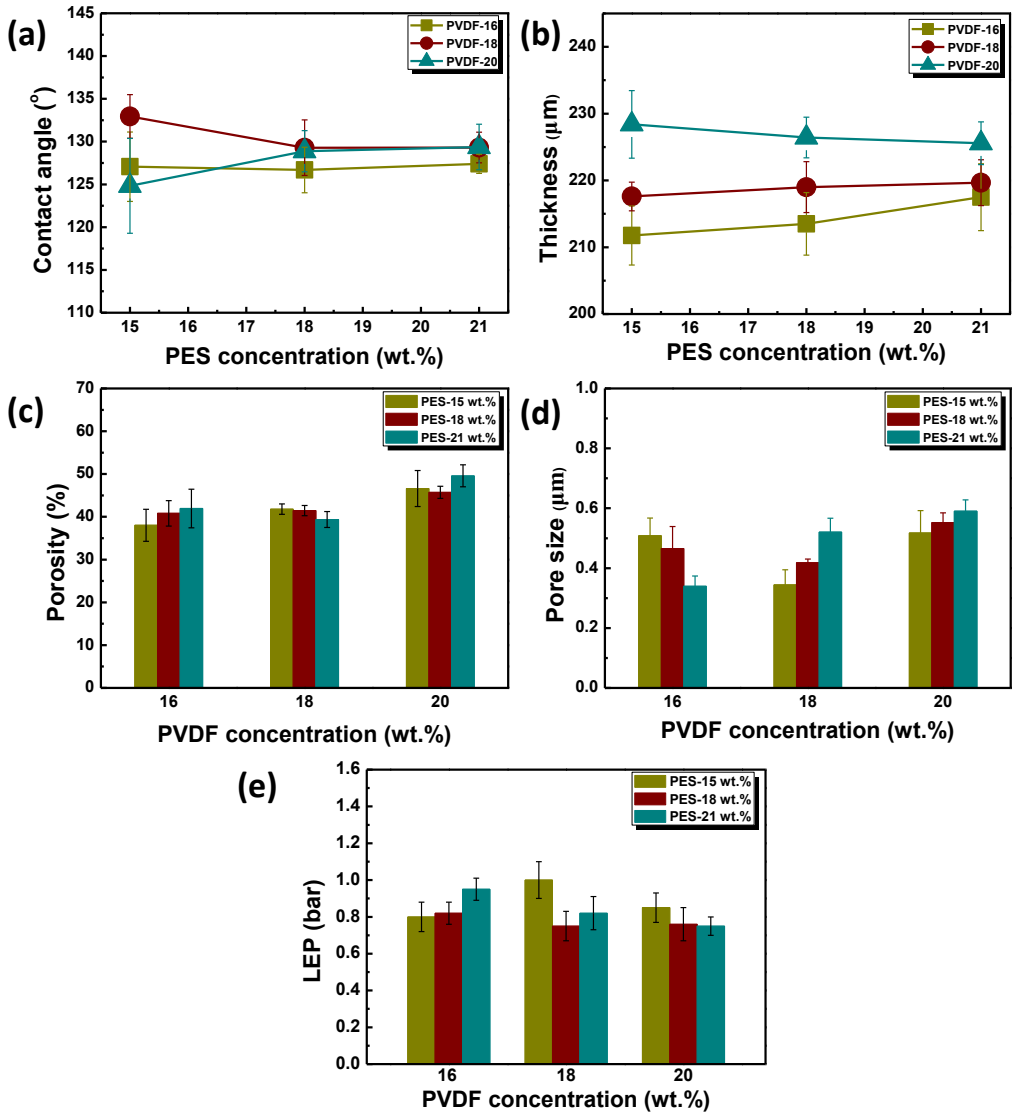


Figure 5.8 (a) Contact angle, (b) thickness, (c) porosity, (d) pore size, and (e) LEP of the PVDF-co membranes

5.2.3 DCMD performance

The fluxes of single-layer PVDF membranes and PVDF-co membranes are shown in Figure 5.9, and all the membranes show salt rejections higher than 99.97%. It could be stated that all the PVDF-co membranes are found to have higher fluxes compared to the single-layer membranes when the PVDF concentration are the same, which can be attributed to the open porous surfaces, thinner thickness, and larger pore sizes. Additionally, the flux increment of PVDF-co-20 membranes are significantly greater than the PVDF-co-16 membranes. This can be explained by the different pore structures,

i.e., cellular pores in PVDF-co-16 membranes while pores are formed by PVDF particulates in PVDF-co-20 membranes showing better pore interconnectivity. Among these membranes, the PVDF-20-21 membrane shows the highest flux due to its largest pore size, as well as the great pore interconnectivity. For the PVDF-16 membranes, the narrower pore size and cellular pore structure induced to relatively lower fluxes. Especially for PVDF-16-21 membrane, although the overall cross-section structures are similar with other two PVDF-co-16 membranes, the net-like fibril surface seems to be denser and the pore size is relatively smaller, which lead to the lowest flux.

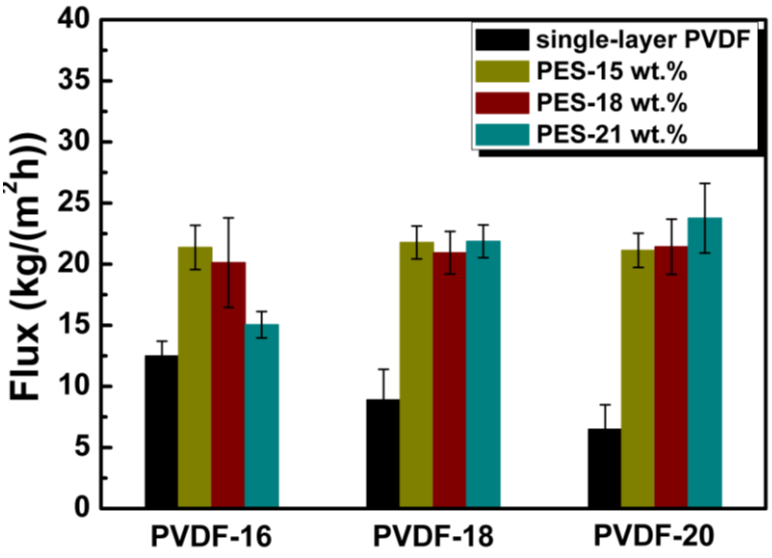


Figure 5.9 DCMD fluxes of the single layer and PVDF-co membranes using 3.5 wt.% NaCl as feed solution. The temperatures of feed and permeate solutions are 60.2±0.5 °C and 19.7±0.3 °C, respectively. The flow rate is 36 L/h on both sides.

The long-term stability of the PVDF-20-21 membrane was evaluated for 50 h using 3.5 wt.% NaCl as feed solution. The observed fluxes and conductivities are represented in Figure 5.10. In view of the flux, it could be stated that the membrane shows steady fluxes in the entire test, which demonstrates a stable membrane performance. Although The salt rejection remains above 99.98%, the permeate solution conductivity slightly increases over time, which indicates that there are defects or partially-wetted pores on the membrane.

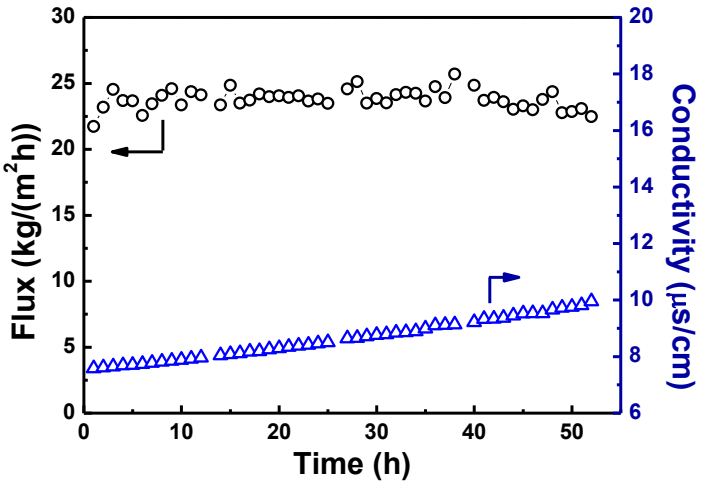


Figure 5.10 Long-term stability of the PVDF-20-21 membrane. The feed solution is 3.5 wt.% NaCl. The temperatures of feed and permeate solutions are 60.6±0.2 °C and 19.9±0.2 °C, respectively. The flow rate is 36 L/h on both sides.

5.3 Conclusions

Porous and symmetric PVDF membranes are fabricated by use of a sacrificial PES layer in a co-casting process. Due to the additional PES layer and the solvent retaining at the PVDF top surface, delayed liquid-liquid demixing occurred, inducing the formation of an open porous surface for the bottom PVDF membranes. Compared to the influence of PES concentration, the PVDF concentration played a more important role in deciding the membrane morphologies. When the PVDF concentration is 16 wt.%, a surface composed of polygonal particles is generated combined with a cellular pore structure. When the concentration increases to 18 wt.%, a completely open top layer with small globules and nodule-like structures is developed. If the PVDF concentration further increases to 20 wt.%, a membrane constituted by larger spherulites can be obtained, which is ascribed to the longer growth time for nuclei because of the higher solution viscosity. Benefitting from the particulate surfaces, the PVDF-co membranes exhibit a higher hydrophobicity (contact angles of 125°-133°) contrasted to the control PVDF membranes (contact angle of 75.6°). Furthermore, the pore sizes of the PVDF-co membranes are enlarged from 0.106-0.147 μm to 0.34-0.59 μm as well. In terms of the DCMD performance, the PVDF-co membranes show increased fluxes in

comparison to the single-layer PVDF membranes, especially for PVDF-co-20 membranes, which can be ascribed to the skinless surface, the larger pore size, and the better pore interconnectivity formed by the large particles. The long-term stability of the membrane with the highest flux was evaluated for 50 h, and steady fluxes are observed. Comparing to the benchmark, a simple co-casting process and cost-effective materials (PVDF, PES, and NMP) are used without high temperature or pressure, the surface hydrophobicity is moderate with contact angles around 130° for PVDF-co-18 and PVDF-co-20 membranes, the pore sizes locate in the range of 0.1-1 μm, and the PVDF layer thicknesses are 30-50 μm. However, the membrane porosities are relatively low due to the limitation of the less-porous non-woven substrates. In addition, the LEP values of the prepared PVDF-co membrane locate in 0.8-1 bar, which is lower than the desired values. Moreover, the MD fluxes are 20.1-23.8 kg/(m^2·h) at feed and permeate temperatures of 60 °C and 20 °C, respectively, which is slightly lower than the desired flux. The biggest restriction of the prepared membranes is the less-porous non-woven substrate, which is similar with that in chapter 4. A more porous and thinner substrate could elevate the MD performance to a higher level with a larger porosity, a thinner membrane, and a higher flux.

References:

[1] G.-d. Kang, Y.-m. Cao, Application and modification of poly(vinylidene fluoride) (PVDF) membranes – A review, J. Membr. Sci., 463 (2014) 145-165.
[2] A. Bottino, G. Camera-Roda, G. Capannelli, S. Munari, The formation of polyvinylidene difluoride microporous membranes by phase separation, J. Membr. Sci., 57 (1991) 1-20.
[3] L.-P. Cheng, T.-H. Young, L. Fang, J.-J. Gau, Formation of particulate microporous poly(vinylidene fluoride) membranes by isothermal immersion precipitation from the 1-octanol/dimethylformamide/poly(vinylidene fluoride) system, Polymer, 40 (1999) 2395-2403.
[4] D.-J. Lin, K. Beltsios, T.-H. Young, Y.-S. Jeng, L.-P. Cheng, Strong effect of precursor preparation on the morphology of semicrystalline phase inversion poly(vinylidene fluoride) membranes, J. Membr. Sci., 274 (2006) 64-72.
[5] X. Li, Y. Wang, X. Lu, C. Xiao, Morphology changes of polyvinylidene fluoride membrane under different phase separation mechanisms, J. Membr. Sci., 320 (2008) 477-482.
[6] S. Munirasu, F. Banat, A.A. Durrani, M.A. Haija, Intrinsically superhydrophobic

PVDF membrane by phase inversion for membrane distillation, Desalination, 417 (2017) 77-86.
[7] S. Nejati, C. Boo, C.O. Osuji, M. Elimelech, Engineering flat sheet microporous PVDF films for membrane distillation, J. Membr. Sci., 492 (2015) 355-363.
[8] A. Bottino, A. Comite, C. Costa, M. Pagliero, Novel hydrophobic PVDF membranes prepared by nonsolvent induced phase separation for membrane distillation, J. Membr. Sci., 596 (2019) 117575.
[9] X. Ding, Y. Cao, H. Zhao, L. Wang, Q. Yuan, Fabrication of high performance Matrimid/polysulfone dual-layer hollow fiber membranes for O2/N2 separation, J. Membr. Sci., 323 (2008) 352-361.
[10] S.A. Hashemifard, A.F. Ismail, T. Matsuura, Co-casting technique for fabricating dual-layer flat sheet membranes for gas separation, J. Membr. Sci., 375 (2011) 258-267.
[11] A. Jomekian, R.M. Behbahani, T. Mohammadi, A. Kargari, CO 2 /CH 4 separation by high performance co-casted ZIF-8/Pebax 1657/PES mixed matrix membrane, J. Nat. Gas Sci. Eng., 31 (2016) 562-574.
[12] R.X. Liu, X.Y. Qiao, T.-S. Chung, Dual-layer P84/polyethersulfone hollow fibers for pervaporation dehydration of isopropanol, J. Membr. Sci., 294 (2007) 103-114.
[13] T.-Y. Liu, R.-X. Zhang, Q. Li, B. Van der Bruggen, X.-L. Wang, Fabrication of a novel dual-layer (PES/PVDF) hollow fiber ultrafiltration membrane for wastewater treatment, J. Membr. Sci., 472 (2014) 119-132.
[14] T. He, M.H.V. Mulder, H. Strathmann, M.Wessling, Preparation of composite hollow fiber membranes: co-extrusion of hydrophilic coatings onto porous hydrophobic support structures, J. Membr. Sci., 207 (2002) 143-156.
[15] S.P. Sun, K.Y. Wang, N. Peng, T.A. Hatton, T.-S. Chung, Novel polyamide-imide/cellulose acetate dual-layer hollow fiber membranes for nanofiltration, J. Membr. Sci., 363 (2010) 232-242.
[16] F.-J. Fu, S. Zhang, S.-P. Sun, K.-Y. Wang, T.-S. Chung, POSS-containing delamination-free dual-layer hollow fiber membranes for forward osmosis and osmotic power generation, J. Membr. Sci., 443 (2013) 144-155.
[17] S. Bonyadi, T.S. Chung, Flux enhancement in membrane distillation by fabrication of dual layer hydrophilic–hydrophobic hollow fiber membranes, J. Membr. Sci., 306 (2007) 134-146.
[18] P. Wang, M.M. Teoh, T.S. Chung, Morphological architecture of dual-layer hollow fiber for membrane distillation with higher desalination performance, Water Res., 45 (2011) 5489-5500.
[19] J. Zhu, L. Jiang, T. Matsuura, New insights into fabrication of hydrophobic/hydrophilic composite hollow fibers for direct contact membrane distillation, Chem. Eng. Sci., 137 (2015) 79-90.
[20] Y. Liu, T. Xiao, C. Bao, Y. Fu, X. Yang, Fabrication of novel Janus membrane by nonsolvent thermally induced phase separation (NTIPS) for enhanced performance in membrane distillation, J. Membr. Sci., 563 (2018) 298-308.
[21] C.C. Pereira, R. Nobrega, C.P. Borges, Membranes obtained by simultaneous casting of two polymer solutions, J. Membr. Sci., 192 (2001) 11-26.
[22] C. Pereira, Hollow fiber membranes obtained by simultaneous spinning of two

polymer solutions: a morphological study, J. Membr. Sci., 226 (2003) 35-50.
[23] F.-J. Fu, S.-P. Sun, S. Zhang, T.-S. Chung, Pressure retarded osmosis dual-layer hollow fiber membranes developed by co-casting method and ammonium persulfate (APS) treatment, J. Membr. Sci., 469 (2014) 488-498.
[24] X.M. Li, Y. Ji, T. He, M. Wessling, A sacrificial-layer approach to prepare microfiltration membranes, J. Membr. Sci., 320 (2008) 1-7.
[25] X.-M. Li, Y. Ji, Y. Yin, Y.-Y. Zhang, Y. Wang, T. He, Origin of delamination/adhesion in polyetherimide/polysulfone co-cast membranes, J. Membr. Sci., 352 (2010) 173-179.
[26] L. Setiawan, L. Shi, W.B. Krantz, R. Wang, Explorations of delamination and irregular structure in poly(amide-imide)-polyethersulfone dual layer hollow fiber membranes, J. Membr. Sci., 423-424 (2012) 73-84.
[27] Q.-C. Xia, M.-L. Liu, X.-L. Cao, Y. Wang, W. Xing, S.-P. Sun, Structure design and applications of dual-layer polymeric membranes, J. Membr. Sci., 562 (2018) 85-111.
[28] D. Li, T.-S. Chung, R. Wang, Morphological aspects and structure control of dual-layer asymmetric hollow fiber membranes formed by a simultaneous co-extrusion approach, J. Membr. Sci., 243 (2004) 155-175.
[29] Y. Ji, X.-M. Li, Y. Yin, Y.-Y. Zhang, Z.-W. Wang, T. He, Morphological control and cross-flow filtration of microfiltration membranes prepared via a sacrificial-layer approach, J. Membr. Sci., 353 (2010) 159-168.
[30] P. Xiao, L.D. Nghiem, Y. Yin, X.-M. Li, M. Zhang, G. Chen, J. Song, T. He, A sacrificial-layer approach to fabricate polysulfone support for forward osmosis thin-film composite membranes with reduced internal concentration polarisation, J. Membr. Sci., 481 (2015) 106-114.
[31] G. Chen, R. Liu, H.K. Shon, Y. Wang, J. Song, X.-M. Li, T. He, Open porous hydrophilic supported thin-film composite forward osmosis membrane via co-casting for treatment of high-salinity wastewater, Desalination, 405 (2017) 76-84.
[32] Y. Han, K. Zhao, Y. Lu, D. Zhu, A method to characterize the compressibility and stability of microfiltration membrane, Desalination, 365 (2015) 1-7.
[33] S. Zhu, M. Shi, S. Zhao, Z. Wang, J. Wang, S. Wang, Preparation and characterization of a polyethersulfone/polyaniline nanocomposite membrane for ultrafiltration and as a substrate for a gas separation membrane, RSC Adv., 5 (2015) 27211-27223.
[34] X. Wu, Z. Xie, H. Wang, C. Zhao, D. Ng, K. Zhang, Improved filtration performance and antifouling properties of polyethersulfone ultrafiltration membranes by blending with carboxylic acid functionalized polysulfone, RSC Adv., 8 (2018) 7774-7784.
[35] D.-J. Lin, K. Beltsios, C.-L. Chang, L.-P. Cheng, Fine Structure and Formation Mechanism of Particulate Phase-Inversion Poly(vinylidene fluoride) Membranes, J. Polym. Sci. B, 41 (2003) 1578-1588.
[36] M. Gu, J. Zhang, X. Wang, H. Tao, L. Ge, Formation of poly(vinylidene fluoride) (PVDF) membranes via thermally induced phase separation, Desalination, 192 (2006) 160-167.

[37] T.-H. Young, D.-J. Lin, J. Gau, W.-Y. Chuang, L.-P. Cheng, Morphology of crystalline Nylon-610 membranes prepared by the immersion-precipitation process: competition between crystallization and liquid–liquid phase separation, Polymer, 40 (1999) 5011-5021.
[38] C. Alexowsky, M. Bojarska, M. Ulbricht, Porous poly(vinylidene fluoride) membranes with tailored properties by fast and scalable non-solvent vapor induced phase separation, J. Membr. Sci., 577 (2019) 69-78.
[39] A. Bowino, G. Capannelli, S. Munari, A. Turturro, Solubility parameters of poly(vinylidene fluoride), J. Polym. Sci. B Polym. Phys., 26 (1988) 785-794.
[40] P. van de Witte, P.J. Dijkstra, J.W.A. van den Berg, J. Feijen, Phase separation processes in polymer solutions in relation to membrane formation, J. Membr. Sci., 117 (1996) 1-31.

Chapter 6

Conclusions and outlook

6.1 General conclusions

Lack of fresh water is understood to be a great global risk in the current age. To alleviate water scarcity, desalination of seawater to produce fresh water is a technologically reliable and economically sustainable method. The currently utilized desalination processes consist of thermal process including multi-stage flash distillation (MSF) and multiple-effect distillation (MED), and membrane separation by reverse osmosis (RO). These technologies are already mature in industry and have been widely established. Nonetheless, there still are some shortcomings. For instance, these technologies are generally energy-intensive (applying either a high temperature or high pressure), and there is a salinity limitation for RO process. Membrane distillation (MD) is a thermal-driven membrane separation process which has been extensively investigated in recent decades. It is promising in desalination due to its several advantages comprising the mild operation conditions related to a relatively low feed temperature compared to distillation, no hydraulic pressure, a high rejection of nonvolatile matter in the feed solution, and the simplicity of the MD setup. However, the technology has not been available at the industrial level, which still need to develop suitable membranes and optimize the membrane module as well as the process design. As the key part to guarantee a high production rate and product quality, the membrane should possess proper structures for high permeate flux and stable anti-wetting performance. Various studies have been conducted to prepare membranes for MD, including nonsolvent-induced phase separation (NIPS), electrospinning, combined with modifications to optimize the membrane structure, morphology, or surface chemistry. However, expensive chemicals and materials with complicated preparation procedures usually are unpractical for a large-scale preparation. Therefore, membrane preparation using a cost-effective material and a simple preparation process is of great interest.

Chapter 6

The potential of using 3D printed (3DP) membranes in membrane distillation is firstly explored in this work. Polyamide (PA) membranes with particulate and porous surface were printed in a laser sintering (LS) process. Thin PVDF layers were coated on the PA membranes utilizing different PVDF concentrations (5 wt.%, 7 wt.%, and 10 wt.%) by dip-coating with different immersion time (15 s, 30 s, 60 s, and 120 s) to reduce the oversized pores. The obtained composite membranes were labeled as PVDF@3DP-x-y, where x and y represent the PVDF concentration and immersion time, respectively. The membrane morphology and pore size results demonstrate the effectiveness of the dip-coating procedure. A continuous and uniform PVDF layer can be constructed with 5 wt.% PVDF solution with immersion intervals above 30 s or a higher concentration of 7 wt.% and 10 wt.%. Results show that the hydrophobicity, thickness, and pore size of the composite membranes are significantly influenced by the PVDF concentration. A lower concentration induces a thinner PVDF layer and the granular morphology of PA membranes could be retained to some degree, which leads to a higher contact angle of 130°; while a higher PVDF concentration generates a thicker and denser flat layer with a relative lower contact angle of 100°. Additionally, PVDF@3DP-10 membranes show the highest thickness of 512-526 μm and pore size of 0.64-1.02 μm, while the PVDF@3DP-5 membranes have the lowest thickness of 350-420 μm and pore size of 1.85-2.58 μm. However, the membrane porosity does not display a substantial difference due to the limitation of the low porosity of the 3DP PA membranes. Moreover, although the composite membranes show a mechanical strength of over 10 MPa, cracks emerged under 0.1 bar during the LEP tests, which may result from the relatively weak adhesion between the not-fully melted PA particles. In the DCMD tests, the composite membranes show relatively low fluxes, below 10 kg/(m^2·h) (feed and permeate temperatures of 60 °C and 20 °C, respectively), due to the rather low porosity and great thickness, as well as some closed pores formed by powder coalescence. This work explored the potential application of 3D printing membranes in MD, and demonstrated the significant role of the membrane substrates in the MD performance. According to the results, further improving the structure of the printed

membranes is essential. For example, since the LS technology is a powder-based process, the structural parameters could be optimized by applying PA particles with a smaller size, which could lead to a thinner thickness and a higher porosity. Moreover, incorporation of small water-soluble materials with PA particles during the printing process followed by washing away after membrane printing may be helpful in enhancing the membrane porosity.

Secondly, a cost-effective and facile bottom-up method was proposed to prepare symmetric PVDF membranes using water as coagulation bath. As confirmed from the SEM images, the obtained membranes composed of interlinked globules are isotropic and porous. A sharp increase of water contact angles from normal casting membranes (71.7°) to the bottom-up membrane (144°) confirms the successful preparation of highly hydrophobic PVDF membranes using a water bath for phase inversion. This ingenious design could effectively delay the solvent/non-solvent exchange rate via the physical barrier effect. Meanwhile, the surface roughness significantly augments from 0.0255 μm of the normal casting membrane to 0.179 μm of the bottom-up membrane using the same dope solution composition. Additionally, the membrane pore size increases from 0.147 μm of the normal casting PVDF-N membrane to 0.99 μm of the PVDF-15 membrane. Nonetheless, the LEP values of the bottom-up membranes are relatively low compared to that of the PVDF-N membrane owing to the larger pore size. Moreover, the DCMD fluxes of PVDF-15 membrane at different feed solution temperatures (8.6-41.4 kg/(m^2·h) from feed temperatures of 40 °C to 70 °C, and the permeate temperature was 20 °C) were almost twice as high as for the normal casting PVDF-N membrane (4.8-24 kg/(m^2·h) from feed temperatures of 40 °C to 70 °C, and the permeate temperature was 20 °C) due to the open porous surface, the thinner polymer layer, and the larger pore size.

Finally, porous and symmetric PVDF membranes are fabricated by use of a sacrificial PES layer in a co-casting process. Due to the additional PES layer and the solvent retaining at the PVDF top surface, delayed liquid-liquid demixing occurred during the phase separation procedure for PVDF, inducing the formation of an open

porous surface and a symmetric structure. Compared to the influence of PES concentration, the PVDF concentration plays a more important role in deciding the membrane morphologies. When the PVDF concentration is 16 wt.%, a surface composed of polygonal particles is generated combined with a cellular pore structure. When the concentration increases to 18 wt.%, a completely open top layer with small globules and nodule-like structures is developed. If the PVDF concentration further increases to 20 wt.%, a membrane constituted by larger spherulites can be obtained, which is ascribed to the longer growth time for nuclei because of the higher solution viscosity. Benefitting from the particulate surfaces, the PVDF-co membranes exhibit a higher hydrophobicity (contact angles of 125°-133°) contrasted to the control PVDF membranes (contact angle of ~75°). Furthermore, the pore sizes of the PVDF-co membranes are enlarged from 0.106-0.147 μm to 0.34-0.59 μm as well. In terms of the DCMD performance, the PVDF-co membranes show increased fluxes of 20.1-23.8 kg/(m^2·h) in comparison to the single-layer PVDF membranes of 12.5- 6.5 kg/(m^2·h) at feed and permeate temperatures of 60 °C and 20 °C, respectively, which can be ascribed to the skinless surface, the larger pore size, a thinner polymer layer, and the better pore interconnectivity. The long-term stability of the membrane with the highest flux was evaluated for 50 h, and steady fluxes (~24 kg/(m^2·h) at feed and permeate temperatures of 60 °C and 20 °C, respectively) are observed.

A comparison between the benchmark in chapter 1 and the obtained results is exhibited in Table 6.1, and it could be concluded that neither of these three methods could 100% reach the expected goals. Among the three works, 3DP membrane is far from what is needed for MD membranes. On the one hand, a high temperature, a special laser beam, the printing instrument, and high-cost printing materials are needed. On the other hand, the dip-coating procedure using PVDF solutions diminish the advantages of no solvent and wastewater discharge, as well as quick fabrication. Moreover, the great thickness, a low porosity, and weak coalescence between powder particles under pressure, lead to low MD fluxes and LEP values. In contrast, the other two works reach most of the goals, such as a simple preparation process without high temperature or

pressure is developed, low-cost polymers and a normal solvent are used, and water is used as the coagulation bath. Moreover, the prepared membranes by these two methods show porous surface with high contact angles of 130°-140°, and most of the membrane pore sizes locate in the range of 0.1-1 μm. However, the porosities and LEP values of the prepared membranes could not attain the expected values. The main restriction for a high porosity of the prepared membrane is the less-porous non-woven substrate (a low porosity of 17%), and the reason for relatively low LEP values is the large pore size. In addition, for the DCMD performance, the PVDF membranes fabricated by bottom-up method show higher fluxes than the PVDF-co membranes. In summary, the bottom-up method is the best among the three investigated methods in terms of the membrane structure and DCMD performance.

Table 6.1 Comparison between the benchmark and results

Benchmark	**PVDF coated 3DP membranes**	**PVDF membranes using bottom-up method**	**PVDF membranes using co-casting method**
Preparation process			
less than 4 steps	x	√	√
No high temperature or pressure	x	√	√
No expensive materials	x	√	√
Membrane			
Membrane surface is open and porous	√	√	√
Contact angle >130°	√	√	√
PVDF layer thickness locates in 30-100 μm	~	√	√
Pore size lies in 0.1-1μm	x	~	√
Porosity is 70%-90%	x	x	x
LEP of water >1 bar	x	~	x
Flux > 25 kg/(m^2·h)	x	√	~

*x: the benchmark is not reached; √: the benchmark is reached; ~: the benchmark is reached for some of the prepared membranes

Due to the advantages of quick fabrication, no solvent and wastewater discharge, and freedom of geometry design for 3D printing technology, its potential in MD application was explored. However, the insufficient resolution (printing accuracy) leads to oversized pores for an MD membrane, thus a PVDF coating is required, which counteracts the advantages of no solvent discharge and quick fabrication. Moreover, a high temperature, a special laser beam, and the printing instrument are needed, which increase the investment. Additionally, according to the obtained results in the thesis, 3D printing technology is difficult to directly print available MD membranes due to its relatively low resolution and accuracy for membrane printing. Although it is still promising to print specialized membranes with complex structures and customized demand with the development of this technology, maybe it is not in the near future. In the current stage, it is more likely to be used to print spacers, modules, and templates with a special geometry design for membrane preparation.

For the bottom-up and co-casting methods which reach most of the benchmarks, utilizing a more porous and thinner support should be able to elevate the MD performance to a higher level with a larger porosity, a thinner membrane, and a higher flux. Moreover, increasing the LEP values by optimizing the membrane structure is also needed. While comparing these two simple methods, the co-casting method seems to be more promising for upscaling than the bottom-up method. Although the polymer solution system in the bottom-up method is simpler with only PVDF/NMP solution than the co-casting process containing two polymer solutions of PVDF/NMP and PES/NMP, the casting process on non-woven support is more feasible than on a glass or metal plate for a large-scale and continuous preparation. Nonetheless, further investigation should be carried out to estimate the energy efficiency, and a pilot-scale preparation needs to be performed to confirm the feasibility of this method.

6.2 Outlook for future work

According to the experiments and results obtained in this thesis, some recommendations for future work are given below.

(1) Employing the 3D printing technology to print membranes is promising due to

its advantages of quick fabrication, no solvent discharge, and freedom of shape and size. However, the printing accuracy is insufficient to prepare membranes that can be used directly in the membrane separation process in the current stage. However, a tentative exploration is still interesting and needed. As there are various 3D printing techniques using different kinds of chemicals and printing principles, different technologies can be explored to prepare membranes. For example, the two-photon polymerization (TPP) technique could print products with a resolution below 100 nm (*J. Membr. Sci.*, 523 (2017) 596; *Appl. Mater. Today*, (2019) 100486), which is still too low for ultrafiltration and nanofiltration membranes but maybe it is enough for the microfiltration and MD membranes. Additionally, for the laser selectivity (LS) technique used in this thesis where a particulate membrane can be printed by powder adhesion, different material powders with a smaller particle size (~1 μm) can be examined while investigating the optimal processing parameters including bed temperature, laser energy, and scanning cycles. Besides, printing two different polymer layers at the same time to develop a hydrophobic/hydrophilic composite membrane will be interesting.

(2) PVDF is a semi-crystalline polymer, which may experience crystallization or liquid-liquid demixing during the phase separation process, thus affecting the membrane morphology. As conclusions from this thesis show that an additional coverage on the PVDF nascent film could effectively reduce the solvent/nonsolvent exchange rate and lead to a skinless membrane with better pore connectivity, other coverage methods could be investigated by applying more cost-effective material or impart the membrane special properties. For example, co-casting a functionalized coating layer on the PVDF solution without delamination could prepare membranes with special applications such as catalysis, degradation, or synthesis on the surface while maintaining a porous and highly-permeable support.

(3) In many studies about treating saline water, the produced water conductivity increased slightly although it could remain sufficiently low, and the rejection is higher than 99.9%. The reason is not totally clear yet. The possible reasons including minor defects on membrane and sea salt aerosols at the solution/membrane interface was

mentioned in a literature (*J. Membr. Sci.*, 599(2020): 117819), but further scientific investigation should be conducted. Additionally, it is important to establish an efficient method and criteria to report the rejection of the prepared membranes as comparing the conductivity of permeate solution to saline feed solution, the rejection factor is always higher than 99.9% according to the equation of $R=1-C_p/C_f$. Moreover, it should be considered carefully whether a membrane is wetted if it could be tested for several days but with very slightly permeate solution conductivity increment.

Curriculum Vitae

Miaomiao Tian



PERSONAL INFORMATION

Date of birth: March 7th, 1989

Nationality: Chinese

Gender: Female

EDUCATION

Oct. 2016-Mar. 2021	PhD, Chemical Engineering
	KU Leuven, Belgium
June 2015- June 2016	Research assistant
	Shanghai Advanced Research Institute, China
Sept. 2012-June 2015	Master, Chemical Technology
	Zhengzhou University, China
Sept. 2008-July 2012	Bachelor, Chemical Engineering and Technology
	Harbin University of Science and Technology, China

CONTACT

Process Engineering for Sustainable Systems (ProcESS)

Department of Chemical Enigineering, KU Leuven

Celestijnenlaan 200F, 3001 Heverlee, Leuven, Belgium

Tel: (+32) 486023586

Email: Miaomiao.tian@kuleuven.be

PUBLICATIONS

(1) **M. Tian**, S. Yuan, F. Decaesstecker, J. Zhu, A. Volodine, B. Van der Bruggen, One-step fabrication of isotropic poly(vinylidene fluoride) membranes for direct contact membrane distillation (DCMD), *Desalination*, 477 (2020) 114265.

(2) **M. Tian**, J. Zhu, Y. Zhang, B. Van der Bruggen, A review on membrane preparation for membrane distillation **(in preparation)**

(3) **M. Tian**, H. De Coninck, J. Zhu, Y. Zhang, B. Van Hooreweder, P. Van Puyvelde, B. Van der Bruggen, Exploring the potential of usage of 3D printed membranes combined with PVDF coating in direct contact membrane distillation (DCMD) **(in preparation)**

(4) **M. Tian**, J. Zhu, S. Yuan, Y. Zhang, B. Van der Bruggen, A co-casting route enables the formation of skinless, hydrophobic poly(vinylidene fluoride) membranes for DCMD **(***Journal of Membrane Science,* **major revision)**

(5) Y. Chen, **M. Tian**, X. Li, Y. Wang, A.K. An, J. Fang, T. He, Anti-wetting behavior of negatively charged superhydrophobic PVDF membranes in direct contact membrane distillation of emulsified wastewaters. *J. Membr. Sci.*, 2017, 535: 230-238